

# Overlooked persistent and bioaccumulative pollutants in Lake Geneva: their measurement, occurrence, and concentration distribution in the water column and sediments

THÈSE N° 6609 (2015)

PRÉSENTÉE LE 23 JUIN 2015

À LA FACULTÉ DE L'ENVIRONNEMENT NATUREL, ARCHITECTURAL ET CONSTRUIT  
LABORATOIRE DE MODÉLISATION DE LA CHIMIE ENVIRONNEMENTALE  
PROGRAMME DOCTORAL EN CHIMIE ET GÉNIE CHIMIQUE

ÉCOLE POLYTECHNIQUE FÉDÉRALE DE LAUSANNE

POUR L'OBTENTION DU GRADE DE DOCTEUR ÈS SCIENCES

PAR

Saer SAMANIPOUR

acceptée sur proposition du jury:

Prof. L. Helm, président du jury  
Prof. J. S. Arey, directeur de thèse  
Dr A. Gerecke, rapporteur  
Prof. E. Reiner, rapporteur  
Prof. U. von Gunten, rapporteur



ÉCOLE POLYTECHNIQUE  
FÉDÉRALE DE LAUSANNE

Suisse  
2015



# Abstract

Organic persistent and bioaccumulative pollutants (PBPs) are continually introduced into the environment as a part of the massive ongoing chemical production that began several decades ago. The PBPs include several chemical families such as: industrial compounds, agricultural chemicals, and pharmaceuticals. However the partitioning properties, concentration distributions in the environment, and environmental fate and behavior of many PBPs have not been investigated. Recent studies have reported on the lack of information regarding the occurrence, fate, and behavior of these PBPs in the environment [1, 2, 3]. The authors emphasized the need for measurements of these PBPs in different environmental compartments in order to better understand their environmental fate and behavior.

In this thesis, I report on the occurrence of legacy and novel PBPs in a deep aquatic system, Lake Geneva. Measuring these compounds in environmental samples is a challenging task due to their trace level concentrations and due to the complexity of the samples, manifest as matrix effect. I developed accelerating sampling techniques and new comprehensive two-dimensional gas chromatography (GC×GC) technique to tackle these challenges. Throughout the thesis I refer to "novel PBPs" as PBPs that are neutral, organic, non-legacy, and that have not been extensively measured in the environment. This terminology is similar to that adopted by Howard and Muir, 2010. I report results for several water column and sediment samples that were analyzed for a suite of 69 PBPs, including novel PBPs, as well as more widely studied compound groups, PBDEs, PCBs, OCPs and halogenated benzenes. This leads to the first reported detection and quantification for three novel PBPs (4-bromobiphenyl (4BBP), tribromobenzene (TBB), and pentachlorothiophenol (PCTP)) in a lake environment.

In Chapter 2 of the thesis I develop an analytical protocol for detection, quantification, and identity confirmation of trace level PBPs in environmental samples. This method takes advantage of the separation power of GC×GC combined to highly sensitive detectors, including electron capture negative chemical ionization time of flight mass spectroscopy (ENCI-TOFMS), micro electron capture detector ( $\mu$ ECD), and flame ionization detector (FID). Chapter 2 evaluates the effectiveness of the application of GC×GC- $\mu$ ECD for the detection and quantification of trace-level PBPs in the lake environment. In particular, I investigate automated baseline correction and peak delineation algorithms for their ability to remove matrix effect and quantify trace level PBPs in complex environmental samples. By employing a suite of chemometric tests, I systematically assess different baseline correction and peak delineation algorithms for

their confidence and accuracy in target analyte quantification. The results of chemometric tests show the crucial importance of the baseline correction algorithm for accurate peak integration. An aggressive baseline correction method systematically produced the best results for the chemometric tests, which indicated a better matrix effect removal. The results of the analytical protocol are also validated using a certified reference material. The validated analytical procedure leads to the successful detection and quantification of 18 trace level target analytes, including 7 PAHs in a light diesel fuel and 11 chlorinated hydrocarbons in a lake water extract. This chapter provides a sensitive and accurate protocol for detection, identity confirmation, and quantification of trace level PBPs in environmental samples. Finally, this chapter also provides guidance for diagnosis of the matrix effect and biased calibration during the quantification of analytes by GC×GC.

Chapters 3 and 4 of the thesis report on the occurrence of novel and legacy PBPs in the water column and sediments of Lake Geneva, a large and deep lake in the western part of Switzerland. The water column of the lake was sampled by deploying passive samplers at five different depths ranging from 70 m to 166.5 m for three consecutive months during the summer of 2011 (ELEM research project). Sediment samples were collected in four locations of the lake at depths ranging from 80 m to 310 m. Several novel PBPs (i.e. 4BBP, TBB, HBB and PCTP) and legacy PBPs, such as pentaBDE technical mixture, hexachlorobenzene (HCB) and PCNB, were included in the list of the target analytes. To confidently detect and quantify the target analytes, the analytical procedure developed in chapter 2 was employed. The water column concentrations of two novel brominated PBPs, 4BBP and TBB, were found to be 0.5-1.0 ng L<sup>-1</sup>, whereas the water column levels of PCTP were estimated to be 3-30000 ng L<sup>-1</sup>. All three novel PBPs were also detected and quantified in the sediments samples. Suspect screening of the GC×GC-ENCI-TOFMS data additionally revealed the presence of a potential precursor of PCTP, pentachloroanisole, in both the water and sediment samples. This is the first report of the occurrence and levels of three novel PBPs (4BBP, TBB, and PCTP) in a lake environment. These chapters also briefly investigate the potential pathways of introduction and elimination of these novel PBPs in the Lake Geneva environment. The occurrence of these novel PBPs and also their relatively high concentrations warrants further investigations of their occurrence in the environment, as well as the evaluation of their environmental risk.

In chapters 3 and 4 I also pre-evaluate the environmental fate and behavior of these novel PBPs. I estimated several environmentally relevant partitioning properties of both legacy and novel PBPs. These properties were estimated employing different modeling methods included EPISuite, a GC×GC retention time based method, ACDLab, and a quantum chemistry modeling approach, depending on the analyte. The estimated partitioning properties were used for evaluation of the potential for bioaccumulation, long range transport, and Arctic contamination. We also estimated equilibrium partitioning distributions of these compounds between the water column and sediments of the lake. Based on both the estimated partitioning properties and the limited available occurrence data for these PBPs, we concluded that bioaccumulation, long range transport, and Arctic contamination may play an important role

in the global fate and behavior of these PBPs. A comparison of PBP levels in lake water and in lake sediments suggested that several target analytes (4BBP and pentaBDE technical mixture) were at or near partitioning equilibrium, whereas for some other target analytes (TBB and PBEB) this was not the case. Finally, avenues are proposed for further investigation of the environmental fate and behavior of the novel PBPs.

In chapter 5, I report on the development of a new fast sampling device for the truly dissolved fraction of hydrophobic compounds in the water column of an aquatic system. Sampling the truly dissolved fraction of PBPs in the water column of an aquatic system is a challenging task, due to the trace level concentrations of these chemicals. Passive sampling approaches are a widely used sampling strategy that can overcome the difficulty of low analyte concentrations in the environment. However, passive sampling techniques necessitate long exposure times, typically 4 to 6 weeks, in order to achieve partitioning equilibrium between the sampler polymer and the water column. In chapter 5, a fast sampler for the truly dissolved fraction of PBPs in the water column was developed with polydimethylsiloxane (PDMS) as the receiving medium. In this chapter I evaluated PBP mass transfer kinetics between water and the PDMS by measuring the depletion of performance reference compounds (PRCs) with three different flow rates (1, 2 and 4 L min<sup>-1</sup>) at several time intervals for 12 PCBs. In order to explain the mass transfer between the water and PDMS, two modeling approaches were tested. An initial prototype of the sampler was built in-house and field-tested during the ELEMOMO field sampling campaign on Lake Geneva. The lab test showed that the rate of mass transfer of hydrophobic compounds was increased by two orders of magnitude compared to conventional passive sampling. The detection and quantification of the trace level PCBs in the water column of Lake Geneva was achieved only after two hours. The rate of mass transfer of the investigated compounds appeared to be highly sensitive to the water flow rate, and it was unexpectedly less sensitive to the chemical and physical properties of the compounds. However, further work is needed in order to completely model the mass transfer process.

Finally, in chapter 6 the water column concentration distributions of trace level PBPs are tentatively evaluated with respect to depth and distance from the shoreline (i.e. vertical and horizontal distribution). The samples collected during the ELEMOMO sampling campaign were analyzed using the protocol developed in chapter 2. The mass transfer model developed in chapter 5 enabled the estimation of the water column concentrations of PBPs. This enabled the construction of a 3-D map of the concentration distribution for each PBP and also facilitated inferences regarding their potential sources in and around the lake. To my knowledge this is the most comprehensive reported concentration distribution measurement of PBPs in a deep aquatic system such as Lake Geneva.

This thesis lays out a comprehensive protocol for the assessment of novel PBPs in aquatic systems, particularly useful for deep and large lakes. The protocol included the development and optimization of analytical procedures, development of novel methods for the rapid sampling of PBPs in a deep lake, and the assessment of the fate and behavior of novel PBPs based on

## **Abstract**

---

their environmental partitioning properties.

# Sommario

La recente produzione massiccia di composti organici persistenti e bioaccumulativi (PBP) ne ha causata l'introduzione nell'ambiente. Con il termine PBP s'intendono composti appartenenti a molteplici famiglie chimiche, tra cui i composti industriali, prodotti chimici agricoli e farmaceutici. I PBP si possono distinguere tra PBP nuovi e quelli già regolamentizzati. Secondo la terminologia adottata da Howard e Muir nel 2010, i PBP nuovi sono composti organici neutri, non regolamentizzati e non rilevati precedentemente.

Salvo che recentemente, le concentrazioni, le proprietà di partizione e il comportamento nell'ambiente di molti PBP non sono stato oggetto di studio. Howard e Muir hanno sottolineato la necessità di misurare questi PBP nei diversi comparti ambientali.

Durante il dottorato, ho misurato i PBP nel Lago di Ginevra e ne ho studiato il comportamento. A causa delle basse concentrazioni ambientali e per la presenza dell'effetto matrice nei campioni analizzati, analizzare questa tipologia di composti in campioni ambientali si è rivelato assai complesso. Avanzati metodi di gascromatografia bidimensionale (GC×GC) sono stati necessari.

In questo documento, riporto i risultati per diversi campioni d'acqua e sedimento, per un totale di 69 PBP, tra cui nuovi PBP, PBDE, PCB e OCP. Tra i PBP già regolamentizzati, ho individuato PBDE, PCB e OCP. Per la prima volta 3 nuovi PBP sono stati rilevati e quantificati in acque di lago: 4-bromobifenile (4BBP), tribromobenzene (TBB), e pentaclorotiofenolo (PCTP).

Nel secondo capitolo della tesi, ho sviluppato un protocollo di analisi per il rilevamento e la quantificazione di PBP in campioni ambientali. Questo metodo sfrutta la capacità di separazione del metodo cromatografico GC×GC combinata all'elevata sensibilità dei vari rivelatori adottati: un rivelatore ad ionizzazione chimica ifenato alla spettroscopia di massa al tempo di volo (ENCI-TOFMS), un micro rivelatore a cattura elettronica ( $\mu$ ECD) e un rivelatore a ionizzazione di fiamma (FID). L'efficacia dell'azione combinata di GC×GC- $\mu$ ECD è stata testata nella rivelazione e la quantificazione di PBP in traccia in matrici ambientali. Inoltre, ho testato molteplici algoritmi automatizzati per la correzione della linea di base e per l'integrazione del picco in funzione della loro capacità di rimuovere l'effetto matrice e quantificare PBP in campioni ambientali complessi. Mediante diversi test chemiometrici, ho sistematicamente valutato diversi metodi della correzione della linea di base e gli algoritmi di integrazione di picco

per la loro accuratezza e la precisione della quantificazione. I risultati dei test chemiometrici hanno dimostrato l'importanza cruciale dell'algoritmo della correzione della linea di base al fine di ottenere un'accurata integrazione del picco. I risultati del protocollo analitico sono stati convalidati usando un materiale di riferimento certificato. La procedura analitica così validata ha rivelato e quantificato 18 inquinanti, tra cui 7 idrocarburi policiclici aromatici in un carburante diesel e 11 idrocarburi clorurati in un estratto di acqua del lago. In questo capitolo vi è quindi riportato un protocollo sensibile e preciso per il rilevamento, l'identificazione, e la quantificazione di PBP in campioni ambientali. Infine, viene anche fornita una guida per la diagnosi degli effetti di matrice e la calibrazione errata durante la quantificazione degli inquinanti mediante GC×GC.

I capitoli 3 e 4 della tesi riguardano la presenza di PBP nuovi e regolamentizzati nell'acqua e nel sedimento del lago di Ginevra. L'acqua del lago è stata campionata utilizzando campionatori passivi a cinque diverse profondità, che vanno dai 70 m ai 166,5 m, per tre mesi consecutivi durante l'estate del 2011 (progetto di ricerca ELEMIO). I campioni di sedimento sono stati raccolti in quattro punti diversi del lago a profondità che vanno da 80 m a 310 m. Tre PBP nuovi (cioè 4BBP, TBB e PCTP) e PBP regolamentizzati, come pentaBDE miscela tecnica, esaclorobenzene (HCB) e PCNB, sono stati analizzati. Per il rilevamento e la quantificazione degli inquinanti considerati, ho adottato la procedura di analisi sviluppato nel capitolo 2. Le concentrazioni medie in acqua dei due nuovi PBP bromurati, 4BBP e TBB, sono di 0.5-1.0 ng L<sup>-1</sup>, mentre i livelli del PCTP in acqua corrispondono a circa 3-30000 ng L<sup>-1</sup>. I tre nuovi PBP sono stati individuati e quantificati nei campioni di sedimento. Lo Suspect screening dei dati di GC×GC-ENCI-TOFMS ha inoltre rivelato la presenza di un potenziale precursore di PCTP, pentaclorotioanisolo, in entrambi i campioni di acqua e sedimento. Questo è il primo rapporto dei livelli della concentrazione di questi nuovi PBP (4BBP, TBB, e PCTP) in un ambiente lacustre. Questi capitoli anche indagano le possibili vie di introduzione e l'eliminazione di questi nuovi PBP nel Lago di Ginevra. Le presenze di questi nuovi PBP e anche le loro concentrazioni relativamente elevate suggeriscono la necessità di ulteriori ricerche di questi composti nell'ambiente, ivi compresa la valutazione del loro rischio ambientale.

Nei capitoli 3 e 4 ho anche valutato il comportamento ambientale di questi nuovi PBP, stimandone diverse proprietà di partizione di rilevanza ambientale. Diversi metodi computazionali sono stati impiegati, inclusi il metodo EPISuite, che si basa sui tempi di ritenzione di GC×GC, ACDLab e, infine, metodi di meccanica quantistica. Le proprietà di partizione stimate sono state quindi utilizzate per la valutazione del potenziale di bioaccumulazione, il trasporto a lunga distanza, e la contaminazione artica. Ho anche valutato l'equilibrio di ripartizione di questi composti tra l'acqua e sedimento del lago. Sulla base delle proprietà stimate e i limitati dati ambientali disponibili per questi PBP, ho concluso che la bioaccumulazione, il trasporto a lunga distanza, e la contaminazione artica costituiscono fattori importanti nel comportamento ambientale di questi PBP. Un confronto tra i livelli di PBP in acqua di lago e nei sedimenti lacustri suggerisce che alcuni inquinanti (4BBP e miscela tecnica pentaBDE) sono prossimi all'equilibrio. Ulteriori accertamenti e studi sono necessari per approfondire il



comportamento e la distribuzione di questi inquinanti nel lago di Ginevra.

Il capitolo 5 si concentra sullo sviluppo di un dispositivo di campionamento veloce per la frazione disciolta di composti idrofobici nell'acqua. Il campionamento dalla frazione disciolta di un PBP nell'acqua di un sistema acquatico ha richiesto un trattamento avanzato a causa delle concentrazioni in traccia di queste sostanze. Il metodo di campionamento passivo adottato prevede lunghi tempi di esposizione, tipicamente tra i 4 a 6 settimane, per raggiungere l'equilibrio di partizionamento tra il campionatore e l'acqua. Nel capitolo 5 di questa tesi, il campionatore veloce per la frazione disciolta del PBP nell'acqua sviluppato utilizza il polidimetilsilossano (PDMS) come mezzo di ricezione. Ho valutato il trasferimento di massa tra acqua e il PDMS misurando la perdita di composti di riferimento (PRCs) utilizzando tre diverse portate d'acqua ( $1 \text{ L min}^{-1}$ ,  $2 \text{ L min}^{-1}$  e  $4 \text{ L min}^{-1}$ ) a diversi intervalli per 12 PCB. Per spiegare il trasferimento di massa tra l'acqua e PDMS, due approcci di modellizzazione sono stati testati. Un primo prototipo del campionatore è stato costruito in-house e testato sul campo durante la campagna di campionamento ELEM0 nel lago di Ginevra. I test di laboratorio hanno mostrato che la velocità di trasferimento di massa di composti idrofobici sono di due ordini di grandezza maggiori rispetto al campionamento passivo. Infatti, la rilevazione dei PCB nell'acqua del lago di Ginevra si è verificata dopo solo due ore di campionamento. Il trasferimento di massa dei composti esaminati si è dimostrato molto sensibile alla velocità dell'acqua e meno sensibile alle proprietà chimiche e fisiche dei composti. Tuttavia, sono necessari ulteriori lavori per modellare il processo di trasferimento di massa.

Infine, nel capitolo 6 ho valutato la distribuzione spaziale dei PBP nell'acqua di lago di Ginevra. I campioni raccolti durante la campagna di campionamento ELEM0 sono stati analizzati utilizzando il protocollo sviluppato nel capitolo 2. Il modello di trasferimento di massa sviluppato nel capitolo 5 mi ha permesso di effettuare una stima delle concentrazioni di PBP nell'acqua. Ho anche delineato una mappa 3-D della distribuzione delle concentrazioni per ciascun PBP nell'acqua del lago, facilitandomi l'individuazione di potenziali fonti di inquinanti all'interno e all'esterno del lago di Ginevra. Si tratta della più completa mappa geochimica di PBP in un sistema lacustre profondo come il lago di Ginevra.

Riassumendo, questa tesi riporta un protocollo completo per la valutazione di nuovi PBP nei sistemi acquatici, che si è peraltro rivelato particolarmente utile per l'applicazione in laghi profondi e ampi. Il protocollo include lo sviluppo e l'ottimizzazione delle procedure analitiche, lo sviluppo di metodi innovativi per il rapido campionamento di PBP in un lago e la valutazione del comportamento ambientale di nuovi PBP in base alle loro proprietà di partizione ambientali.

## keywords

Persistent and bioaccumulative pollutants (PBPs), halogenated organic pollutants, analytical chemistry, GC×GC- $\mu$ ECD/FID, GC×GC-ENCI-TOFMS, water, sediment, novel PBPs, PCBs, PBDEs, OCPs, extraction, lake, fate and behavior, modeling, sampling, method development,

## Sommario

---

and instrument development.

# Contents

|  |            |
|--|------------|
| <b>Abstract (English/Italiano)</b>   | <b>iii</b> |
| <b>Introduction</b>  | <b>1</b>   |
| <b>1 Introduction</b>  | <b>1</b>   |
| 1.1 Motivations . . . . .  | 1          |
| 1.2 Present study . . . . .  | 3          |
| <b>2 Analyte quantification with comprehensive two-dimensional gas chromatography: Assessment of methods for baseline correction, peak delineation, and matrix effect elimination for real samples</b> | <b>5</b>   |
| 2.1 Introduction . . . . .   | 6          |
| 2.2 Methods . . . . .  | 11         |
| 2.2.1 Chemicals . . . . .  | 11         |
| 2.2.2 Standards preparation for the external standard calibration method (ESM)   | 13         |
| 2.2.3 Sample preparation for the standard addition method (SAM) . . . . .  | 13         |
| 2.2.4 Sample analysis by GC×GC- $\mu$ ECD, GC×GC-FID, and GC×GC-ENCI-TOFMS   | 13         |
| 2.2.5 Analyte peak integration methods . . . . .   | 15         |
| 2.2.6 Analyte quantification methods . . . . .   | 19         |
| 2.2.7 Chemometric tests used to assess the peak integration methods . . . . .  | 21         |
| 2.3 Results and discussion . . . . .   | 26         |
| 2.3.1 Successful detection and integration of target analytes, and resulting signal-to-noise ratios . . . . .  | 27         |
| 2.3.2 Quantitative performance assessment of peak integration methods . . . . .  | 33         |
| 2.4 Conclusions . . . . .  | 52         |
| <b>3 Overlooked Persistent and Bioaccumulative Brominated Pollutants in the Deep Water Column of Lake Geneva: 1,3,5-tribromobenzene and 4-bromobiphenyl</b>  | <b>55</b>  |
| 3.1 Introduction . . . . .   | 56         |
| 3.2 Experimental section . . . . .   | 58         |
| 3.2.1 Sampling location . . . . .  | 58         |
| 3.2.2 Target analyte selection . . . . .   | 59         |
| 3.2.3 Chemicals . . . . .  | 60         |
| 3.2.4 Water column sampling . . . . .  | 60         |

## Contents

---

|          |   |           |
|----------|---|-----------|
| 3.2.5    | Sample preparation and clean-up . . . . .   | 60        |
| 3.2.6    | GC×GC- $\mu$ ECD and GC×GC-ENCI-TOFMS conditions . . . . .  | 61        |
| 3.2.7    | Target analyte quantification . . . . .   | 62        |
| 3.2.8    | Chemical property estimation . . . . .  | 62        |
| 3.3      | Results and Discussion . . . . .  | 62        |
| 3.3.1    | Successful detection, identity confirmation, and quantification of target analytes by GC×GC- $\mu$ ECD and GC×GC-ENCI-TOFMS . . . . .                           | 62        |
| 3.3.2    | Concentrations and trends of target Br-PBPs in the water column of Lake Geneva . . . . .  | 63        |
| 3.3.3    | Occurrence of target Br-PBPs in the lake sediments . . . . .  | 67        |
| 3.3.4    | Potential sources of the target analytes . . . . .  | 69        |
| 3.3.5    | Physical and chemical property estimation and predicted environmental behaviors of TBB and 4BBP . . . . .   | 71        |
| <b>4</b> | <b>Pentachlorothiophenol, a newly identified aquatic pollutant</b>  | <b>75</b> |
| 4.1      | Introduction . . . . .  | 76        |
| 4.2      | Methods . . . . .   | 78        |
| 4.2.1    | Target analyte selection . . . . .  | 78        |
| 4.2.2    | Chemicals . . . . .   | 78        |
| 4.2.3    | Environmental sampling . . . . .  | 78        |
| 4.2.4    | Sample preparation . . . . .  | 79        |
| 4.2.5    | Sediment samples extraction and clean up . . . . .  | 80        |
| 4.2.6    | Analysis by GC×GC- $\mu$ ECD and GC×GC-ENCI-TOFMS . . . . .   | 80        |
| 4.3      | Results and discussion . . . . .  | 81        |
| 4.3.1    | Estimated PDMS-water partitioning coefficient of target analytes . . . . .  | 81        |
| 4.3.2    | Estimation of environmentally relevant properties . . . . .   | 82        |
| 4.3.3    | Detection and confirmation of target analytes in environmental samples by GC×GC- $\mu$ ECD and GC×GC-ENCI-TOFMS . . . . .                                       | 83        |
| 4.3.4    | Matrix effect elimination and accurate quantification of the target analytes in environmental samples . . . . .   | 84        |
| 4.3.5    | PCTP, HCB and PCNB in the water column and sediments of Lake Geneva   | 84        |
| 4.3.6    | The fate and behavior of PCTP in the Lake Geneva environment . . . . .  | 89        |
| 4.3.7    | Implications . . . . .  | 90        |
| <b>5</b> | <b>Development, modeling and field test of an in-situ accelerated sampler for the truly dissolved fraction of organic pollutants in deep and shallow water.</b> | <b>93</b> |
| 5.1      | Introduction . . . . .  | 94        |
| 5.2      | Experimental . . . . .  | 96        |
| 5.2.1    | Chemicals . . . . .   | 96        |
| 5.2.2    | Loading of performance reference compounds (PRCs) onto PDMS polymer strips . . . . .  | 96        |
| 5.2.3    | Laboratory desorption experiment . . . . .  | 97        |
| 5.2.4    | Accelerated sampler prototype . . . . .   | 97        |

|          |  |            |
|----------|--|------------|
| 5.2.5    | Field sampling in Lake Geneva . . . . .  | 98         |
| 5.2.6    | Extraction of PDMS strips after deployment . . . . .   | 100        |
| 5.2.7    | Sample analysis . . . . .  | 100        |
| 5.2.8    | GC×GC- $\mu$ ECD and GC×GC-ENCI-TOFMS conditions . . . . .   | 100        |
| 5.2.9    | Quality assurance . . . . .  | 101        |
| 5.3      | Theoretical background . . . . .   | 101        |
| 5.3.1    | One compartment Linear model of sorption kinetics . . . . .  | 101        |
| 5.4      | Results and discussion . . . . .   | 103        |
| 5.4.1    | Application of the one-compartment linear model to laboratory desorption kinetic data . . . . .                              | 103        |
| 5.4.2    | Development and application of a two-compartment non-linear model of sorption kinetics . . . . .                             | 104        |
| 5.4.3    | Application of the two-compartment non-linear model to the laboratory desorption kinetics experiment . . . . .               | 107        |
| <b>6</b> | <b>Hydrophobic organic pollutant concentrations exhibit strong spatial gradients in the deep water column of Lake Geneva</b> | <b>121</b> |
| 6.1      | Introduction . . . . .   | 122        |
| 6.2      | Methods . . . . .  | 123        |
| 6.2.1    | Water sampling location . . . . .  | 123        |
| 6.2.2    | Chemicals . . . . .  | 126        |
| 6.2.3    | Sample preparation . . . . .   | 126        |
| 6.2.4    | GC×GC- $\mu$ ECD and GC×GC-ENCI-TOFMS instrument conditions . . . . .  | 129        |
| 6.2.5    | Target analyte quantification in the environmental samples . . . . .   | 130        |
| 6.3      | Results and discussion . . . . .   | 131        |
| 6.3.1    | Successful detection and quantification of HOPs in the deep water column and sediments of Lake Geneva . . . . .              | 131        |
| 6.3.2    | Comparison of pollutant concentrations measured by passive sampler and by accelerated sampler . . . . .                      | 132        |
| 6.3.3    | Occurrence and general trends of the target analytes in the water column of Lake Geneva . . . . .                            | 134        |
| 6.3.4    | Classification of the water column sampling locations and the variability within each class . . . . .                        | 135        |
| 6.3.5    | Spatial distribution of HOPs in the deep water column . . . . .  | 136        |
| 6.3.6    | Occurrence of the target analytes in the sediments of the lake . . . . .   | 141        |
| 6.3.7    | Environmental implications . . . . .   | 145        |
| <b>7</b> | <b>Conclusions</b>   | <b>149</b> |
| 7.1      | Main findings and implications . . . . .   | 149        |
| 7.2      | Remaining challenges . . . . .   | 151        |
| 7.3      | Future work . . . . .  | 151        |

## Contents

---

|          |  |            |
|----------|--|------------|
| <b>A</b> | <b>Supporting information to Chapter 3: Overlooked Persistent and Bioaccumulative Brominated Pollutants in the Deep Water Column of Lake Geneva: 1,3,5-tribromobenzene and 4-bromobiphenyl</b> | <b>153</b> |
| A.1      | Passive sampling methodology . . . . .   | 153        |
| A.2      | Sediment samples extraction and clean up . . . . .   | 154        |
| A.3      | GC×GC- $\mu$ ECD and GC×GC-ENCI-TOFMS analysis conditions . . . . .  | 155        |
| A.4      | Target quantification . . . . .  | 156        |
| <b>B</b> | <b>Supporting information to Chapter 4: Pentachlorothiophenol, a newly identified aquatic pollutant</b>  | <b>161</b> |
| B.1      | Water concentration estimation of the target analytes . . . . .  | 161        |
| B.1.1    | Preprocessing and extraction of the PDMS strips . . . . .  | 162        |
| B.2      | Sediment samples extraction and clean up . . . . .   | 162        |
| B.3      | GC×GC- $\mu$ ECD and GC×GC-ENCI-TOFMS instrument conditions . . . . .  | 163        |
| B.4      | Computational estimates of aqueous $pK_a$ values . . . . .   | 164        |
| B.4.1    | Free energy of the proton in aqueous phase . . . . .   | 164        |
| B.4.2    | Quantum chemical computation of the $K_{sw}^{app}$ . . . . .   | 164        |
| B.5      | Quality assurance . . . . .  | 165        |
|          | <b>Bibliography</b>  | <b>198</b> |

# 1 Introduction

## 1.1 Motivations

Little is known concerning the vast majority of man-made chemicals released into the environment [3, 1, 4]. The US-EPA has registered about 82,000 chemicals [4], whereas the European Chemical Agency (ECHA) lists more than 140,000 compounds commercialized in Europe [5]. Howard and Muir, in 2010, identified 610 compounds with wide commercial use (i.e. a US/Canada production volume  $> 1$  t/y) that were predicted to be bioaccumulative and persistent in the environment (thus persistent and bioaccumulative pollutants, PBPs) and also were somewhat overlooked by the environmental science community. Further investigations showed that potential transformation products of some of these 610 compounds also met the criteria for environmental persistence and bioaccumulation [1]. These PBPs include several chemical families such as: industrial compounds, personal care products, agricultural chemicals, and pharmaceuticals. Most of the 610 PBPs are neutral and more than 60% of them are halogenated. However the concentration distributions in the environment, partitioning properties, and environmental fate and behavior of 80% of these PBPs have not been investigated widely [3, 1, 4]. The above studies reported on the lack of information regarding the occurrence, fate, and behavior of these PBPs in the environment [3, 1, 4]. The authors emphasized the need for measurements of these PBPs in different environmental compartments in order to better understand their environmental fate and behavior.

Overall, most of organic PBPs released into the environment have not been measured, and there is no information about their fate and behavior [6, 7]. Recent exploratory studies detected several pollutants (first environmental detection), in different environmental samples, such as water, precipitation, biota, and sediment [8, 9, 10, 11, 12, 13, 14], which warrants the need for further investigation of the PBPs in the water column of lakes. Throughout this manuscript we refer to the 610 organic pollutants listed by Howard and Muir as PBPs.

Measurement of PBPs due to their trace level concentrations and complexity of the matrix

## Chapter 1. Introduction

---

encountered in analysis of environmental samples is a challenging task [15, 16, 17, 18]. The conventional sampling methodologies to overcome these issues are large volume sampling [19, 17] and passive sampling [20, 21, 22]. For the large volume sampling of PBPs, special care must be taken in sample handling and storage [23, 24, 18]. Moreover, large volume sampling appears to be sensitive to the suspended solids and the dissolved organic matter in the aquatic system [25]. Finally, large volume sampling is impractical for water depths > 100 m, due to the possibility of cross-contamination caused by the use of long tubes and pumping systems [17, 18]. Compared to large volume sampling The passive sampling methodology is inexpensive, stable, and easy to handle [23, 26, 27]. However, passive sampling has the disadvantage of long exposure times, such as 4 to 8 weeks, depending on the chemical and physical properties of the target compound and the hydrological conditions of the sampled system [28, 29]. Additionally, the issue of biofilm formation appears to be relevant for passive sampling, due to the long exposure times required [30]. Most passive sampling efforts have been conducted in shallow water [24, 22], due to the logistical challenges of deep water deployments [29, 31, 28].

The deep water column of aquatic systems has not been explored extensively for the truly dissolved (TD) fraction of PBPs. The TD fraction of a PBP excludes PBP mass that is associated with suspended particles, dissolved organic matter, or particulate organic carbon [32]. Hence, the TD fraction of PBPs in aquatic systems is considered widely important even when present at trace level concentrations [17, 7, 33, 32, 25]. The PBPs mainly have been investigated in the shallow water column (depth < 20 m) of the aquatic systems [19, 34, 35, 36, 37, 21, 9, 38, 17]. The lack of published data in the deep water column is mainly due to the difficulties in sampling the TD fraction of PBPs (mentioned above). There have been few attempts to develop new sampling systems for measuring PBPs in the deep water columns of aquatic systems that are able to overcome the issues of cost, time, energy and the difficulty of sample handling [31, 28]. To my knowledge, there is no rapid sampling system available that can sample trace levels of the truly dissolved fraction of PBPs in the deep water column of aquatic systems, without being affected by suspended solids and/or dissolved organic matter.

Finally, limited published data are available regarding the spatial distributions of PBPs in the water column of deep and large lakes. The spatial concentration distribution of PBPs in lakes, both vertical and horizontal, is considered an indication of the environmentally relevant processes affection the fate and behavior of that PBP [39, 32, 34, 35, 40, 41, 42, 43, 44, 45, 46, 47, 48]. Recent investigations have highlighted the importance of input flux, through air-water exchange, tributaries, and dry and wet deposition, particularly for highly urbanized areas [49, 50, 36, 45, 46, 35, 34]. Additionally, there are limited works that have evaluated the vertical concentration distribution of PBPs in both the deep and shallow water column [51, 52, 53]. The mentioned studies also have indicated the possibility of the existence of significant vertical and horizontal gradients of PBPs in the water column of an aquatic system. To my knowledge, there is no published work that has evaluated the spatial concentration distribution of PBPs in the deep water column of a large lake, such as Lake Geneva, Switzerland.



### 1.2 Present study

In this thesis, I report on the occurrence of legacy and novel PBPs in a deep aquatic system, Lake Geneva. I employed comprehensive two-dimensional gas chromatography (GC×GC) to tackle the problem of complexity of the environmental samples. Throughout the thesis I refer to "novel PBPs" as PBPs that are neutral, organic, non-legacy, and that have hardly been measured in the environment. This terminology is similar to that adopted by Howard and Muir, 2010. This thesis consists of five research reports treating five individual questions each in an independent chapter.

In Chapter 2 of the thesis I developed an analytical protocol for detection, quantification, and identity confirmation of trace level PBPs in environmental samples. This method took advantage of the separation power of GC×GC combined to highly sensitive detectors, including electron capture negative chemical ionization time-of-flight, mass spectrometry (ENCI-TOFMS), micro electron capture detector ( $\mu$ ECD), and flame ionization detector (FID). Chapter 2 evaluates the effectiveness of the application of GC×GC- $\mu$ ECD for the detection and quantification of trace-level PBPs in the lake environment. This protocol enabled the successful detection and quantification of 18 trace level PBPs in real environmental samples.

Chapters 3 and 4 of the thesis present focused investigations of selected novel and legacy PBPs in the deep water column and sediments of Lake Geneva. The water column of the lake was sampled by deploying passive samplers at five different depths ranging from 70 m to 166.5 m for three consecutive months during the summer of 2011 (ELEM0 research project). Sediment samples were collected in four locations of the lake at depths ranging from 80 m to 310 m. These field data enabled several inferences about the sources and sinks of these pollutants in the lake. In chapters 3 and 4 I also pre-evaluated the environmental fate and behavior of these novel PBPs based on their estimated partitioning properties. Finally, avenues are proposed for further investigation of the environmental fate and behavior of these novel PBPs.

In chapter 5, I report on the development and testing of a new rapid sampling device for the truly dissolved fraction of hydrophobic compounds in the water column of an aquatic system. A two-compartment non-linear model was developed to describe the mass transfer of 11 PCBs between the PDMS and water. Finally, an initial prototype of the sampler was built in-house and field-tested during the ELEM0 field sampling campaign on Lake Geneva. The accelerated sampler, accurately measured the trace level TD concentration of 4 PCBs in the deep water column of Lake Geneva.

Finally, in chapter 6, the water column concentration distributions of trace level PBPs are evaluated with respect to depth and distance from the shoreline (i.e. vertical and horizontal concentration distributions). The samples collected during the ELEM0 sampling campaign

## **Chapter 1. Introduction**

---

were analyzed using the protocol developed in Chapter 2. The mass transfer model developed in Chapter 5 enabled the estimation of the water column concentrations of PBPs. Surprisingly large gradients are found, with several PBPs exhibiting concentration differences that exceeded one order of magnitude at different locations in the lake. This enabled the construction of the concentration distribution in both vertical and horizontal dimensions for each PBP and also facilitated inferences regarding their potential sources in and around the lake. This is the most comprehensive reported concentration distribution of PBPs in the water column of a deep aquatic system, such as Lake Geneva, based on direct measurements.

## **2 Analyte quantification with comprehensive two-dimensional gas chromatography: Assessment of methods for baseline correction, peak delineation, and matrix effect elimination for real samples**

Published as: *J. Chrom. A.* 2015, 1375, 123–139.

Authors: Saer Samanipour, Petros Dimitriou-Christidis, Jonas Gros, Aureline Grange, J. Samuel Arey

Contributions: This chapter was prepared by Saer Samanipour with editorial comments by all coauthors, particularly J. Samuel Arey.

### Abstract

Comprehensive two-dimensional gas chromatography (GC×GC) is used widely to separate and measure organic chemicals in complex mixtures. However, approaches to quantify analytes in real, complex samples have not been critically assessed. We quantified 7 PAHs in a certified diesel fuel using GC×GC coupled to flame ionization detector (FID), and we quantified 11 target chlorinated hydrocarbons in a lake water extract using GC×GC with electron capture detector ( $\mu$ ECD), further confirmed qualitatively by GC×GC with electron capture negative chemical ionization time-of-flight mass spectrometer (ENCI-TOFMS). Target analyte peak volumes were determined using several existing baseline correction algorithms and peak delineation algorithms. Analyte quantifications were conducted using external standards and also using standard additions, enabling us to diagnose matrix effects. We then applied several chemometric tests to these data. We find that the choice of baseline correction algorithm and peak delineation algorithm strongly influence the reproducibility of analyte signal, error of the calibration offset, proportionality of integrated signal response, and accuracy of quantifications. Additionally, the choice of baseline correction and the peak delineation algorithm are essential for correctly discriminating analyte signal from unresolved complex mixture signal, and this is the chief consideration for controlling matrix effects during quantification. The diagnostic approaches presented here provide guidance for analyte quantification using GC×GC.

### 2.1 Introduction

Comprehensive two-dimensional gas chromatography (GC×GC) is used widely for the analysis of complex mixtures, as it can resolve thousands of peaks within single chromatograms [54, 55]. GC×GC has been used in the analysis of petroleum, environmental samples, foods, and biological fluids [54]. Even though GC×GC provides very good separation capacity, analyte co-elution still arises in very complex samples [56]. Analyte quantification remains challenging due to the inherent complexity of two-dimensional data and the typical presence of co-eluting (overlapping) peaks [57, 58].

During the past decade, several investigations have quantified analytes using GC×GC data [58]. In 1998, Beens et al introduced the notion of analyte quantification with GC×GC-FID, employing the external standard calibration method [59]. Later studies applied external standard calibration as a means to quantify small aromatic hydrocarbons in gasoline, suspected allergens in fragrances, and polychlorinated biphenyls (PCBs) in soil and sediment [55, 60, 61, 62, 63]. Some of these studies used internal standards to normalize the peak volumes of the target analytes [55, 60, 63]. The studies mentioned above used univariate detectors, either FID (flame ionization detector) or ECD (electron capture detector). These were important contributions to the development of quantification methods for GC×GC. However the analytes quantified in these studies were usually well-resolved peaks at high con-

centrations [55, 61, 62, 63]. Kallio and Hyötyläinen emphasized the necessity of well-resolved peaks in order to achieve accurate integrated peak volumes [62]. Additionally, Adahchour et al expressed concern regarding the quality of quantifications performed on univariate data produced by GC×GC using the external standard calibration method [64]. They stated that external calibration was not suitable for quantification in cases involving poorly resolved peaks.

The complexity of typical GC×GC chromatograms warrants sophisticated data processing methods [57, 58, 65, 66]. After data acquisition, analyte signal quantification involves the following major data processing tasks: baseline correction, peak detection, and peak delineation [65, 66, 67, 68, 69]. To facilitate discussion of these different data processing operations, we conceptually decompose the GC×GC detector signal into four additive components (Figure 2.1; Eq. 2.1), defined as follows:

- The *resolvable analyte signal* is the signal attributed to analytes that are wholly or partly resolved by the instrument [65, 66, 70]. We do not assign a threshold of chromatographic resolution [71] to the resolvable analyte signal, since the ability to differentiate resolved signal from unresolved signal depends upon the baseline correction and peak delineation algorithms applied. In the present work, we are interested in quantifying resolvable analyte signal, or peak volume, of target analytes.
- The *unresolved signal* arises from chemical elutants that are not reasonably resolved from one another. This is operationally defined by the combination of baseline correction and peak delineation algorithm applied. The unresolved signal corresponds to the "chemical blank" in earlier chemometrics literature [72, 73]. The *matrix effect* arises from failure to discriminate properly between the unresolved signal and the resolvable analyte signal. Matrix effects are defined and explained further in section 2.2.6.
- The *instrument background signal* is the signal produced by the instrument in the absence of sample, excluding random signal fluctuations.
- The *noise* is zero-mean random fluctuation of the signal, inherent to the instrument detector [57, 65].

Distinguishing and separating these signal components is an important goal of GC×GC data processing. Since here we are focused on analyte quantification, we also define the *non-analyte signal*, which is the unresolved signal plus instrument background signal plus noise (Eq. 2.1). The non-analyte signal is called the "constant error" in earlier chemometrics literature [74], and this signal component can be quantified by measuring the Total Youden Blank, assuming

that non-additive signal interactions (matrix interferences) are not present [72, 75].

$$\begin{aligned} \text{Total instrument signal} &= \text{analyte signal} && (2.1) \\ &+ \text{instrument background signal} \\ &+ \text{unresolved signal} \\ &+ \text{noise} \end{aligned} \left. \vphantom{\begin{aligned} \text{Total instrument signal} \\ &+ \text{instrument background signal} \\ &+ \text{unresolved signal} \\ &+ \text{noise} \end{aligned}} \right\} \text{non-analyte signal}$$

Throughout this article, we refer to a *peak integration method* as a particular combination of algorithms that leads to a unique value for the integrated resolvable analyte signal, or peak volume, attributed to a given analyte in the GC×GC chromatogram. An individual peak integration method is composed of one baseline correction algorithm combined with one peak delineation algorithm. These methods are discussed below. The term *quantification method* refers to a method that uniquely maps an observed peak volume to an estimated analyte concentration in an environmental sample. For this purpose, we applied both the external standard calibration method (ESM) and the standard addition calibration method (SAM) [76, 77, 78], and these methods are explained in section 2.2.6.

After signal acquisition, the first step in GC×GC data processing is usually the baseline correction, which involves estimation and removal of the baseline. Here, the baseline is defined operationally as the signal that is subtracted from the total chromatogram signal before peak integration [57, 65]. The approach taken for defining the baseline may vary depending on the objective of the analyst. For example, for quantification of resolvable analytes, an appropriate baseline correction method ideally should remove the non-analyte signal component, leaving behind only the resolvable analyte signal [65, 66, 79, 80]. Alternatively, for the quantification of the sample total chemical signal, it may instead be desirable for the baseline correction method to remove only the instrument background signal component, leaving behind both the resolvable analyte signal and the unresolved signal [79, 80].

Several strategies have been proposed for performing a baseline correction [57]. It may be appropriate to define the analytical blank as the baseline and remove this signal from the sample signal. The analytical blank is defined as a sample identical to the original sample, but excluding the analyte of interest [78]. In principal this should produce the non-analyte signal chromatogram. However it is often not possible to obtain the analytical blank [65]. Available automated algorithms offer more general approaches to estimating the baseline. The "deadband baseline" correction algorithm uses the statistical properties of white noise to define regions of the chromatogram called deadbands and then calculates and removes this signal from the chromatogram [69, 81]. The deadband baseline is intended to estimate the signal trend that would arise in the absence of chemical elutants [69]. This baseline correction algorithm thus estimates and removes the instrument background signal, but it does not remove the unresolved signal component (Figure 2.1). A second algorithm, the "local linear baseline" correction, fits a straight line to intervals as wide as the peak width within each

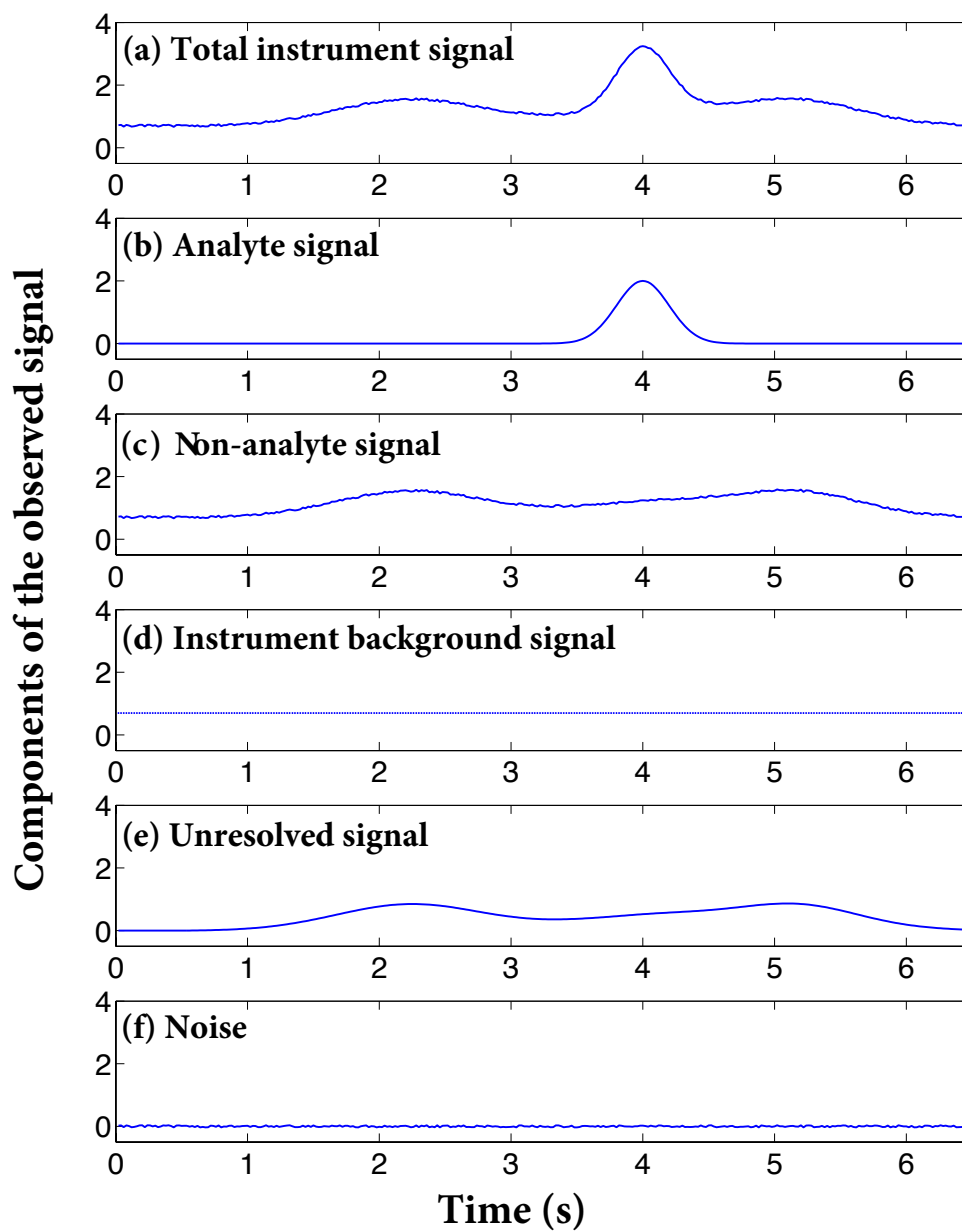


Figure 2.1 – Conceptual schematic of the disaggregated components of the sample signal in a single modulation period of the GC $\times$ GC chromatogram. (a) The observed total instrument signal; (b) the resolvable analyte signal; (c) the non-analyte signal; (d) the instrument background signal; (e) the unresolved signal; and (f) the noise.

modulation period of the GC×GC chromatogram, which is then subtracted from the total instrument signal [57]. The local linear baseline correction method thus attempts to estimate and remove the non-analyte signal (instrument background signal plus unresolved signal and noise), leaving behind the resolvable analyte signal. However, complications can arise in cases of the presence of unresolved material and low signal-to-noise ratios [65]. Finally, the Eilers algorithm takes a different approach, which is to estimate the baseline by fitting a higher order polynomial to the signal contained in each GC×GC modulation period [82]. The Eilers method thus estimates the non-analyte signal and attempts to isolate the resolvable analyte signal. Amigo et al compared different baseline correction methods with simulated conventional GC data, including the Eilers method and the local linear baseline correction method [57]. They found that the Eilers method more accurately isolated the resolvable analyte signal in cases of overlapping peaks. In summary, existing baseline estimation methods use widely differing algorithms and assumptions. However the impact of the GC×GC baseline estimation algorithm on analyte quantification has not been extensively tested.

After baseline correction and peak detection, the *peak delineation* step defines the boundaries of each detected peak, thereby indicating the two-dimensional region of the GC×GC chromatogram signal that should be aggregated together for an individual peak volume [56, 57, 69]. Together, baseline correction and the peak delineation completely determine the integrated volume of a detected peak. The "two-step" and "inverted watershed" algorithms are automated approaches commonly used for peak delineation in GC×GC [65]. These two methods do not require any prior information about analyte or sample identity in order to perform the peak delineation, thus they are called automated peak delineation methods. The two-step algorithm first detects one-dimensional peaks in each individual modulation period using the first and second derivatives of the signal. In the second step, the algorithm decides which one-dimensional peaks in adjacent GC×GC modulation periods should be merged together to create a two-dimensional peak, based on a parameterized tolerance level for shifting of the peak retention time in between each modulation [56]. This is a modified version of the method developed and used for processing conventional GC chromatograms [66]. The inverted watershed algorithm, also known as the drain algorithm, finds the pixel with the locally highest intensity in each detected peak and then identifies neighboring pixels that belong to the two-dimensional peak ("blob"), until it reaches the baseline [69]. In cases of complex mixtures, inaccurate delineation of the peak boundaries introduces uncertainty into the peak volume [62, 65]. Nevertheless, to our knowledge, these peak delineation approaches have not been compared for their abilities to produce accurate analyte quantifications in real samples.

There are several possible ways in which uncertainty or error may arise during these GC×GC data processing steps [65, 66, 70, 83]. The baseline correction, peak detection, and peak delineation are all important sources of uncertainty [65, 66, 70]. Vivó-Truyols et al and Latha et al both evaluated errors arising during the peak detection step [67, 84]. Taken together, these two studies find that for complex samples, the commonly utilized algorithms have a



high probability of failure during peak detection, suggesting that further developments are needed. Another important source of error is the peak delineation step [65, 85, 86]. The two-step algorithm can exhibit sensitivity to peak tailing in the second dimension and to irregularities in the peak shape within each modulation [65, 85]. This may lead to inaccurate definition of the peak boundaries and resulting peak volumes [85]. Additionally, this algorithm may be sensitive to the peak width in the second dimension [85]. In some cases this was found to cause up to 80% error in the volume of the peak. The inverted watershed peak delineation algorithm has been found to be adversely affected by high level of noise and by overlapping peaks, leading to errors in the defined peak boundaries such as split peaks [65, 70].

To our knowledge, no published study has yet evaluated currently available baseline correction and peak delineation algorithms for their ability to produce reliable analyte quantifications from univariate GC×GC chromatograms of real, complex samples [65, 70]. In order to address this need, we performed an assessment and comparison of several different peak integration algorithms that have been developed for GC×GC.

## 2.2 Methods

### 2.2.1 Chemicals

We used a PAH standard mixture (EPA Method 8310 PAH mixture) that contained 18 polycyclic aromatic hydrocarbons in dichloromethane (DCM) solvent, purchased from Restek Switzerland. We also used a certified diesel fuel ("certified PAHs in diesel"), consisting of a solution of two PAH-free, synthetic, light diesel fuels combined with known concentrations of 7 PAHs in DCM. The certified diesel fuel was provided by Restek Switzerland (Table 2.1). An analytical PCB standard mixture and an organochlorinated pesticide standard mixture both were purchased from Sigma-Aldrich Switzerland. The PCB standard mixture consisted of a  $1 \mu\text{g L}^{-1}$  solution of each of 11 PCBs in hexane and the organochlorinated pesticide standard mixture contained  $0.1 \mu\text{g L}^{-1}$  of each of 18 pesticides in hexane (Table 2.1). Pesticide grade hexane and ACS grade pentane were obtained from VWR Switzerland.

Table 2.1 – Complete list of target analytes considered in this investigation and their GC×GC-FID and GC×GC- $\mu$ ECD retention times ( $t_r$ ) in the first and the second dimensions.

| Polycyclic aromatic hydrocarbons analyzed by GC×GC-FID |  |                |              |   |
|--|--|----------------|--------------|---|
| Abbreviation   | Compound name  | $t_{r1}$ (min) | $t_{r2}$ (s) | Concentration in certified diesel fuel sample (mg L <sup>-1</sup> ) |
| PAH1   | naphthalene  | 9.60           | 2.32         | 0.25  |
| PAH2   | 1-methylnaphthalene  | 12.80          | 2.26         | 0.60  |
| PAH3   | 2-methylnaphthalene  | 13.20          | 2.36         | 0.43  |
| PAH4   | acenaphthylene   | 16.67          | 2.88         | 0.11  |
| PAH5   | fluorene   | 20.13          | 2.94         | 0.13  |
| PAH6   | phenanthrene   | 24.80          | 3.58         | 0.28  |
| PAH7   | acenaphthene   | 31.33          | 4.00         | 0.05  |
| Chlorinated hydrocarbons analyzed by GC×GC- $\mu$ ECD  |  |                |              |   |
| Abbreviation   | Compound name  | $t_{r1}$ (min) | $t_{r2}$ (s) | Presence in the lake water extract confirmed by GC×GC-ENCI-TOFMS    |
| std1   | 2,4,5,6-tetrachloro- <i>m</i> -xylene                                | 30.80          | 3.22         | nd <sup>a</sup>   |
| std2   | $\alpha$ -hexachlorocyclohexane                                      | 33.18          | 4.14         | detected <sup>b</sup>   |
| std3   | $\beta$ -hexachlorocyclohexane                                       | 34.28          | 5.44         | nd  |
| std4   | $\gamma$ -hexachlorocyclohexane                                      | 35.75          | 4.32         | nd  |
| std5   | $\delta$ -hexachlorocyclohexane                                      | 36.30          | 5.68         | nd  |
| std6   | 2,2',5'-trichlorobiphenyl  | 37.77          | 3.60         | detected  |
| std7   | 2,4,4'-trichlorobiphenyl   | 41.98          | 3.22         | detected  |
| std8   | 1,4,5,6,7,8,8-heptachloro-3a,4,7,7a-tetrahydro-4,7-methano-1H-indene | 43.45          | 2.94         | nd  |
| std9   | 2,2',3,5'-tetrachlorobiphenyl  | 45.28          | 3.04         | detected  |
| std10  | aldrin   | 46.75          | 2.78         | detected  |
| std11  | 2,2',5,5'-tetrachlorobiphenyl  | 46.93          | 3.18         | detected  |
| std12  | heptachloro- <i>exo</i> -epoxide                                     | 50.05          | 2.92         | detected  |
| std13  | $\gamma$ -chlordane  | 52.07          | 2.80         | detected  |
| std14  | 2,2',4,5,5'-pentachlorobiphenyl                                      | 53.53          | 2.62         | detected  |
| std15  | $\beta$ -endosulfan  | 55.73          | 2.78         | detected  |
| std16  | $\alpha$ -chlordane  | 56.28          | 2.54         | nd  |
| std17  | 1-chloro-4-[2,2-dichloro-1-(4-chlorophenyl)ethyl]benzene             | 56.47          | 3.40         | nd  |
| std18  | 1,1-bis-(4-chlorophenyl)-2,2-dichloroethene                          | 57.57          | 3.20         | nd  |
| std19  | endrin ketone  | 59.22          | 2.50         | detected  |
| std20  | 2,3',4,4',5-pentachlorobiphenyl                                      | 59.22          | 3.24         | detected  |
| std21  | endrin aldehyde  | 61.60          | 2.98         | nd  |
| std22  | 2,2',3,3',4,4'-hexachlorobiphenyl                                    | 61.78          | 2.30         | nd  |
| std23  | 2,2',3,5,5',6-hexachlorobiphenyl                                     | 63.98          | 2.40         | detected  |
| std24  | endosulfan sulfate   | 65.08          | 3.40         | nd  |
| std25  | 1,1,1-trichloro-2,2-bis(4-chlorophenyl)ethane                        | 69.12          | 2.48         | detected  |
| std26  | 2,2',3,4,4',5,5'-heptachlorobiphenyl                                 | 70.58          | 2.14         | detected  |
| std27  | 1-chloro-4-[2,2-dichloro-1-(4-chlorophenyl)ethyl]benzene             | 75.53          | 2.12         | nd  |
| std28  | methoxychlor   | 78.83          | 2.22         | detected  |
| std29  | 2,2',3,3',4,4',5,5'-octachlorobiphenyl                               | 84.88          | 2.44         | detected  |

<sup>a</sup> "nd" refers to a chemical that was not detected in the lake water extract using GC×GC-ENCI-TOFMS; <sup>b</sup> "detected" refers to a compound having confirmed presence in the lake water extract with GC×GC-ENCI-TOFMS.

### 2.2.2 Standards preparation for the external standard calibration method (ESM)

The PAH standard mixture was diluted in hexane by a factor of 250, resulting in a  $2 \text{ mg L}^{-1}$  solution in hexane, which was considered the stock solution for the six-level ESM. Dilutions were used to create six concentration levels (0.1, 0.2, 0.5, 1, 1.5 and  $2 \text{ mg L}^{-1}$ ), with three replicates at each concentration level. All concentration levels were prepared in  $200 \mu\text{L}$  of hexane. We generated a chlorinated hydrocarbon standard mixture by performing a hundred-fold dilution of the purchased PCB standards mixture and a ten-fold dilution of organochlorinated pesticide standards mixture in hexane. The resulting stock solution had a concentration of  $0.01 \mu\text{g L}^{-1}$  of each PCB and each organochlorinated pesticide, and this solution was used for the preparation of five concentration levels (0.0005, 0.001, 0.002, 0.005 and  $0.01 \mu\text{g L}^{-1}$ ), with three replicates at each chlorinated hydrocarbon concentration level.

### 2.2.3 Sample preparation for the standard addition method (SAM)

A ten-fold diluted solution of the certified diesel fuel, in hexane, was spiked with the PAH standards mixture to generate five amendment levels of 0, 0.1, 0.2, 0.3, and  $0.4 \text{ mg L}^{-1}$  of each PAH. Three replicates were prepared at each addition level. This enabled us to create a five-level standard addition with three replicates at each PAH concentration level.

A sample of lake water extract, taken to represent the dissolved fraction of hydrophobic organic pollutants in the water column of Lake Geneva, was collected as follows. Sampling was performed by deploying a polydimethylsiloxane (PDMS) passive sampler ( $10 \times 1 \times 0.05 \text{ cm}$ ) in the lake for a period of one month. Extraction was performed by shaking the PDMS strip in  $20 \text{ mL}$  pentane for 8 h, three consecutive times, subsequently combining the resulting  $60 \text{ mL}$  of pentane, and then switching the solvent to hexane. No clean-up step was included in the extraction process. The final volume of environmental extract was reduced to  $3 \text{ mL}$  of hexane using a rotary evaporator (Buchi R210 Switzerland). Fifteen equal aliquots of  $100 \mu\text{L}$  of the lake sample extract were prepared, and three of them were brought to a final volume of  $200 \mu\text{L}$  with hexane. The other twelve aliquots were spiked with different volumes of the  $0.01 \mu\text{g L}^{-1}$  chlorinated hydrocarbon standard mixture and then brought to a final volume of  $200 \mu\text{L}$  with hexane. This procedure enabled us to create a standard addition of the concentration levels 0, 0.0005, 0.001, 0.002 and  $0.005 \mu\text{g L}^{-1}$  for each chlorinated hydrocarbon, with three replicates at each chlorinated hydrocarbon addition level.

### 2.2.4 Sample analysis by GC×GC- $\mu\text{ECD}$ , GC×GC-FID, and GC×GC-ENCI-TOFMS

GC×GC- $\mu\text{ECD}$  and GC×GC-FID measurements were carried out on a Leco Corp instrument equipped with a modified Agilent 7890A GC system having a split/splitless injector, a dual-stage quadruple-jet modulator, and both  $\mu\text{ECD}$  and FID detectors. The separations were carried out on a  $30 \text{ m}$  length,  $0.25 \text{ mm}$  inner diameter (i.d.),  $0.25 \mu\text{m}$  film thickness RTX-1

column (Restek, USA) as the first dimension, and 2 m length, 0.1 mm i.d., 0.1  $\mu\text{m}$  film thickness BPX-50 column as the second dimension (Restek, USA). Helium was the carrier gas used and the instrument was set to produce a constant flow rate of  $1.5 \text{ mL min}^{-1}$ . The first column oven temperature program was:  $45 \text{ }^\circ\text{C}$  initially held for 1 min; then increased to  $160 \text{ }^\circ\text{C}$  at  $2.5 \text{ }^\circ\text{C min}^{-1}$  and then held for another minute; and finally increased to  $300 \text{ }^\circ\text{C}$  at  $1.8 \text{ }^\circ\text{C min}^{-1}$  and held for 10 min. The second column oven was programmed as:  $57 \text{ }^\circ\text{C}$  held for 1 min; then increased to  $172 \text{ }^\circ\text{C}$  at  $3.2 \text{ }^\circ\text{C min}^{-1}$  and held for 1 min; and finally increased to  $312 \text{ }^\circ\text{C}$  at  $2.8 \text{ }^\circ\text{C min}^{-1}$  and kept at that temperature for 33.4 min. These instrument oven programs were used for all samples and all standards mixtures. All injections were carried out in splitless mode. Additionally, after each injection the instrument ovens were baked out at  $300\text{ }^\circ\text{C}$  for 30 min. The injector port liner was replaced at the beginning of each day to avoid carryover from previous injections. For the diesel fuel and for the PAH standards mixtures, we used the FID and we used a modulation period of 8 s. For the lake water extract and chlorinated hydrocarbon standard mixtures we used the  $\mu\text{ECD}$  and we employed a modulation period of 11 s. For both the FID and  $\mu\text{ECD}$  chromatograms, data was collected at a sampling rate of 50 Hz. All chromatograms were acquired using ChromaTOF software (Leco).

The chlorinated hydrocarbon standards and the lake water extract were also analyzed by a GC×GC coupled to an electron capture negative chemical ionization (ENCI)-time of flight-mass spectrometer (TOFMS) (Zoex Corp. USA). The separation was carried out on a 30 m length, 0.25 mm inner diameter (i.d.), 0.25  $\mu\text{m}$  film thickness RXI-1MS column (Restek, USA) as the first dimension, and a 1 m length, 0.1 mm i.d., 0.1  $\mu\text{m}$  film thickness BPX-50 column (Restek, USA) as the second dimension. Helium was the carrier gas, and methane was used as the ionization agent. The first column oven temperature program was:  $32 \text{ }^\circ\text{C}$  initially held for 1 min; then increased to  $300 \text{ }^\circ\text{C}$  at  $4.5 \text{ }^\circ\text{C min}^{-1}$  and then held for another minute. The second column oven was programmed as:  $67 \text{ }^\circ\text{C}$  held for 1 min; then increased to  $300 \text{ }^\circ\text{C}$  at  $4.2 \text{ }^\circ\text{C min}^{-1}$  and held for 1 min. The temperature of the transfer line and the ionization chamber were  $250 \text{ }^\circ\text{C}$  and  $220 \text{ }^\circ\text{C}$ , respectively. An 8 s modulation period was used during the analysis. The TOFMS acquired 50 spectra per seconds with a mass range of 50 to 600  $m/z$  via GCsquare (Zoex) with a mass resolution of 4000 (full width at half maximum) and a mass precision of  $\pm 2$  milli-mass-units (mmu) over the calibrated mass range 50 to 600  $m/z$ , where the mass precision was defined as the difference between the measured mass for the standard and the suspect peak in the environmental sample. The detector was operated at 2234 V. The ionization source emission current for our analysis was 0.1 mA.

### **Protocol for positive confirmation of chlorinated hydrocarbon target analytes with GC×GC-ENCI-TOFMS**

The presence of chlorinated hydrocarbon target analytes was confirmed in the lake water extract using GC×GC-ENCI-TOFMS. The confirmation procedure was carried out by comparing the external standards chromatogram to the sample chromatogram analyzed under

the same chromatographic conditions. The lake water extract and the chlorinated hydrocarbon standards mixture ( $0.01 \mu\text{g L}^{-1}$ ) were both analyzed with GC $\times$ GC-ENCI-TOFMS. The resulting chromatograms were baseline corrected over each recorded  $m/z$  value using the deadband baseline correction method [69]. Chromatograms were then processed with GC Image software, which produces a unique mass spectrum for each detected chromatographic peak by averaging the mass spectra of all the pixels within the delineated boundaries of the two-dimensional peak. The laboratory quality assurance protocol developed by the European Union requires the monitoring of a minimum of two  $m/z$  values for each compound in order to meet the conformity criteria for structure identification [87]. Previous investigation of inter-laboratory variations in the fragmentation pattern and ion intensity ratios of ENCI indicated that ion intensity ratios are unreliable parameters for analyte identification, particularly in the case of TOFMS [88]. Therefore, we focused on the  $m/z$  values rather than the ion intensity ratios. We extracted three  $m/z$  values from the averaged spectrum of each standard peak of the external standard chromatogram. These three  $m/z$  values included the molecular ion, if available, and the two (or three) expected fragments for each standard [88, 89]. We compared the selected  $m/z$  values of the external standard peak to the mass spectrum of the same chromatographic peak in the lake water extract chromatogram. We considered a target analyte to have confirmed presence in the lake water extract when the chromatographic peak of the target analyte occurred inside of the expected GC $\times$ GC retention time window ( $\pm 12.1$  s in the first dimension and  $\pm 0.1$  s in the second dimension) and all the three expected  $m/z$  values were present in the suspected peak of the sample chromatogram. When assigning a match of  $m/z$  values, we allowed a tolerance of  $\pm 2$  mmu between the  $m/z$  value of the external standard and  $m/z$  value of the sample peak. A similar structure identification procedure has been used previously for the detection of trace level halogenated compounds in environmental samples using GC-ENCI-quadrupole mass spectrometry [90, 91, 92].

### **2.2.5 Analyte peak integration methods**

The algorithms that we chose to evaluate were selected based on their availability and technical compatibility. We used ChromaTOF (Leco Corporation) implementations of the local linear baseline algorithm and two-step peak delineation algorithm [66, 85]. We used the GC Image (GC Image, LLC [81]) implementations of the deadband baseline algorithm and inverted watershed peak delineation algorithm [69, 81]. We also applied the Eilers baseline estimation algorithm [82], implemented in Matlab (R2010.10.b, Mathworks, Inc., Natick, MA) [93]. Based on the inter-compatibility of data formats accepted by the different software packages, we tried several different combinations of baseline algorithms and peak delineation algorithms, and this is summarized in Table 2.3. However some data format incompatibilities precluded some combinations, as explained in section 2.2.5 below. We also applied an in-house algorithm for peak integration described in a previous publication [79].

This quantification assessment was performed using both univariate FID and  $\mu\text{ECD}$  data. We

did not consider the integration of multivariate (i.e., mass spectral) detector data, which is discussed elsewhere [65, 94].

### Baseline estimation algorithms

Several baseline estimation algorithms were compared. For the local linear, deadband, and Eilers baseline algorithms, the baseline correction step was conducted before the peak delineation step. Thus the baseline estimation step was operationally independent of the peak delineation step. However the peak delineation results are dependent on the baseline estimation method used.

Baseline correction method parameters were set as follows. For the local linear baseline correction (ChromaTOF), we applied the default, recommended settings, as follows. The baseline offset was set in the middle of the noise (0.5). The minimum signal-to-noise ratios for the base peak and the sub-peaks were set at 10 and 3, respectively. For the deadband baseline correction (GC Image), we applied the default baseline correction parameters, listed in Table 2.2. The Eilers baseline correction was carried out using Matlab code developed by Eilers [82]. The three baseline parameters are  $\lambda$ ,  $p$  and  $d$ . We chose the recommended values of 0.02 and 2 for  $p$  and  $d$ , respectively [82]. For the major parameter  $\lambda$ , which defines the aggressiveness of the algorithm, a recommended value is not given, and we tried three different values:  $10^{6.5}$ ,  $10^5$  and  $10^4$ . Low  $\lambda$  values ( $10^4$ ) lead to an aggressive baseline estimation, whereas high  $\lambda$  values ( $10^{6.5}$ ) lead to a more conservative baseline.

### Peak detection and peak matching

We employed the automated peak detection and peak matching algorithms implemented in the GC Image [95] and ChromaTOF software packages, and these were used to assign peaks for the inverted watershed and two-step peak delineation algorithms, respectively. The matching algorithms in both packages use a retention window parameter as a criterion for proposing a match, or assignment of a peak considered chemically equivalent in two GC×GC chromatograms. The retention window defines the acceptable shifts in the first and second dimensions between two matched peaks. For both algorithms, we defined the maximum shift in the first dimension as the length of the modulation period plus a tolerance level of 10% of the modulation period. For the second dimension we used a window of 0.1 s as the maximum acceptable shift. This led to a retention window of 8.8 s × 0.1 s for GC×GC-FID chromatograms of PAH standards and the certified diesel fuel, and a retention window of 12.1 s × 0.1 s for GC×GC- $\mu$ ECD chromatograms of chlorinated hydrocarbon standards and the lake water extract. All automated peak matches were additionally confirmed by visual inspection. We accepted all proposed peak matches, with the exception of std23 at the lowest concentration level in the external standard chromatogram. This mis-assignment was due to

Table 2.2 – The parameter settings for the deadband baseline correction and inverted watershed delineation algorithms implemented in the GC Image software. Each parameter in the table is explained in the user manual of GC Image software.

| Deadband baseline correction   |       |                    |  |
|--|-------|--------------------|--|
| parameter  | value | unit               |  |
| Stride   | 1     | modulation         |  |
| Distribution   | 7     | unitless           |  |
| Filter window size   | 7     | pixel              |  |
| Number of dead band pixels   | 5     | pixel              |  |
| Gradient filter window size  | 7     | pixel              |  |
| Blob detection and peak delineation<br>with inverted watershed algorithm |       |                    |  |
| Signal smoothing<br>before peak delineation                              |       |                    |  |
| First column   | 0.1   | pixel              |  |
| Second column  | 1     | pixel              |  |
| Blob filter  |       |                    |  |
| Minimum area   | 15    | pixel              |  |
| Minimum volume   | 0.0   | detector intensity |  |
| Minimum peak   | 10    | unitless           |  |

the presence of another nearby peak present in the solvent that had a retention time similar to std23. We corrected this match manually. Finally, the Gaussian-peak fit method does not include an automated peak detection algorithm; for this method we assigned peaks manually.

### Peak delineation and peak integration

Baseline-corrected chromatograms were analyzed using both the two-step (ChromaTOF) and inverted watershed (GC Image) peak delineation algorithms. Each peak integration method was defined as a single combination of a baseline estimation algorithm and a peak delineation algorithm. We denote peak integration methods with a shorthand abbreviation of two capital letters, where the first letter represents the baseline estimation method and the second letter represents the peak delineation algorithm (Table 2.3). Technical compatibilities allowed the following combinations: the local linear baseline algorithm was applied together with the two-step and inverted watershed peak delineation algorithms, leading to the LT and LI peak integration methods. The deadband baseline algorithm and Eilers baseline algorithm were each applied together with the inverted watershed algorithm, leading to the DI and EI peak integration methods. Data importation limitations of the ChromaTOF package precluded us from accessing its two-step peak delineation algorithm with chromatograms that had been baseline corrected with the deadband algorithm or Eilers algorithm. For the assignment of analyte peaks in GC×GC chromatograms, we employed the automated peak matching algorithm implemented in GC Image [95], as explained in detail in the previous section (Peak

detection and peak matching).

We also applied an algorithm developed in our group that optimizes a local linear baseline fitted simultaneously with the optimization of a gaussian function to describe the analyte signal [79]. We called the algorithm "Gaussian-peak fit", denoted LG. It should be noted that the implementation of the local linear baseline in the LG algorithm is not equivalent to the local linear baseline algorithm in ChromaTOF. However for ease of presentation we have grouped both these algorithms together under the notation "L". Since the Gaussian-peak fit baseline and peak delineation are optimized simultaneously, their present implementations are not easily interchanged with baseline and peak delineation algorithms in the other software programs. The LG algorithm can be applied to well-resolved peaks but may give poor results or convergence failure for co-eluting peaks. The LG algorithm has been applied previously to the integration of resolved hopane peaks in GC×GC chromatograms of petroleum mixtures [79, 80]. The LG algorithm parameters were set as follows: The "max shift" parameter, which represents the maximum extent of shift that is allowable between the local apices of adjacent second-dimension signal slices that are considered as part of one analyte peak, was set to 5 pixels. The "peak cutoff" parameter, which is the minimum value of the integrated area of a second-dimension signal slice that can be considered as resolved analyte, was set to 5000 FID units. The "peak width cutoff" parameter, which is the maximum width of a second-dimension signal slice that can be considered as part of a single analyte, was set to 20 pixels. Finally, the "peak search cutoff" parameter describes the maximum distance from the apex of a second-dimension slice that the algorithm may search (in the second dimension) for information that is used to delineate the boundary and baseline of the peak. This value was set to 20 pixels. In this study, we applied the LG algorithm to peak integration of PAHs in the certified diesel fuel. However, for many of the chlorinated hydrocarbons in the lake water extract, the LG algorithm suffered convergence problems and hence these results are not reported.

Table 2.3 – Peak integration methods used for GC×GC chromatogram analysis. Each peak integration method is composed of a combination of a baseline estimation algorithm (columns) and a peak delineation algorithm (rows).

|                                  |                 | Baseline correction algorithm |          |                              |
|----------------------------------|-----------------|-------------------------------|----------|------------------------------|
|                                  |                 | ChromaTOF                     | GC Image | Matlab                       |
| Peak<br>delineation<br>algorithm | Software        |                               |          |                              |
|                                  | Method type     | Local linear                  | Deadband | Eilers                       |
|                                  | ChromaTOF       | LT                            | -        | -                            |
|                                  | GC Image        | LI                            | DI       | El <sub>λ</sub> <sup>1</sup> |
| Matlab                           | LG <sup>a</sup> |                               |          |                              |

<sup>a</sup> The linear local baseline correction method implemented in this method is not equivalent to the linear local baseline algorithm in ChromaTOF.



### 2.2.6 Analyte quantification methods

After we applied the peak integration methods to the GC×GC-FID and GC×GC- $\mu$ ECD chromatograms, we quantified target analytes using the external standard calibration method (ESM) and also the standard addition calibration method (SAM). These calculations and related data analysis were carried out using Matlab [93]. We preferred the use of SAM instead of internal standard (IS) normalization. The IS method assumes that the matrix effect is similar for both the IS and the target analyte [96]. However the SAM re-normalizes the chromatogram for each target analyte using the analyte itself [76, 77].

#### Analyte quantification using the external standard calibration method

The ESM is performed by recording the analyte signal at several different levels of injected standard concentration, in the absence of the sample matrix. We assumed a linear model [77, 78]:

$$y = b_{ESM}x + e_{ESM} \quad (2.2)$$

where  $y$  is the peak volume of the analyte,  $x$  is the concentration of the injected standard,  $b_{ESM}$  is the slope (instrument sensitivity) and  $e_{ESM}$  is the offset, which may be interpreted as the error associated with quantification of the analyte in the absence of sample matrix [97]. The offset can be considered negligible if zero lies within the confidence interval of the offset [76]. This corresponds to the assumption that the analytical signal is zero when the analyte's concentration is zero [78]. In the present study we included the offset in the quantification even if the offset was statistically equivalent to zero [98]. In order to estimate the concentration of a chemical in the sample, the analytical signal of the sample should be interpolated using:

$$x_0 = \frac{y_0 - e_{ESM}}{b_{ESM}} \quad (2.3)$$

where  $y_0$  is the integrated analyte signal in the sample, and  $x_0$  is the estimated concentration of the analyte in the sample using the ESM. The ESM model is shown schematically in Figure 2.2. The ESM does not account for matrix effects, by design [77, 97, 99]. However, in a complex sample, matrix effect is one of the most common problems [72, 100].

PAH analytes in the certified diesel fuel were quantified using a six-level ESM with three replicates at each concentration level. Chlorinated hydrocarbons in the lake water extract were quantified using a five-level ESM with three replicates at each concentration level.

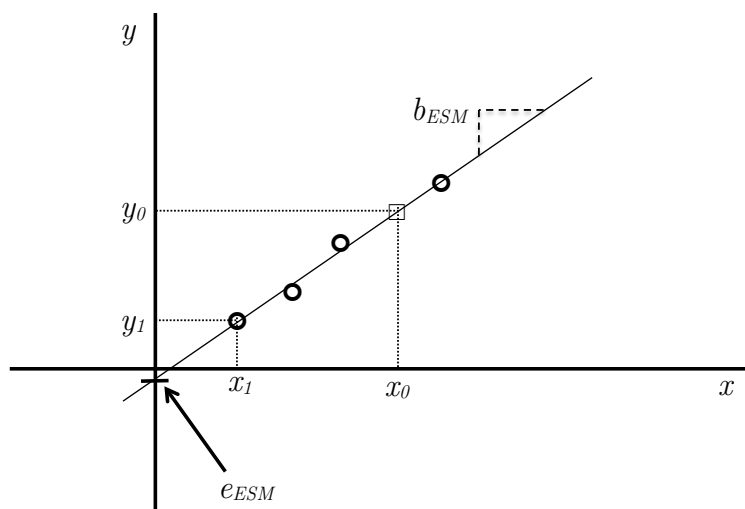


Figure 2.2 – Example schematic of the external standard calibration method based on Eq. 2.2. Fictitious data are presented for illustrative purposes. Labeled:  $b_{ESM}$  is the slope,  $e_{ESM}$  is the offset,  $y_0$  is the integrated analyte signal in the sample,  $x_0$  is the ESM estimate of the analyte concentration in the sample,  $x_1$  is the lowest concentration level of the ESM, and  $y_1$  is the integrated signal at the  $x_1$  concentration level.

### Analyte quantification with the standard addition calibration method and diagnosis of matrix effects

The matrix effect is defined as a change in apparent instrument sensitivity ( $b$ ) that arises when the analyte is measured in a complex sample compared to when it is measured as a pure standard [78, 97, 101]. In the context of analyte quantification with GC×GC, the matrix effect arises from failure of the peak integration method to correctly distinguish the intended analyte signal from the unresolved signal of the sample (Figure 2.1). The matrix effect assumes that the apparent instrument sensitivity is not dependent on changes in analyte concentration. This requirement is consistent with the assumed additivity of the signal components defined in Eq. 2.1. Matrix effects confound quantification by the ESM. However matrix effects can be corrected using the standard addition method (SAM) [76, 78], which is an in-situ re-normalization of the apparent analyte signal [75, 101].

The model for the standard addition method is:

$$y = b_{SAM}x + f \quad (2.4)$$

where  $b_{SAM}$  is the slope of the SAM,  $x$  is the added concentration of an analyte to the sample, and  $f$  is the offset of the SAM. The SAM offset,  $f$ , represents the integrated analyte signal in

the sample,  $y_0$ , plus the uncertainty of the SAM model,  $e_{SAM}$ :

$$f = y_0 + e_{SAM} \quad (2.5)$$

In Eq. 2.5,  $e_{SAM}$  is attributed to the sum of the uncertainty of  $f$  ( $e_f$ ) and the uncertainty of  $y_0$  ( $e_{y0}$ ). In general, however, it is not possible to distinguish  $e_f$  from  $e_{y0}$ , and it is also not possible to diagnose the presence of incorrigible errors in  $e_{SAM}$  [73, 74, 102]. Therefore the magnitude of  $e_{SAM}$  is taken as a measure of overall uncertainty of the integrated analyte signal of the original sample.

In order to quantify the chemical of interest in the sample, the standard addition model is used via:

$$x_0 = \frac{f}{b_{SAM}} \quad (2.6)$$

where  $x_0$  is the SAM estimate of the analyte concentration in the sample. The SAM model is shown schematically in Figure 2.3.

For PAH analytes in the certified diesel fuel and for chlorinated hydrocarbon analytes in the lake water extract, we performed a SAM that included four spike levels plus the unspiked sample, with three replicates at each level. Eq. 2.4 was fitted to the SAM data for each analyte, and Eq. 2.6 was used for the quantification. The native analyte concentration and the integrated analyte signal of the unspiked sample are denoted  $x_0$  and  $y_0$ , respectively.

Finally, non-additive interactions between the different signal components can also affect the analyte quantification. The term *matrix interference* is used to describe a change in apparent instrument sensitivity that is dependent on both the analyte concentration and the presence of sample matrix [74, 78, 103]. This represents a non-additive interaction between the sample matrix and the analyte, which contradicts the additivity of signal components assumed by Eq. 2.1 [72, 74, 103]. In the present study we did not correct for the presence of matrix interferences. However, we did diagnose for matrix interferences, which is discussed further in section 2.2.7.

### 2.2.7 Chemometric tests used to assess the peak integration methods

Several chemometric tests were applied in order to compare the performance of the different peak integration methods described in section 2.2.5. The results of these tests were used to make inferences about sources of uncertainty in the analyte quantification. This allowed us to compare and assess different combinations of baseline estimation algorithms and peak delineation algorithms as applied to analyte quantification in real, complex samples.

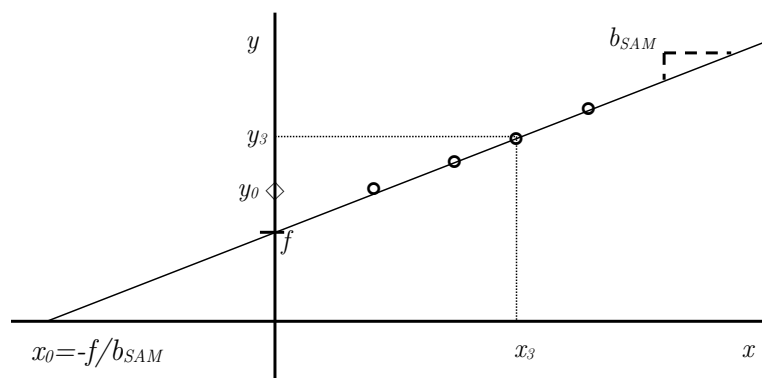


Figure 2.3 – Example schematic of the standard addition calibration method based on Eqs. 2.4 and 2.5. Fictitious data are presented for illustrative purposes. The  $x$  axis represents the target analyte concentration that is added to the unspiked sample, and the  $y$  axis represents the corresponding integrated analyte signal. Labeled:  $b_{SAM}$  is the slope,  $f$  is the offset,  $x_0$  is the SAM estimate of the concentration of the analyte in the unspiked sample, and  $y_0$  is the integrated analyte signal in the unspiked sample.

### Test of reproducibility of integrated analyte signal

To evaluate the uncertainty in measured analyte concentration associated with the sample dilution operation and run-to-run instrument variability, we defined the relative standard error statistic as [86]:

$$RSE(\%) = 100 \cdot \frac{\sqrt{\frac{\sum_{i=1}^n (y_i - \bar{y})^2}{n-1}}}{\bar{y}} \quad (2.7)$$

where  $RSE$  is the relative error of the signal from the injected replicates,  $y_i$  is the integrated analyte signal (peak volume) of each replicate  $i$  at a given external standard concentration level or standard addition concentration level,  $\bar{y} = \sum_{i=1}^n y_i / n$  is the average peak volume of the three replicates at each concentration level, and  $n$  is the number of replicates at the external standard or standard addition concentration level [98].

### Test of proportionality of the integrated signal response

The analyte quantification methods employed here, ESM and SAM, both rely on linear instrument response to changes in analyte concentration [71, 77, 78]. The two detectors utilized in this study were FID and  $\mu$ ECD, which produce a linear and additive signal from zero until the saturation point [104, 105, 106]. We confirmed that we remained in the linear range of raw detector output. However, the integrated signal assigned to an analyte may exhibit non-

linear response due to shortcomings in the applied baseline correction and peak delineation algorithms. Thus, when signal non-proportionality was observed for injected standards, we interpret this as biased calibration [103] arising from poor handling of baseline and peak delineation [65, 85, 86]. When we observed non-proportionality in real samples, we interpret this as apparent matrix interference arising from errors in baseline correction and peak delineation. Matrix interferences and biased calibration are not easy to detect and are considered as incorrigible error [102, 103].

We used the following definition of an average response factor (*ARF*) to evaluate proportional response of injected standards:

$$ARF = \frac{\sum_{l=1}^{n-1} \sum_{m>l}^n \left( \frac{y_m - e_{ESM}}{x_m} \right) \frac{x_l}{x_l}}{\sum_{i=1}^{n-1} (i)}. \quad (2.8)$$

where  $y_m$  and  $y_l$  are the integrated analyte signals at  $x_m$  and  $x_l$  levels of concentration, respectively;  $n$  is number of the levels of concentration;  $m$  and  $l$  are the indices for different levels of concentration, where  $m > l$ ; and  $e_{ESM}$  is the offset of the external standard method (Figures 2.4 and 2.5). Eq. 2.8 is defined such that  $x_m$  is larger than  $x_l$  for each combination of  $l$  and  $m$  that is considered in the summation. *ARF* represents an average of the response factor over all combinations of concentration levels used in the ESM. A good peak integration algorithm should result in an average response factor close to one. A value of  $ARF < 1$  indicates an insufficient integrated signal response (under-response) with increasing injected analyte mass, whereas  $ARF > 1$  indicates exaggerated signal response (over-response) with increasing injected analyte mass. Eq. 2.8 was considered as a diagnostic for biased calibration that arises from errors in baseline correction or peak delineation.

For standard addition data, we used the following modification to Eq. 2.8 to assess the proportionality of signal response:

$$ARF = \frac{\sum_{l=1}^{n-1} \sum_{m>l}^n \left( \frac{y_m - f}{x_m} \right) \frac{x_l}{x_l}}{\sum_{i=1}^{n-2} (i)}. \quad (2.9)$$

where  $f$  is the offset of the SAM (Eq. 2.4). In both Eqs. 2.8 and 2.9, the *ARF* is a unitless value representing the extent of agreement with perfect proportionality, which is given by a *ARF* value equal to one. Eq. 2.9 was viewed as a diagnostic for matrix interference arising from problems with baseline correction or peak delineation.

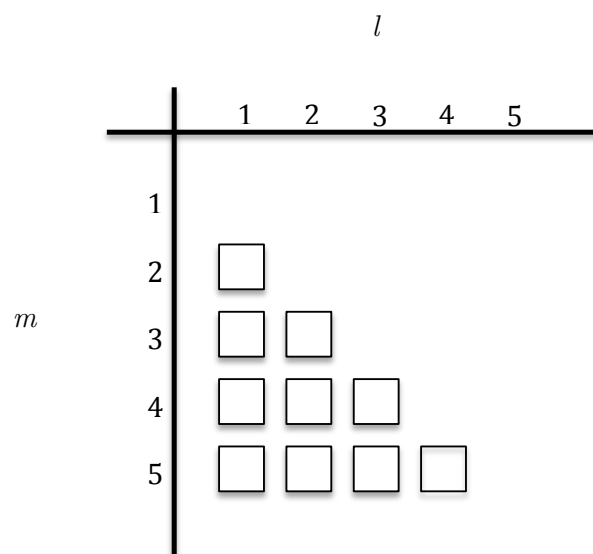


Figure 2.4 – The combination matrix for Eq. 2.8, where the  $m$  and  $l$  are indices of different concentration levels of ESM, and where  $m > l$ . Each square represents a term that contributes to the summation in Eq. 2.8. The reported  $ARF$  value for each peak integration method is an average of all computed response factor values for that method.

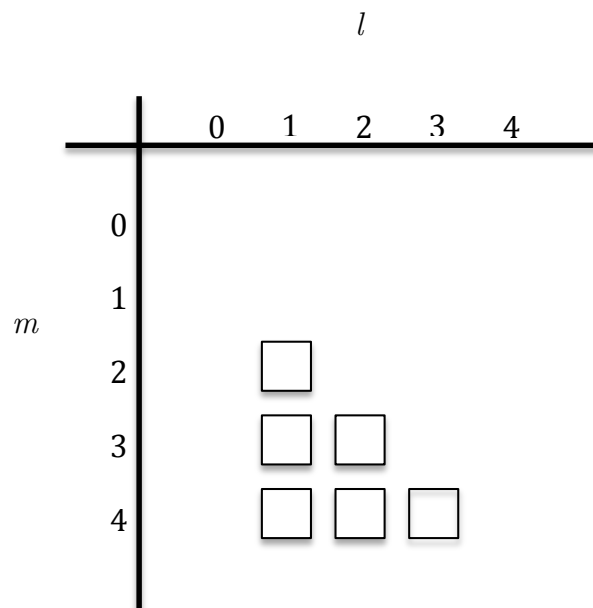


Figure 2.5 – The combination matrix for Eq. 2.9, where the  $m$  and  $l$  are indices of different concentration levels of SAM, and where  $m > l$ . Each square represents a term that contributes to the summation in Eq. 2.9. The reported  $ARF$  value for each peak integration method is an average of all computed response factor values for that method. Index 0 represents the unamended sample, and index 1 represents the lowest amendment level.

### Tests of relative error for the ESM offset and the SAM offset

The magnitude of the ESM offset is interpreted to reflect the uncertainty introduced by the calibration method into the quantification [77, 78, 102]. A non-zero offset can result from a poor baseline correction or peak delineation, particularly in the case of complex samples [98, 107]. In order to produce an offset equal to zero, an integration algorithm should accurately isolate the resolved analyte signal from the chromatogram non-analyte signal. Thus we evaluated the relative offset error, defined as:

$$e_{rel,ESM}(\%) = 100 \cdot \frac{e_{ESM}}{y_0} \quad (2.10)$$

where  $e_{rel,ESM}$  is the offset error in %,  $y_0$  is the integrated analyte signal in the sample, and  $e_{ESM}$  is the offset of the ESM. The  $e_{rel,ESM}$  statistic provides an estimate of the relative uncertainty of the analyte concentration as determined by the ESM, assuming no matrix effect. A value of  $e_{rel,ESM} > 50\%$  was operationally defined as an indication that the external standard peak volumes were inadequate for the quantification.

The SAM offset,  $f$ , is an estimate of the integrated analyte signal in the sample,  $y_0$ , plus the uncertainty of the standard addition model,  $e_{SAM}$  (Eq. 2.5). The discrepancy between the observed analyte signal for the unspiked sample ( $y_0$ ) and the SAM offset ( $f$ ) represents a measure of the uncertainty ( $e_{SAM}$ ) introduced into the quantification by the standard addition model (Eq. 2.11) [78, 97]. We defined the SAM relative offset error as the ratio of the offset error divided by  $y_0$ :

$$e_{rel,SAM}(\%) = 100 \cdot \left( \frac{f - y_0}{y_0} \right) = 100 \cdot \left( \frac{e_{SAM}}{y_0} \right) \quad (2.11)$$

where  $f$  has been determined using only the spiked samples and  $y_0$  is the integrated instrument signal for the unspiked sample in the SAM. Ideally, the offset,  $f$ , should equal the integrated instrument signal,  $y_0$ . Thus an accurate peak integration method should give a  $e_{rel,SAM}$  value close to zero. We used the  $e_{rel,SAM}$  as a diagnostic for the adequacy of the SAM for the quantification of the target analytes. If  $e_{rel,SAM} > 50\%$  for a given target analyte, we considered that the SAM was inadequate for the quantification of that target analyte.

### Assessment of the change in apparent instrument sensitivity induced by the matrix

Matrix effects change the apparent instrument sensitivity for an analyte, where the sensitivity is defined as the slope of the line describing the increase in analyte signal with increasing analyte concentration [74, 77, 78, 97, 108]. For a given analyte, the slope of the ESM indicates instrument sensitivity in the absence of matrix, whereas the slope of the SAM indicates instrument sensitivity in the presence of matrix [76]. Cardone et al defined the *proportional*

*error factor* as a way to diagnose and compensate for matrix effects [75]:

$$P = \frac{b_{SAM}}{b_{ESM}} \quad (2.12)$$

The value of  $P$  represents the change in apparent instrument sensitivity caused by the matrix effect [77]. Thus a peak integration method that avoids the introduction of matrix effects will produce a  $P$  factor close to 1. The significance of  $P \neq 1$  can be established by evaluating the  $P$  confidence interval [76]. Cardone et al suggested a practical way to perform the so-called *P correction*, in which the analyte is quantified by correcting the ESM results for matrix effects [74]:

$$x_0 = \frac{y_0 - e_{ESM}}{P \times b_{ESM}} = \frac{y_0 - e_{ESM}}{b_{SAM}} \quad (2.13)$$

### 2.3 Results and discussion

We conducted a comparative assessment of peak integration methods using a suite of target analytes evaluated in two different types of complex environmental samples with two different types of instrument detectors. These were: (1) 7 PAHs that had been added to a certified diesel fuel and analyzed using GC×GC-FID (Figures 2.6 and 2.8); and (2) 29 chlorinated hydrocarbons, including both PCBs and chlorinated pesticides, that were analyzed in a water column extract from Lake Geneva using GC×GC- $\mu$ ECD (Table 2.1, and Figures 2.7 and 2.8). These analytes were quantified using both the external standard method and the standard addition method. Additionally, both the chlorinated hydrocarbon standards and the lake water extract were further analyzed by GC×GC-ENCI-TOFMS (Figure 2.9). This latter analysis enabled a qualitative confirmation of the presence of chlorinated hydrocarbon target analytes in the lake water extract.

Several chemometric tests (sections 2.2.6 and 2.2.7) were applied to the analyte peak volume data obtained from both GC×GC-FID and GC×GC- $\mu$ ECD measurements. For each test, we report either mean results or else the frequency with which the test result falls within an acceptable interval. The maximum or minimum values of each chemometric test were also viewed as representing the "worst case" performance for the considered samples. Finally, we conducted Kruskal-Wallis one-way analysis of variance ([109]) on the results of each test. The Kruskal-Wallis method produces a non-parametric statistic that indicates whether the median test results can be considered as meaningfully different among the different peak integration methods, expressed as a  $p$  value or significance level. A finding of  $p < 0.05$  indicates that at least two of the peak integration methods give significantly different test results. For each chemometric test, we computed the Kruskal-Wallis statistic of the test residuals after subtracting the mean test value of all peak integration methods for each analyte.



### 2.3.1 Successful detection and integration of target analytes, and resulting signal-to-noise ratios

All of the peak integration methods successfully integrated the analyte signal of the 7 PAH standards and the 29 chlorinated hydrocarbon standards for all concentration levels of external standard chromatograms. Additionally, all of the integration methods detected and integrated the 7 PAH analytes having confirmed presence in the certified diesel fuel analyzed by GC×GC-FID. However, not all 29 chlorinated hydrocarbon target analytes were detected in the GC×GC- $\mu$ ECD chromatograms of the lake water extract (Table 2.4).

Unsuccessful integrations of analytes in GC×GC- $\mu$ ECD chromatograms of the lake water sample were diagnosed as: failure to detect the analyte peak; delineation of an incoherent peak; or convergence failure of the algorithm. These problems were attributed to the presence of unresolved signal overlapping with the analyte signal. For example, octachlorobiphenyl (std29), which had retention times of 84.88 min in the first dimension and 2.44 s in the second dimension, fell in a region of significantly elevated signal that often appears in  $\mu$ ECD chromatograms of PDMS extract. None of the peak integration methods were able to integrate this peak. These peak volume omissions affected 13 chlorinated hydrocarbon analytes for the LI, LI, DI, and EI<sub>λ</sub> peak integration methods, leaving us with 16 analytes that were successfully detected and integrated in all lake water extract chromatograms using these methods. However if we detected an analyte in all concentration levels of the standard addition except the unspiked sample, we still included that analyte for subsequent data analysis. The LG method exhibited failure to converge for most (18 out of 29) of the chlorinated hydrocarbon analytes in the lake water extract. This mostly occurs due to overlapping peaks, which the algorithm is not designed to handle.

The lake water extract and the chlorinated hydrocarbon standards also were analyzed by GC×GC-ENCI-TOFMS. The highly sensitive soft chemical ionization enabled us to detect the molecular ion and/or fragment ions of trace level chlorinated hydrocarbon target analytes in the lake water extract [88, 89, 110, 111]. To our knowledge, the present work is the first to publish the use of GC×GC coupled to TOFMS with negative chemical ionization. GC×GC-ENCI-TOFMS analysis enabled us to confirm the presence of 17 out of 29 target analytes in the lake water extract. Our inability to confirm the presence of the remaining 12 target analytes in the lake water extract was attributed either to the absence of these analytes in the lake water extract or to the detection limits of GC×GC-ENCI-TOFMS, which has lower sensitivity than GC×GC- $\mu$ ECD. For all 17 detected chlorinated hydrocarbons, we observed agreement to within  $\pm 2$  mmu for at least three m/z values when comparing the external standard spectrum with the sample spectrum of the same analyte peak (see section 2.2.4).

Several target analytes that had been confirmed in the lake water extract (via GC×GC-ENCI-

TOFMS) were also successfully detected and integrated in GC×GC- $\mu$ ECD chromatograms. The inverted watershed algorithm (LI, DI,  $EI_\lambda$ ) resulted in the highest number of GC×GC- $\mu$ ECD integrated peaks that were also confirmed by GC×GC-ENCI-TOFMS, depending on the baseline correction algorithm used (Table 2.4). For example, the DI method detected and successfully integrated 24 of the 29 target analytes. Of these 24 analytes, 15 were separately confirmed by GC×GC-ENCI-TOFMS, and the remaining 9 were not found by GC×GC-ENCI-TOFMS. This also means that the DI algorithm failed to find 2 of the 17 analytes that had been confirmed by GC×GC-ENCI-TOFMS. The LT and LG peak integration methods produced lower numbers of successfully detected and integrated chlorinated hydrocarbon target analytes that had confirmed presence in the lake water sample.

In subsequent chemometric tests (section 2.3.2), we considered only the chlorinated hydrocarbon analytes that had confirmed presence and that were successfully integrated in GC×GC- $\mu$ ECD chromatograms using the LT, LI, DI, and  $EI_\lambda$  peak integration methods. We evaluated all five peak integration methods for 7 PAHs in the GC×GC-FID chromatograms of the certified diesel fuel, and we evaluated four of the algorithms (LT, LI, DI,  $EI_\lambda$ ) for the 11 confirmed chlorinated hydrocarbon analytes that were successfully integrated in GC×GC- $\mu$ ECD chromatograms of the lake water extract. We neglected consideration of the LG method applied to the chlorinated hydrocarbon analytes, due to the low success rate of this method with the lake water extract matrix.

For the thus selected 18 successfully integrated target analytes (7 PAHs and 11 confirmed chlorinated hydrocarbons), we computed signal-to-noise ratios of analyte peaks for the sample chromatograms and also for chromatograms of the lowest concentration level of the external standard. A signal-to-noise ratio (S/N) >10 guarantees that the integrated analyte signal is larger than the Limit of Quantification (LOQ) [76]. The S/N was computed with GC Image, using the ratio of the absolute signal value, measured at the apex of the peak, to the white noise level as measured by the deadband baseline. We found values of S/N >100 for the lowest concentration level of all 7 PAH standards ( $0.1 \text{ mg L}^{-1}$ ) and all 11 chlorinated hydrocarbon standards ( $0.0005 \text{ } \mu\text{g L}^{-1}$ ). Additionally, we found S/N > 100 for these same 7 PAHs in the diesel fuel and 11 chlorinated hydrocarbon peaks in the lake water extract. Thus the integrated signal was larger than the LOQ for all target analytes that were considered in subsequent chemometric assessments (section 2.3.2).

Table 2.4 – The number of peaks successfully detected and integrated by different peak integration algorithms, when applied to environmental samples. The integration method acronyms are explained in Table 2.3.

|   | Known polycyclic aromatic hydrocarbons<br>in the certified diesel fuel |    |                   |                 |                 |    |    |
|---|--|----|-------------------|-----------------|-----------------|----|----|
|   | Peak integration method  |    |                   |                 |                 |    |    |
| Instrument method   | LT   | LI | EI <sub>6.5</sub> | EI <sub>5</sub> | EI <sub>4</sub> | DI | LG |
| Integrated peaks<br>from<br>GC×GC-FID<br>(7 target analytes)  | 7  | 7  | 7                 | 7               | 7               | 7  | 7  |
|   | Target chlorinated hydrocarbons<br>in the lake water extract           |    |                   |                 |                 |    |    |
|   | Peak integration method  |    |                   |                 |                 |    |    |
| Instrument method   | LT   | LI | EI <sub>6.5</sub> | EI <sub>5</sub> | EI <sub>4</sub> | DI | LG |
| Integrated peaks<br>from<br>GC×GC- $\mu$ ECD<br>(29 target analytes)                                  | 18   | 19 | 24                | 25              | 25              | 24 | 11 |
| Integrated peaks<br>from<br>GC×GC- $\mu$ ECD<br>and confirmed by<br>GC×GC-ENCI-TOFMS<br>(17 analytes) | 9  | 12 | 15                | 17              | 17              | 15 | 5  |
| Integrated peaks<br>from<br>GC×GC- $\mu$ ECD<br>but not found by<br>GC×GC-ENCI-TOFMS<br>(12 analytes) | 9  | 7  | 9                 | 8               | 8               | 9  | 6  |

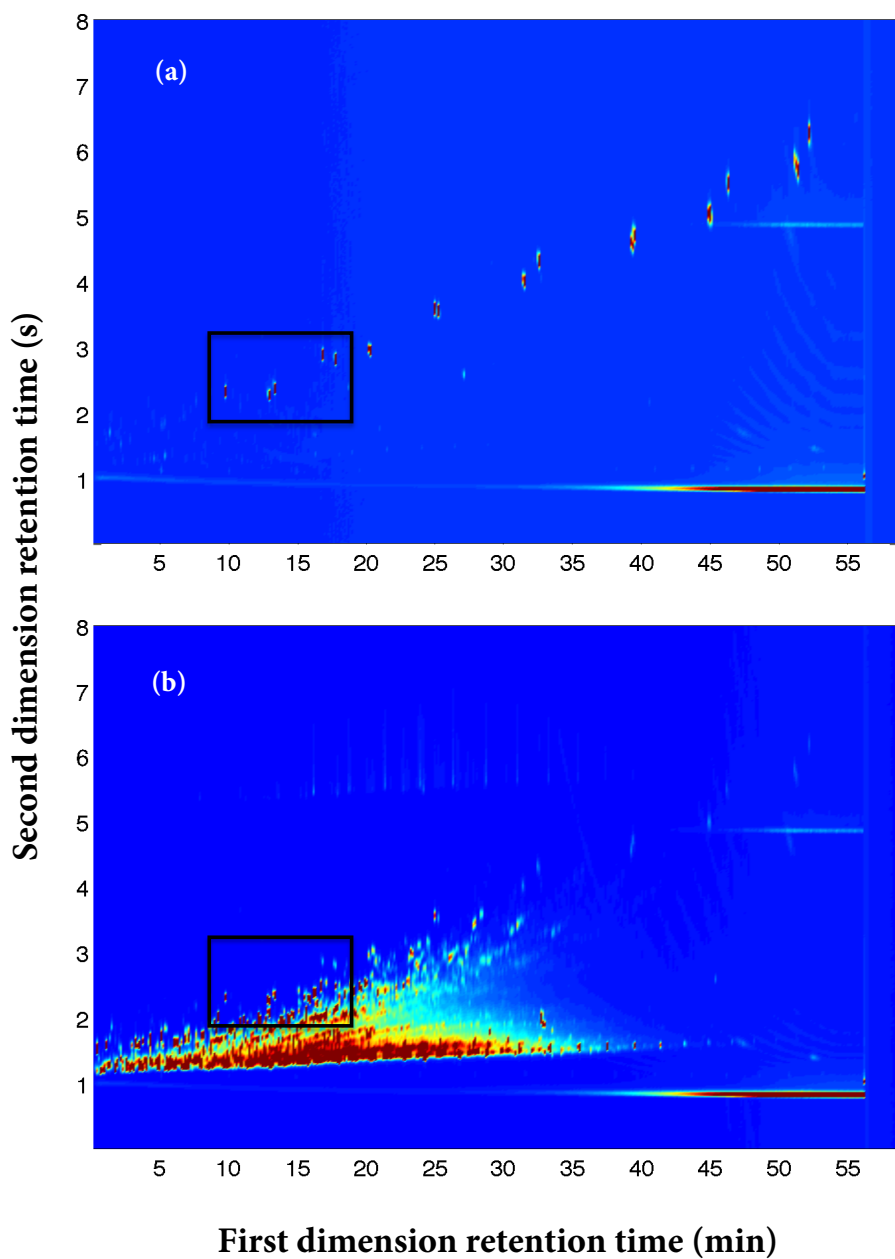


Figure 2.6 – GC×GC-FID chromatograms of (a) the PAH standard mixture and (b) the certified diesel fuel. Both chromatograms have been baseline corrected using the deadband method [81]. The black rectangle shows a subregion of the chromatogram that is expanded in Figure 2.8.

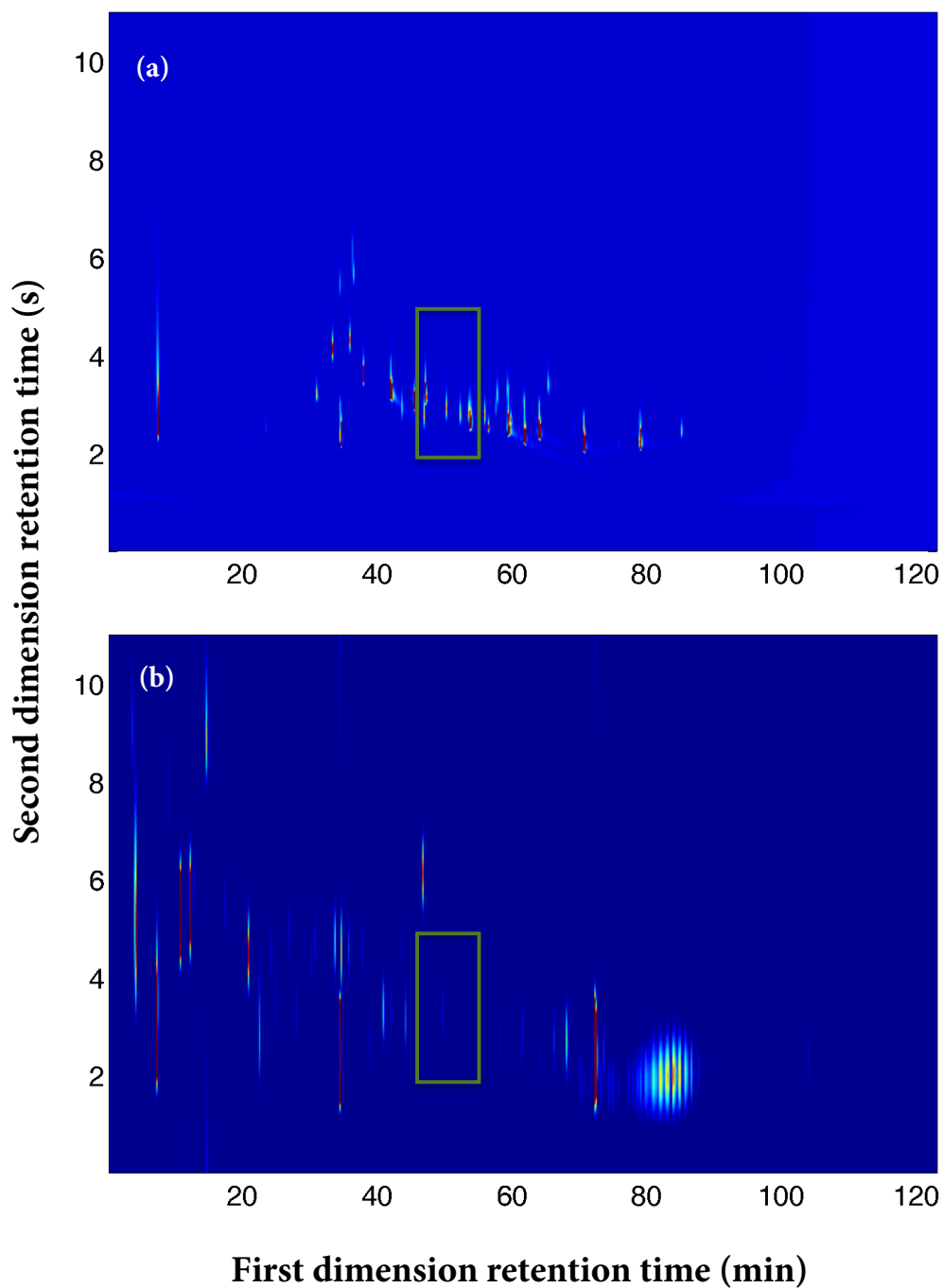


Figure 2.7 – GC×GC- $\mu$ ECD chromatograms of (a) the chlorinated hydrocarbon standard mixture and (b) the lake water extract. Both chromatograms have been baseline corrected using the deadband method [81]. The green rectangle shows a subregion of the chromatogram that is expanded in Figure 2.8.

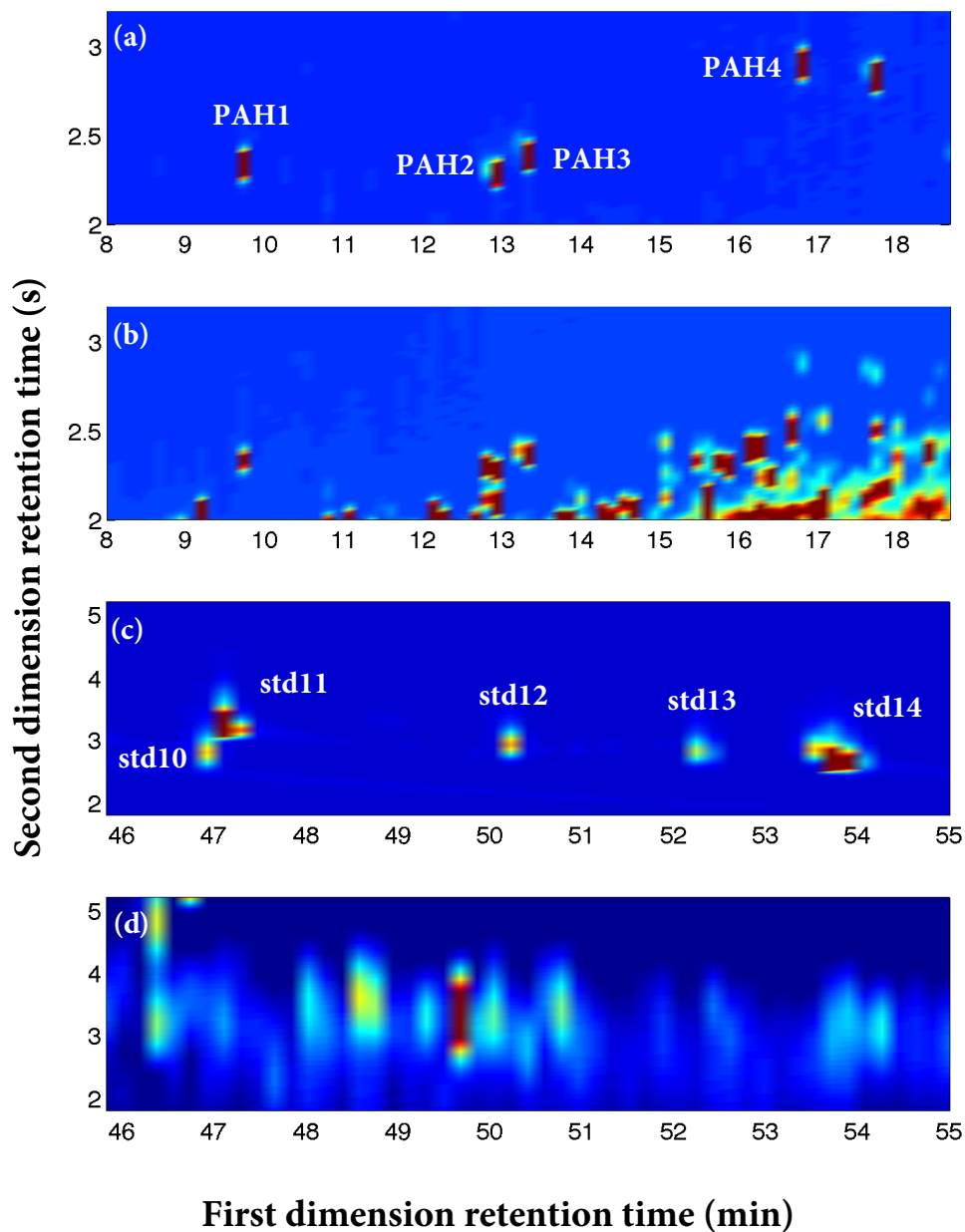


Figure 2.8 – Zoom of subregions of GC×GC chromatograms of (a) the PAH standard mixture; (b) the certified diesel fuel; (c) the chlorinated hydrocarbon standard mixture; and (d) the lake water extract. All chromatograms have been baseline corrected using the deadband method [81].

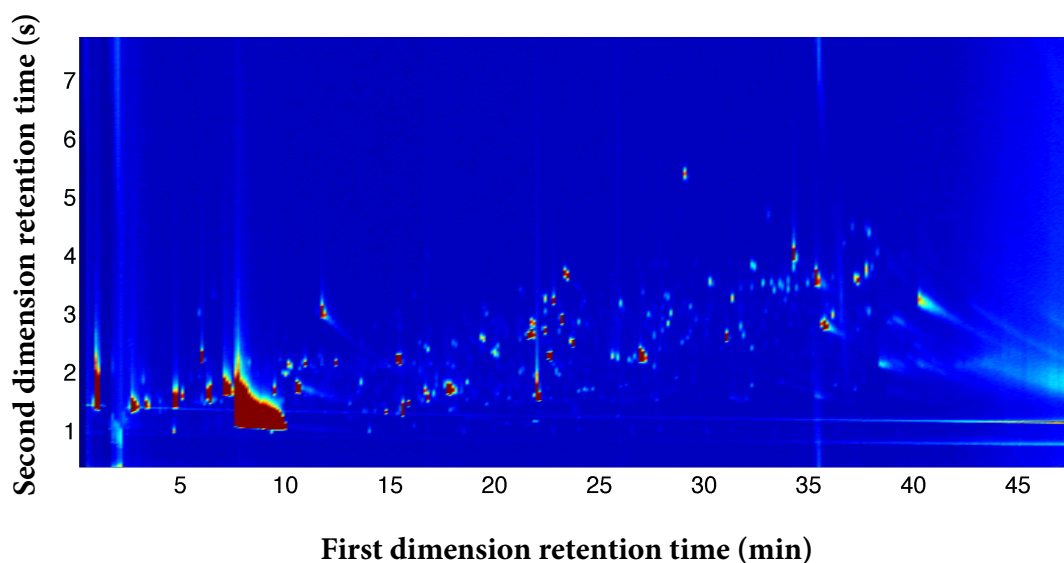


Figure 2.9 – GC×GC-ENCI-TOFMS total ion chromatogram of the lake water extract, baseline corrected using the deadband method [81].

### 2.3.2 Quantitative performance assessment of peak integration methods

Based on the results discussed in section 2.3.1, we conducted several chemometric tests on peak volumes produced by the different peak integration methods. We considered GC×GC-FID data of 7 PAH analytes in the certified diesel fuel and GC×GC- $\mu$ ECD data of 11 confirmed chlorinated hydrocarbon analytes in the lake water extract. The PAH standards have been introduced into the certified diesel mixture in known quantities, hence their concentrations are known *a priori*. This enabled a side-by-side assessment of the quantification accuracy of these PAHs for the different peak integration methods that we tested. The lake water extract offered the opportunity to further test the same peak integration methods, but in a more realistic context where the target analyte concentrations in the matrix are not known.

#### Reproducibility of the integrated peak volume over replicate injections

A reliable peak integration method should provide quantitatively reproducible peak volumes when applied to multiple analyses of the same standard or sample. The observed variability in analyte peak volumes for replicate injection samples provides a lower bound on the quantitative reliability of a peak integration method. Hence we viewed the relative standard error (%) of the peak volume,  $RSE$  (Eq. 2.7), as a prime indicator of the skill of a peak integration method.

External standard chromatograms allowed us to evaluate replicate variability of peak volumes

under the best chromatographic circumstances, where analyte peaks are well-separated, well-shaped, and unimpeded by matrix effects (Table 2.5). Under these conditions, some peak integration methods produced more reliable peak volumes than others for the test set of 18 external standard peaks. The EI<sub>4</sub> method gave the most repeatable peak volumes overall, with average *RSE* values of 5.7% for PAHs and 8.9% for chlorinated hydrocarbons (Figs. 2.10 and 2.11). The LG method performed comparably to the EI<sub>4</sub> method for the PAH standard set. The other peak integration methods, including LT, LI, EI<sub>6,5</sub>, EI<sub>5</sub>, and DI, performed less well than EI<sub>4</sub> for the PAH standards. For chlorinated hydrocarbon analytes, the peak integration methods produced results that were comparable to each other, with the exception of the LI method, which produced poor repeatability for the lowest concentration level of std6 due to slight tailing in the second dimension. The Kruskal-Wallis statistic indicates that differences in *RSE* values given by different peak integration methods are significant, with  $p < 0.01$  for both the PAH standard set and the chlorinated hydrocarbon standards set (Table 4). For chlorinated hydrocarbon standards, *RSE* values were inversely correlated to concentration level for all peak integration methods (Figure 2.11). This suggests intuitively that the analyte signal was increasingly difficult to separate from instrument noise with decreasing injected standard concentration level.

When confronted with a complex environmental sample, none of the peak integration methods produced quantitatively repeatable volumes (e.g.,  $RSE \leq 20\%$ ) for all target analytes. PAHs in the diesel fuel were reasonably separated from the hydrocarbon unresolved complex mixture, and for these compounds all peak integration methods gave good results, with average *RSE* values ranging from 2.5 to 3.8%. However, the peak volumes of target chlorinated hydrocarbons in the lake sample matrix proved more difficult, with average *RSE* values ranging from 7.9% (EI<sub>6,5</sub>) to 17.5% (DI), depending on the method. Again, the EI<sub>4</sub> peak integration method appeared to perform the best overall, with average *RSE* values of 2.5% for PAHs in the certified diesel fuel and 8.2% for chlorinated hydrocarbons in the lake water extract. The peak integration methods EI<sub>4</sub> and EI<sub>5</sub> gave reliable peak volume repeatability for all of the chlorinated hydrocarbon target analytes except for std26 in the unspiked lake water sample chromatogram. For this peak, EI<sub>4</sub> and EI<sub>5</sub> gave *RSE* values of 43.9% and 51.9% respectively, and this appeared to be due to co-elution with unresolved signal. All of the peak integration methods produced a large *RSE* (%) value for std26 in the unspiked lake sample, which demonstrates the challenge of complex samples for these methods. Compared to the EI<sub>4</sub> methods, other peak integration methods performed less well, with the DI method producing the highest average *RSE* value (17.5%) and highest maximum *RSE* value (89.7%), again arising from std26. For chlorinated hydrocarbons in the lake water extract, differences in *RSE* values given by different peak integration methods were significant, characterized by a Kruskal-Wallis statistic of  $p < 0.01$ . Among most of the methods, the largest peak volume variability appeared to arise from improper demarcation of the baseline and co-elution between the target analyte signal and the unresolved signal.



### 2.3. Results and discussion

The reproducibility of the integrated peak volume provides a direct measure of the ability of the peak integration method to handle slight changes in analyte peak shape from one chromatogram to another. Overall, the EI<sub>4</sub> and EI<sub>5</sub> peak integration methods were consistently found to produce the most repeatable peak volumes for external standards and also for analytes in environmental samples, irrespective of the detector type (FID or  $\mu$ ECD). Other methods performed less well. The sharp contrast in performances of the EI<sub>λ</sub> and DI methods, especially in the presence of unresolved complex mixture, illustrates the importance of using an appropriate baseline method for achieving reproducible integration of the resolvable analyte signal. These two peak integration methods use the same peak delineation algorithm (inverted watershed) and differ only in baseline algorithm.

Table 2.5 – Average and maximum relative standard error (*RSE* %) of integrated peak volumes for each peak integration method, computed using Eq. 2.7 for different sample sets. The peak integration method acronyms are explained in Table 2.3.

| External standard chromatograms   |      |      |                   |                 |                 |      |      |                             |
|---|------|------|-------------------|-----------------|-----------------|------|------|-----------------------------|
| PAH standards (GC×GC-FID)   |      |      |                   |                 |                 |      |      |                             |
| Peak integration method   |      |      |                   |                 |                 |      |      |                             |
|   | LT   | LI   | EI <sub>6.5</sub> | EI <sub>5</sub> | EI <sub>4</sub> | DI   | LG   | <i>p</i> value <sup>a</sup> |
| Average <i>RSE</i> (%) <sup>b</sup>   | 9.8  | 10.1 | 9.5               | 9.5             | 5.7             | 10.1 | 5.6  | <0.01                       |
| Max <i>RSE</i> (%) <sup>c</sup>   | 19.6 | 21.1 | 21.2              | 21.0            | 20.0            | 20.9 | 18.5 | -                           |
| Chlorinated hydrocarbon standards (GC×GC- $\mu$ ECD)                          |      |      |                   |                 |                 |      |      |                             |
| Peak integration method   |      |      |                   |                 |                 |      |      |                             |
|   | LT   | LI   | EI <sub>6.5</sub> | EI <sub>5</sub> | EI <sub>4</sub> | DI   | LG   | <i>p</i> value <sup>3</sup> |
| Average <i>RSE</i> (%) <sup>b</sup>   | 8.9  | 9.9  | 8.5               | 9.8             | 8.9             | 8.1  | -    | <0.01                       |
| Max <i>RSE</i> (%) <sup>c</sup>   | 16.5 | 85.3 | 17.2              | 22.4            | 17.5            | 17.7 | -    | -                           |
| Standard addition chromatograms   |      |      |                   |                 |                 |      |      |                             |
| PAH analytes in the certified diesel fuel (GC×GC-FID)                         |      |      |                   |                 |                 |      |      |                             |
| Peak integration method   |      |      |                   |                 |                 |      |      |                             |
|   | LT   | LI   | EI <sub>6.5</sub> | EI <sub>5</sub> | EI <sub>4</sub> | DI   | LG   | <i>p</i> value <sup>a</sup> |
| Average <i>RSE</i> (%) <sup>b</sup>   | 3.8  | 2.8  | 2.5               | 2.8             | 2.5             | 2.6  | 2.7  | 0.6                         |
| Max <i>RSE</i> (%) <sup>c</sup>   | 15.2 | 6.3  | 5.4               | 6.1             | 7.3             | 8.0  | 7.3  | -                           |
| Chlorinated hydrocarbon analytes in the lake water extract (GC×GC- $\mu$ ECD) |      |      |                   |                 |                 |      |      |                             |
| Peak integration method   |      |      |                   |                 |                 |      |      |                             |
|   | LT   | LI   | EI <sub>6.5</sub> | EI <sub>5</sub> | EI <sub>4</sub> | DI   | LG   | <i>p</i> value <sup>a</sup> |
| Average <i>RSE</i> (%) <sup>b</sup>   | 8.8  | 11.0 | 7.9               | 11.4            | 8.2             | 17.5 | -    | <0.01                       |
| Max <i>RSE</i> (%) <sup>c</sup>   | 45.8 | 80.2 | 86.7              | 51.9            | 43.9            | 89.7 | -    | -                           |

<sup>a</sup> Kruskal-Wallis one-way analysis of variance *p* value; <sup>b</sup> The averaged *RSE* (%) is the mean *RSE* value for all standards and levels of concentration of the sample type, where a single *RSE* (%) value is based on 3 replicate injections of a single analyte at a single concentration level; <sup>c</sup> Maximum *RSE* (%) value in the sample set.

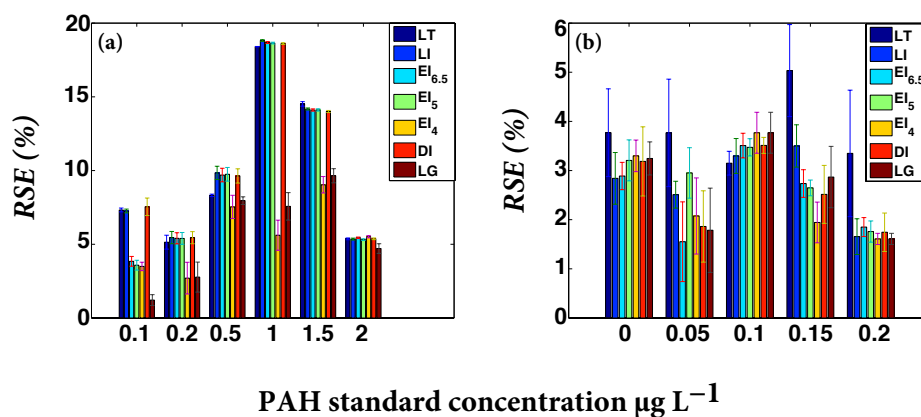


Figure 2.10 – Average relative standard error (*RSE*) values in % for: (a) PAH standards mixture; and (b) PAH standard additions of the certified diesel fuel sample. The peak integration method acronyms are explained in Table 2.3 of the main text. The error bars represent the variability of *RSE* of different analytes within each level of concentration.

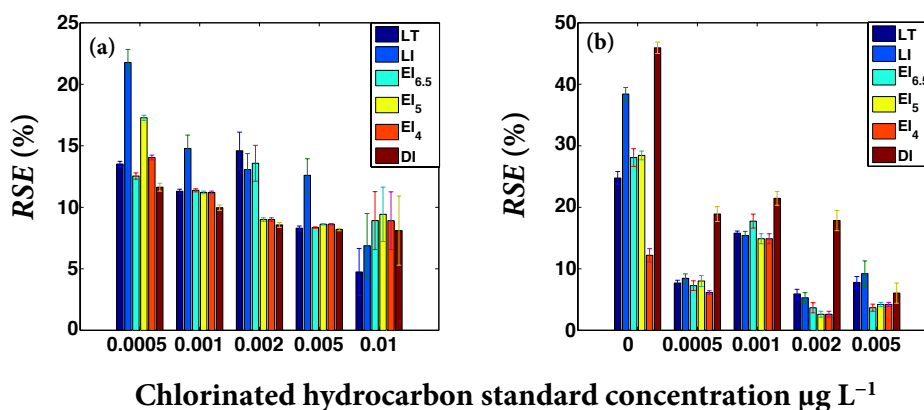


Figure 2.11 – Average relative standard error (*RSE*) values in % for: (a) chlorinated hydrocarbon standards; and (b) chlorinated hydrocarbons additions of the lake water extract sample. The peak integration method acronyms are explained in Table 2.3 of the main text. The error bars represent the variability of *RSE* of different analytes within each level of concentration.

### Proportional response of integrated peak volume with respect to injected analyte concentration

For the analyte concentrations explored here, both the FID and  $\mu$ ECD detectors were expected to produce linear response. Hence the peak volume of a target analyte should increase proportionally with increasing injected analyte mass, once zeroed to the offset. To evaluate the ability of peak integration methods to faithfully produce proportional response across different concentration levels, we computed the average response factor statistic,  $ARF$ , for both external standard signal data (Eq. 2.8) and standard addition signal data (Eq. 2.9).

The  $EI_\lambda$  peak integration methods produced the best analyte signal proportionality results for external standard data. These methods produced average response factor values of  $0.9 < ARF < 1.1$  for all 7 PAH standards and all 11 chlorinated hydrocarbon standards (Table 2.6, and Figures 2.12 and 2.13). The LT algorithm performed only slightly less well. Other algorithms performed well for most standards, but the DI and LI methods both produced aberrant  $ARF$  values of 1.39 and -0.53, respectively, for std6. At the higher standard concentration levels, the DI method apparently failed to delineate the peak boundaries correctly, splitting this peak into two parts. Consistent with the  $ARF$  results, integrated analyte signal exhibited a strong linear correlation with injected concentration in most cases, revealing squared correlation coefficient values of  $r^2 > 0.98$  for all methods and all standards, with the exception of the DI method applied to std6.

All peak integration methods gave good analyte signal proportionality results for standard addition data of the 7 PAHs in diesel fuel, finding  $0.9 < ARF < 1.1$  for all of these analytes. These peaks were reasonably well-separated from the hydrocarbon unresolved complex mixture. However the peak integration methods had more difficulty with chlorinated hydrocarbon analytes in the lake water extract, where several analytes co-eluted with unresolved signal. The  $EI_5$  and  $EI_4$  methods produced  $0.9 < ARF < 1.1$  for the largest number of analytes, compared to other methods. However these two methods gave inflated  $ARF$  values for both std13 and std15, attributed to difficulty handling peak tailing in both the first and second dimensions. Other peak integration methods gave poorer signal proportionality results for chlorinated hydrocarbon standard addition data. For example, the LI peak integration method resulted in negative  $ARF$  values of -1.75 and -1.07 for std6 and std26. Both of these peaks were slightly tailed in the second dimension and also overlapped with unresolved signal. In these cases, the inverted watershed algorithm split the tail into a separate peak, a behavior that has been previously documented for this delineation method [65]. These outcomes can be viewed as matrix interferences that arise from difficulty in handling the baseline and/or peak delineation. This problem also affected the standard addition offset for these peaks, as discussed in the next section. Similar problems were observed for handling of std6 by the DI peak integration method, leading artifactually to a negative slope for the standard addition of this analyte.

The *ARF* test demonstrates the importance of the peak integration method for obtaining the correct apparent signal response to concentration variation. We interpreted non-proportional signal response as an indication that the peak integration method was unable to properly delineate the resolvable analyte signal from the unresolved signal and this was viewed as a matrix interference (section 2.2.7). The peak integration methods that appeared least affected were  $EI_4$  and  $EI_5$ . The contrast between the performances of  $EI_4$  and other methods demonstrates the importance of both the baseline correction and peak delineation for obtaining correct apparent signal response behavior.

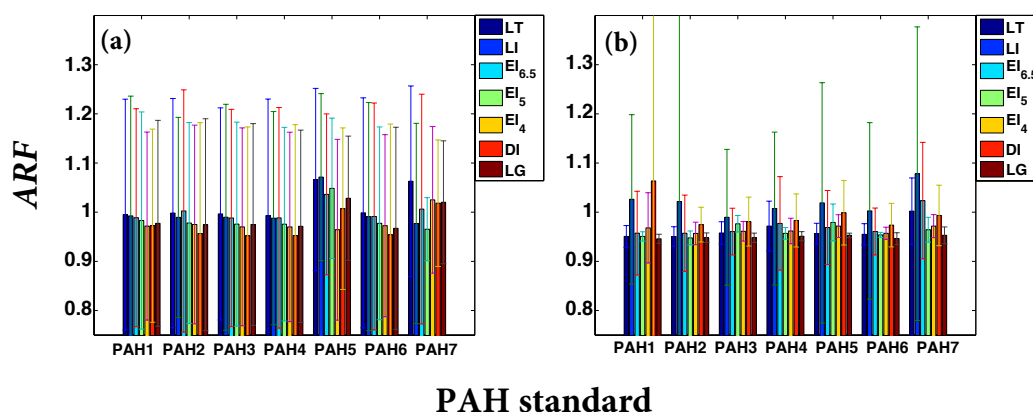


Figure 2.12 – The average response factor (*ARF*) values for: (a) PAH standards; (b) PAH standard addition of the certified diesel fuel sample, based on Eqs. 2.8 and 2.9. The peak integration method acronyms are explained in Table 2.3 of the main. The error bars are the 95% confidence interval computed using the bootstrap method with 1000 synthetic samples.

## 2.3. Results and discussion

Table 2.6 – Average response factor (*ARF*) statistics for the peak integration methods, for different sample sets, based on Eqs. 2.8 and 2.9. The peak integration method acronyms are explained in Table 2.3.

| External standard chromatograms   |      |       |                   |                 |                 |       |      |                             |
|---|------|-------|-------------------|-----------------|-----------------|-------|------|-----------------------------|
| PAH standard (GC×GC-FID)  |      |       |                   |                 |                 |       |      |                             |
| Peak integration method   |      |       |                   |                 |                 |       |      |                             |
|   | LT   | LI    | EI <sub>6.5</sub> | EI <sub>5</sub> | EI <sub>4</sub> | DI    | LG   | <i>p</i> value <sup>a</sup> |
| Max <i>ARF</i> value <sup>b</sup>   | 1.00 | 1.00  | 1.00              | 0.99            | 1.07            | 1.00  | 1.06 | 0.01                        |
| Min <i>ARF</i> value <sup>c</sup>   | 0.97 | 0.96  | 0.95              | 0.95            | 0.96            | 0.95  | 0.97 | -                           |
| Number of analytes having<br>0.9 < <i>ARF</i> < 1.1<br>(out of 7 analytes)  | 7    | 7     | 7                 | 7               | 7               | 7     | 7    | -                           |
| Chlorinated hydrocarbon standards (GC×GC-μECD)                              |      |       |                   |                 |                 |       |      |                             |
| Peak integration method   |      |       |                   |                 |                 |       |      |                             |
|   | LT   | LI    | EI <sub>6.5</sub> | EI <sub>5</sub> | EI <sub>4</sub> | DI    | LG   | <i>p</i> value <sup>a</sup> |
| Max <i>ARF</i> value <sup>b</sup>   | 1.11 | 1.39  | 1.09              | 1.07            | 1.10            | 1.10  | -    | <0.01                       |
| Min <i>ARF</i> value <sup>c</sup>   | 0.94 | 0.93  | 0.93              | 0.92            | 0.93            | -0.53 | -    | -                           |
| Number of analytes having<br>0.9 < <i>ARF</i> < 1.1<br>(out of 11 analytes) | 10   | 10    | 11                | 11              | 11              | 9     | -    | -                           |
| Standard addition chromatograms   |      |       |                   |                 |                 |       |      |                             |
| PAH analytes in the certified diesel fuel (GC×GC-FID)                       |      |       |                   |                 |                 |       |      |                             |
| Peak integration method   |      |       |                   |                 |                 |       |      |                             |
|   | LT   | LI    | EI <sub>6.5</sub> | EI <sub>5</sub> | EI <sub>4</sub> | DI    | LG   | <i>p</i> value <sup>a</sup> |
| Max <i>ARF</i> value <sup>b</sup>   | 1.06 | 1.02  | 0.99              | 1.01            | 1.02            | 1.00  | 1.08 | <0.01                       |
| Min <i>ARF</i> value <sup>c</sup>   | 0.95 | 0.94  | 0.95              | 0.95            | 0.95            | 0.95  | 0.95 | -                           |
| Number of analytes having<br>0.9 < <i>ARF</i> < 1.1<br>(out of 7 analytes)  | 7    | 7     | 7                 | 7               | 7               | 7     | 7    | -                           |
| Chlorinated hydrocarbons in the lake water extract (GC×GC-μECD)             |      |       |                   |                 |                 |       |      |                             |
| Peak integration method   |      |       |                   |                 |                 |       |      |                             |
|   | LT   | LI    | EI <sub>6.5</sub> | EI <sub>5</sub> | EI <sub>4</sub> | DI    | LG   | <i>p</i> value <sup>a</sup> |
| Max <i>ARF</i> value <sup>b</sup>   | 1.77 | 1.58  | 2.00              | 1.25            | 1.25            | 1.54  | -    | 0.08                        |
| Min <i>ARF</i> value <sup>c</sup>   | 0.90 | -1.75 | 1.03              | 0.98            | 0.98            | -0.20 | -    | -                           |
| Number of analytes having<br>0.9 < <i>ARF</i> < 1.1<br>(out of 11 analytes) | 3    | 6     | 5                 | 9               | 8               | 4     | -    | -                           |

<sup>a</sup> Kruskal-Wallis one-way analysis of variance *p* value; <sup>b</sup> The Max *ARF* is the maximum *ARF* value observed for the set of analytes in the studied sample; <sup>c</sup> The Min *ARF* is the minimum *ARF* value observed for the set of analytes in the studied sample.

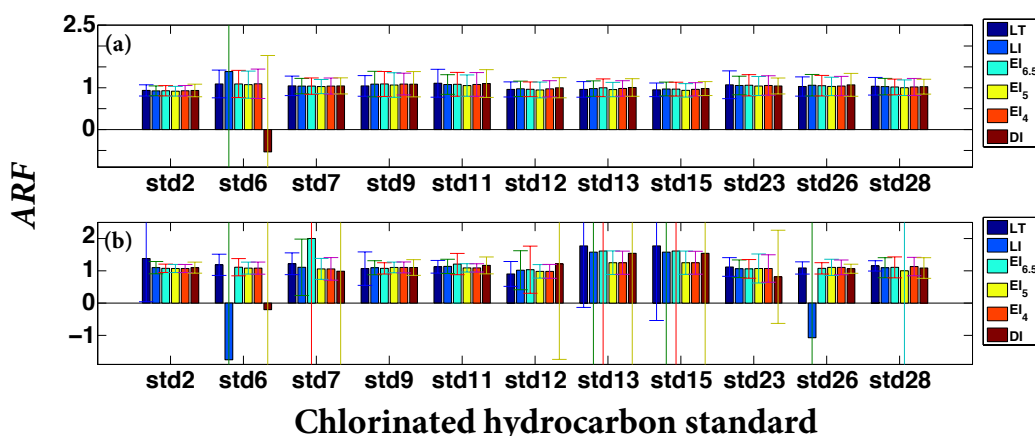


Figure 2.13 – The average response factor ( $ARF$ ) values for: (a) chlorinated hydrocarbon standards; (b) chlorinated hydrocarbon standard addition of the lake water extract sample, based on Eqs. 2.8 and 2.9. The peak integration method acronyms are explained in Table 2.3 of the main. The error bars are the 95% confidence interval computed using the bootstrap method with 1000 synthetic samples.

### Magnitude of the offset as an indicator of fidelity of the peak integration method

The magnitudes of the relative offset errors,  $e_{rel,ESM}$  and  $e_{rel,SAM}$ , provide information about the extent to which the resolvable analyte signal has been correctly isolated from the instrument background signal and the unresolved signal. These metrics are given by Eqs. 2.10 and 2.11. The relative offset errors also indicate the adequacy of the quantification method for concentration estimation of analytes. We defined a relative offset error ( $e_{rel,ESM}$  or  $e_{rel,SAM}$ ) value of  $> 50\%$  as indicating that the approach is unreliable for quantification of that analyte in that sample.

For external standard data, the relative offset errors were varied, with  $e_{rel,ESM}$  values ranging from  $-0.48\%$  for PAH2 (with method  $EI_4$ ) to  $361\%$  for std26 (with method LI). However some peak integration methods consistently produced smaller offset errors than others (Table 2.7). The  $EI_4$ , DI, and LG peak integration methods provided low average  $e_{rel,ESM}$  values and also low maximum  $e_{rel,ESM}$  values for the PAH standard set, compared to other methods. Among the PAH standards, PAH7 led to the worst relative offset error results for all peak integration methods. This may have arisen because PAH7 was at a lower concentration in the diesel fuel ( $0.05 \text{ mg L}^{-1}$ ) than the other target PAH analytes. The  $EI_\lambda$  and LI methods produced the lowest average  $e_{rel,ESM}$  values and lowest maximum  $e_{rel,ESM}$  values for the chlorinated hydrocarbon standards. The  $EI_\lambda$  and LI methods also produced the highest number of analytes having  $e_{rel,ESM} < 50\%$  for both the PAH standard set and chlorinated hydrocarbon standard set. Hence these two peak integration methods enabled the quantification of a larger number of analytes than did the other methods. Among the chlorinated hydrocarbon standards, the

LT method gave an especially poor  $e_{rel,ESM}$  value of 361% for std9. For this standard the LT method produced a small  $y_0$  value compared to all the other peak integration methods, attributed to the co-elution of unresolved signal with this peak. The two-step algorithm, which is sensitive to the peak width in the second dimension, appeared to define inappropriate boundaries of std9 in the lake water extract chromatogram. The LT method also produced the largest number of analytes having  $e_{rel,ESM} > 50\%$  in the lake water extract; these analytes were thus considered non-quantifiable.

All peak integration methods gave standard addition relative offset errors,  $e_{rel,SAM}$ , that were  $< 50\%$  for all 7 target PAHs in diesel fuel (Table 2.7) indicating that peak volume results would be eligible for quantification by SAM in all cases. The LG, EI<sub>4</sub>, and EI<sub>5</sub> peak integration methods produced the lowest average  $e_{rel,SAM}$  values (4.3, 6.6, and 7.7%) and also the lowest maximum magnitude  $e_{rel,SAM}$  values for the PAHs in diesel fuel. However, offset errors were higher for the chlorinated hydrocarbons in the lake water extract, many of which co-eluted with unresolved signal from the complex mixture. The EI<sub>4</sub> and EI<sub>5</sub> methods produced the lowest average  $e_{rel,SAM}$  value and also the lowest maximum values for chlorinated hydrocarbons in the lake water extract (LG was not applied to this sample). The EI<sub>4</sub> and EI<sub>5</sub> methods also resulted in high numbers of analytes considered eligible for quantification ( $e_{rel,SAM} < 50\%$ ) in the lake water extract. The LT, DI, and LI peak integration methods fared less well. The LT method produced only 3 analytes considered eligible for quantification by SAM in the lake water extract. The poorer performance of these peak integration methods was attributed to baseline corrections that were not aggressive enough to isolate the analyte signal from the unresolved signal. When unresolved signal is present, an overly conservative baseline inflates the apparent volume of the peak, causing an overestimation of the peak volume. For the LT, LI, DI and EI<sub>6.5</sub> peak integration methods, improper demarcation of the baseline was believed to lead to an overall overestimation of the standard addition offset and therefore a large offset error.

Overall, analysis of the offset errors suggests that the EI<sub>4</sub>, EI<sub>5</sub>, and LG peak integration methods provide more accurate delineations of resolvable analyte signal compared to other methods. For both the  $e_{rel,ESM}$  and  $e_{rel,SAM}$  data sets, differences among the peak delineation methods were found significant according to the Kruskal-Wallis statistic ( $p$  values  $< 0.01$ ). Proper demarcation of the baseline is especially important for controlling the offset error [98, 112]. We find that the lowest offset errors are consistently obtained using the baseline estimation method of Eilers (EI<sub>4</sub> and EI<sub>5</sub> methods) or using a baseline that is optimized simultaneously together with the peak delineation (LG method).

### Diagnosis of matrix effects

Matrix effects change the apparent sensitivity of the instrument, and this is diagnosed by the proportional error factor,  $P$  (Eq. 2.12). Based on the results of the peak volume reproducibility

Table 2.7 – The average absolute value and maximum magnitude of the relative offset error (%) ( $e_{rel,ESM}$  and  $e_{rel,SAM}$ , Eqs. 2.10 and 2.11), and the number of analytes with relative offset error below 50%, for each peak integration method. The peak integration method acronyms are explained in Table 2.3.

| External standard chromatograms                                  |        |        |                   |                 |                 |       |       |                |
|--|--------|--------|-------------------|-----------------|-----------------|-------|-------|----------------|
| PAH standards  |        |        |                   |                 |                 |       |       |                |
| Peak integration method  |        |        |                   |                 |                 |       |       |                |
|  | LT     | LI     | El <sub>6.5</sub> | El <sub>5</sub> | El <sub>4</sub> | DI    | LG    | <i>p</i> value |
| Average absolute value of $e_{rel,ESM}$ (%)                      | 30.8   | 32.4   | 30.7              | 38.1            | 17.7            | 21.4  | 22.7  | <0.01          |
| Max absolute magnitude of $e_{rel,ESM}$ (%)                      | -118.0 | -132.0 | -115.6            | -161.0          | -63.4           | -71.0 | -74.4 | -              |
| Number of analytes with $e_{rel,ESM}$ < 50% (out of 7 analytes)  | 6      | 6      | 5                 | 5               | 6               | 6     | 5     |                |
| Chlorinated hydrocarbon standards                                |        |        |                   |                 |                 |       |       |                |
| Peak integration method  |        |        |                   |                 |                 |       |       |                |
|  | LT     | LI     | El <sub>6.5</sub> | El <sub>5</sub> | El <sub>4</sub> | DI    | LG    | <i>p</i> value |
| Average absolute value of $e_{rel,ESM}$ (%)                      | 114.3  | 18.2   | 17.5              | 16.7            | 19.9            | 25.5  | -     | <0.01          |
| Max absolute magnitude of $e_{rel,ESM}$ (%)                      | 361.1  | 41.4   | 34.8              | 36.3            | 46.9            | 76.1  | -     | -              |
| Number of analytes with $e_{rel,ESM}$ < 50% (out of 11 analytes) | 3      | 10     | 11                | 11              | 11              | 10    | -     |                |
| Standard addition chromatograms                                  |        |        |                   |                 |                 |       |       |                |
| PAH analytes in the certified diesel fuel                        |        |        |                   |                 |                 |       |       |                |
| Peak integration method  |        |        |                   |                 |                 |       |       |                |
|  | LT     | LI     | El <sub>6.5</sub> | El <sub>5</sub> | El <sub>4</sub> | DI    | LG    | <i>p</i> value |
| Average absolute value of $e_{rel,SAM}$ (%)                      | 11.0   | 10.8   | 11.7              | 7.7             | 6.6             | 9.5   | 4.3   | <0.01          |
| Max absolute magnitude of $e_{rel,SAM}$ (%)                      | -32.7  | 18.5   | -36.8             | -25.5           | -22.4           | 28.8  | -7.5  | -              |
| Number of analytes with $e_{rel,SAM}$ < 50% (out of 7 analytes)  | 7      | 7      | 7                 | 7               | 7               | 7     | 7     |                |
| Chlorinated hydrocarbon analytes in the lake water extract       |        |        |                   |                 |                 |       |       |                |
| Peak integration method  |        |        |                   |                 |                 |       |       |                |
|  | LT     | LI     | El <sub>6.5</sub> | El <sub>5</sub> | El <sub>4</sub> | DI    | LG    | <i>p</i> value |
| Average absolute value of $e_{rel,SAM}$ (%)                      | 140.0  | 80.6   | 48.7              | 24.2            | 29.5            | 53.5  | -     | <0.01          |
| Max absolute magnitude of $e_{rel,SAM}$ (%)                      | 296.0  | 361.8  | 217.6             | 70.2            | 69.7            | 264.3 | -     | -              |
| Number of analytes with $e_{rel,SAM}$ < 50% (out of 11 analytes) | 3      | 8      | 8                 | 9               | 8               | 7     | -     |                |



tests (section 2.3.2), we defined a proportional error interval of  $0.8 < P < 1.2$  as indicating an absence of matrix effect. Under the analysis conditions used here, matrix-altered sensitivity is attributed to the inability of the peak integration method to accurately discriminate resolvable analyte signal from the unresolved signal arising from poorly separated constituents in the sample. Matrix interferences were diagnosed separately (section 2.3.2). Hence the compared  $P$  factors of different peak integration methods were viewed as a diagnostic of their comparative skill for avoiding the introduction of matrix effects into the quantification.

For the PAHs in diesel fuel, the  $P$  factors ranged from 0.73 for PAH7 (with method LT) to 1.93 for PAH2 (with method LG). The EI<sub>4</sub>, DI, and LG peak integration methods produced acceptable  $P$  factors ( $0.8 < P < 1.2$ ) for 5 out of 7 PAHs, indicating the absence of matrix effects (Table 2.8 and Figures 2.14 and 2.15). However, all of the peak integration methods produced  $P$  factors outside of the acceptable range for PAH2 and PAH3, indicating the presence of a substantial matrix effect for these two PAHs. These peaks eluted in close proximity to the raised signal produced by unresolved hydrocarbon complex mixture (Figure 2.8), apparently leading to difficulties in demarcating an appropriate baseline and peak boundaries.

For chlorinated hydrocarbons in the lake water extract, the EI<sub>4</sub> and EI<sub>5</sub> peak integration methods produced  $P$  factors within the acceptable range ( $0.8 < P < 1.2$ ), indicating absence of the matrix effects, for 10 out of 11 analytes. Conversely, the LT method elicited substantial apparent matrix effects for 6 out of 11 analytes. For the LT peak integration method, we interpreted that the local linear baseline correction frequently was unable to discriminate adequately between analyte signal and unresolved signal from the complex mixture, which led to an overestimation of peak volume in many cases (section 2.3.2). Additionally, the two-step algorithm often was unable to define the peak boundaries precisely, sometimes incorporating the tails of surrounding peaks to the analyte peak of interest. These failures may have led to a systematic overestimation of the peak volume for the higher concentration levels compared to the lower concentration levels of standard addition, and thus an inflated  $P$  factor. A similar situation was observed for the LI peak integration method. Compared to other methods, the LI method tended to expand the peak boundaries, especially for the higher concentration levels of standard addition. Thus the  $P$  factors produced by the LI method were slightly larger than those of the LT method. The DI peak integration method was unable to produce acceptable  $P$  factors for 7 out of 11 chlorinated standards, indicating frequent substantial matrix effects, and this was mainly attributed to a baseline correction method that was insufficiently aggressive to discriminate the unresolved signal from the analyte signal. Similarly, the Eilers baseline correction with the  $\lambda=10^{6.5}$  apparently was not aggressive enough to remove the unresolved signal from the analyte signal.

When judged by the  $P$  factor, the EI<sub>4</sub> and EI<sub>5</sub> peak integration methods were found to be the most effective at eliminating matrix effects for target analytes in the both the certified

## Chapter 2. Analyte quantification with GC×GC

diesel fuel and the lake water extract, despite the abundant unresolved signal arising from complex mixture in these samples. A comparison of results of the DI and EI<sub>λ</sub> methods demonstrated that increased aggressiveness of the baseline correction method resulted in dramatic improvement in the *P* factor, indicating improved discrimination of the resolvable analyte signal from the unresolved complex mixture signal. Notably, the large variability in the *P* factor from compound to compound illustrates that the conventional internal standard method (IS) would fail to remove the matrix effect for many of these analytes.

Table 2.8 – Summary of proportional error factor results, *P*<sup>a</sup>, indicative of the presence of matrix effects produced by each peak integration method for 7 PAHs in diesel fuel and 11 chlorinated hydrocarbons in the lake water extract.

| PAHs in the certified diesel fuel                                       |                         |      |                   |                 |                 |       |      |
|---|-------------------------|------|-------------------|-----------------|-----------------|-------|------|
|   | Peak integration method |      |                   |                 |                 |       |      |
|   | LT                      | LI   | EI <sub>6.5</sub> | EI <sub>5</sub> | EI <sub>4</sub> | DI    | LG   |
| Max <i>P</i> factor <sup>b</sup>  | 1.91                    | 1.76 | 1.83              | 1.85            | 1.84            | 1.83  | 1.93 |
| Min <i>P</i> factor <sup>c</sup>  | 0.73                    | 0.79 | 0.79              | 0.79            | 0.84            | 0.81  | 0.84 |
| Number of analytes with<br>0.8 < <i>P</i> < 1.2<br>(out of 7 analytes)  | 4                       | 4    | 4                 | 4               | 5               | 5     | 5    |
| Chlorinated hydrocarbons in the lake water extract                      |                         |      |                   |                 |                 |       |      |
|   | Peak integration method |      |                   |                 |                 |       |      |
|   | LT                      | LI   | EI <sub>6.5</sub> | EI <sub>5</sub> | EI <sub>4</sub> | DI    | LG   |
| Max <i>P</i> factor <sup>b</sup>  | 1.36                    | 1.51 | 1.42              | 1.13            | 1.13            | 1.52  | -    |
| Min <i>P</i> factor <sup>c</sup>  | 0.96                    | 0.62 | 1.04              | 0.71            | 0.77            | -0.22 | -    |
| Number of analytes with<br>0.8 < <i>P</i> < 1.2<br>(out of 11 analytes) | 5                       | 2    | 5                 | 10              | 10              | 4     | -    |

<sup>a</sup> The *P* factor was computed with Eq. 2.12; <sup>b</sup> The max *P* factor was the single highest *P* factor among all analytes for each peak integration method; <sup>c</sup> The min *P* factor was the single smallest *P* factor among all analytes for each peak integration method.

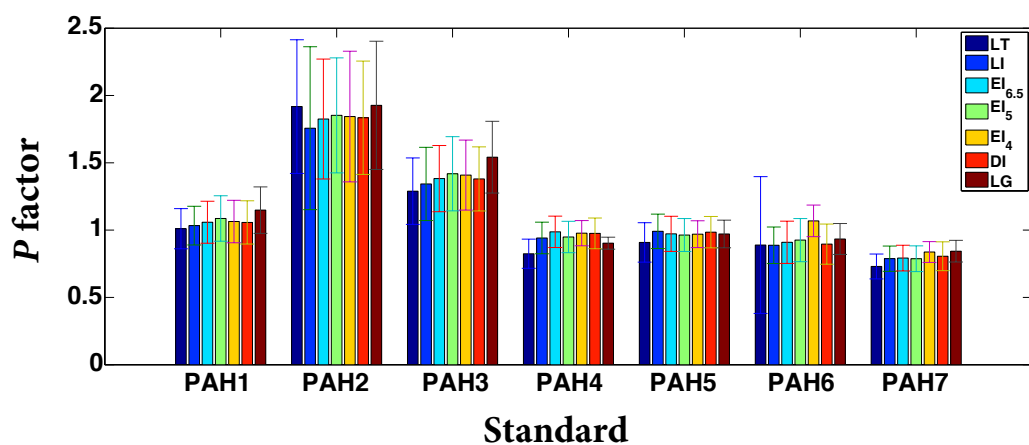


Figure 2.14 – Average  $P$  factors of 7 PAHs in the certified diesel fuel, computed using Eq. 2.12. The peak integration method acronyms are explained in Table 2.3 of the main text. The error bars show the 95% confidence interval computed using the bootstrap method with 1000 synthetic samples.

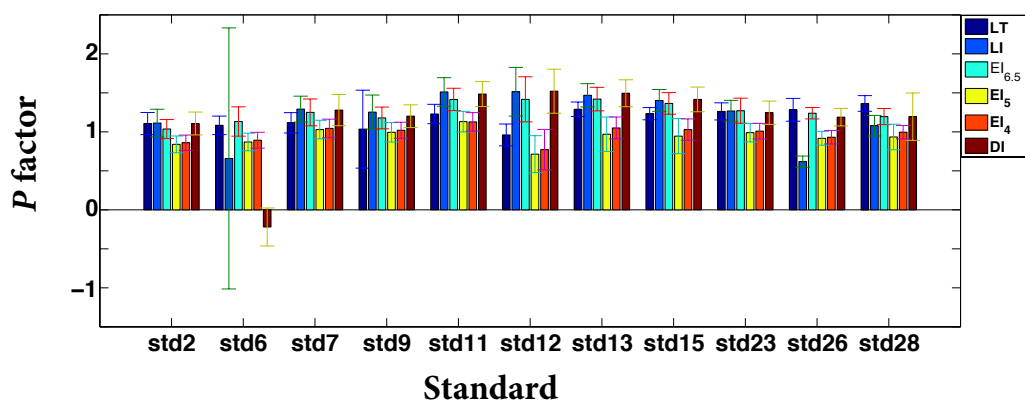


Figure 2.15 – Average  $P$  factors of 11 chlorinated hydrocarbons in the lake water extract, computed using Eq. 2.12. The peak integration method acronyms are explained in Table 2.3 of the main text. The error bars show the 95% confidence interval computed using the bootstrap method with 1000 synthetic samples.

### Quantification of PAHs in diesel fuel by GC×GC-FID

The concentration of each target PAH in the certified diesel fuel was estimated using three methods: the external standard method (Eq. 2.3); the standard addition method (Eq. 2.6); and the external standard method with  $P$  correction (Eq. 2.13). These determinations were compared to the known PAH concentrations in this reference material (Table 2.9).

The external standard method successfully quantified PAH1, PAH5, and PAH6 with accuracy of  $< 0.07 \text{ mg L}^{-1}$  when using peak volumes given by any of the peak integration methods (Table 2.9). The ESM was considered inadequate to perform quantifications for PAH7, which was present in the diesel fuel at a concentration of only  $0.05 \text{ mg L}^{-1}$ , based on the high ESM offset errors observed for all peak integration methods (see section 2.3.2). For PAH4, which was present at  $0.11 \text{ mg L}^{-1}$ , ESM quantifications with the EI<sub>6,5</sub>, EI<sub>5</sub>, and LG methods were considered ineligible based on high ESM offset errors. However the remaining methods (LT, LI, EI<sub>4</sub>, and DI) led to reasonable ESM quantifications having accuracy of  $< 0.03 \text{ mg L}^{-1}$  for PAH4. The ESM gave poor results for PAH2 and PAH3, with errors of roughly  $0.60 \text{ mg L}^{-1}$  and  $0.30 \text{ mg L}^{-1}$ , respectively, for all the peak integration methods. This corresponds to 100% overestimation of PAH2, and a 70% overestimation of PAH3, using any of the peak integration methods. This outcome was attributed to a significant matrix effect that affected all of the peak integration methods, already diagnosed by the large  $P$  factors for these two PAHs (section 2.3.2).

Standard additions led to improved quantification results for PAHs, using peak volumes given by any of the peak integration methods (Table 2.9). Compared to the ESM, the SAM produced drastically improved quantifications for both PAH2 and PAH3, confirming the previous diagnosis that these two PAHs were impacted by matrix effect. When corrected for matrix effects, some peak integration methods still produced better peak volumes than others. Using the SAM quantification based on EI<sub>4</sub>, EI<sub>5</sub>, or LG peak integration methods, we achieved a quantification error of  $0.07 \text{ mg L}^{-1}$  or less for all 7 PAHs in diesel fuel. This provided quantitatively meaningful concentration estimates for several of the PAHs, which had concentrations ranging from  $0.05$  to  $0.60 \text{ mg L}^{-1}$ . The uncertainty levels provided by Restek were  $\pm 10\%$  for each of the known PAH concentrations in the certified diesel fuel reference material.

Among the peak integration methods assessed here, the EI<sub>4</sub>, EI<sub>5</sub>, and LG methods produced the best quantifications for PAHs in diesel fuel, but only after correction for matrix effects using standard addition. In previous sections, the EI<sub>4</sub> and EI<sub>5</sub> peak integration methods were found to produce the best results for peak volume reproducibility, average response factor, and offset error. These methods both feature an aggressive baseline correction. All of peak integration methods produced erroneous peak volumes for PAH2 and PAH3, despite that these two compounds appeared reasonably well-separated in the GC×GC chromatogram. A

standard addition procedure effectively eliminated these matrix effects.

### **Quantification of target chlorinated hydrocarbons in the lake water extract by GC×GC- $\mu$ ECD**

In contrast to the PAHs in the certified diesel fuel, the concentrations of the 11 target chlorinated hydrocarbons in the lake water extract are not known *a priori*, although their presence has been confirmed qualitatively by GC×GC-ENCI-TOFMS (section 2.3.1). Hence we can assess the quantifications of chlorinated hydrocarbons by GC×GC- $\mu$ ECD only using indirect measures.

External standard method quantification depended strongly on the peak integration method used to determine the analyte peak volume (Table 2.10). The three EI $_{\lambda}$  methods led to valid ESM quantifications for all 11 of the considered target chlorinated hydrocarbon analytes. However the DI, LI, and LT methods fell short of this success rate, due to either a large ESM offset error (section 2.2.7) or due to failure to detect the analyte in the sample. For example, using LT peak volumes, the ESM was able to quantify only 3 of the 11 target analytes. Among the analytes that were quantified, different peak integration methods led to ESM quantifications that often disagreed by  $> 0.5 \mu\text{g mL}^{-1}$  (Figure 2.16). This represents substantial disagreement for a set analytes having estimated concentrations ranging from 0.1 to  $4.2 \mu\text{g mL}^{-1}$ .

Compared to the external calibration procedure, the standard addition method produced fewer valid quantifications. The EI $_{\lambda}$  and LI peak integration methods enabled SAM quantifications of 8 or more of the 11 target chlorinated hydrocarbon analytes, whereas the DI and LT methods led to a lower success rate for quantification. Unsuccessful quantifications resulted from either a large SAM relative offset error or failure to detect the analyte in the unspiked sample (section 2.3.2).

However the standard addition procedure leads to substantially improved agreement among the quantification estimates produced by different peak integration methods, compared to quantifications by external standard method (Table 2.11 and Figure 2.16). Among the analytes that could be quantified by SAM, different peak integration methods led to quantifications that exhibited improved agreement with each other, usually within  $< 0.5 \mu\text{g mL}^{-1}$ . Compared to the ESM quantifications, the standard additions eliminated consideration of the most difficult or "pathological" cases (those exhibiting a large offset error) and compensated for matrix effects for the remaining analytes.

These results indicate that the peak integration methods differ markedly in their ability to eliminate matrix effects. To further evaluate this hypothesis, we compared SAM quantification

## Chapter 2. Analyte quantification with GC×GC

Table 2.9 – Quantifications of 7 PAH standards (mg L<sup>-1</sup>) in diesel fuel using ESM, SAM, and ESM with *P* correction. The peak integration method acronyms are explained in Table 2.3.

| Quantification by external standard method (Eq. 2.3)                           |                  |                 |                 |                   |                 |                 |                 |                 |
|--|------------------|-----------------|-----------------|-------------------|-----------------|-----------------|-----------------|-----------------|
| Peak integration method  |                  |                 |                 |                   |                 |                 |                 |                 |
|  | ref <sup>a</sup> | LT              | LI              | El <sub>6.5</sub> | El <sub>5</sub> | El <sub>4</sub> | DI              | LG              |
| PAH1   | 0.25             | 0.31            | 0.31            | 0.31              | 0.30            | 0.29            | 0.31            | 0.30            |
| PAH2   | 0.60             | 1.21            | 1.20            | 1.21              | 1.20            | 1.17            | 1.22            | 1.20            |
| PAH3   | 0.43             | 0.73            | 0.73            | 0.72              | 0.72            | 0.71            | 0.72            | 0.74            |
| PAH4   | 0.11             | 0.09            | 0.10            | nq <sup>b</sup>   | nq <sup>b</sup> | 0.08            | 0.10            | nq <sup>b</sup> |
| PAH5   | 0.13             | 0.18            | 0.17            | 0.17              | 0.17            | 0.18            | 0.17            | 0.17            |
| PAH6   | 0.25             | 0.31            | 0.32            | 0.31              | 0.31            | 0.29            | 0.31            | 0.33            |
| PAH7   | 0.05             | nq <sup>b</sup> | nq <sup>b</sup> | nq <sup>b</sup>   | nq <sup>b</sup> | nq <sup>b</sup> | nq <sup>b</sup> | nq <sup>b</sup> |
| AAD <sup>c</sup>   | -                | 0.18            | 0.18            | 0.21              | 0.21            | 0.17            | 0.18            | 0.21            |
| Max AD <sup>d</sup>  | -                | 0.62            | 0.60            | 0.61              | 0.60            | 0.58            | 0.62            | 0.60            |
| Quantification by standard addition method (Eq. 2.6)                           |                  |                 |                 |                   |                 |                 |                 |                 |
| Peak integration method  |                  |                 |                 |                   |                 |                 |                 |                 |
|  | ref <sup>a</sup> | LT              | LI              | El <sub>6.5</sub> | El <sub>5</sub> | El <sub>4</sub> | DI              | LG              |
| PAH1   | 0.25             | 0.29            | 0.29            | 0.27              | 0.26            | 0.27            | 0.28            | 0.24            |
| PAH2   | 0.60             | 0.63            | 0.69            | 0.66              | 0.64            | 0.64            | 0.66            | 0.61            |
| PAH3   | 0.43             | 0.57            | 0.55            | 0.52              | 0.50            | 0.50            | 0.52            | 0.46            |
| PAH4   | 0.11             | 0.07            | 0.079           | 0.05              | 0.05            | 0.07            | 0.07            | 0.07            |
| PAH5   | 0.13             | 0.16            | 0.15            | 0.15              | 0.14            | 0.15            | 0.16            | 0.15            |
| PAH6   | 0.25             | 0.32            | 0.33            | 0.31              | 0.30            | 0.25            | 0.33            | 0.32            |
| PAH7   | 0.05             | 0.03            | 0.03            | 0.03              | 0.02            | 0.038           | 0.04            | 0.03            |
| AAD <sup>c</sup>   | -                | 0.05            | 0.06            | 0.05              | 0.04            | 0.03            | 0.05            | 0.03            |
| Max AD <sup>d</sup>  | -                | 0.14            | 0.09            | 0.09              | 0.07            | 0.07            | 0.09            | 0.07            |
| Quantification by external standard method with <i>P</i> correction (Eq. 2.13) |                  |                 |                 |                   |                 |                 |                 |                 |
| Peak integration method  |                  |                 |                 |                   |                 |                 |                 |                 |
|  | ref <sup>a</sup> | LT              | LI              | El <sub>6.5</sub> | El <sub>5</sub> | El <sub>4</sub> | DI              | LG              |
| PAH1   | 0.25             | 0.31            | 0.30            | 0.29              | 0.28            | 0.27            | 0.29            | 0.26            |
| PAH2   | 0.60             | 0.63            | 0.68            | 0.66              | 0.65            | 0.64            | 0.67            | 0.63            |
| PAH3   | 0.43             | 0.57            | 0.54            | 0.52              | 0.51            | 0.50            | 0.53            | 0.48            |
| PAH4   | 0.11             | 0.11            | 0.10            | nq <sup>b</sup>   | nq <sup>b</sup> | 0.08            | 0.10            | nq <sup>b</sup> |
| PAH5   | 0.13             | 0.20            | 0.18            | 0.18              | 0.17            | 0.18            | 0.18            | 0.17            |
| PAH6   | 0.25             | 0.34            | 0.36            | 0.34              | 0.33            | 0.27            | 0.35            | 0.35            |
| PAH7   | 0.05             | nq <sup>b</sup> | nq <sup>b</sup> | nq <sup>b</sup>   | nq <sup>b</sup> | nq <sup>b</sup> | nq <sup>b</sup> | nq <sup>b</sup> |
| AAD <sup>c</sup>   | -                | 0.07            | 0.07            | 0.06              | 0.06            | 0.04            | 0.06            | 0.04            |
| Max AD <sup>d</sup>  | -                | 0.14            | 0.11            | 0.10              | 0.08            | 0.07            | 0.09            | 0.10            |

<sup>a</sup> The reference concentration of each PAH in the certified diesel fuel (listed uncertainty is  $\pm 10\%$ ); <sup>b</sup> The offset error of this PAH standard was larger than 50%, thus the analyte was considered non-quantifiable (nq); <sup>c</sup> AAD of concentration is the absolute average deviation between the reference concentrations and the estimated concentration, excluding the nq values, using each peak integration method; <sup>d</sup> Max AD is the maximum absolute deviation between the reference concentrations and the estimated concentrations using each peak integration method.

results to ESM quantification results, among the analytes that could be quantified with both methods (Table 2.11). We find that the EI<sub>4</sub> peak integration method produces quantifications that are in agreement to within 0.25  $\mu\text{g mL}^{-1}$ , on average, when using SAM versus when using ESM for the quantification. The EI<sub>5</sub> method gives results similar to EI<sub>4</sub>, whereas the LI and LT integration methods exhibit much larger discrepancies for quantification by SAM versus by ESM. This result lends direct support to the interpretation that the EI<sub>4</sub> and EI<sub>5</sub> methods eliminated some matrix effects that confound the ESM quantification, whereas other peak integration methods exhibited less skill at this task. This conclusion is consistent with the findings presented in sections 2.3.2 and 2.3.2.

Table 2.10 – Quantification of target chlorinated hydrocarbon concentrations ( $\mu\text{g mL}^{-1}$ ) in the lake water extract sample by ESM, SAM, and ESM with *P* correction. The peak integration method acronyms are explained in Table 2.3.

| Quantification by external standard method<br>(Eq. 2.3)                           |                 |                 |                   |                 |                 |                 |
|---|-----------------|-----------------|-------------------|-----------------|-----------------|-----------------|
| Peak integration method   |                 |                 |                   |                 |                 |                 |
|   | LT              | LI              | El <sub>6.5</sub> | El <sub>5</sub> | El <sub>4</sub> | DI              |
| std2  | 1.6             | 2.0             | 1.9               | 1.5             | 1.4             | 2.0             |
| std6  | nq <sup>a</sup> | 1.8             | 1.6               | 1.0             | 0.9             | nq <sup>a</sup> |
| std7  | nq <sup>a</sup> | 1.1             | 1.0               | 0.5             | 0.4             | 1.1             |
| std9  | nq <sup>a</sup> | 0.8             | 0.8               | 0.5             | 0.4             | nq <sup>a</sup> |
| std11   | nq <sup>a</sup> | 0.4             | 0.6               | 0.4             | 0.6             | 0.1             |
| std12   | 1.7             | 1.7             | 1.7               | 4.2             | 3.8             | 1.6             |
| std13   | nq <sup>a</sup> | 3.7             | 3.5               | 1.7             | 1.1             | 3.6             |
| std15   | 0.2             | 3.6             | 3.5               | 1.7             | 1.1             | 3.6             |
| std23   | nq <sup>a</sup> | 0.4             | 0.6               | 0.5             | 0.3             | 0.5             |
| std26   | nd <sup>b</sup> | 0.5             | 0.5               | 0.9             | 0.8             | 1.0             |
| std28   | nd <sup>b</sup> | nd <sup>b</sup> | 1.7               | 1.2             | 1.0             | 1.1             |
| Quantification by standard addition method<br>(Eq. 2.6)                           |                 |                 |                   |                 |                 |                 |
| Peak integration method   |                 |                 |                   |                 |                 |                 |
|   | LT              | LI              | El <sub>6.5</sub> | El <sub>5</sub> | El <sub>4</sub> | DI              |
| std2  | 1.3             | 1.8             | 1.9               | 1.7             | 1.6             | 1.9             |
| std6  | nq <sup>a</sup> | 4.0             | 1.9               | 1.5             | 1.4             | nq <sup>a</sup> |
| std7  | 0.8             | 0.9             | 0.7               | 0.6             | 0.5             | nq <sup>a</sup> |
| std9  | nq <sup>a</sup> | 1.2             | 1.4               | 0.8             | 0.7             | 1.5             |
| std11   | nq <sup>a</sup> | nq <sup>a</sup> | 0.8               | 0.7             | 0.8             | nq <sup>a</sup> |
| std12   | 3.0             | 2.4             | 2.6               | nq <sup>a</sup> | nq <sup>a</sup> | 2.4             |
| std13   | nq <sup>a</sup> | 3.0             | 3.0               | 1.7             | 1.3             | 3.0             |
| std15   | nq <sup>a</sup> | 3.0             | 3.0               | 1.7             | 1.3             | 3.0             |
| std23   | nq <sup>a</sup> | 0.8             | nq <sup>a</sup>   | 0.7             | 0.6             | 0.7             |
| std26   | nd <sup>b</sup> | nq <sup>a</sup> | nq <sup>a</sup>   | 1.50            | nq <sup>a</sup> | nq <sup>a</sup> |
| std28   | nd <sup>b</sup> | nd <sup>b</sup> | nq <sup>a</sup>   | nq <sup>a</sup> | nq <sup>a</sup> | nq <sup>a</sup> |
| Quantification by external standard method<br>with <i>P</i> correction (Eq. 2.13) |                 |                 |                   |                 |                 |                 |
| Peak integration method   |                 |                 |                   |                 |                 |                 |
|   | LT              | LI              | El <sub>6.5</sub> | El <sub>5</sub> | El <sub>4</sub> | DI              |
| std2  | 1.4             | 1.8             | 1.8               | 1.8             | 1.6             | 1.8             |
| std6  | nq <sup>a</sup> | 2.7             | 1.4               | 1.2             | 1.0             | nq <sup>a</sup> |
| std7  | nq <sup>a</sup> | 0.8             | 0.8               | 0.5             | 0.4             | nq <sup>a</sup> |
| std9  | nq <sup>a</sup> | 0.7             | 0.6               | 0.5             | 0.3             | nq <sup>a</sup> |
| std11   | nq <sup>a</sup> | nq <sup>a</sup> | 0.4               | 0.4             | 0.5             | nq <sup>a</sup> |
| std12   | 1.8             | 1.1             | 1.2               | nq <sup>a</sup> | nq <sup>a</sup> | 1.0             |
| std13   | nq <sup>a</sup> | 2.5             | 2.5               | 1.7             | 1.0             | 2.4             |
| std15   | 0.1             | 2.6             | 2.6               | 1.8             | 1.1             | 2.5             |
| std23   | nq <sup>a</sup> | 0.3             | nq <sup>a</sup>   | 0.5             | 0.2             | 0.4             |
| std26   | nd <sup>b</sup> | nq <sup>a</sup> | nq <sup>a</sup>   | 1.0             | nq <sup>a</sup> | nq <sup>a</sup> |
| std28   | nd <sup>b</sup> | nd <sup>b</sup> | nq <sup>a</sup>   | nq <sup>a</sup> | nq <sup>a</sup> | nq <sup>a</sup> |

<sup>a</sup> non-quantifiable (nq) because either the offset error of ESM or the offset error of SAM was larger than 50%; <sup>b</sup> "nd" indicates that a peak was not detected by the automated matching algorithms in the sample.



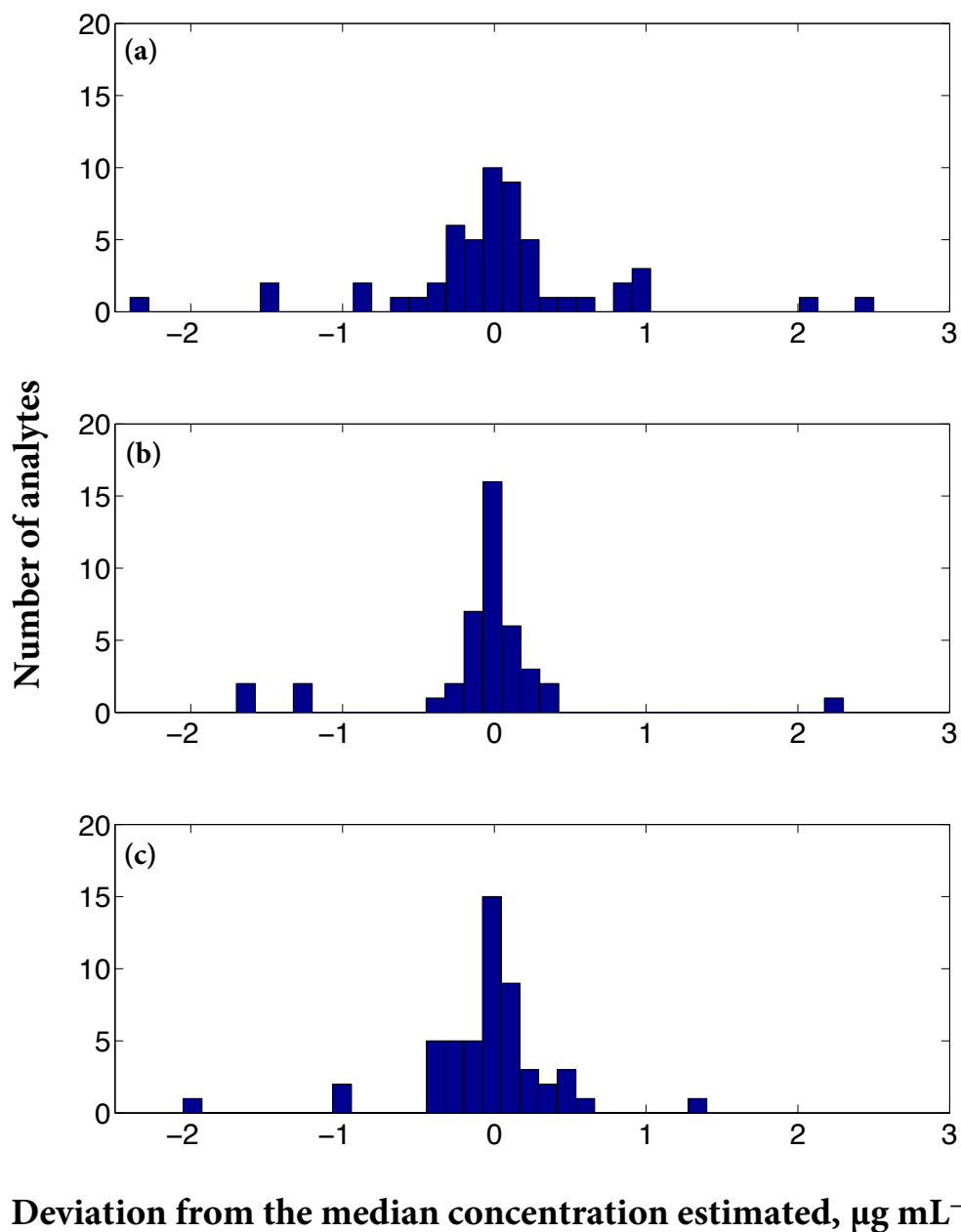


Figure 2.16 – The deviation of the quantified concentration produced by each peak integration method from the median quantified concentration of all peak integration methods, for all quantified analytes, in  $\mu\text{g mL}^{-1}$ : (a) using the external standard calibration method; (b) using the standard addition calibration method; (c) using the external standard calibration method with  $P$  correction.

Table 2.11 – The averaged differences between the concentrations quantified by SAM and by ESM for chlorinated hydrocarbons ( $\mu\text{g mL}^{-1}$ ). The peak integration method acronyms are explained in Table 2.3.

| Quantified by SAM vs by ESM                           |       |       |                   |                 |                 |       |
|---|-------|-------|-------------------|-----------------|-----------------|-------|
| Peak integration method                               |       |       |                   |                 |                 |       |
| Chlorinated standard mix                              | LT    | LI    | EI <sub>6.5</sub> | EI <sub>5</sub> | EI <sub>4</sub> | DI    |
| AAD of conc ( $\mu\text{g mL}^{-1}$ ) <sup>a</sup>    | 0.800 | 0.675 | 0.413             | 0.244           | 0.250           | 0.500 |
| Max AD of conc ( $\mu\text{g mL}^{-1}$ ) <sup>b</sup> | 1.30  | 2.20  | 0.900             | 0.600           | 0.500           | 0.800 |
| Quantified by SAM vs by ESM with <i>P</i> correction  |       |       |                   |                 |                 |       |
| Peak integration method                               |       |       |                   |                 |                 |       |
| Chlorinated standard mix                              | LT    | LI    | EI <sub>6.5</sub> | EI <sub>5</sub> | EI <sub>4</sub> | DI    |
| AAD of conc ( $\mu\text{g mL}^{-1}$ ) <sup>a</sup>    | 0.133 | 0.490 | 0.346             | 0.227           | 0.164           | 0.422 |
| Max AD of conc ( $\mu\text{g mL}^{-1}$ ) <sup>b</sup> | 0.200 | 1.20  | 1.00              | 0.50            | 0.200           | 1.20  |

<sup>a</sup> AAD of concentration is the absolute average deviation between the concentration quantified by SAM and the concentration quantified using ESM, excluding the nq values, for each peak integration method; <sup>b</sup> Max AD is the maximum absolute deviation between the concentration quantified by SAM and the concentration quantified by ESM, excluding the nq values, for each peak integration method.

## 2.4 Conclusions

Recent years have featured extensive developments in new methods for analyzing GC×GC data, including methods to demarcate the baseline and methods to detect and delineate analyte peaks. Taken together, a baseline algorithm and a peak delineation algorithm formulate a complete peak integration method. However little has been done to evaluate peak integration methods for their ability to produce reliable quantifications of analytes in GC×GC chromatograms of real samples. Here, we attempt to address the gap that lies between existing GC×GC peak integration methods and the objective criteria needed to achieve confident analyte quantification in real samples analyzed by GC×GC-FID and GC×GC- $\mu$ ECD.

Using chemometric tests that can be applied to real samples, we assessed several peak integration methods for their abilities to distinguish resolvable analyte signal from unresolved signal and from the instrument background signal. We find that proper demarcation of the baseline is important for achieving a low offset error, good integrated analyte signal reproducibility, proportional integrated signal response, avoidance of matrix effects, and good analyte quantification. The magnitude of the offset error is found to be a good indicator of proper demarcation of the baseline. Some baseline algorithms were found to be overly conservative, including both the GC Image deadband algorithm and the ChromaTOF local linear baseline. These baselines led to inflated offset errors and decreased reliability at analyte quantification. In contrast, the Eilers algorithm, when parameterized to estimate an aggressive

baseline ( $\lambda = 10^4$  or  $10^5$ ), was associated with the best performance in all of our chemometric tests, and this also produced the best analyte quantifications. Our results show that proper demarcation of the baseline is crucial for obtaining reliable, quantitative results from GC×GC univariate data.

Delineation of GC×GC analyte peaks is challenging, and the choice of algorithm is important. The GC Image inverted watershed algorithm and ChromaTOF two-step algorithm both were successful for achieving quantitative delineation of most analytes. However the inverted watershed algorithm sometimes produced inappropriate fragmentations of analyte peaks, leading to large errors in proportional integrated signal response and analyte quantification. Both the inverted watershed and two-step algorithms also sometimes incorporated surrounding unresolved signal together with the analyte signal. This behavior was associated with poor proportional signal response, inflated offset error, and/or altered apparent instrument sensitivity. Interestingly, the choice of baseline algorithm has a substantial impact on the skill of the peak delineation algorithm, even though these algorithms are usually applied in two separate steps. With conservative baseline corrections that aggregate unresolved signal together with the analyte signal, the peak delineation algorithms were prone to define the peak boundary over a region that further exceeded the analyte signal footprint. These combined effects can lead to substantial overestimates of the integrated peak volume.

We show that peak integration methods differ in their tendency to eliminate or generate apparent matrix effects. This is a key consideration when choosing the combination of algorithms to apply to a complex sample. Apparent matrix effects arise from improper discrimination of the analyte signal from the unresolved signal, and thus both the baseline algorithm and peak delineation algorithm are important. Using a traditional standard addition procedure, we find that some peak integration methods avoid matrix effects much more consistently than others. Among the algorithms tested here, the choice of baseline algorithm constituted the chief factor for controlling apparent matrix effects. When judged by either proportional signal response or by apparent instrument sensitivity, the aggressive Eilers baseline ( $\lambda = 10^4$  or  $10^5$ ) led to the most successful elimination of matrix effects. Simply by applying the inverted watershed peak delineation algorithm with two different baseline algorithm (Eilers baseline versus deadband baseline), we find dramatic differences in the resulting severity of apparent matrix effects (Table 2.8). This illustrates clearly the importance of the baseline correction step for controlling matrix effects.

Peak detection was not investigated extensively in this study. Nonetheless, we find that different peak integration methods lead to different sets of detected peaks in the GC×GC chromatogram, and the baseline plays an important role for peak detection. For example, when applied to a GC×GC- $\mu$ ECD chromatogram of lake water extract that was baseline-corrected with an aggressive Eilers algorithm, the inverted watershed delineation algorithm successfully

detected all 17 chlorinated hydrocarbon analytes that had been independently confirmed by GC×GC-ENCI-TOFMS. However when the same chromatogram was subjected to less aggressive baseline algorithms, the inverted watershed algorithm found only 15 or fewer of the confirmed analytes (Table 2.4).

A source of error not discussed in this work is the propagation of analysis replicate uncertainty into the final analyte quantification. These random errors are embedded in our quantification results, which are based on replicate GC×GC analyses of real samples. However we did not specifically diagnose for the impact of replicates variability on our quantification results, which could be handled by applying a propagation of error analysis.

The proposed chemometric tests in this investigation are useful for diagnosing and handling certain sources of error that arise during the quantification of analytes by GC×GC- $\mu$ ECD and GC×GC-FID. However, these tests do not provide a rigorous diagnosis of the reasons behind the failure of a certain combination of baseline correction and peak delineation method, and further study is needed in this direction. Among the peak integration methods assessed here, the EI<sub>4</sub>, EI<sub>5</sub> and LG methods gave the best results for chemometric tests. However, the LG method suffered a high rate of convergence failure when applied to complex matrix. Presently we recommend the EI<sub>4</sub> and EI<sub>5</sub> peak integration methods for analyte quantification of real samples. The aggressive baseline provided by the Eilers algorithm (using  $\lambda = 10^4$  or  $10^5$ ) was associated with the best chemometric test results and the most accurate analyte quantification results. Compared to other baseline methods, the aggressive Eilers baseline also improved the delineation behavior of the inverted watershed algorithm, leading to the fewest incidences of improperly split peaks, for example. Additionally, the EI<sub>4</sub> and EI<sub>5</sub> methods performed better than other methods for eliminating unresolved signal that gave rise to apparent matrix effects. However it is important to recognize that none of the peak integration methods tested here were immune to matrix effects, manifest as overlap or co-elution between the target analyte signal and the unresolved signal. Ultimately, the analyst has to decide which algorithms are most appropriate for quantifying signal data on a case by case basis. Further assessments of these and other methods for peak detection and peak integration, including methods dedicated to signal deconvolution, would be very useful follow-up work to the present study. The diagnostic approaches presented here should provide guidance for further efforts to assess the performance of these and other algorithms, including further studies with other analytes and other samples.

### **3 Overlooked Persistent and Bioac-cumulative Brominated Pollutants in the Deep Water Column of Lake Geneva: 1,3,5-tribromobenzene and 4-bromobiphenyl**

Submitted to: *Environ. Sci. Technol.* 2015 (es-2015-01534y).

Authors: Saer Samanipour, Deedar Nabi, J. Samuel Arey

Contributions: This chapter was prepared by Saer Samanipour with editorial comments by all coauthors, particularly J. Samuel Arey.

### Abstract

We detected and quantified two brominated pollutants, 1,3,5-tribromobenzene (TBB) and 4-bromobiphenyl (4BBP), in the deep water column of Lake Geneva, using comprehensive two dimensional gas chromatography coupled to electron capture detector (GC×GC- $\mu$ ECD) and electron capture negative chemical ionization time-of-flight mass spectroscopy (GC×GC-ENCI-TOFMS). These compounds have not been previously detected in lakes, nor they have been investigated extensively in the environment. Averaged water column concentrations were  $625 \pm 68 \text{ pg L}^{-1}$  for TBB and  $668 \pm 86 \text{ pg L}^{-1}$  for 4BBP over the depth range 70 to 166.5 m, during the summer of 2011. These water column concentrations were one to two orders of magnitude higher than for pentabromoethylbenzene and the polybrominated diphenylethers BDE99, BDE100, and BDE153. Observed vertical concentration trends in the lake water column provide insight into the removal processes affecting these brominated pollutants. Based on analysis of sediment and treated wastewater effluent samples, we concluded that wastewater effluent, urban run-off, and atmospheric deposition are plausible sources of TBB and 4BBP into the lake. Based on their estimated chemical properties, both of these pollutants exhibit likely persistence in the environment, bioaccumulation potential, long range transport potential, and Arctic contamination potential. Wider studies of TBB and 4BBP are recommended.

### 3.1 Introduction

Many nonpolar organic brominated pollutants have been found to persist in the environment, bioaccumulate, and pose an important risk to human health and ecosystem through their toxicity [113, 114, 115, 116, 7]. Most of these compounds are brominated flame-retardants (BFRs) [117, 113] or industrial chemicals [10, 4] having wide commercial use [3, 4]. These brominated persistent and bioaccumulative pollutants (Br-PBPs) are expected to occur and potentially accumulate in surface water systems based on inputs from urban wastewater and run-off, atmospheric deposition, and associated long-range transport [19, 118, 119, 120, 121, 122, 123, 124, 125]. For example, polybrominated diphenyl ethers (PBDEs) and polybrominated biphenyls (PBBs) have been found in the water column and precipitation of the Great Lakes, in biota from the Baltic Sea and North Sea, in surface waters in the Arctic, and in lake sediments in Europe [19, 118, 119, 120, 121, 122, 123, 124, 125]. Many of the PBBs and PBDEs have been widely studied for their environmental fate and behavior [126, 117]. As a result, the US production and use of the most commonly used PBBs (e.g., Firemaster<sup>®</sup> technical mixture) was stopped in 1974 [114], and production in Europe was discontinued after 2000 [120]. Global restrictions have been placed on the production and use of PBDEs employed as flame retardants (e.g., pentaBDE technical mixture) [115].

However, many potential Br-PBPs are currently produced that have undergone much less scrutiny for their environmental impact. This includes so called novel brominated flame-

retardants (NBFRs), which became used as replacements for the discontinued BFRs, PBDEs and PBBs [127]. Howard and Muir recently identified 80 Br-PBPs of various origins that have annual global production volume  $> 1 \text{ t y}^{-1}$  and are considered potentially persistent and bioaccumulative in the environment [3]. Amongst these 80 pollutants, published environmental occurrence data are considered limited for 21 compounds, when compared to well-investigated pollutants such as PBDEs [3]. Hereafter we refer to these pollutants as novel Br-PBPs.

In the present study we conducted a further prioritization on the 21 novel Br-PBPs, which led us to four high priority compounds: 1,3,5-tribromobenzene (TBB), 4-bromobiphenyl (4BBP), pentabromoethylbenzene (PBEB), and hexabromobenzene (HBB). For 4BBP and TBB, very limited published occurrence data are available. 4BBP has been detected in River Daqing sediments, China [128], and TBB was measured in snow cores in Devon Ice Cap, Nunavut, Canada [10]. No other environmental occurrence data are reported for these two pollutants. 4BBP and TBB may have industrial origin [10, 4, 3] and may conceivably arise in the environment as degradation products of PBBs and HBB, respectively [129, 130, 131, 132, 133, 134, 135]. 4BBP and TBB have not been reported in lake systems, even though lakes are well-known convergence areas for persistent pollutants from wastewater treatment plants, urban run-off, and long range transport [32, 136, 7, 19, 119]. PBEB and HBB are presently used NBFRs [126] and have been relatively more widely investigated in the environment [117, 137, 138, 139].

Additionally, little is known about the depth profiles of Br-PBPs in the water column of deep water bodies. Published water column measurements of Br-PBPs in lakes are limited to surface samples having depths  $< 10 \text{ m}$  [19, 36, 37, 9, 38, 49, 21]. However, several modeling studies have suggested that vertical gradients could arise for hydrophobic compounds in the water column, due to transformation or transport processes affecting these pollutants [140, 40, 136, 47]. The measured vertical profiles of polycyclic aromatic hydrocarbons (PAHs) in open seas have demonstrated that such gradients can exist [51]. To our knowledge there are no data available regarding the depth profiles of Br-PBPs in the water column of deep lakes, such as Lake Geneva.

The Br-PBPs are particularly difficult to measure in environmental samples with conventional analytical tools such as gas chromatography coupled to mass spectrometry (GC-MS), due to the complexity of the analyzed matrices and the trace concentration levels of these compounds in the environment [33, 141, 137, 142, 119, 143, 120, 121, 122]. Br-PBPs are difficult to detect with conventional electron impact (EI) ionization used with GC-MS, due to the low sensitivity of EI for these compounds. A much less common technology, GC-MS with electron capture negative chemical ionization (ENCI), is effective for measurement of Br-PBPs [144].

In two recent studies, we developed and validated a highly sensitive analytical method for the

detection, quantification and identity confirmation of trace level halogenated hydrocarbons in environmental samples [15, 16]. This method employs comprehensive two dimensional gas chromatography (GC×GC) coupled to the highly sensitive micro electron capture detector (GC×GC- $\mu$ ECD) and GC×GC coupled to electron capture negative chemical ionization time-of-flight mass spectrometry (GC×GC-ENCI-TOFMS), which enable us to successfully detect and quantify  $\text{pg L}^{-1}$  levels of halogenated hydrocarbons in aquatic samples [15]. By comparison, GC×GC-TOFMS with conventional electron impact (EI) ion source has poorer sensitivity towards halogenated hydrocarbons such as Br-PBPs [145, 146, 147, 148, 149]. Our previous study also evaluated several signal integration approaches for analyte quantification and matrix effect elimination for halogenated hydrocarbons analyzed by GC×GC- $\mu$ ECD [15]. Finally, GC×GC has the additional advantage that environmental partitioning properties can be estimated for nonpolar pollutants based on their GC×GC retention times as long as they have boiling point  $\leq 402$  °C [150].

In the present study, we aimed to: (1) search for the overlooked brominated pollutants TBB and 4BBP as well as (the more widely studied pollutants) PBEB and HBB in the water column and sediments of Lake Geneva, using GC×GC- $\mu$ ECD and GC×GC-ENCI-TOFMS; (2) evaluate concentration trends of these novel Br-PBPs with respect to water depth in the deep lake; (3) and assess the likely characteristic environmental behaviors of these novel Br-PBPs, based on chemical properties estimated by GC×GC retention times and other quantitative structure activity relationship (QSAR) methods.

## 3.2 Experimental section

### 3.2.1 Sampling location

Our sampling site, Lake Geneva, is one of the largest fresh water resources in Europe, having a surface area of  $580 \text{ km}^2$  and a maximum depth of 310 m [151]. Lake Geneva is the main drinking water source for more than 520,000 people [152]. Commercial and recreational fishing in Lake Geneva together amount to approximately 1000 tons of fish per year, used 100% for local consumption [153].

The water column sampling location was located at  $46^{\circ}49'82.88''$  N and  $6^{\circ}58'10.55''$  E (World Geodetic System, WGS84), about 1200 m distance from the lake shore and 500 m distance from the effluent discharge of Lausanne's Vidy wastewater treatment plant (WWTP), which serves a population equivalent of approximately 220,000. This sampling site has a total water depth of 167 m. During the summer of 2011, for the three consecutive months, June, July and August, we deployed two passive samplers at five different water depths. To deploy the passive samplers, we used a stainless steel chain connected to a buoy and a stainless steel bottom release. The sampling depths were: 70, 107, 147, 162 and 166.50 m. The deepest sampling



point was 0.5 m above the sediment bed. We were not permitted to place samplers more shallow than 70 m due to the operation of fishing trawlers at these depths. To protect from biofilm formation and from bioturbation, the passive samplers were placed inside solvent pre-washed stainless steel cages. The cages were then deployed at the desired depths.

We also collected sediment cores at four widely separated locations of the lake (Figure 4.1), using either a Benthos gravity corer from a boat (Sed1 and Sed4) or a human-occupied MIR submersible (Sed2 and Sed3) during the ELEMO field campaign, 2011 [151]. The sediment samples were collected in locations having total depths of: 167 m (Sed1), 310 m (Sed2), 180 m (Sed3) and 80 m (Sed4). After collection, sediment samples were brought immediately to the lab and stored at  $-20^{\circ}\text{C}$  until extraction for analysis.

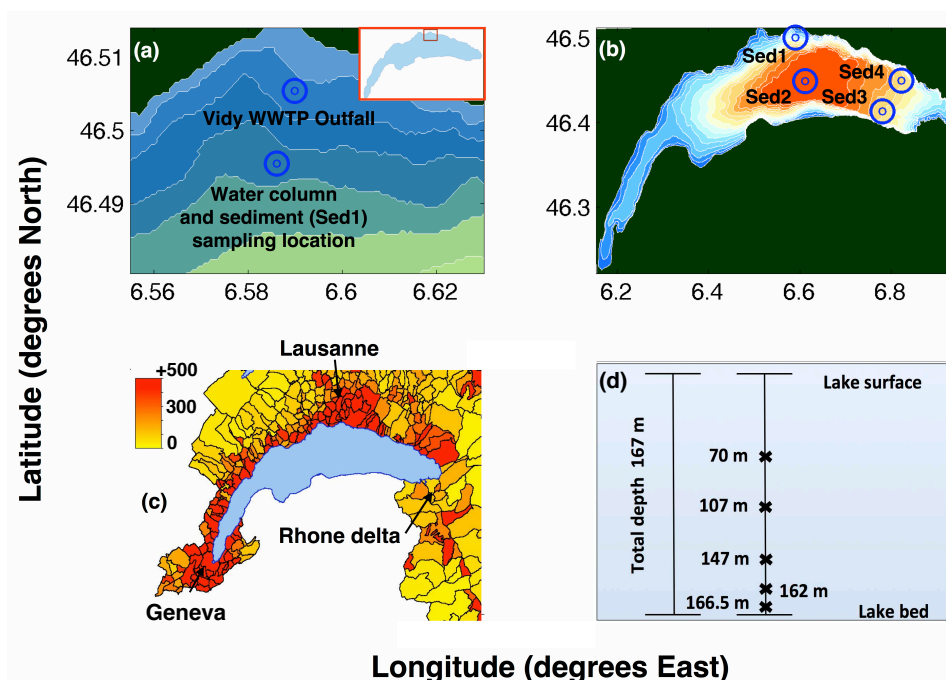


Figure 3.1 – Maps depicting (a) sampling location for the water column and sediment (Sed1) in Lake Geneva, with lake bathymetry contours of 45 m overlaid; (b) the four sediment sampling locations, with bathymetry contours of 20 m overlaid; and (c) population density of the Lake Geneva area ( $\text{person km}^{-2}$ ), by municipality, 2007 (source: bfs.admin.ch). (d) Schematic showing depths at which the water column samplers were deployed.

### 3.2.2 Target analyte selection

To identify Br-PBPs of high priority, we performed a prioritization screening on the 21 novel Br-PBPs listed in the Howard and Muir 2010 paper [3]. The screening criteria were that chemicals must be: (1) amenable to GC- $\mu\text{ECD}$  without derivatization; (2) neutral; (3) thermally

### Chapter 3. Overlooked brominated pollutants in Lake Geneva

---

stable; (4) available as analytical chemical standards from research chemical suppliers; (5) registered in the European Union's Registration, Evaluation and Authorization of Chemicals (REACH) database; (6) and not banned from production in Europe. Applying these criteria led us to four high priority novel Br-PBPs: 4-bromobiphenyl (4BBP), 1,3,5-tribromobenzene (TBB), hexabromobenzene (HBB), and pentabromoethylbenzene (PBEB).

We additionally analyzed for the legacy pentaBDE technical mixture, which consisted of 2,2',4,4'-tetrabromodiphenyl ether (BDE47), 2,2',4,4',5-pentabromodiphenyl ether (BDE99), 2,2',4,4',6-pentabromodiphenyl ether (BDE100), 2,2',4,4',5,5'-hexabromodiphenyl ether (BDE153), and 2,2',4,4',5,5'-hexabromodiphenyl (HBBP). Throughout the present article we refer to this technical mixture as "pentaBDEs". These compounds had a historical high volume of production [122], and are considered to constitute one of the most toxic PBDE technical mixtures distributed in commerce [154]. This mixture has been widely investigated in the environment in different parts of the world, including Switzerland [119, 143, 142, 121, 122, 123, 124, 155, 156]. Our findings for the pentaBDEs provided a point of comparison for interpreting the levels and trends of the novel Br-PBPs in Lake Geneva.

#### 3.2.3 Chemicals

We purchased analytical standards PCB 30, PCB 50, PCB 145, PCB 204, 4-bromobiphenyl, 1,3,5-tribromobenzene, 2,3,4,5,6-pentabromoethylbenzene, and hexabromobenzene from Sigma-Aldrich Switzerland. We purchased technical pentaBDE mixture (EPA method 527) from AccuStandard Switzerland (see Table B.1 in Supporting Information). Diatomaceous earth, Florisil, and sodium sulfate were purchased from Sigma-Aldrich. We obtained pesticide grade hexane, ACS grade acetone, and ACS grade pentane from VWR Switzerland.

#### 3.2.4 Water column sampling

Passive samplers are often employed for measurements of persistent and bioaccumulative pollutants in aquatic systems, due to their low expense to deploy, ease of storage and transport, and stability over time [157, 158, 159, 160]. The rate constant describing pollutant uptake into strips from the water column ( $k_e$ ) was estimated based on the rates of disappearance of several performance reference compounds (PRCs) during the sampling period (Eq. A.1 in Appendix) [161, 30, 162]. For more information see Appendix, section A.1.

#### 3.2.5 Sample preparation and clean-up

##### Extraction of the passive samplers deployed in the lake

For passive sampling of the water column we used polydimethylsiloxane sheets (PDMS, AlteSil Laboratory Sheet, UK) of thickness 0.5 mm. PDMS exhibits linear mass transfer behavior

over a wide range of sorbate  $K_{ow}$  values [163, 164]. The PDMS sheets were cut into strips of  $10 \times 1 \times 0.05 \text{ cm}^3$  and had an average weight of  $1.98 \pm 0.20 \text{ g}$ . The strips were then cleaned using Soxhlet extraction with methanol for 24 hours [22, 165, 166, 167] and subsequently stored at  $-20 \text{ }^\circ\text{C}$ . Five cleaned strips were used as the PDMS blank. Before the field deployment we loaded the PDMS strips with four PRCs (PCB 30, PCB 50, PCB 145, PCB 204) to a concentration of  $20 \text{ ng g}^{-1}$  of each standard. The details of the PRC loading process are explained elsewhere [162]. After the loading step, five strips were used to determine the initial PRC concentrations in the strips. After deployment in the lake, extraction of the strips was carried out by soaking them in 20 mL of pentane for eight hours, three consecutive times. The volume of the final extract (60 mL) was reduced to 1 mL by rotary evaporation and simultaneously solvent-exchanged to hexane. The final extract was stored at  $-20 \text{ }^\circ\text{C}$  until analysis. We did not perform any clean-up step on the final extract.

For quality assurance, we analyzed four different types of blanks. These were: the 5 PDMS blanks (explained above); the solvent blanks, which were the solvents used for extraction (pentane and hexane); 3 field blanks, which were extracts of loaded strips brought to the field but not deployed; and the method blank, which was a solvent extract of the glassware used for the extraction and rotary evaporation.

### Sediment samples extraction and clean-up

We culled sediment from the top 1 cm of each sediment core (Figure A.1). Only the center section of the sediment core was taken, thereby excluding sediment in contact with the plastic walls of the coring tube. The resulting sediment samples had an approximate dry weight of 5 g each. Each lake sediment sample was air dried and then homogenized (EPA method EPA-823-B-01-002, revision of October 2001). 0.5 g of each homogenized sediment sample was extracted using Accelerated Solvent Extraction (ASE), which was a modified version of EPA Method 3545A, Revision 1 February 2007 [16]. Further method details are given in section A.2 of Appendix.

### 3.2.6 GC×GC- $\mu$ ECD and GC×GC-ENCI-TOFMS conditions

We analyzed water column extracts and sediment extracts with a Leco Corp GC×GC- $\mu$ ECD instrument equipped with a modified Agilent 7890A GC system having a split/splitless injector and a dual-stage quadrupole-jet modulator. We separated the samples using a 30 m length, 0.25 mm inner diameter (i.d.), 0.25  $\mu\text{m}$  film thickness RTX-1 column (Restek, USA) as the first dimension, and 2 m length, 0.1 mm i.d., 0.1  $\mu\text{m}$  film thickness BPX-50 column as the second dimension (Restek, USA). Further instrument details are provided in Supporting Information, section A.3.

GC×GC coupled to electron capture negative chemical ionization (ENCI)-time of flight-mass spectrometer (TOFMS) (Zoex Corp. USA) was used to additionally analyze three lake water extracts and two sediment sample extracts. Instrument details are reported in Supporting Information, section A.3.

### 3.2.7 Target analyte quantification

All chromatograms were baseline-corrected using the Eilers baseline [82] via Matlab. The three unitless algorithm parameters,  $\lambda$ ,  $p$  and  $d$ , were set to  $10^4$ , 0.02, and 2, respectively. The Eilers baseline is effective for eliminating poorly resolved background signal in complex samples analyzed by GC×GC [15, 80]. After baseline correction, analyte peaks were integrated with the inverted watershed algorithm implemented in the GC Image package (GC Image, LLC [81]). The peak integration parameters in the GC Image software were set to default values (Table A.2). This combination of baseline correction and peak integration algorithms was recently shown to give good performance for analyte quantification by GC×GC- $\mu$ ECD and GC×GC-FID [15].

### 3.2.8 Chemical property estimation

We estimated several environmentally relevant chemical properties of both the novel and legacy Br-PBP target analytes. Where experimental property data were available, we gave priority to those values. For TBB, 4BBP, PBEB, HBB, and BDE47, several partitioning properties were estimated using GC×GC retention times [150]. For compounds having boiling point > 402 °C (BDE99, BDE100, BDE153, and HBBP), we used EPISuite [168]. We also assessed target analytes for persistence using BIOWIN [168] and the expert judgment criteria for biodegradability potential [169, 3].

## 3.3 Results and Discussion

### 3.3.1 Successful detection, identity confirmation, and quantification of target analytes by GC×GC- $\mu$ ECD and GC×GC-ENCI-TOFMS

With GC×GC- $\mu$ ECD we successfully detected and quantified 7 out of 9 target Br-PBPs in water extracts and 4 out of 9 target Br-PBPs in sediment extracts (Figure A.2, Table 3.2 and Table A.3). GC×GC- $\mu$ ECD is seldom applied for trace analysis of halogenated pollutants, despite being roughly two orders of magnitude more sensitive than conventional GC-MS for halogenated analytes. Here we achieved excellent separation of the target analytes, even though limited sample clean-up was applied (Figures A.2). Limit-of-quantification (LOQ) values range from 1.0-50 pg L<sup>-1</sup> for water column samples and from 3.5-4.0 pg g<sup>-1</sup> for sediment samples, depending on the analyte (Table 3.1).

For selected samples, GC×GC-ENCI-TOFMS analysis provided further successful identity confirmation for the Br-PBPs, delivering far better separation and sensitivity for halogenated compounds than conventional GC-MS with electron impact source. We applied a five-point criterion for target analyte identity confirmation by GC×GC-ENCI-TOFMS. These were: positive matches between standard peak and sample analyte peak for retention times in both the first and second dimension, and positive matches between standard peak and target peak for three  $m/z$  values within a tolerance level of 5 mmu (Table 3.1). This procedure is in conformity with criteria for identity confirmation established by the European Union [87]. Using this methodology, we observed 100% agreement between GC×GC- $\mu$ ECD and GC×GC-ENCI-TOFMS for positive detection of Br-PBPs, and we also observed 100% agreement for negative detection (absence) of Br-PBPs, over all 9 target compounds in 5 different samples (Table 3.1). Further details on methods used for detection, quantification, and identity confirmation of halogenated analytes by GC×GC- $\mu$ ECD and GC×GC-ENCI-TOFMS are provided in our recent report [15].

In collaboration with the ENCI-TOFMS manufacturer (Tofwerk, Switzerland), we evaluated the mass precision of the GC×GC-ENCI-TOFMS instrument, where the mass precision is defined as the difference between the exact mass of the fragment and the measured accurate mass of that fragment. We evaluated the mass precision based on an injection of 100 pg of octafluoronaphthalene (OFN) into the instrument. This demonstrated that under optimized conditions (i.e. methane pressure, temperature of ionization chamber, and the fitting of the mass calibration models) the instrument produces a mass precision of  $\pm 2$  mmu for the 271.9872 spectral fragments produced by OFN. However, we did not optimize the instrument conditions for our target analytes. Therefore we assume that the non-optimized instrument has (not better than) unit mass accuracy for the absolute  $m/z$  values of injected standards, and thus we report only unit mass values for the major fragments of these mass spectra (Table 3.1). However, we still assume that the instrument has a high mass precision for the purposes of comparing injected standards with target analyte peaks in samples. For the pollutants listed in Table 3.1, we consistently observed mass differences of  $\leq 5$  mmu between the spectra of the standards and the target peaks in environmental samples, despite that the system was not optimized to produce the accurate masses of the target analytes. This justifies our criteria for positive detection of target analytes outlined above in this section.

#### 3.3.2 Concentrations and trends of target Br-PBPs in the water column of Lake Geneva

Although never reported previously in lakes, 4BBP and TBB were found to have water column concentrations approaching  $1 \text{ ng L}^{-1}$ , one to two orders of magnitude higher than the legacy pentaBDEs. The depth-averaged concentration of 4BBP was  $625 \pm 68 \text{ pg L}^{-1}$  and the

Table 3.1 – GC×GC-ENCI-TOFMS retention times and monitored m/z values, and the frequency of positive detection of the target analytes in selected samples by GC×GC- $\mu$ ECD and GC×GC-ENCI-TOFMS.

| Less studied Target analytes | Acronym | Compound                               | $t_{R1}^d$ (min) | $t_{R2}^e$ (s) | Molecular weight $M_w$ | Mass spectra <sup>c</sup> |                    |                    |                    | Water samples   |            |             |  | Sediment samples |            |             |  |
|------------------------------|---------|--|------------------|----------------|------------------------|---------------------------|--------------------|--------------------|--------------------|-----------------|------------|-------------|--|------------------|------------|-------------|--|
|                              |         |  |                  |                |                        | (m/z) <sub>1</sub>        | (m/z) <sub>2</sub> | (m/z) <sub>3</sub> | (m/z) <sub>4</sub> | GC×GC $\mu$ ECD | ENCI-TOFMS | GC×GC TOFMS | GC×GC- $\mu$ ECD LOQ (pg L <sup>-1</sup> ) | GC×GC $\mu$ ECD  | ENCI-TOFMS | GC×GC TOFMS | GC×GC- $\mu$ ECD LOQ (pg g <sup>-1</sup> ) |
|                              | TBB     | 1,3,5-tribromobenzene                  | 14.47            | 2.78           | 314.7999               | 79                        | 233                | 235                | -                  | 3/3             | 3/3        | 3/3         | 50   | 0/2              | 0/2        | 0/2         | 3.8  |
|                              | 4BBP    | 4-bromobiphenyl                        | 20.37            | 3.54           | 233.1039               | 81                        | 233                | 235                | -                  | 3/3             | 3/3        | 3/3         | 14   | 2/2              | 2/2        | 2/2         | 4.0  |
|                              | PBBB    | 2,3,4,5,6-pentabromomethylbenzene      | 32.53            | 4.55           | 500.6453               | 81/8 <sup>f</sup>         | 500 <sup>g</sup>   | 502 <sup>g</sup>   | -                  | 3/3             | 3/3        | 3/3         | 2.2  | 2/2              | 2/2        | 2/2         | 4.0  |
|                              | HBB     | hexabromobenzene                       | 36.93            | 5.42           | 551.4882               | 81                        | 233                | 235                | 315                | 0/3             | 0/3        | 0/2         | 30   | 0/2              | 0/2        | 0/2         | 3.5  |
|                              | BDE147  | 2,2',4,4'-tetrabromodiphenyl ether     | 38.13            | 4.68           | 485.7914               | 79                        | 366                | 368                | 370                | 0/3             | 0/3        | 0/3         | 1.0  | 0/2              | 0/2        | 0/2         | 4.0  |
|                              | BDE199  | 2,2',4,4',5'-pentabromodiphenyl ether  | 42.93            | 5.10           | 564.6875               | 79                        | 159                | 161                | 163                | 3/3             | 3/3        | 3/3         | 1.0  | 2/2              | 2/2        | 2/2         | 3.8  |
|                              | BDE100  | 2,2',4,4',6'-pentabromodiphenyl ether  | 41.87            | 4.86           | 564.6875               | 79                        | 159                | 161                | 163                | 3/3             | 3/3        | 3/3         | 2.1  | 0/2              | 0/2        | 0/2         | 3.6  |
|                              | BDE153  | 2,2',4,4',5,5'-hexabromodiphenyl ether | 47.17            | 5.22           | 643.5836               | 79                        | 159                | 161                | 163                | 3/3             | 3/3        | 3/3         | 1.0  | 2/2              | 2/2        | 2/2         | 4.0  |
|                              | HBBP    | 2,2',4,4',5,5'-hexabromobiphenyl       | 46.25            | 5.30           | 627.5843               | 81/8 <sup>f</sup>         | 627 <sup>g</sup>   | 629 <sup>g</sup>   | -                  | 3/3             | 3/3        | 3/3         | 1.0  | 0/2              | 0/2        | 0/2         | 3.8  |

<sup>a</sup> In 3 PDMS strips collected at 166.5 m during June, July, and August, 2011; <sup>b</sup> In Sed1 and Sed2 collected at the passive sampling location and center of the lake; <sup>c</sup> Mass spectrum m/z values shown are from the present study unless indicated otherwise; <sup>d</sup> First dimension GC×GC retention time; <sup>e</sup> Second dimension GC×GC retention time; <sup>f</sup> Koljic et al [170]; <sup>g</sup> Hoffmann et al [171].

depth-averaged concentration of TBB was  $668 \pm 86 \text{ pg L}^{-1}$  over three the month sampling period (Figure 3.2). For PBEB the concentration was  $7 \pm 1.8 \text{ pg L}^{-1}$ , and HBBP was not detected (LOD of  $10 \text{ pg L}^{-1}$ ). By comparison, measured levels of the pentaBDEs ranged from  $2 \pm 0.8 \text{ pg L}^{-1}$  (HBBP) to  $27 \pm 7 \text{ pg L}^{-1}$  (BDE99). These pentaBDEs levels are comparable to water column concentrations of the same compounds reported in all five Great Lakes [19, 38] and in rivers and lakes in Europe, including Lake Thun and Greifensee in Switzerland [122, 124]. Higher levels of pentaBDE compounds have been reported in Niuchao Lake, China ( $4020 \text{ pg L}^{-1}$  winter and  $520 \text{ pg L}^{-1}$  summer) [36]. The surprisingly high water column levels of 4BBP and TBB in Lake Geneva warrant concern, and further environmental measurements of these pollutants are needed.

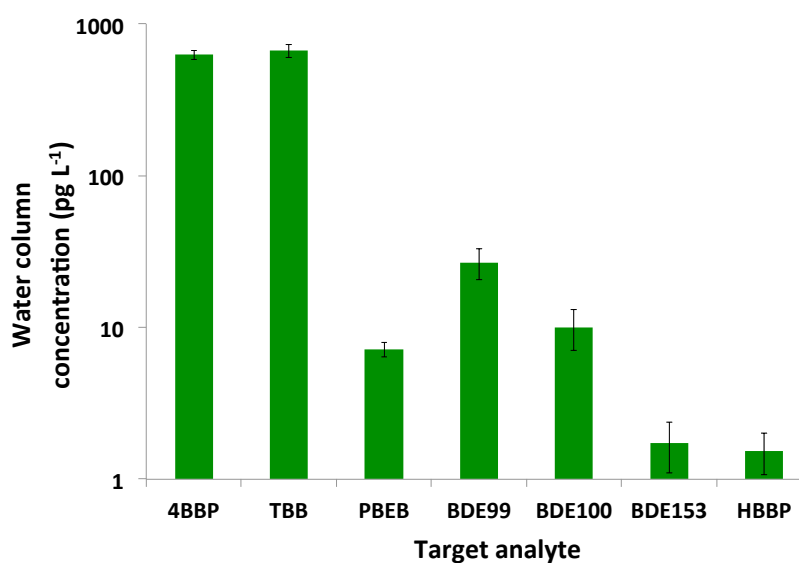


Figure 3.2 – The average water column concentrations of the target analytes. The error bars show the concentration variability ( $\pm 2$  standard deviations) over 30 water column samples taken at five different depths during three sampling periods (June, July, and August 2011).

Water column concentrations of 4BBP and PBEB exhibited no statistically significant trend over the sampled depth range of 70 to 165.5 m, whereas vertical concentration trends were observed for TBB and the legacy pentaBDE compounds (Figures 3.3 and A.3). The vertically uniform concentrations of 4BBP and PBEB suggest a situation of slow change, in which compound source or removal processes (assumed to be near the lake surface or at the sediment bed) are slow relative to vertical transport in the water column. We assumed that the water column in this sampling area had experienced complete vertical mixing during the winter prior to the sampling campaign; the 2011 winter holomixis was reported to have reached a depth of 200 m [172]. TBB and BDE100 both exhibit a trend of decreasing concentration with increasing depth, over the sampled depth range. This may indicate active biodegradation of

### Chapter 3. Overlooked brominated pollutants in Lake Geneva

---

these pollutants at the sediment bed [129, 131, 130, 148, 173]. Anaerobic dehalogenation has been previously documented for PBDEs in other sediments (Table 3.3) [148, 173]. Finally, the legacy compounds BDE153, BDE99, and HBBP exhibited decreased relative concentrations at 70 m depth, followed by elevated concentrations at 107 m depth, and decreased concentrations at 147-166.5 m depth (Figures 3.3 and A.3). The hump-shaped vertical concentration profiles of these three pentaBDEs may indicate removal due to direct photolysis near the lake surface and anaerobic dehalogenation at the sediment bed. Again, we assumed that these compounds had vertically homogenized water concentrations during the previous winter's holomixis. When exposed to direct sunlight, BDE153, BDE99, and HBBP all undergo direct photolysis within hours, whereas this process is much less rapid for BDE100 (Table A.4) [174, 175]. These relative magnitudes in the rates of direct photolysis are roughly consistent with the observed concentration trends of BDE153, BDE99, HBBP, and BDE100 between 70 and 107 m (Figures 3.3 and A.3). Photolysis rates are not reported in the literature for TBB, 4BBP, and PBEB. At all measurement locations, all measured pollutants except BDE153 and HBBP exhibited statistically unchanging concentrations over the three individual one-month measurement periods of June, July, and August 2011. The temporal stability of measured concentrations further lends confidence to the interpretation that the observed vertical trends are meaningful.

The lake appeared well-stratified at the passive sampling location, exhibiting a thermocline between 15-35 m depth (Figure 3.4). At the sampled depth range (70-167 m) the water column temperature varied between 5.9 °C at 70 m depth and 5.6 °C at 167 m depth. The temperature profile at the passive sampling location suggests that the water column of the lake at that location may be reasonably vertically well mixed. However, the concentration profiles of some of the analyzed PBPs (e.g. TBB and BDE153) indicated the presence of statistically meaningful concentration differences with respect to the depth, as discussed above. In the absence of more sophisticated (e.g., 3-dimensional and time-dependent) modeling of the lake physics, it is not straightforward to interpret the water mass mixing in this area of the lake. Therefore these temperature profile data were considered insufficient to make quantitative inferences about vertical or horizontal transport of PBPs at this sampling location.

Limited published data are available regarding the vertical concentration trends or gradients for hydrophobic compounds in aquatic systems, especially in the deep water column. However, modeling efforts have suggested that hydrophobic compounds could exhibit vertical gradients in large aquatic or marine systems, due to the simultaneous influences of currents and turbulent mixing, air-water exchange, atmospheric deposition, sedimentation, and transformation reactions [140, 136, 47, 40]. Lake Geneva exhibits a spatially and temporally complex physical structure, diverse pollutant inputs, and highly variable forcing from the overlying wind field [176, 172]. Thus, confident interpretations of the observed pollutant concentration trends would require more measurement data and the modeling of relevant sources and processes affecting these hydrophobic compounds. Nonetheless, the observed water column trends at our sampling site suggest insight into the relative susceptibilities of these Br-PBPs



toward removal by anaerobic degradation at the sediment bed and photolysis in the upper water column.

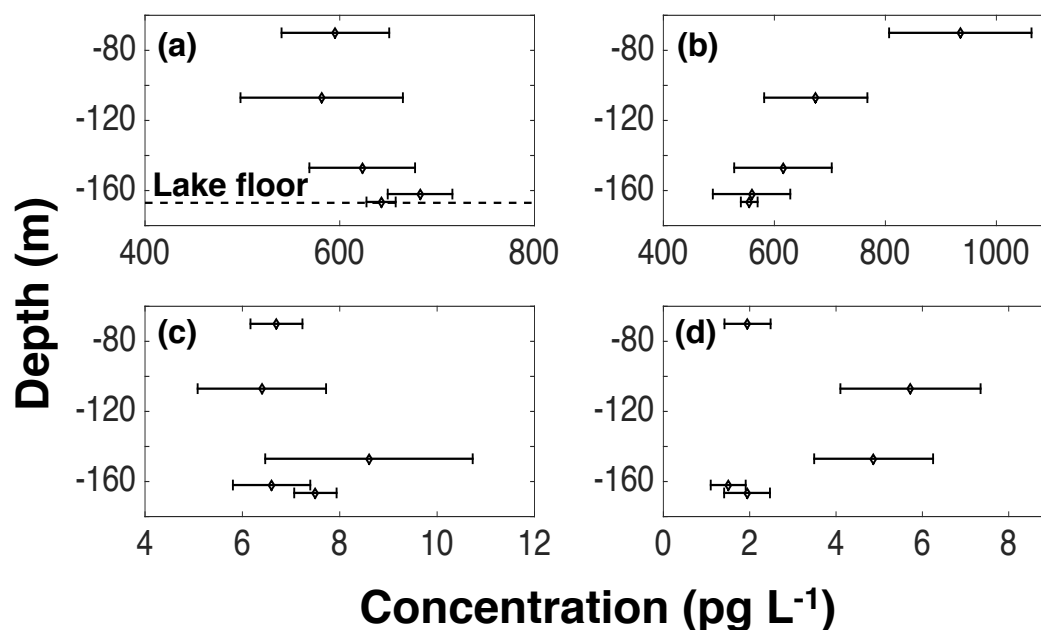


Figure 3.3 – Water column concentration with respect to depth for (a) 4BBP; (b) TBB; (c) PBEB; and (d) BDE153. The error bars indicate the observed concentration variability (95% confidence interval) over the three-month sampling period.

### 3.3.3 Occurrence of target Br-PBPs in the lake sediments

At the same site where water column samples were taken (Figure 3.3), sediment concentrations of 4BBP, PBEB, BDE99, and BDE153 were successfully quantified (Sed1, Table 3.2). At this sampling site, sediment concentrations of 4BBP, BDE99, and BDE153 were found to be approximately explained by partitioning equilibrium with the overlying water column. For these three compounds, the sediment-water concentration ratio ( $C_{Sed1}/C_{water}$ ) were reasonably consistent with with estimated equilibrium partitioning coefficient ( $K_d$ ) values, exhibiting discrepancies of a factor of 6 or less (Table 3.3).  $K_d$  values were estimated by assuming that these Br-PBPs sorb to the organic matter of the sediment [32] based on a measured fraction of organic carbon ( $f_{oc}$ ) value of 0.059 reported [177] at a nearby location (Table 3.3). However for PBEB the  $C_{Sed1}/C_{water}$  ratio was 28 times smaller than the estimated  $K_d$ . This discrepancy may be explained by active biodegradation of PBEB in the sediment or error in the estimated  $K_d$  value. For TBB, BDE100, and HBBP, which were not detected in Sed1, we used the sediment limit-of-detection (LOD) value to estimate an upper bound on the possible  $C_{Sed1}/C_{water}$  value. For TBB, sediment concentrations are at least 33 times lower than can be explained by partitioning equilibrium with the water column, according to our estimated  $K_d$ . Based on this finding and the observed water column gradient for this pollutant (Figure 3.3), we

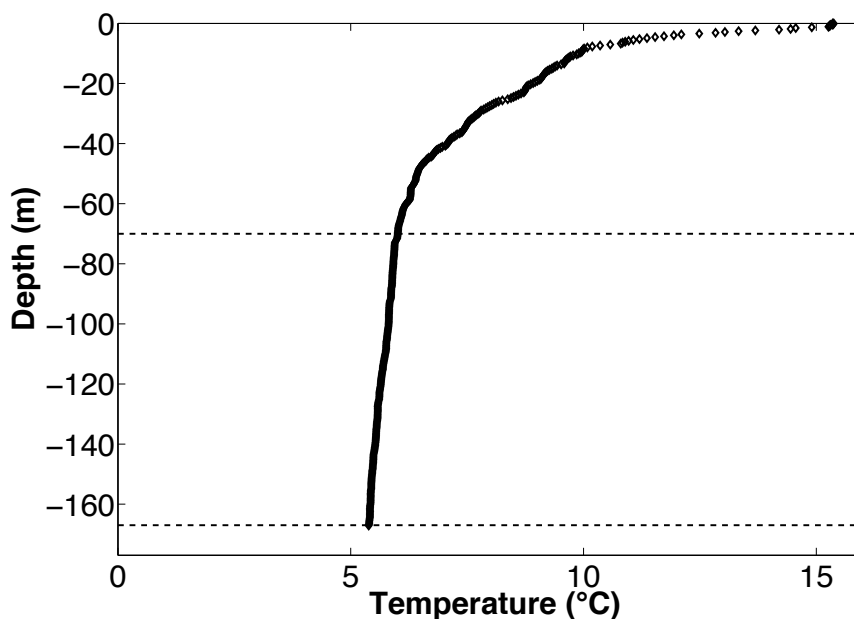


Figure 3.4 – Water column temperature profile of Lake Geneva at the passive sampling location. The dotted lines depict the sampled depth range. Data are provided by Neil Graham, University of Geneva.

propose that sediments of the lake in that location may rapidly eliminate TBB via anaerobic degradation. HBBP was not detected in any of sediment samples and was detected in the water column only during August, 2011; therefore we did not draw any conclusions about this compound. Finally, HBB and BDE47 were detected neither in the water column nor in the sediments.

We observed elevated concentrations of all target analytes in sediment samples collected in the middle of the deep lake (Sed2) and near the highly urbanized area of Lausanne (Sed1) relative to samples collected in eastern region of the lake (Sed3 and Sed4), as shown in Table 3.2. The observed concentration distributions at these four sampling sites may provide insight into the sources of these pollutants into the lake, and this is discussed further in the next section. The highest measured 4BBP sediment concentration in Lake Geneva ( $187.0 \text{ pg g}^{-1}$ ) was higher than the 4BBP concentration reported in the River Daqing sediment samples in China (up to  $40 \text{ pg g}^{-1}$ ). For BDE99, we observed sediment concentrations in Lake Geneva that were comparable to levels reported in sediments of Lake Thun, Switzerland, ( $200\text{-}1600 \text{ pg g}^{-1}$ ) and for BDE153 we observed sediment levels that were two orders of magnitude smaller than reported in Llobregat River, Spain ( $17,000 \text{ pg g}^{-1}$ , Table 3.2). Concentrations of BDE99 were smaller than the reported levels in other American and European lakes and rivers sediment by between one to three orders of magnitude (Table 3.2) [122, 125, 124, 182, 178, 179, 180].

Table 3.2 – Sediment concentrations of the detected target analytes in the sediment samples.<sup>a</sup>

| Target analyte | Concentration in the sediments of Lake Geneva (pg g <sup>-1</sup> ) <sup>b</sup> |       |                    |                    | Literature values for other sediments (pg g <sup>-1</sup> )           |
|----------------|--|-------|--------------------|--------------------|---|
|                | Sed1   | Sed2  | Sed3               | Sed4               |   |
| 4BBP           | 59.5   | 187.0 | < 4.0 <sup>c</sup> | < 4.0 <sup>c</sup> | nd-40.0 <sup>d</sup>  |
| PBEB           | 4.5  | 13.7  | < 4.0 <sup>c</sup> | < 4.0 <sup>c</sup> | nd-32.0 <sup>e</sup> , nd-10.0 <sup>f</sup> , and nd-100 <sup>g</sup> |
| BDE99          | 65.9   | 89.6  | < 4.0 <sup>c</sup> | 15.5               | nd-10,000 <sup>f</sup> , and 200-1,600 <sup>h</sup>                   |
| BDE153         | 28.6   | 33.0  | < 4.0 <sup>c</sup> | 5.2                | nd-17,000 <sup>f</sup>  |

<sup>a</sup> TBB, HBB, BDE47, BDE100 and HBBP were not detected in any of sediment samples; <sup>b</sup> The concentration is expressed per dry weight of the sediment sample; <sup>c</sup> The target was detected in the sample, however its concentration was smaller than the sediment LOQ; <sup>d</sup> Sediment samples of 14 rivers from Hai River Basin, China [128]; <sup>e</sup> Sediment samples from Loselva River, Norway [178]; <sup>f</sup> Sediment samples from Llobergat River, Spain [179]; <sup>g</sup> Sediment samples from San Francisco Bay [180]; <sup>h</sup> Sediment samples from Lake Thun, Switzerland [125, 124].

### 3.3.4 Potential sources of the target analytes

TBB and 4BBP have several conceivable sources in the environment, but little is known about their global production and distribution volumes. Both TBB and 4BBP have estimated global production volumes of > 1 t y<sup>-1</sup>, [3] and the major producer of these chemicals is China [175]. 4BBP is utilized in industrial synthesis of different chemicals, including rodenticides, pharmaceuticals, and personal care products [183, 184, 185]. Similarly, TBB is used as a reagent in production of different pharmaceuticals and personal care products [186, 187]. TBB is also used as an added flame retardant together with HBB during the production of organic polymers [188, 189]. TBB and 4BBP are additionally found to be the anaerobic dehalogenation products of HBB and HBBP, after several successive dehalogenation reactions [129, 130, 131, 135, 132]. PBEB and HBB are still in use as NBFs [117].

We considered plausible pathways for the introduction of TBB and 4BBP into Lake Geneva. The presence of these compounds seemed unlikely to be explained by dehalogenation of higher brominated congeners. Although TBB and 4BBP are dehalogenation products of HBB and HBBP, respectively, they are not the main products of these pathways [132, 135, 129, 130, 131]. Additionally, in our search of the GC×GC-ENCI-TOFMS data of all of the analyzed sediment samples, we failed to find the target ions for 1,3,4,5-tetrabromobenzene and 2,2-dibromobiphenyl, which are the transformation intermediates that would be expected to produce TBB and 4BBP upon dehalogenation, respectively [129, 130, 131, 135, 132]. Therefore the surprisingly high levels of TBB and 4BBP in the water column of the lake are unlikely to be explained by *in situ* production of these compounds through the anaerobic dehalogenation of HBB and HBBP, respectively. Considering their industrial use, TBB and 4BBP may plausibly be present in industrial and urban waste water effluents. In a recent study by our group, TBB was

Table 3.3 – Comparison of the estimated sediment-water equilibrium partitioning constant<sup>a</sup> ( $K_d$ ) with the sediment-water column concentration ratio ( $C_{Sed1}/C_{water}$ ) at sampling site Sed1.

| Compound | Estimated<br>log $K_d^a$<br>(L kg <sup>-1</sup> ) | Observed<br>log $C_{Sed1}/C_{water}^b$ | Anaerobic<br>dehalogenation<br>half life (weeks) |
|----------|---|--|--|
| TBB      | 2.28 <sup>c</sup>                                 | ≤ 0.76 <sup>d</sup>                    | not determined <sup>e</sup>                      |
| 4BBP     | 2.78 <sup>c</sup>                                 | 1.98 ± 0.06                            | 1 <sup>f</sup>                                   |
| PBEB     | 4.24 <sup>c</sup>                                 | 2.80 ± 0.09                            | not determined <sup>e</sup>                      |
| BDE100   | 3.92 <sup>g</sup>                                 | ≤ 2.86 <sup>d</sup>                    | 2 <sup>g</sup> , 25 <sup>h</sup>                 |
| BDE99    | 2.92 <sup>i</sup>                                 | 2.99 ± 0.22                            | 2 <sup>g</sup> , 25 <sup>h</sup>                 |
| BDE153   | 4.41 <sup>i</sup>                                 | 4.29 ± 0.04 <sup>j</sup>               | 2 <sup>g</sup> , 25 <sup>h</sup>                 |
| HBBP     | 6.60 <sup>i</sup>                                 | ≤ 3.59 <sup>j, d</sup>                 | 50 <sup>k</sup>                                  |

<sup>a</sup> Estimated as  $K_d = f_{oc} \times K_{oc-w}$ , where  $f_{oc} = 0.059$  is the fraction of organic carbon in sediments reported at a location about 200 m distance from the Sed1 site and at a total depth of 100 m [181, 177]; <sup>b</sup> Measured sediment-water concentration ratio (L kg<sup>-1</sup>), based on levels observed in the Sed1 sample (July, 2011) and the averaged water column concentration during June-August 2011; <sup>c</sup> Based on  $K_{oc-w}$  estimated from GC×GC retention times according to the model of Nabi et al [150]; <sup>d</sup> This upper bound value is computed using the sediment LOD, defined as LOQ/3 (Table 3.1); <sup>e</sup> No data are available for anaerobic degradation half-life of this compound; <sup>f</sup> This value was measured with inoculated Woods Pond (Lenox, Mass.) sediments after one week of acclimation [131]; <sup>g</sup> This value was determined using three different cultures of anaerobic dehalogenating bacteria (inoculated) added to San Francisco Bay sediments [148]; <sup>h</sup> This value was determined using two different sediment samples collected from Er-Jen River and Nan-Kan River basins without inoculation [173]; <sup>i</sup> Based on a  $K_{oc-w}$  value estimated using EPISuite; <sup>j</sup> This value is based on the water concentration measured only during August 2011, since water concentrations were < LOD during the months of June and July; <sup>k</sup> This value is based on river and/or lake sediment microorganisms incubated with reduced anaerobic mineral medium and non-inoculated sediment [129].

detected but not quantified in Lausanne's Vidy WWTP effluent (Table 3.4), which indicates the involvement of WWTPs as a potentially prominent source of TBB into the lake. 4BBP was not detected in Vidy WWTP effluent. The largest tributary into the lake, the Rhône River [153], did not appear to be a major source of 4BBP, based on the finding that two sediment samples nearest to the Rhône delta, Sed3 and Sed4, contain much lower levels of 4BBP than the sediment samples Sed1 and Sed2 (Table 3.2). For TBB, the role of the Rhône is less clear, since this compound was not detected in any of the four sediment samples.

Further insights may be gained by comparing the observed distributions of the four Br-PBPs that were successfully quantified in sediment samples. Inspection of Table 3.2 shows that 4BBP, PBEB, BDE99, and BDE153 all exhibit similar trends in concentration among the four analyzed sediment samples: the highest levels of all four compounds are observed for Sed2 (near the middle of the lake), followed by Sed1 (near the urbanized Lausanne area), and with lowest levels observed for Sed3 and Sed4 (near the Rhône delta). This similarity in concentration trends may indicate similarity in sources of the four compounds. Atmospheric deposition is considered to be a major source for the introduction of PBDEs into Swiss lakes, including Lake Geneva [124]. BDE99, BDE100, and BDE153 were also detected in Lausanne's Vidy WWTP effluent, indicating that this is a proximate source of these compounds [16].

Taking together the above considerations, we conclude that atmospheric deposition and possibly WWTP effluents and urban run-off are the most plausible sources of TBB and 4BBP in Lake Geneva. However, further environmental sampling would be needed to confirm the importance of proximate sources of these lake pollutants.

#### **3.3.5 Physical and chemical property estimation and predicted environmental behaviors of TBB and 4BBP**

To assess the wider fate and environmental behavior of TBB and 4BBP, we compiled data for several environmentally relevant properties based on literature and our own estimates (Tables 3.5 and A.4). This enabled us to make inferences about the long range transport potential, Arctic contamination potential, and bioaccumulation potential of these pollutants.

##### **Long range transport potential (LRTP) and Arctic contamination potential (ACP)**

We screened 4BBP and TBB for environmental persistence, long range transport potential (LRTP) and Arctic contamination potential (ACP). Both pollutants met criteria for environmental persistence defined as an estimated atmospheric oxidation half life  $> 1$  d and by expert judgement (see references [3, 169]). 4BBP and TBB also were found to have both LRTP and ACP as defined by the criteria:  $4 < \log K_{ow} < 8$ ,  $6 < \log K_{oa} < 9$ , and  $-3 < \log K_{aw} < 1$  [190]. Previously reported detection of TBB in a snow core in Nunavut, Canada [10] may be viewed

### Chapter 3. Overlooked brominated pollutants in Lake Geneva

Table 3.4 – Occurrence of Br-PBP target analytes in the Lausanne's Vidy WWTP effluent (taken from [16]).

| Compound | Detection by GC×GC-ENCI-TOFMS <sup>a</sup> | Concentration in Liquid phase <sup>b</sup> (ng L <sup>-1</sup> ) |
|----------|--|--|
| TBB      | detected                                   | <0.4 <sup>c</sup>  |
| 4BBP     | not detected                               | not determined   |
| PBEB     | not detected                               | not determined   |
| HBB      | detected                                   | <30 <sup>c</sup>   |
| BDE47    | detected                                   | <2 <sup>c</sup>  |
| BDE100   | detected                                   | <9 <sup>c</sup>  |
| BDE99    | detected                                   | not determined   |
| BDE153   | detected                                   | <10 <sup>c</sup>   |
| HBBP     | not detected                               | not determined   |

<sup>a</sup> Based on the GC×GC-ENCI-TOFMS analysis of a PDMS passive sampler deployed in the effluent stream for 24 h, using the five point criterion method for identity confirmation; <sup>b</sup> The WWTP effluent liquid phase concentration was determined from filtered grab samples analyzed by GC×GC- $\mu$ ECD; <sup>c</sup> Upper bound on the possible concentration for compounds that were detected but had levels below the reported LOQ by [16].

as supporting evidence for its potential for long range transport and associated Arctic contamination. Among our target analytes, the pentaBDEs, HBB, and PBEB all have been previously investigated for LRTP and ACP [191, 192, 37, 121, 193, 10], whereas 4BBP and TBB have not. Based on their estimated partitioning properties and plausible persistence properties, we conclude that long range transport and Arctic contamination are likely important processes affecting the global fate and behavior of TBB and 4BBP.

#### Bioaccumulation potential

According to our chemical property estimates, 4BBP and TBB meet the bioaccumulation potential criteria set by Howard and Muir, 2010 [3], defined as  $\log K_{ow} > 3$  and bio-concentration factor (BCF)  $> 500$ . These criterion are slightly more conservative than the criteria used by REACH, which is BCF  $> 2000$  [194]. Previously reported occurrences of 4BBP in biological samples are consistent with its predicted tendency to bioaccumulate. 4BBP has been reportedly found in human tissues of cancer patients in China [195] and human breast milk in Denmark and Finland [196]. Biotic occurrence data is absent for TBB. However TBB is a structural analogue of trichlorobenzene, which is considered as bioaccumulative and persistent [197]. Based on estimated partitioning properties and limited existing occurrence data, we interpret that 4BBP and TBB have a high likelihood of bioaccumulation potential and that this process likely plays an important role in the environmental and human health impacts of these compounds. HBB has been measured in several biotic samples in the environment including bird eggs (Peregrine Falcon, Glaucous Gulls, and Herring Gulls)

and freshwater fish (northern snakehead fish and mud carp) [179, 198, 199, 200, 201]. Similarly both PBEB and pentaBDEs have been found to bioaccumulate in the environment both based on their properties and their previously reported occurrences in biotic media [200, 180, 202, 142, 203, 193, 191, 204, 205, 206, 207, 199, 208, 209]. Further investigations into the bioaccumulation behavior of 4BBP and TBB are warranted.

#### **Toxicity**

Previously reported laboratory experiments indicate that both 4BBP and TBB are toxic [210, 211, 212, 213, 214]. High dosages of 4BBP cause liver cancer in rats and mice [212]. Both TBB and HBB cause liver damage [210, 211], and in repeated high dosages they cause liver failure [211]. There is no published report regarding the toxicity of PBEB. The pentaBDEs constituted the first PBDE technical mixture that was banned globally in part due to toxicity [154, 215]. Further toxicology studies of 4BBP and TBB are warranted.

#### **Recommendation**

Here we report TBB and 4BBP at near  $\sim 1 \text{ ng L}^{-1}$  concentrations in the water column of Lake Geneva. Surprisingly, these pollutants have never been reported in any lake. These pollutants are considered most likely to have entered the lake primarily by atmospheric deposition and/or in municipal wastewater effluents, and/or urban run-off. Based on estimates of their chemical properties, TBB and 4BBP exhibited likely persistence in the environment and have potential to bioaccumulate, undergo long range transport, and contaminate Arctic regions. These pollutants also may be toxic. We recommend urgent environmental risk assessment studies and prompt evaluation of whether regulatory restrictions should be placed on the production and use of TBB and 4BBP.

Table 3.5 – Estimated chemical and physical properties of the high priority novel Br-PBPs.

| Properties  | Symbols  | Compound name                                 |   |   |  |
|---|--|---|---|---|--|
|   |  | 4BBP  | TBB   | HBB   | PBBB   |
| Melting point                                     | $T_m$ (°C)                                     | 72.89 <sup>a</sup>                            | 122.80 <sup>a</sup>                           | 327.0 <sup>a</sup>                              | 138.00 <sup>b</sup> , 137.69 <sup>a</sup>      |
| Boiling point                                     | $T_b$ (°C)                                     | 312.46 <sup>a</sup>                           | 271.00 <sup>a</sup>                           | 417.5 <sup>a</sup>                              | 363.21 <sup>a</sup>                            |
| Pure solid vapor pressure                         | $P_s$ (mm Hg)                                  | $1.5 \times 10^{-3c}$ , $2.4 \times 10^{-3a}$ | $7.5 \times 10^{-3c}$ , $1.5 \times 10^{-3a}$ | $1.58 \times 10^{-3c}$ , $3.17 \times 10^{-4b}$ | $3.7 \times 10^{-6c}$ , $4.65 \times 10^{-6a}$ |
| Water solubility                                  | $C_{sat}^w$ (mg L <sup>-1</sup> )              | 4.651 <sup>c</sup> , 0.653 <sup>e</sup>       | 20.325 <sup>c</sup> , 0.790 <sup>e</sup>      | 0.34 <sup>c</sup> , 0.35 <sup>b</sup>           | 0.219 <sup>c</sup> , 0.105 <sup>e</sup>        |
| Henry's law constant                              | $k_H$ (atm·m <sup>3</sup> mole <sup>-1</sup> ) | $1.65 \times 10^{-4a}$                        | $3.41 \times 10^{-4a}$                        | $7.92 \times 10^{-5a}$                          | $2.97 \times 10^{-6a}$                         |
| Air-water partition constant                      | $\log K_{aw}$                                  | -2.27 <sup>c</sup> , -2.17 <sup>a</sup>       | -1.73 <sup>c</sup> , -1.86 <sup>a</sup>       | -3.85 <sup>c</sup> , -4.06 <sup>a</sup>         | -3.14 <sup>c</sup> , -3.49 <sup>a</sup>        |
| Octanol-water partition constant                  | $\log K_{ow}$                                  | 4.96 <sup>c</sup> , 4.59 <sup>f</sup>         | 4.19 <sup>c</sup> , 4.66 <sup>a</sup>         | 5.80 <sup>c</sup> , 5.85 <sup>a</sup>           | 5.97 <sup>c</sup> , 7.48 <sup>a</sup>          |
| Octanol-air partition constant                    | $\log K_{oa}$                                  | 7.14 <sup>c</sup> , 6.82 <sup>a</sup>         | 6.12 <sup>c</sup> , 6.52 <sup>a</sup>         | 9.61 <sup>c</sup> , 10.97 <sup>a</sup>          | 10.13 <sup>c</sup>                             |
| Organic carbon-water partition constant           | $\log K_{oc-w}$ (L kg <sup>-1</sup> )          | 4.08 <sup>c</sup> , 4.01 <sup>a</sup>         | 3.58 <sup>c</sup> , 2.85 <sup>a</sup>         | 5.55 <sup>c</sup> , 4.68 <sup>a</sup>           | 5.54 <sup>c</sup> , 6.49 <sup>a</sup>          |
| Dissolved organic carbon-water partition constant | $\log K_{DOC-w}$ (L kg <sup>-1</sup> )         | 4.62 <sup>c</sup> , 4.84 <sup>i</sup>         | 4.05 <sup>c</sup> , 4.40 <sup>i</sup>         | 6.33 <sup>c</sup> , 6.82 <sup>i</sup>           | 6.31 <sup>c</sup> , 6.96 <sup>i</sup>          |
| PDMS-water partition constant                     | $\log K_{PDMS-w}$                              | 4.84 <sup>f</sup>                             | 4.84 <sup>j</sup>                             | 6.21 <sup>j</sup>                               | 6.64 <sup>j</sup>                              |
| Bioconcentration factor                           | $\log BCF$                                     | 5.11 <sup>c</sup> , 3.12 <sup>a</sup>         | 4.60 <sup>c</sup> , 2.77 <sup>a</sup>         | 6.61 <sup>c</sup> , 3.97 <sup>a</sup>           | 4.15 <sup>c</sup> , 6.62 <sup>a</sup>          |

<sup>a</sup> Estimated using EPISuite [168]; <sup>b</sup> Covaci et al [117]; <sup>c</sup> Estimated based on measured GC×GC retention times using the method of Nabi et al [150]; <sup>d</sup> Hardy et al [154]; <sup>e</sup> Yalkowsky et al [216]; <sup>f</sup> Doucette et al [217]; <sup>g</sup> Braekvelt et al [218]; <sup>h</sup> Estimated using the method developed by Kwan et al [141]; <sup>i</sup> Estimated using the method developed by Schwarzenbach et al [32]; <sup>j</sup> Estimated using the method developed by Booi et al [219]; <sup>k</sup> Perron et al [220].



## **4 Pentachlorothiophenol, a newly identified aquatic pollutant**

**Main author: Saer Samanipour**

**Contributions: This chapter was prepared by Saer Samanipour with editorial comments by J. Samuel Arey.**

**Daniel Trogolo (EPFL) performed the quantum chemical computations.**

### Abstract

Pentachlorothiophenol (PCTP) was successfully detected and semiquantitatively determined in both the water column and sediments of Lake Geneva, based on measurements using comprehensive two dimensional gas chromatography coupled to electron capture detector (GC×GC- $\mu$ ECD) and comprehensive two dimensional gas chromatography coupled to electron capture negative chemical ionization time-of-flight mass spectroscopy (GC×GC-ENCI-TOFMS). This is the first published report of PCTP in an aquatic system. The average water column concentration of PCTP in the deep lake was estimated to lie between 3 ng L<sup>-1</sup> and 3000 ng L<sup>-1</sup>, and its sediment concentrations varied between < 2.2 ng kg<sup>-1</sup> and 153.8 ng kg<sup>-1</sup>. Two potential precursors of PCTP, hexachlorobenzene (HCB) and pentachloronitrobenzene (PCNB), were successfully detected and quantified in the sediments of the lake. We also detected HCB, but not PCNB, in the water column of the lake. We estimated several environmentally relevant partitioning properties of these three compounds. These properties were used as a basis to make inferences about the potential sources of PCTP into the lake. We also detected pentachloromethylthiobenzene (PCMTB), which is a known degradation products of PCTP in soil and plant roots. The detection of PCMTB may indicate the involvement of PCNB in the introduction of PCTP into Lake Geneva.

### 4.1 Introduction

Pentachlorothiophenol (PCTP) was recently proposed as a new potential persistent and bioaccumulative pollutant (PBP) by Howard and Muir, based on its estimated chemical physical properties and its US-Canada volume of production of > 1 t y<sup>-1</sup> [3, 2]. However, very little is known about the environmental distribution of PCTP and about its fate and behavior. Properties relevant to the partitioning or degradation of PCTP have not been measured and the few properties available are estimated. Only one previous study has reported PCTP in the environment: Arinaitwe et al recently detected PCTP in aerosol particles in east Africa using conventional gas chromatography coupled to electron capture negative chemical ionization mass spectroscopy (GC-ENCI-MS) [12]. The current study is the first report of detection and quantification of PCTP in an aquatic system.

Several different plausible sources could potentially lead to the occurrence of PCTP in the environment, including both industrial waste and/or direct production. PCTP was classified as a high volume of production chemical (> 1000 t/y) in Europe by 1993 [221]. Recently, PCTP was entered in the list of persistent, bioaccumulative and toxic substances by the Registration, Evaluation, Authorisation and Restriction of Chemicals (REACH regulation) and also was considered for further regulations [222]. Today PCTP is still in use in Europe however, its global production volume is unknown and the major producer and distributor is China [223]. PCTP is used in the rubber industry during the vulcanization of tires [224]. PCTP is one of the main reactants used in the industrial production of pentachloronitrobenzene (PCNB) [225]. PCTP also

has been utilized as an intermediate in synthesis of several organic compounds [224, 226, 225] and in Raman Spectroscopy as a surface enhancer [227]. Therefore, the wastewater effluents of different industries such as rubber industry [228], chemical companies [225], and pharmaceutical companies [226] may plausibly contain PCTP. PCTP may also conceivably arise in the environment as a degradation product of the commercial chemical precursors PCNB and hexachlorobenzene (HCB) [229, 230, 231, 232, 233, 234, 235, 236, 237, 238, 239, 240, 241, 242]. Published experiments on the biodegradation of PCNB in soil and in the roots of plants reported PCTP as one of the degradation products [240, 241, 229, 230, 231, 232, 233, 234, 235, 237]. PCNB is a widely used fungicide, particularly in Japan and China [243]. Other transformation products of PCNB have been detected and quantified in soil samples in Japan and sea waters in Singapore [244, 245]. Finally, PCTP also can be produced through enzymatic transformation of HCB in the liver of rodents and humans [236, 242, 230, 237, 238]. Thus PCTP is monitored in urine samples of the industrial workers as an indicator of HCB exposure [246, 247, 248]. HCB was one of the twelve chlorinated compounds considered for global ban or reduced emission during the International Convention of Organic Pollutants in Stockholm, 2004 [249].

Typically employed analytical protocols for analyzing hydrophobic organic pollutants are unlikely to successfully detect and quantify PCTP in complex environmental samples. Oxidative clean up steps with either sulfuric acid or metallic Cu are commonly used to eliminate confounding matrix prior to analysis [17, 63, 250]. However, these sample preparation procedures will also oxidize the thiol group in PCTP, and thus PCTP would not be detected. Indeed, the only previously reported detection of PCTP in the environment was made without using any clean up step. Instead, successive fractionations were applied to decrease sample matrix effect, followed by GC-ENCI-MS analysis [12].

Comprehensive two-dimensional gas chromatography (GC×GC) [54, 58, 63, 146, 147, 251, 15], which can be thought of as a tandem fractionation process, is another analysis approach that can be used to mitigate the matrix effect for analysis of trace level PBPs in complex environmental samples. The resolving power of GC×GC makes it possible to minimize or bypass the clean up process, thus widening the spectrum of trace level PBPs that can be detected and quantified in complex environmental samples [16]. We recently developed a method for detection and quantification of halogenated pollutants in complex environmental samples by GC×GC coupled to micro electron capture detector (GC×GC- $\mu$ ECD) and electro capture negative chemical ionization time-of-flight mass spectroscopy (GC×GC-ENCI-TOFMS), and this approach would be appropriate for analysis of PCTP [15].

The aims of the present investigation were to: (1) analyze the water column and sediments of Lake Geneva for PCTP and its precursors (i.e. PCNB and HCB [252, 248, 253, 244, 254]) using GC×GC- $\mu$ ECD and GC×GC-ENCI-TOFMS; (2) evaluate the potential sources and sinks of PCTP in the lake environment; (3) estimate the environmentally relevant physical and

chemical properties of PCTP and its precursors in order to pre-evaluate the environmental fate and behavior of these compounds. We additionally performed a suspect screening of pentachloromethylthiobenzene (PCMTB) in the samples analyzed using GC×GC-ENCI-TOFMS, since this compound is a known degradation product of PCTP [233, 236, 242].

## 4.2 Methods

### 4.2.1 Target analyte selection

Howard and Muir published a list of 610 compounds with production volumes  $> 1 \text{ t y}^{-1}$  that may have potential to be bioaccumulative and persistent in the environment and that have been somewhat overlooked by the environmental community [2]. We further screened these compounds, considering only those that are: thermally stable; amenable to GC-ECD; available as analytical standards from commercial research suppliers; registered in Registration, Evaluation and Authorization of Chemicals (REACH) database; and not banned or limited in their global volume of production. This resulted in a list of 12 compounds [16], one of which is PCTP. We also analyzed for PCNB and HCB, which are potential environmental precursors for PCTP [233, 236, 242, 228].

### 4.2.2 Chemicals

Analytical standards PCB 30, PCB 50, PCB 145, PCB 204, pentachlorothiophenol (PCTP), pentachloronitrobenzene (PCNB) and hexachlorobenzene (HCB) were purchased from Sigma-Aldrich Switzerland. We also purchased diatomaceous earth, Florisil<sup>®</sup>, and sodium sulfate from Sigma-Aldrich Switzerland. Pesticide grade hexane, ACS grade acetone, ACS grade methanol, and ACS grade pentane were obtained from VWR Switzerland.

### 4.2.3 Environmental sampling

Lake Geneva is a large freshwater lake with  $580 \text{ km}^2$  surface area and 310 m maximum depth [151, 153]. The lake provides drinking water for more than 520,000 people and supports both commercial and recreational fishing [255]. More than 10 large wastewater treatment plant (i.e., which each serves a population equivalent of  $> 10,000$ ) and 20 small wastewater treatment plants (which each serves population equivalent of between 1,000 and 10,000) discharge their treated effluent into the lake [153]. Several studies have reported legacy PBPs in the sediments and biota of Lake Geneva [256, 257, 258, 259, 254, 260], whereas the water column of the lake has been mainly monitored for pharmaceuticals [261, 262, 152] and some nonpolar brominated compounds [53].

We deployed passive sampling strips, in duplicate at depths of 70, 107, 147, 162 and 166.5 m, at a site which has a bottom depth of 167 m, near Vidy Bay at  $46^{\circ}49'82.88'' \text{ N}$  and  $6^{\circ}58'10.55'' \text{ E}$

(World Geodetic System, 1984). Sampling was carried out for three consecutive one-months periods during June, July, and August of 2011. The samplers were deployed in solvent pre-washed stainless steel cages attached to a vertical stainless steel chain connected to a buoy and a bottom weight. The cages were used to protect the PDMS strips from bioturbation.

Sediment cores were collected at four locations in the lake (Figure 4.1). Two cores (Sed1 and Sed4) were taken by boat with a Benthos gravity corer, and two cores (Sed2 and Sed3) were retrieved with human-occupied MIR submersibles during the 2011 ELEM0 sampling campaign [151].

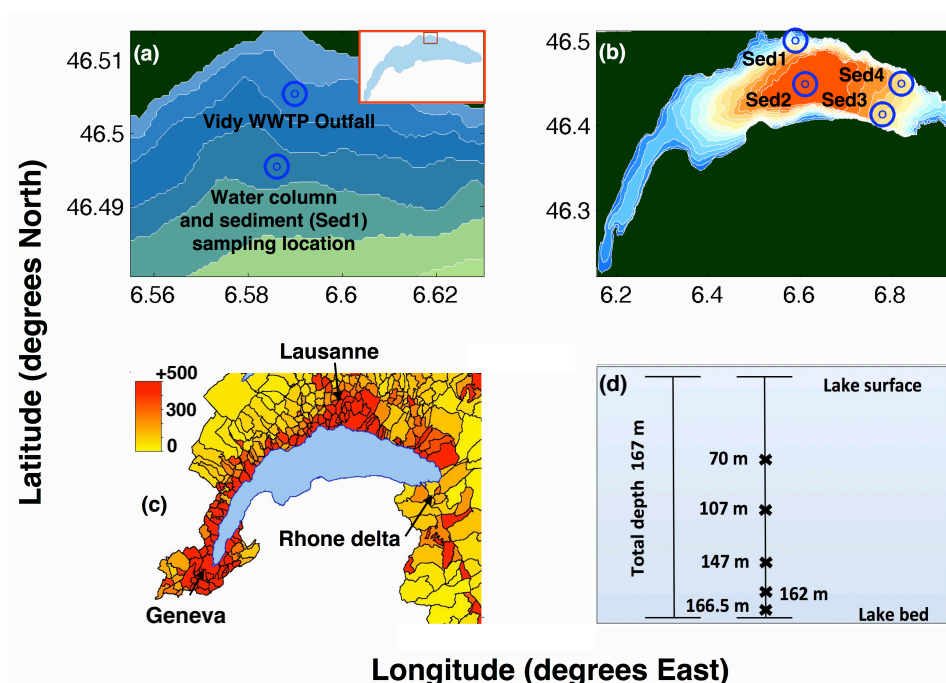


Figure 4.1 – Maps depicting: (a) sampling site for the sediment (Sed1) and the water column in Lake Geneva, with lake bathymetry contours of 45 m overlaid; (b) the four sediment sampling locations, with bathymetry contours of 20 m contours overlaid; and (c) population density of Lake Geneva area, by municipality, 2007 (source: bfs.admin.ch). (d) Schematic showing depths at which the water column samplers were deployed.

#### 4.2.4 Sample preparation

##### Passive sampling

Passive samplers are used widely for measuring hydrophobic organic chemicals in aquatic systems, owing to their inexpensive deployment, ease of storage and transport, and stability [263, 158, 160, 157]. Passive samplers measure the truly dissolved fraction of chem-

icals in water, thereby excluding the chemical fraction associated with suspended particles and dissolved organic matter [25]. We employed performance reference compounds (PRCs)[161, 264, 21, 265] for estimation of the rate of mass transfer ( $k_e$ ) of each target analyte between the water and the passive sampler. The concentration estimation of target analytes using the PRCs is explained in Appendix.

We employed polydimethylsiloxane (PDMS) as passive sampler material due to the demonstrated linearity of mass transfer of PBPs over a wide range of  $K_{ow}$  values [265]. Each PDMS strip was loaded with four PRCs (PCB30, PCB50, PCB145, and PCB204) and deployed in the lake. At the end of each sampling period, the strips were immediately extracted using pentane and stored at  $-20\text{ }^{\circ}\text{C}$  until analysis. The detailed procedures for PDMS strips loading, extraction, and quality control are provided in Appendix B.1.

### 4.2.5 Sediment samples extraction and clean up

The top 1 cm of each core was sampled. We only collected the center section of the sediment core, therefore we excluded the sediment in contact with the plastic tubing (Figure A.1). These sediment samples were air dried and homogenized according to the method EPA-823-B01-002, revision October 2001. We used accelerated solvent extraction for the extraction of 0.5 g of homogenized sediment sample based on method EPA 3545A, revision 1st February 2007. Further method details are available in Appendix B.2.

### 4.2.6 Analysis by GC×GC- $\mu$ ECD and GC×GC-ENCI-TOFMS

A Leco Corp GC×GC- $\mu$ ECD system was used for initial identification and quantification of target analytes in both water column and sediment extracts. The instrument was a modified Agilent 7890A GC system with split/splitless injector equipped with a dual stage quadruplet jet modulator, and FID/ $\mu$ ECD detectors. The separations were carried out on a 30 m, 0.25 mm inner diameter (i.d.), 0.25  $\mu\text{m}$  film thickness RTX-1 column from Restek (Restek, USA) as the first dimension and 2 m, 0.1 mm i.d., 0.1  $\mu\text{m}$  film thickness RTX-50 column as the second dimension. Helium was used as the carrier gas. Further instrument and analysis details are provided in Appendix B.3.

To further confirm the presence of our target analytes, we analyzed three lake water extracts and two sediment sample extracts by GC×GC-ENCI-TOFMS (Zoex Corp. USA). Instrument settings and analysis details are given in Appendix B.3.

### Quantum chemical computations

All quantum chemical computations were performed using the Gaussian09 program [266]. To estimate partition properties of both neutral and anionic PCTP, the following protocol was used. Gas phase geometries were optimized with the B2PLYPD [267, 268]/aug-cc-pVTZ [269, 270, 271, 272] model chemistry. Harmonic vibrational frequency calculations were carried out with the B2PLYPD/aug-cc-pVTZ method. Single point energy calculations on gas phase geometries were conducted using the B2PLYPD model chemistry, in water, *n*-octanol, *n*-hexadecane, and propylacetate solvent using the SMD [273] implicit solvation model as implemented in Gaussian09.

For  $pK_a$  calculations, the CBS-QB3 [274, 275] method was applied: geometry optimizations were conducted with the B3LYP [276, 277]/6-311G [278] model chemistry. Thermal contributions to the Gibbs free energy were computed as implemented in CBS-QB3 composite method. Solvation free energies were assessed with the B2PLYPD/aug-cc-pVTZ model chemistry and the SMD implicit solvation model [273].

## 4.3 Results and discussion

### 4.3.1 Estimated PDMS-water partitioning coefficient of target analytes

We estimated the PDMS-water partition coefficient,  $K_{sw}$ , of our target analytes, needed to convert the measured concentrations in passive samplers into water column concentrations in the lake (Table 4.1). For the  $K_{sw}$  value of the nonpolar target analyte, HCB, we obtained an experimentally determined value by Kwon et al [167]. For  $K_{sw}$  value of PCNB, we first estimated the  $K_{ow}$  value for this target analyte using EPISuite [168]. This estimated  $K_{ow}$  value was then entered in a linear free energy relationship (LFER) developed by Kwon et al [167] to estimate the  $K_{sw}$  (Table 4.1). For PCTP, the  $K_{sw}$  is speciation dependent, since this compound can deprotonate at neutral pH. Therefore, we needed to determine or estimate the  $pK_a$  of PCTP in water, as well as the species-specific  $K_{sw}$  values of both the neutral and anionic form [279, 280, 32]. We employed a quantum chemical computation approach to estimate the  $pK_a$  of PCTP, giving a value of  $4.3 \pm 1.00$ . Further details regarding these calculations are provided in Appendix B.3.

For PCTP, we estimated the apparent PDMS-water partitioning constant ( $K_{sw}$ ). The apparent partitioning constant ( $K_p^{app}$ ) of an ionizable compound between water and an organic phase is defined as [279, 280, 32]:

$$K_p^{app} = \alpha_i \cdot K_p^{HA} + (1 - \alpha_i) K_p^{A^-} \quad (4.1)$$

where  $K_p^{app}$  is the apparent partition coefficient between water and the organic phase (in this

## Chapter 4. Pentachlorothiophenol, a newly identified aquatic pollutant

Table 4.1 – Estimated and experimental chemical and physical properties of the target analytes.

| Chemical-physical property                   | Acronym                 | PCTP               |                   |                       | PCNB              | HCB               |
|--|-------------------------|--------------------|-------------------|-----------------------|-------------------|-------------------|
|  |                         | A <sup>-</sup>     | HA                | Apparent <sup>a</sup> | N <sup>b</sup>    | N <sup>b</sup>    |
| Partitioning constant between PDMS and water | log $K_{sw}$ (unitless) | -9.49 <sup>c</sup> | 5.04 <sup>c</sup> | 1.80                  | 4.06 <sup>d</sup> | 4.91 <sup>e</sup> |

<sup>a</sup> The reported property is the apparent value, estimated using Eq. 4.1, assuming an environmental pH of 7.5 (measurements via CIPEL) and a  $pK_a$  of 4.26; <sup>b</sup> "N" indicates a neutral compound that does not dissociate at neutral pH; <sup>c</sup> The property was estimated using SMD method; <sup>d</sup> Estimated via EPISuite [168]; <sup>e</sup> Experimental value by Kwon et al [167].

case PDMS),  $K_p^{HA}$  is the partition coefficient of the protonated species for two those phases,  $K_p^{A^-}$  is the partition coefficient deprotonated species for the two phases, and  $\alpha_i$  is the neutral fraction of an organic acid, given by:

$$\alpha_i = \frac{1}{1 + \frac{K_{i,a}}{[H^+]}} = \frac{1}{1 + 10^{pH - pK_{i,a}}} \quad (4.2)$$

where  $K_{i,a}$  is the dissociation constant of an acid in water. As for the  $pK_a$  value of PCTP, we used quantum chemical calculations to estimate the  $K_p^{HA}$  and  $K_p^{A^-}$  of PCTP in both water and PDMS (Table 4.1). These estimated parameters were then entered in Eq. 4.1 to estimate the apparent  $K_{sw}$  of PCTP.

### 4.3.2 Estimation of environmentally relevant properties

Several environmentally relevant partitioning properties of the target analytes were estimated using different approaches (Table 4.2). These partitioning properties enabled us to make inferences about the fate and behavior of PCTP in the Lake Geneva environment. In order to estimate the properties of the neutral target analyte, HCB, we used a recently developed model based on GC×GC retention times [150]. We used EPISuite for estimation of partitioning properties of PCNB [168]. For environmental partitioning properties of PCTP, we employed Advanced Chemistry Development (ACD/Labs) V11.02 [281] which takes into account both the environmental pH and  $pK_a$  of the analyzed chemical.

For the air-water partitioning coefficient ( $K_{aw}$ ), we assumed that the ionized fraction is not present in the gas phase [32], thus the apparent air water partition coefficient of an ionizable target analyte was estimated using:

$$K_{aw}^{app} = \alpha_i \cdot K_{aw}^{HA} \quad (4.3)$$

For the partitioning properties where we could not neglect the presence of the dissociated species in non aqueous phases (i.e.  $K_{ow}$ ,  $K_{oc}$ , and BCF) we used Eq. 4.1.



Table 4.2 – Estimated and experimental chemical and physical properties of the target analytes.

| Chemical-physical property                                    | Acronym   | PCTP            |                          |                       | PCNB              | HCB                       |
|---|---|-----------------|--------------------------|-----------------------|-------------------|---------------------------|
|   |   | A <sup>-a</sup> | HA                       | Apparent <sup>b</sup> | N <sup>c</sup>    | N <sup>d</sup>            |
| Partitioning constant between octanol and water               | log $K_{ow}$ (mol L <sup>-1</sup> · mol <sup>-1</sup> L)    | 2.22            | 5.19 <sup>e</sup>        | 2.58                  | 5.03              | 5.45 (5.47 <sup>f</sup> ) |
| Partitioning constant between air and water                   | log $K_{aw}$ (mol L <sup>-1</sup> · mol <sup>-1</sup> L)    | -               | -2.31 <sup>e</sup>       | -5.55 <sup>g</sup>    | -3.71             | -1.48                     |
| Partitioning constant between organic carbon and water        | log $K_{oc-w}$ (mol kg <sup>-1</sup> · mol <sup>-1</sup> L) | 1.15            | 4.63 <sup>e</sup>        | 1.60                  | 3.87 <sup>h</sup> | 4.67                      |
| Bioconcentration factor                                       | log BCF (mol kg <sup>-1</sup> · mol <sup>-1</sup> L)        | 0.70            | 5.69 <sup>e</sup>        | 2.46                  | 2.87              | 5.75                      |
| Water solubility (mg L <sup>-1</sup> )                        | -   | -               | 1.15                     | -                     | 0.44              | 0.67                      |
| Boiling point (°C)  | -   | -               | 315.71 <sup>c</sup>      | -                     | 335.5             | 291.43 <sup>c</sup>       |
| Melting point (°C)  | -   | -               | 231.5 <sup>c</sup>       | -                     | 144.0             | 231.8 <sup>c</sup>        |
| Acid dissociation constant                                    | $pK_a$  | -               | 4.26 ± 1.00 <sup>i</sup> | -                     | -                 | -                         |
|   |   | -               | 3.14 ± 0.50 <sup>h</sup> | -                     | -                 | -                         |
|   |   | -               | 2.58 <sup>j</sup>        | -                     | -                 | -                         |
| Reduction potential of the non-protonated radical species (V) | $E_{red}^0$   | 0.55            | -                        | -                     | -                 | -                         |

<sup>a</sup> The reported property belongs to the ionized dissociated species (A<sup>-</sup>) assuming a  $pK_a$  of 4.3 ± 1 and a pH of 10 at 25 °C, estimated using Advanced Chemistry Development (ACD/Labs) V11.02 [281], unless it is specified differently; <sup>b</sup> The reported property is the apparent value, estimated using Eq. 4.1, assuming an environmental pH of 7.5 (measurements by CIPLE [260]); <sup>c</sup> Estimated using EPISuite [168] unless it is specified otherwise; <sup>d</sup> The reported property belongs to the neutral species, N, estimated using model based on GC×GC retention times [150] unless it is mentioned otherwise; <sup>e</sup> The property of the neutral species (HA) was estimated assuming a  $pK_a$  of 4.3 ± 1 and a pH of 2 at 25 °C, estimated using Advanced Chemistry Development (ACD/Labs) V11.02 [281]; <sup>f</sup> Experimental value of Kwon et al [167]; <sup>g</sup> Estimated using equation 4.3, Schwarzenbach et al [32]; <sup>h</sup> Estimated using Advanced Chemistry Development (ACD/Labs) V11.02 [281]; <sup>i</sup> The property was estimated using the computational protocol described in Methods; <sup>j</sup> Estimated value taken from [282].

Additionally, we estimated the one-electron reduction potential of the non-protonated radical species, PCTP<sup>•</sup> / PCTP<sup>-</sup> couple, based on computed aqueous bond dissociation enthalpy ( $BDE_{aq}$ ) of the S-H bond of PCTP[282] and the theoretical  $pK_a$  the value for PCTP that we computed. We took advantage of the thermodynamic cycle that links  $pK_a$ ,  $E_{red}^0$ , and  $BDE_{aq}$ , as described in paragraph 3.1 of Warren's study [283].

$$E_{red}^0 = \frac{BDE_{aq} - 1.37pK_a - C_{H,aq}}{23.06} \quad (4.4)$$

where the factor  $C_{H,aq}$  represents the H<sup>+</sup> / H<sup>•</sup> standard reduction potential in water and corresponds to 55.8 kcal mol<sup>-1</sup> [283]. For the PCTP<sup>•</sup> / PCTP<sup>-</sup> half-reaction, the resulting estimated reduction potential is 0.55 V.

#### 4.3.3 Detection and confirmation of target analytes in environmental samples by GC×GC- $\mu$ ECD and GC×GC-ENCI-TOFMS

We employed a recently developed protocol for detection, quantification and identity confirmation of the target analytes using GC×GC- $\mu$ ECD and GC×GC-ENCI-TOFMS [15]. Target analytes were initially detected in both water column and sediment sample extracts by

## Chapter 4. Pentachlorothiophenol, a newly identified aquatic pollutant

---

GC×GC- $\mu$ ECD based on a 2-D retention time match with known standards, with a retention time tolerance of  $\pm 0.08$  min in the first dimension and  $\pm 0.3$  s in the second dimension. The presence of the target analytes was further confirmed by GC×GC-ENCI-TOFMS analysis for three selected water column extracts and two sediment samples. From the standard mixture chromatogram we extracted three  $m/z$  values from the averaged spectrum of each individual target analyte peak using GC Image software package (GC Image, LLC [81]). These three  $m/z$  values were the molecular ion, if available, and two (or three) expected fragments for each target analyte [230]. We compared the three  $m/z$  values of the target analyte in the standard mixture chromatogram to the suspected target analyte peak in the environmental sample chromatogram (see Table 4.3). A target analyte had confirmed presence in the environmental sample chromatogram if the suspected peak matched all three  $m/z$  values of the standard within a tolerance  $\pm 5$  mmu and the retention times also matched within  $\pm 0.08$  min in the first dimension and  $\pm 0.3$  s in the second dimension (Table 4.3). This procedure is in conformity with the European Union quality assurance of laboratories [87]. This procedure resulted in 100% agreement between positive detections by GC×GC- $\mu$ ECD and GC×GC-ENCI-TOFMS for all 3 target analytes in the 5 samples.

### 4.3.4 Matrix effect elimination and accurate quantification of the target analytes in environmental samples

We successfully quantified the target analytes in both water and sediment extracts using GC×GC- $\mu$ ECD. To limit the impact of matrix effects we employed an aggressive baseline correction, which was the Eilers baseline correction method [82] implemented via Matlab [93]. For the peak delineation algorithm, we used the inverted watershed algorithm [69]. Recent work has shown that this combination of algorithms leads to good results for quantification of target analytes in real samples by GC×GC, compared to other tested algorithms [15]. In particular, the choice of baseline algorithm is important for reducing the impact of apparent matrix effect [15]. The combination of the optimized separation via GC×GC and the data processing algorithms enabled the successful detection and quantification of the target analytes (Figure B.2). For analyte quantification, we used a five point external standard calibration curve with three replicates at each level of concentration. Chemometric tests indicated that external standard curves were unbiased and had low offset error (see Appendix, Quality assurance).

### 4.3.5 PCTP, HCB and PCNB in the water column and sediments of Lake Geneva

PCTP and HCB were successfully detected and quantified in all 30 water extracts, whereas PCNB (LOD of  $3.3 \text{ pg L}^{-1}$ ) was not detected in any of the water column samples. The averaged water column concentration of PCTP ranged between  $193.7 \text{ ng L}^{-1}$  and  $225.2 \text{ ng L}^{-1}$ , whereas for HCB the averaged water column concentration varied between  $0.016 \text{ ng L}^{-1}$  and  $0.155 \text{ ng L}^{-1}$  (see Table B.4 and Figures 4.2 and B.2). The average water column concentrations of reported HCB at this site in Lake Geneva,  $60.0 \text{ pg L}^{-1}$ , was 3 times larger than that reported in Lake Baikal,  $20.0 \text{ pg L}^{-1}$  [284], whereas it was about one order of magnitude larger

Table 4.3 – GC×GC-ENCI-TOFMS retention times and monitored m/z values; the method limit of quantification (LOQ) by GC×GC- $\mu$ ECD, and frequency of detection of the target analytes in selected samples by GC×GC-ENCI-TOFMS and by GC×GC- $\mu$ ECD.

| Compound                       | $t_{r1}^c$ (min) | $t_{r2}^d$ (s) | $t_{r1}^c$ (min) |        |        | Water samples   |                     |   | Sediment samples                                      |                     |  |
|--------------------------------|------------------|----------------|------------------|--------|--------|---|---------------------|---|---|---------------------|--|
|                                |                  |                | (m/z)1           | (m/z)2 | (m/z)3 | Frequency of positive detection<br>GC×GC<br>$\mu$ ECD | GC×GC<br>ENCI-TOFMS | GC×GC- $\mu$ ECD<br>LOQ (pg L <sup>-1</sup> ) | Frequency of positive detection<br>GC×GC<br>$\mu$ ECD | GC×GC<br>ENCI-TOFMS | GC×GC- $\mu$ ECD<br>LOQ (ng kg <sup>-1</sup> ) |
| pentachlorothiophenol (PCTP)   | 30.40            | 4.18           | 246              | 281    | 283    | 3/3   | 3/3                 | 1.9   | 2/2   | 2/2                 | 2.0  |
| hexachlorobenzene (HCB)        | 16.42            | 2.33           | 284              | 285    | 286    | 3/3   | 3/3                 | 2.0   | 2/2   | 2/2                 | 4.0  |
| pentachloronitrobenzene (PCNB) | 17.24            | 2.52           | 247              | 249    | 251    | 0/3   | 0/3                 | 10.0  | 2/2   | 2/2                 | 4.5  |

<sup>a</sup> The frequency of detection in 3 selected PDMS strips during June-August of 2011 at 166.5 m depth; <sup>b</sup> The frequency of detection in Sed1 and Sed2; <sup>c</sup> GC×GC first dimension retention time, min; <sup>d</sup> GC×GC second dimension retention time, s.

## Chapter 4. Pentachlorothiophenol, a newly identified aquatic pollutant

---

than reported average concentrations in remote mountain lakes in Europe ( $6 \text{ pg L}^{-1}$ ) [285]. However, the dissolved HCB concentration in Lake Geneva was comparable to HCB water column concentrations in the Great Lakes [19]. The absolute water column concentration of PCTP may lay between  $3 \text{ ng L}^{-1}$  and  $3000 \text{ ng L}^{-1}$ . This large level of uncertainty is due to the inherent uncertainties in the estimates of the two crucial parameters of  $\text{p}K_a$  and apparent  $K_{sw}$  of PCTP. The estimated  $\text{p}K_a$  value of PCTP using the quantum chemical approach may have an uncertainty of 1 log unit, and the  $K_{sw}^{HA}$  also estimated by the quantum chemical approach has an uncertainty of perhaps 0.6 log unit. Therefore, the absolute average water column concentration PCTP may have an uncertainty of  $\sim 1.5$  log units.

For both PCTP and HCB we observed a homogenous distribution of concentration as a function of time and depth during all three months which was in agreement with trends observed in concentration profiles of hydrophobic brominated hydrocarbons, 4-bromobiphenyl and pentabromoethylbenzene at this site in the lake [53]. This uniform vertical concentration distribution suggests a situation of slow change in compound source and removal process relative to vertical mixing at this location of the lake. It is worth noticing that even though the absolute concentration of PCTP in the water column of the lake is not well defined due to the inherent uncertainties in the two key parameters  $\text{p}K_a$  and apparent  $K_{sw}$ , the relative concentrations of PCTP are well constrained. Therefore, the observed concentration trend for PCTP in the water column is meaningful, independently from the uncertainty inherent in the absolute average water column concentration.

We detected PCTP, HCB and PCNB in all four sediment samples (Table 4.4 and Figure B.2). PCTP concentrations in the sediment extracts varied from non-quantified ("nq") to  $6.8 \text{ ng kg}^{-1}$ , whereas HCB and PCNB concentrations ranged between  $9.2 \text{ ng kg}^{-1}$  and  $318.4 \text{ ng kg}^{-1}$ , and from nq to  $153.8 \text{ ng kg}^{-1}$ , respectively, Table 4.4. This is the first report of PCTP in sediments of a lake. The average measured HCB sediment concentration of  $158.1 \text{ ng kg}^{-1}$  was about one order of magnitude smaller than the levels reported 30 years ago by Thomas et al in Lake Geneva [254]. However, the Lake Geneva sediment concentration of HCB is comparable to levels reported in sediments of Lake Redó, Spain ( $180 \text{ ng kg}^{-1}$ ) [286]. Observed PCNB levels in Lake Geneva sediments appeared to be two to three orders of magnitude smaller than levels reported in sediment samples from 20 major river basins in the US [241].

For all three target analytes, we observed higher concentrations in the sediment samples Sed1 and Sed2, which were collected in Vidy Bay and in the center of the lake, compared to the other sediment samples. The sediment spatial distribution of the target analytes provides insight into the potential sources of these target analytes. We discuss the plausible sources of our target analytes in the later section "The fate and behavior of PCTP in the Lake Geneva environment".

Table 4.4 – Concentrations of the target analytes in the sediment of Lake Geneva.

| Target analyte | Sediment concentration (ng kg <sup>-1</sup> ) <sup>a</sup> |       |                    |                    |   | log                         |                                 |
|----------------|--|-------|--------------------|--------------------|---|-----------------------------|---------------------------------|
|                | Sed1   | Sed2  | Sed3               | Sed4               | Literature value reported in other sediments (ng kg <sup>-1</sup> ) | $K_d$ (L kg <sup>-1</sup> ) | $C_s/C_w$ (L kg <sup>-1</sup> ) |
| PCTP           | 4.6  | 6.8   | < 2.0 <sup>b</sup> | 2.5                | -   | 0.38 <sup>c</sup>           | -1.41                           |
| HCB            | 245.6  | 318.4 | 9.2                | 61.0               | 750-1250 <sup>d</sup> , 180 <sup>e</sup> , 160.0 <sup>e</sup>       | 3.65                        | 3.45                            |
| PCNB           | 153.8  | 107.9 | < 4.5 <sup>b</sup> | < 4.5 <sup>b</sup> | up to 180,000 <sup>g</sup>  | -                           | 2.65                            |

<sup>a</sup> The concentration is normalized by the dried weight of the sediment sample; <sup>b</sup> The target analyte was detected in the sample but its concentration was smaller than the method limit of quantification (LOQ) <sup>c</sup> Estimated using a  $pK_a$  of 4.3 and an environmental pH of 7.5; <sup>d</sup> This value was reported in 1984 by Thomas et al for sediments of Lake Geneva [254]; <sup>e</sup> This value was reported for sediments of Lake Redó, Spain [286]; <sup>f</sup> This value was reported for the sediments of Lake Geneva, 2006, close to the outfall of Vidy Bay WWTP [177]; <sup>g</sup> This value is the maximum value reported in the sediments of 20 major river basins in the US [241].

The concentration distribution of HCB between sediment and water at the Sed1 sampling location appeared to be explained by partitioning equilibrium of HCB between these two compartments. We compared the measured concentration ratio of HCB in sediment and in water ( $C_{Sed1}/C_w$ ), to the equilibrium sediment-water partition coefficient of this pollutant,  $K_d$ , defined as  $K_{oc-w} \times f_{oc}$  [32]. The  $f_{oc}$  is the fraction of organic carbon in the sediment, measured at a location about 200 m from the Sed1 site, having a total depth of 100 m [177, 181]. For HCB, the absolute deviation of log transformed  $C_{Sed1}/C_w$  and the estimated log  $K_d$  was 0.21 log units, suggesting that the water column and sediment are at partitioning equilibrium at this site.

The sediment-water concentration distribution ratio of PCTP of 0.04 was about 60 times smaller than the estimated apparent  $K_d$  of 2.40. The water column concentration of PCTP has a large level of uncertainty due to the inherent errors in the estimated  $pK_a$  and estimated apparent  $K_{sw}$ . The estimated apparent  $K_d$  is also affected by the uncertainty of  $pK_a$  and estimated apparent  $K_{oc-w}$ . Therefore, an assessment of the sediment-water partitioning equilibrium state proved to be difficult. Measurements of these chemical property parameters are needed.

PCNB was not detected in the water column of the lake. We estimated the expected water column concentration of PCNB based on its concentration in sediment, assuming partitioning equilibrium between the two compartments. The lack of detection of PCNB in the water column was attributed to the fact that PDMS was not an adequate medium for sampling PCNB in water [16, 287].

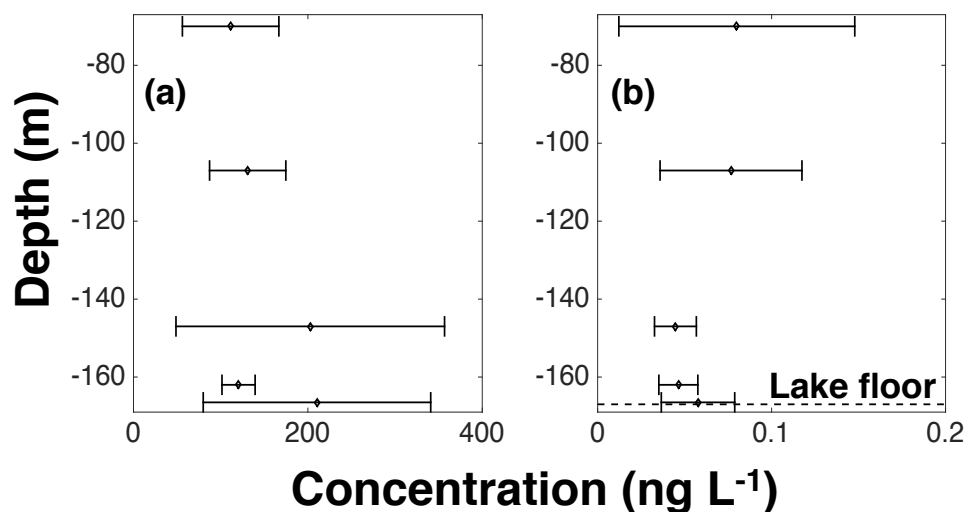


Figure 4.2 – The concentration profiles of (a) PCTP and (b) HCB in the water column of Lake Geneva. The error bars represent the observed concentration variability over the three-month sampling period.

#### Suspect screening of pentachloromethylthiobenzene (PCMTB) in the environmental samples

We detected PCMTB in both the water column and sediment samples of the lake, employing a suspect screening of GC×GC-ENCI-TOFMS chromatograms. We did not include PCMTB in our initial set of target analytes. However, given the potential role of PCMTB for understanding the occurrence of PCTP, we evaluated our samples analyzed using GC×GC-ENCI-TOFMS for PCMTB. To perform the suspect screening, we employed a protocol similar to the method of Hernández et al [288]. We analyzed the GC×GC-ENCI-TOFMS chromatograms of the five selected samples for five  $m/z$  values for PCMTB reported previously (see Table 4.5) [228]. There was only one resolved peak in the environmental samples that contained all five  $m/z$  values. This peak had a first dimension retention time of 45.14 min and second dimension retention time of 4.68 s. Based on the PCMTB boiling point (323.42 °C estimated via EPISuite [168]) and  $\log K_{ow}$  of 5.51 (estimated using ACD/Labs [281]), we found good agreement between the retention times of the suspected peak in the environmental samples and predicted retention window of PCMTB, estimated from its boiling point and  $\log K_{ow}$  (i.e., first dimension retention time between 44 min and 46 min, and second dimension retention time between 3 s and 5 s). This result provides high confidence that PCMTB is present in our samples. To further confirm this result and also to quantify PCMTB in environmental samples, the use of an analytical standard would be necessary.

Table 4.5 – Previously reported m/z values for PCMTB, and comparison to the suspect peak.

| m/z value literature <sup>a</sup> | m/z this study | fragment                  |
|-----------------------------------|----------------|---------------------------|
| 296                               | 296            | M <sup>b</sup>            |
| 246                               | 246            | M - CH <sub>3</sub> - Cl  |
| 211                               | 211            | M- CH <sub>3</sub> - 2×Cl |
| 174                               | 174            | M- 3×Cl - SH              |
| 139                               | 139            | M- 4×Cl - SH              |

<sup>a</sup> Benz et al [228]; <sup>b</sup> M represents the molecular ion.

#### 4.3.6 The fate and behavior of PCTP in the Lake Geneva environment

There are several plausible pathways that could introduce PCTP into Lake Geneva. The European production and consumption of PCTP decreased from > 1000 t/y, in 1993 [221], to < 4 t/y [222]. PCTP can be released into the environment as an industrial waste [224, 226, 227, 225], or it can be produced by degradation of HCB and PCNB [229, 230, 231, 232, 233, 234, 235, 236, 237, 238, 239, 240, 241, 242]. We found no information about the production and consumption levels of PCNB in Switzerland. One of the main metabolites of PCNB, i.e. pentachloroaniline, has been detected and quantified in different soil samples in Switzerland [289]. Moreover, we detected PCMTB, which is one of the degradation products of PCTP, in sediment and the water column of Lake Geneva (Figure 4.3). This information may suggest that the degradation of PCNB in soil, plants, sludge and sediment is a production pathway for PCTP, even though PCNB was not detected in the water column of the lake (possibly due to the lack of affinity for PDMS). Interestingly, a recent study reported PCNB in Vidy Bay WWTP effluent (Table 4.6) [16]. Thus, the effluents of WWTPs and runoffs may be an important source for PCTP into the lake systems. The other important PCTP precursor, HCB, had higher concentration levels and also different spatial distribution in the sediments of the lake when compared to PCNB and PCTP. These higher levels were attributed to the heavy past use of this pollutant in the Lake Geneva area [177, 254], whereas the sediment spatial distribution may be attributed to the different sources of HCB compared to PCTP and PCNB. The only pathway for degradation of HCB to form PCTP mainly takes place in the liver of animals and humans exposed to HCB [230, 236, 237, 238]. However, considering the ban posed on HCB and also its levels in the Swiss environment [290], this pathway appeared unlikely to be a relevant process for the environmental production of PCTP. We also evaluated the sediment spatial concentration distribution of PCTP and PCNB. The sediment spatial distribution of PCTP and PCNB may suggest the involvement of the highly urbanized area of Lausanne in the introduction of these pollutants into the lake. Considering different potential introduction ways of PCTP into the lake, we think that both the direct release through WWTP effluents and urban runoffs, and also the degradation product of PCNB may be important sources of PCTP in the lake area.

Once in the water column of a lake, PCTP may partition into biota, dissolved organic carbon (DOC) in the water column, and organic carbon bound to sediments (OC) and particulate

## Chapter 4. Pentachlorothiophenol, a newly identified aquatic pollutant

Table 4.6 – Occurrence of the target analytes in the Lausanne's Vidy WWTP effluent (taken from reference [16]).

| Target analyte | Detection by GC×GC-ENCI-TOFMS <sup>a</sup> | Concentration in Liquid phase <sup>b</sup> (ng L <sup>-1</sup> ) |
|----------------|--|--|
| PCTP           | na <sup>c</sup>                            | not determined   |
| HCB            | not detected                               | not determined   |
| PCNB           | not detected                               | 0.6  |

<sup>a</sup> Based on the GC×GC-ENCI-TOFMS analysis of a PDMS passive sampler deployed in the effluent stream for 24 h, using the five point criterion method for identity confirmation; <sup>b</sup> The WWTP effluent liquid phase concentration was determined from filtered grab samples analyzed by GC×GC- $\mu$ ECD; <sup>c</sup> Sample was not analyzed for this target analyte.

organic carbon in the water column (POC)[32]. Based on the estimated  $pK_a$  of PCTP of 4.2, this pollutant is more than 99.9 % dissociated at the lake pH of 7.5. This lowers the tendency of PCTP to partition into the hydrophobic phases such as DOC, POC, and OC (Figure 4.3). However, the estimated apparent BCF of PCTP ( $10^{2.46}$ ) suggests that the partitioning into the biota may still be important. For air-water exchange processes, the small apparent  $K_{aw}$  ( $10^{-5.55}$ ) indicates that this compound has a very low vapor phase concentration relative to the aqueous phase, at partitioning equilibrium.

The estimated reduction potential of 0.55 V (versus SHE) for the deprotonated PCTP radical suggests that the PCTP anion would be easily oxidized by several common lake water oxidants, as shown in Table 4.7. These aquatic oxidants would be able (from a thermodynamic view) to take an electron away from the PCTP anion. For example, triplet excited state dissolved organic matter (<sup>3</sup>DOM\*) has an estimated reduction potential of approximately 1.36-1.95 vs NHE, according to estimates by Canonica et al [291]. In sunlit aquatic waters, <sup>3</sup>DOM\* and carbonate radical are in much higher concentration than hydroxyl radical [32]. Thus these oxidants may play an important role in the degradation of PCTP in the lake environment. However, further work would be needed to test these hypotheses.

### 4.3.7 Implications

This is the first report of the concentration of PCTP in the water column and sediments of an aquatic system. Due to the high separation power of GC×GC, we were able to detect and quantify PCTP in the water column samples without performing any clean up step on the lake water extracts, and with only limited clean up carried out on the sediment samples of Lake Geneva. We employed GC×GC- $\mu$ ECD for quantification and GC×GC-ENCI-TOFMS for the identity confirmation of PCTP in the environmental samples. PCTP has been detected and quantified in atmospheric particulates collected from east Africa recently [12] and also in the sediment samples collected in Tokyo Bay, Japan (personal communication by Dr. Y. Zushi)



Table 4.7 – Environmentally relevant oxidants, their reaction and the  $E_{red}^0$  (V).

| Oxidant                  | Reaction in water                                | $E_{red}^0$ (V)        |
|--------------------------|--|------------------------|
| HO $\cdot$               | HO $\cdot$ +e $^{-}$ $\rightarrow$ HO $^{-}$     | 1.9                    |
| O $_3$                   | O $_3$ +e $^{-}$ $\rightarrow$ O $_3^{-}$        | 1.0                    |
| $^1$ O $_2$              | $^1$ O $_2$ +e $^{-}$ $\rightarrow$ O $_2^{-}$   | 0.83                   |
| HO $_2$ /O $_2^{-}$      | HO $_2$ +e $^{-}$ $\rightarrow$ HO $_2^{-}$      | 0.75                   |
| ArO $\cdot$ <sup>b</sup> | ArO $\cdot$ +e $^{-}$ $\rightarrow$ ArO $^{-}$   | 0.79                   |
| RO $\cdot$ <sup>c</sup>  | RO $\cdot$ +e $^{-}$ $\rightarrow$ RO $^{-}$     | 1.2                    |
| ROO $\cdot$ <sup>c</sup> | ROO $\cdot$ +e $^{-}$ $\rightarrow$ ROO $^{-}$   | 0.77                   |
| CO $_3^{-}$              | CO $_3^{-}$ +e $^{-}$ $\rightarrow$ CO $_3^{2-}$ | 1.6                    |
| NO $_3$                  | NO $_3$ +e $^{-}$ $\rightarrow$ NO $_3^{-}$      | 2.3                    |
| $^3$ DOM*                | -  | 1.36-1.95 <sup>d</sup> |

<sup>a</sup> Data is taken from reference [32]; <sup>b</sup> Ar stands for phenyl; <sup>c</sup> R stands for alkyl; <sup>d</sup> Data is taken from reference [291].

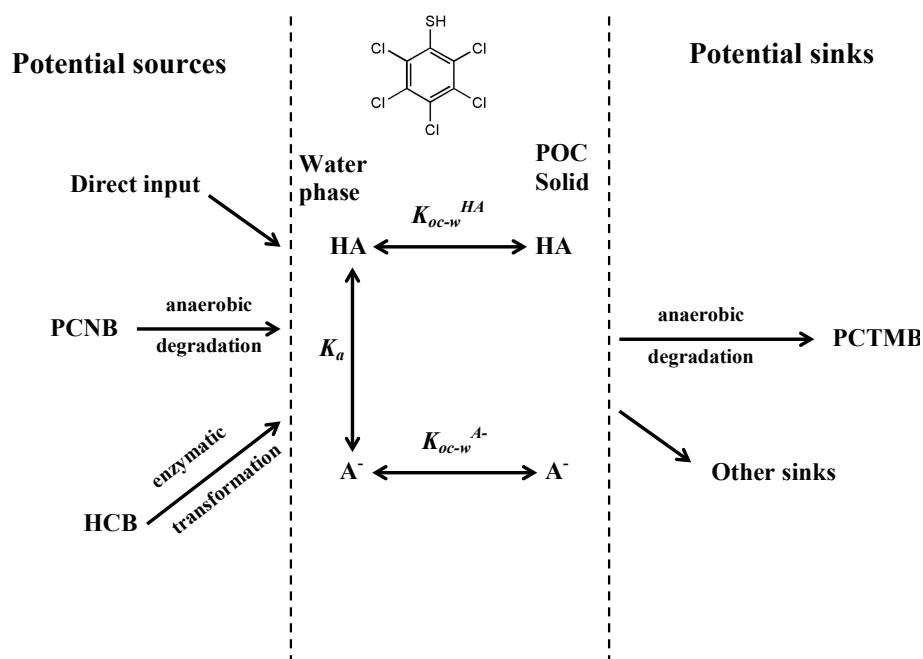


Figure 4.3 – Plausible sources and sinks for PCTP in the lake environment.

#### Chapter 4. Pentachlorothiophenol, a newly identified aquatic pollutant

---

using high resolution GC×GC-EI-TOFMS. In all three cases of detection and quantification of PCTP, the clean up step during the sample preparation was limited compared to what is common in the literature [250, 17, 63] and the use of advanced separation techniques such as GC×GC-TOFMS was needed. In our opinion, the lack of environmental occurrence data of PCTP is likely due to the inadequacy of the methods used commonly for sample preparation and analysis.

For the water column sampling, the use of passive samplers deployed in steel cages minimizes the formation of biofilm [292], therefore the clean up step can be avoided. For sediment samples, matrix effect is more important. Nonetheless, with the separation power of GC×GC coupled with different detectors and combined with adequate data processing tools [15, 63], the analyst can detect and quantify trace levels of PCTP in these complex environmental samples. In future work, the application of polymers with higher affinity for ionizable pollutants (e.g. polyacrylate) may be more effective for sampling of water.

In upcoming work we are planning to measure both the  $pK_a$  and the apparent  $K_{sw}$  of PCTP at pH of 7.5, using HPLC-MS, in order to improve the water column concentration estimate of PCTP.

## **5 Development, modeling and field test of an in-situ accelerated sampler for the truly dissolved fraction of organic pollutants in deep and shallow water.**

**Main author: Saer Samanipour**

**Contributions: This chapter was prepared by Saer Samanipour with editorial comments by J. Samuel Arey.**

**Angelos Mallios and Richard Camilli, from Woods Hole Oceanographic Institution (WHOI), contributed to the development and field test of the accelerated sampler.**

**Justine Politano (EPFL) contributed to the modeling efforts.**

**Sanjeev Dasari (EPFL) contributed to the laboratory desorption experiments.**

### Abstract

An accelerated sampler was developed to measure the truly dissolved fraction of hydrophobic organic compounds (HOPs) in aquatic systems. This sampler collects the truly dissolved fraction of HOPs in the water column by flushing water at high velocity past a polymeric sampling phase, in-situ. The sampler was initially developed and tested with controlled laboratory experiments. A two-compartment mass transfer model was developed and was applied to the depletion profiles of 11 PCBs in laboratory experiments, at three water flow rates of 1, 2, and 4 L min<sup>-1</sup>. The mass transfer model consisted of a bulk polymer compartment that participated in an absorption process, and a surface compartment that hosted an adsorption/desorption process. This model successfully described the mass transfer kinetics of PCBs between the polymer and water. To conduct a field test, a prototype of the accelerated sampler was deployed in the benthic water column of Lake Geneva at depths of 120-125 m and 140-145 m. We also deployed passive samplers at similar depths at a location about 500 m distance from the accelerated sampling site, for two consecutive months of June and July of 2011. Both water column sampling methods enabled successful quantification of 4 out of 11 PCBs in the water column. We compared the average water column concentrations of these 4 PCBs as measured using the conventional passive sampling methodology and using the accelerated sampler. We found an excellent agreement between the two sampling methodologies. The absolute concentration deviation between the two methods were smaller than 53% for all four PCBs, which was within measurement error. The accelerated sampler enabled us to measure ~ 0.001 pg L<sup>-1</sup> levels of truly dissolved fraction of HOPs in the deep water column of this aquatic system only after 2 h of deployment, without being affected by suspended solids and dissolved organic matter in the water column.

### 5.1 Introduction

Measuring hydrophobic organic pollutants (HOPs) in aquatic environments is a challenging task due to the trace level concentrations of these compounds and due to the complex matrix encountered in environmental samples [15, 16, 17, 18]. Large volume sampling [19, 17] and passive sampling methodologies [20, 21, 22] are the conventional methods for measuring these compounds in the water column of aquatic systems. Large volume sampling of HOPs requires particular care in sample handling and storage [23, 24, 18]. A recent study showed that large volume sampling is sensitive to the suspended solids and the dissolved organic matter in the aquatic system [25]. Additionally, large volume sampling is not a practical approach for water depths > 100 m, due to the possibility of cross-contamination caused by the use of long tubes and pumping system [17, 18]. By comparison, the passive sampling methodology is inexpensive, stable, and easy to handle [23, 26, 27]. However, passive sampling necessitates exposure times of 4 to 8 weeks, depending on the water concentration levels, hydrophobicity of the target analytes, and the hydrological conditions [28, 29]. Additionally, passive samplers may encounter problems with biofilm formation, due to the long exposure times required [30]. Most passive sampling efforts have been conducted in shallow water [24, 22], due to the

logistical challenges of deep water deployments [29, 31, 28].

Little published data are available regarding the concentration of the truly dissolved (TD) fraction of HOPs in deep waters. The TD fraction of a HOP is the fraction of the HOP that is dissolved in water and that is not associated with suspended particles, dissolved organic matter, particulate organic carbon [32]. This fraction (i.e. TD fraction) tends to bioaccumulate into the biota due to its high bioavailability [32]. Therefore when HOPs are analyzed in aquatic systems, the TD fraction is considered widely important even when present at trace level concentrations [17, 7, 33, 32, 25]. There have been several attempts to measure HOPs in the water column of aquatic systems [35, 34, 19, 17], however these studies were mainly limited to the surface water. There are a few published works in development of new sampling systems that are able to overcome the issues of cost, time, energy and the difficulty of sample handling, for sampling of HOPs in the deep water columns of aquatic systems [31, 28]. Petrick et al developed an *in situ* system that uses an immersible pump, to push water through a glass fibre filter followed by an XAD resin [31]. This sampling system was test at 4000 m depth, with the maximum depth of deployment of 6000 m. However, this system uses plastic tubes for the connections, and this may cause cross-contamination due to the absorption of HOPs to the plastic tubings. This sampling system also difficult to deploy in aquatic systems with a high concentration of suspended solids. The higher concentration of suspended solids may cause the glass filter to clog and therefore the sampler may not reach the limit of quantification for that HOP. Llorca et al used a passive sampling based system to measure polycyclic aromatic hydrocarbons in an outlet of a wastewater treatment plant in Spain, having a sampling depth of 1 m [28]. However, their sampling system required a sampling time of 5 days in order to be able to accurately quantify their target analytes. To our knowledge there is no fast sampling system available that can sample trace levels of the truly dissolved fraction of HOPs in deep water column of aquatic systems, without being affected by suspended solids and/or dissolved organic matter in the water column.

The aim of this study is to develop, model, and field test an accelerated sampler that can sample the truly fraction of HOPs in the both shallow and deep water column of an aquatic system. We developed a pumped flow device with the ability to sample quantitatively the truly dissolved fraction of HOPs within 5 hours in deep and shallow water. We developed a mass transfer model to describe the uptake of HOPs from water into the sampling polymer, based on controlled laboratory experiments. The performance of the accelerated sampler and mass transfer model were field validated by comparing the accelerated sampler results with field measurements obtained using conventional passive samplers.

## Chapter 5. Accelerated sampler

Table 5.1 – The list of performance reference compounds (PRCs) used in this study and their chemical-physical properties.

| PRCs used during the laboratory experiment |         |          |                   |                   |         |         |
|--|---------|----------|-------------------|-------------------|---------|---------|
| Compound                                   | Acronym | $M_w^a$  | $\log K_{ow}^b$   | $K_{pw}^c$        | $D_w^d$ | $D_p^e$ |
| 2,3,6-trichlorobiphenyl                    | PCB27   | 255.961  | 5.69 <sup>f</sup> | 4.73 <sup>i</sup> | 5.27    | 7.41    |
| 2,4,5-trichlorobiphenyl                    | PCB31   | 255.961  | 5.69 <sup>f</sup> | 4.73 <sup>i</sup> | 5.27    | 6.03    |
| 2,2',4,6'-tetrachlorobiphenyl              | PCB51   | 286.922  | 5.84 <sup>f</sup> | 5.10 <sup>i</sup> | 4.82    | 3.63    |
| 2,2',5,5'-tetrachlorobiphenyl              | PCB52   | 286.922  | 5.84 <sup>g</sup> | 5.38 <sup>h</sup> | 4.82    | 3.63    |
| 2,2',4,5,5'-pentachlorobiphenyl            | PCB101  | 323.883  | 6.38 <sup>g</sup> | 5.71 <sup>h</sup> | 4.46    | 3.02    |
| 2,3,3',4,4'-pentachlorobiphenyl            | PCB105  | 323.883  | 6.61 <sup>h</sup> | 5.89 <sup>h</sup> | 4.46    | 3.16    |
| 2,3',4,4',5-pentachlorobiphenyl            | PCB118  | 323.883  | 6.61 <sup>h</sup> | 5.87 <sup>h</sup> | 4.46    | 2.82    |
| 2,2',3,4,4',5'-hexachlorobiphenyl          | PCB138  | 357.844  | 7.06 <sup>h</sup> | 6.20 <sup>h</sup> | 4.15    | 2.57    |
| 2,2',3,4',5,6-hexachlorobiphenyl           | PCB149  | 360.878  | 7.28 <sup>f</sup> | 6.37 <sup>i</sup> | 4.15    | 2.69    |
| 2,2',3,4,4',5,5'-heptachlorobiphenyl       | PCB180  | 395.3232 | 7.36 <sup>g</sup> | 6.40 <sup>h</sup> | 3.89    | 2.40    |
| 2,2',3,3',4,4',5,5'-octachlorobiphenyl     | PCB194  | 429.7683 | 8.92 <sup>g</sup> | 8.02 <sup>i</sup> | 3.67    | 1.86    |
| PRCs used for environmental sampling       |         |          |                   |                   |         |         |
| 2,4,6-trichlorobiphenyl                    | PCB30   | 255.961  | 5.69 <sup>f</sup> | 4.73 <sup>h</sup> | 5.27    | 6.03    |
| 2,2',4,6-tetrachlorobiphenyl               | PCB50   | 286.922  | 5.84 <sup>f</sup> | 5.10 <sup>h</sup> | 4.82    | 3.63    |
| 2,2',3,4,6,6'-hexachlorobiphenyl           | PCB145  | 360.878  | 7.28 <sup>f</sup> | 6.37 <sup>h</sup> | 4.15    | 2.69    |
| 2,2',3,4,4',5,6,6'-octachlorobiphenyl      | PCB204  | 429.7683 | 8.92 <sup>f</sup> | 8.02 <sup>h</sup> | 3.67    | 1.86    |

<sup>a</sup> The molecular weight of the PRC ( $\text{g mole}^{-1}$ ); <sup>b</sup> The partitioning constant of the compound between octanol and water; <sup>c</sup> The polydimethylsiloxane (PDMS) and water partitioning constant of the PRC; <sup>d</sup> The diffusion coefficient of the PRC ( $\times 10^{-10}$ ) in water having units  $\text{m}^2 \text{s}^{-1}$ , estimated using reference [32]; <sup>e</sup> The diffusion coefficient of the PRC ( $\times 10^{-11}$ ) in PDMS having units  $\text{m}^2 \text{s}^{-1}$ . Value is taken from the reference [293]; <sup>f</sup> Estimated using EPISuite [168]; <sup>g</sup> Value taken from reference [294]; <sup>h</sup> Value taken from reference [295]; <sup>i</sup> Value estimated using the LFER in reference [167].

## 5.2 Experimental

### 5.2.1 Chemicals

An analytical standard mixture of polychlorinated biphenyls (PCBs) was purchased from Sigma-Aldrich Switzerland. This mixture consisted of 11 PCBs in a solution of heptane (Table 5.1). We also obtained PCB30, PCB 50, PCB 145, PCB 204 standards from Sigma-Aldrich. Pesticide grade methanol, hexane, and pentane were purchased from VWR Switzerland.

### 5.2.2 Loading of performance reference compounds (PRCs) onto PDMS polymer strips

We used polydimethylsiloxane sheets (PDMS, AlteSil Laboratory Sheet, UK) with a thickness of 0.5 mm. We chose PDMS due to its exhibited linearity in the mass transfer for compounds

having a wide range of hydrophobicity, i.e.  $K_{ow}$  [164, 163, 219]. We cut the PDMS sheets into strips of  $10 \times 1 \times 0.05 \text{ cm}^3$ , which resulted in an average strip weight of  $1.98 \pm 0.20 \text{ g}$ . To clean the strips, we extracted them with methanol using Soxhlet extraction for a duration of 24 h. The cleaned PDMS strips were then stored in a glass container at  $-20 \text{ }^\circ\text{C}$ .

The cleaned PDMS strips were loaded with performance reference compounds (PRCs) [162, 165] using the method of Booij et al. [162]. For the laboratory desorption experiment we loaded the strips with 100 ng of each individual PCB present in the PCB standard mixture (Table 5.1). For the environmental deployment we loaded the PDMS strips with 4 PRCs, which were PCB30, PCB50, PCB145, and PCB204, at  $20 \text{ ng g}^{-1}$  each.

### 5.2.3 Laboratory desorption experiment

The laboratory desorption experiment consisted of a SP-400 immersible pump (Fulz Pumps, Inc, USA), emplaced in a 50 L glass container with a distilled water inflow, and with the PRC-loaded PDMS strip suspended in stainless steel pipes that carried pump water outflow (Figure 5.1). The desorption experiment was carried out at 3 different flow rates of  $1 \text{ L min}^{-1}$ ,  $2 \text{ L min}^{-1}$ , and  $4 \text{ L min}^{-1}$ . We evaluated the depletion of 11 PCBs over time periods of 120 min, 360 min, and 240 min for the desorption experiments, at flow rates of  $1 \text{ L min}^{-1}$ ,  $2 \text{ L min}^{-1}$ , and  $4 \text{ L min}^{-1}$ , respectively. However, for the  $1 \text{ L min}^{-1}$  experiment we were unable to sample the depletion levels over periods longer than 120 min due to difficulties of maintaining this water flow rate with the SP-400 pump.

The glass container and the pump were washed by distilled water and rinsed with solvent, hexane, prior to each experiment. Before starting each experiment we flushed the pump and the stainless steel pipes with distilled water for 30 min, in order to avoid cross-contamination. Finally, for the laboratory experiment, the PRC-loaded PDMS strip was positioned downstream from the pump. This setup enabled us to prevent cross-contamination that would otherwise be caused by sorption of PRCs to the pump and the surface of glass container.

### 5.2.4 Accelerated sampler prototype

The accelerated sampler consisted of an SP-400 immersible pump system attached to 60 cm of stainless steel pipes at the pump intake. The PRC-loaded PDMS strip was placed inside of the intake pipe for the deployment in the environment. The pump system was connected to a control-box, used to regulate the water flow rate. This prototype was analogous to the laboratory setup used for the desorption experiment. However, in the field sampler prototype, we decided to have the PRC-loaded PDMS strips placed upstream from the pump. This positioning of pump and the PDMS strip enabled us to avoid interferences from cross-contamination in between field measurements. Finally, the pumps used for the field experiment were not

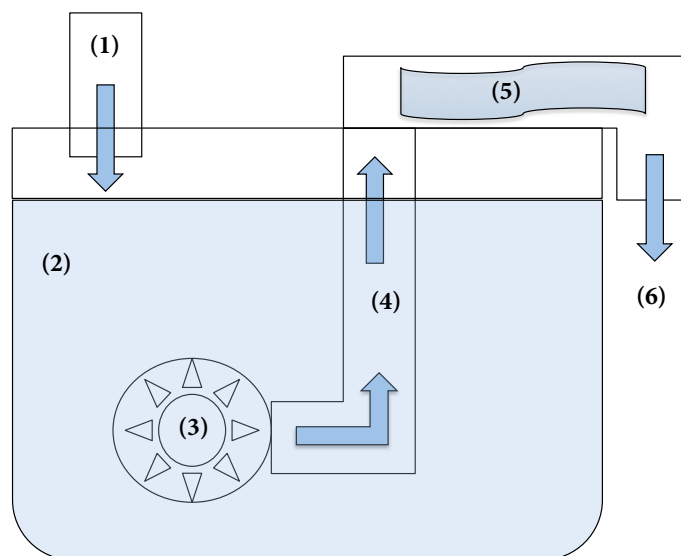


Figure 5.1 – A simplified schematic of the desorption experiment. The numbers indicate different components of the experimental setup: (1) distilled water inflow, (2) glass container filled with water, (3) SP-400 immersible pump, (4) stainless steel pipe, (5) the PDMS strip, (6) water outflow. The arrows indicate the direction of the water flow.

utilized for the laboratory experiments.

### 5.2.5 Field sampling in Lake Geneva

We deployed both conventional passive samplers and also a prototype of the accelerated sampler in Vidy Bay, Lake Geneva (Figure 5.3). The passive samplers served as a reference measurement in order to evaluate the performance of the accelerated sampler. The conventional passive samplers were deployed at five different depths between 70 and 166.5 m for an exposure period of 1 month, during two sampling periods of June and July, 2011. This location is about 1200 m from the northern shore of the lake and has a total depth of 167 m, having 46°49'82.88" N and 6°58'10.55" E (World Geodetic System, 1984). For the field test, the accelerated sampler was deployed twice, both times at locations about 500 m east of the passive sampling location. These accelerated sampler deployments were conducted on June 12<sup>th</sup> and July 2<sup>nd</sup>, 2011 at 120-125 and 140-145 m depths, respectively using the human-occupied MIR scientific submersibles, which followed the trajectories shown in Figure 5.2. These deployments were carried out for exposure times of 73 min and 178 min, respectively, and with an average pump water flow rate of 4 L m<sup>-1</sup>.



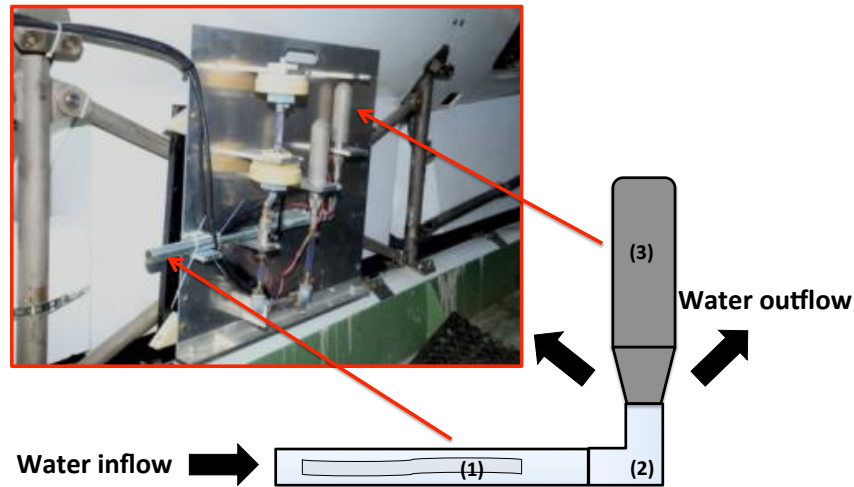


Figure 5.2 – A simplified schematic of the prototype of the accelerated sampler deployed using the MIR human-occupied scientific submersibles, and also a photograph of the accelerated sampler integrated into the MIR chassis. Labeled in the schematic are (1) the PRC-loaded PDMS strip, (2) stainless steel pipe, and (3) the SP-400 immersible pump system.

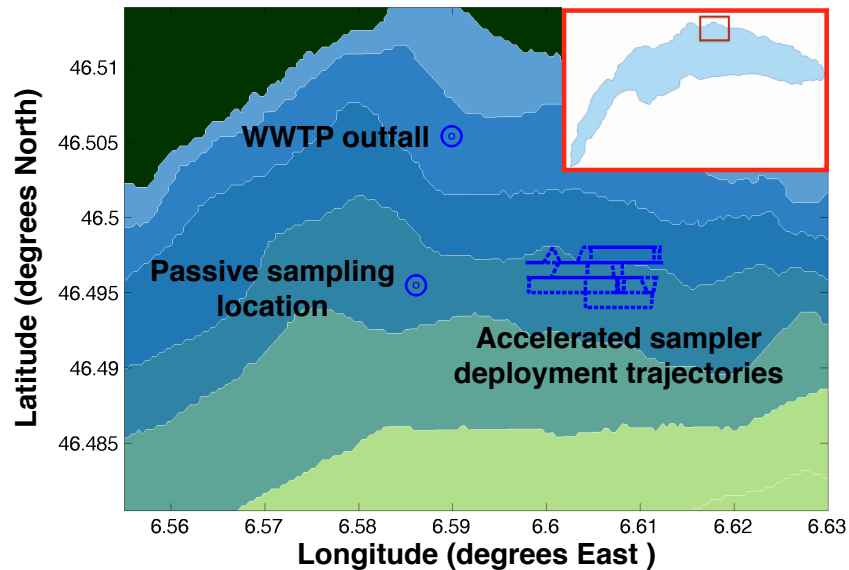


Figure 5.3 – Map showing the locations of conventional passive sampling, Lausanne's Vidé wastewater treatment plant (WWTP) outfall, and the trajectories of the accelerated sampler deployed using MIR submersibles, in World Geodetic System (WGS84) coordinates. Bathymetry contours of 45 m are overlaid.

### 5.2.6 Extraction of PDMS strips after deployment

All PDMS strips, including those from the desorption experiment, field passive sampling, environmental deployment of the accelerated sampler, and also controls were extracted with 20 mL of pentane for 8 h, three consecutive times. The final extract volume (60 mL) was reduced to 1 mL and simultaneously was switched to hexane, using a rotary evaporator. The final extracts were stored at - 20 °C until analysis.

### 5.2.7 Sample analysis

#### GC-ECD conditions

We analyzed the PDMS extracts from the laboratory depletion experiments using a Hewlett-Packard (HP 6890) gas chromatography (GC) system coupled to an electron capture detector (ECD). The separations were carried out on a 60 m length, 0.25 mm inner diameter (i.d.), 0.25  $\mu\text{m}$  film thickness SPB-Octyl column (Sigma-Aldrich, Switzerland). The oven temperature program was started at 80 °C and held for 30 s, then initially increased to a temperature of 150 °C with a ramp rate of 150 °C  $\text{min}^{-1}$ , where it was held at 150 °C for 1 min. The second temperature ramp was a 2.5 °C  $\text{min}^{-1}$  increase from 150 °C to 285 °C, where it was held at 285 °C for 30 min. We injected 1  $\mu\text{L}$  of the sample extracts on-column and employed a constant carrier gas (helium) flow rate.

#### 5.2.8 GC $\times$ GC- $\mu$ ECD and GC $\times$ GC-ENCI-TOFMS conditions

PDMS strip extracts from both the passive sampler field deployments and also the accelerated sampler field deployments were analyzed using a Leco Corp comprehensive two dimensional gas chromatograph coupled with a micro electro capture detector (GC $\times$ GC- $\mu$ ECD) instrument, which is a modified Agilent 7890A GC system. This system was equipped with a split/split-less injector and a dual-stage quadruple-jet modulator. We analyzed the environmental sample extracts employing a first dimension column of 30 m length, with 0.25 mm i.d., 0.25  $\mu\text{m}$  film thickness RTX-1 (Restek, USA), and a second dimension column of 2 m length, with a 0.1 mm i.d., and 0.1  $\mu\text{m}$  film thickness BPX-50 (Restek, USA). The main oven temperature program consisted of: an initial temperature of 45 °C, held for 1 min, and then increased to 160 °C at 2.5 °C  $\text{min}^{-1}$ , and from 160 °C to 300 °C at 1.8 °C  $\text{min}^{-1}$ , held at that temperature for 10 min. The secondary oven temperature program was a first ramp from 57 °C to 172 °C at 3.2 °C  $\text{min}^{-1}$ , held for 1 min, and then a second ramp from 172 °C to 312 °C with a ramp-rate of 2.8 °C  $\text{min}^{-1}$  and held for 33.4 min. A modulation period of 15 s was chosen. We used helium as carrier gas with a constant flow rate of 1.5 mL  $\text{min}^{-1}$ .

To further confirm the identity of the target analytes in the environmental extracts, we analyzed 3 PDMS strip extracts from the passive sampler deployment and 2 extracts from the accelerated sampler deployment with a GC $\times$ GC coupled to an electron capture negative

chemical ionization time-of-flight mass spectrometer (ENCI-TOFMS) (Zoex Corp. USA). For identity confirmation of the target analytes by GC×GC-ENCI-TOFMS, we used a previously established method [53, 16, 15]. The instrument program is detailed elsewhere [53, 16].

#### 5.2.9 Quality assurance

For sample preparation and analysis control, we analyzed four different blanks. These blanks comprised of: a PDMS blank, which was an extract of five pre-cleaned PDMS strips; a glassware blank, which was the solvent extraction of the glassware and rotary evaporator used for the extraction; a field blank, which was a loaded PDMS strip brought to the field but not deployed; and finally a solvent blank. All glassware utilized in the analysis was first hand-washed and oven-baked at 450 °C overnight. We also baked the GC systems at 300 °C for 30 min before each standard and sample injection.

### 5.3 Theoretical background

#### 5.3.1 One compartment Linear model of sorption kinetics

We first describe a model that is widely used to describe sorption kinetics of pollutants associated with uniphase passive sampler devices [296, 164, 21, 162, 219, 297, 264], here referred to as the one-compartment linear model.

This model assumes that the mass transfer between the bulk water and the passive sampler material takes place by diffusion through a thin water boundary layer (WBL) at the sampler-water interface and diffusion within the passive sampler material (Figure 5.4). The mass transfer flux is a linear function of the concentration difference of the HOP between the water bulk phase and passive sampler phase. The interface between passive sampler phase and WBL is assumed to be at partitioning equilibrium, and the bulk water phase is assumed well-mixed. In this case, the mass flux of a HOP between bulk water and the PDMS polymer can be described by [32]:

$$F_{p-w} = v_{tot}(C_w \cdot K_{pw} - C_p) \quad (5.1)$$

where  $F_{p-w}$  has units of mass time<sup>-1</sup> length<sup>-2</sup>,  $C_w$  is the concentration of HOP in bulk water,  $C_p$  is the concentration of the HOP in the PDMS phase,  $K_{pw}$  is the equilibrium partition constant of the HOP between water and the PDMS phase, and  $v_{tot}$  is the total velocity of mass transfer from bulk water to the PDMS, with units of length time<sup>-1</sup> (Figure 5.4). Assuming a steady-state transfer between the two phases, the total velocity of mass transfer,  $v_{tot}$ , is given by:

$$\frac{1}{v_{tot}} = \frac{1}{v_p} + \frac{K_{pw}}{v_w} \quad (5.2)$$

## Chapter 5. Accelerated sampler

---

where  $v_p$  represents the velocity of diffusive mass transfer within the polymer material, and  $v_w$  represents the velocity of mass transfer across the WBL. Under the assumption that transport through both the WBL and the polymer phase are governed by steady state diffusion, each mass transfer velocity can be approximated by the ratio of the diffusion coefficient of the HOP in that phase and the thickness of the phase layer, or:

$$v_p = \frac{D_p}{\delta_p} \quad (5.3)$$

$$v_w = \frac{D_w}{\delta_w} \quad (5.4)$$

where the  $D_p$  is diffusion coefficient of the HOP in the polymer;  $D_w$  is the diffusion coefficient of the HOP in water;  $\delta_p$  is the 1/2 of the thickness of the polymer strip [164, 21, 162, 161, 294]; and  $\delta_w$  is the thickness of WBL. Thus Eq. 6.2 can be rewritten as:

$$\frac{1}{v_{tot}} = \frac{\delta_p}{D_p} + \frac{\delta_w \cdot K_{pw}}{D_w} \quad (5.5)$$

Therefore Eq. 6.1 can be written as:

$$F_{p-w} = \frac{1}{\frac{\delta_p}{D_p} + \frac{\delta_w K_{pw}}{D_w}} (C_w \cdot K_{pw} - C_p) \quad (5.6)$$

In this case the concentration variation of HOPs in the polymer with respect to time can be explained by:

$$\frac{dC_p}{dt} = F_{p-w} \cdot \left(\frac{A_p}{V_p}\right) = \frac{1}{2\delta_p \left(\frac{\delta_p}{D_p} + \frac{\delta_w K_{pw}}{D_w}\right)} (C_w \cdot K_{pw} - C_p) \quad (5.7)$$

where the  $A_p$  and  $V_p$  are the surface area and the volume of the polymer, and therefore  $\frac{A_p}{V_p} = \frac{1}{2\delta_p}$ .

To describe uptake of an HOP by the polymer, we assume that:  $C_p(t=0) = 0$ ; and  $C_w$  is constant with time. In this case we can solve Eq. 5.7 to obtain:

$$C_p = C_w \cdot K_{pw} (1 - \exp(-k_e t)) \quad (5.8)$$

In Eq. 5.8 the parameter  $k_e$  has unit of  $\text{time}^{-1}$  and represents the rate constant of mass transfer between water and polymer, and it is described as follows:

$$k_e = \frac{1}{2\delta_p \left(\frac{\delta_p}{D_p} + \frac{\delta_w K_{pw}}{D_w}\right)} \quad (5.9)$$

The same rate of mass transfer,  $k_e$ , also can be used for describing the depletion of the PRCs

from the polymer to the water phase. In this case we assume that the  $C_w = 0$  and  $C_p(t = 0) = C_p^0$ , where  $C_p^0$  is the initial concentration of the HOP in the polymer phase. Solving Eq. 5.7 gives:

$$C_p = C_p^0 \exp(-k_e \cdot t) \quad (5.10)$$

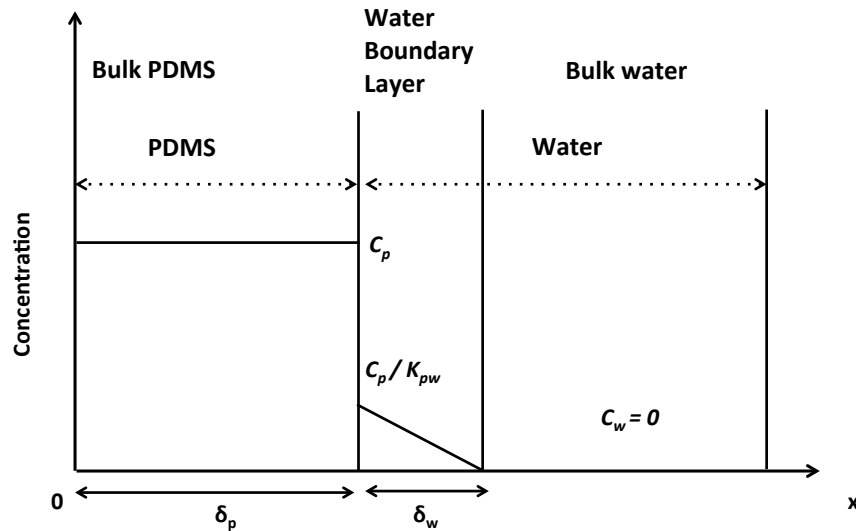


Figure 5.4 – The schematic of the one compartment model, illustrating the PRC concentration profiles expected during the laboratory desorption experiment.  $C_p$  is the concentration of the PRC in PDMS,  $C_w$  is the concentration of PRC in water,  $K_{pw}$  is the partitioning constant of PRC between the two phases,  $\delta_p$  is half of the PDMS strip thickness, and  $\delta_w$  is the thickness of water boundary layer.

## 5.4 Results and discussion

### 5.4.1 Application of the one-compartment linear model to laboratory desorption kinetic data

As a starting point in this study, we attempted to apply the conventional one-compartment linear model to describe the depletion kinetics of HOPs from PDMS polymer during the laboratory desorption experiment. We used Eq. 5.10 to describe the depletion profiles of the 11 PCBs, with  $k_e$  as a fitting parameter (Table 5.2).

The goodness-of-fit parameters suggested that the one compartment model does not adequately explain the experimental data (Table 5.2). Squared regression coefficient values ( $R^2$ )

were  $< 0.6$  for 31 cases out of 33, and root mean square error of the fit (RMSE) values were  $\sim 0.1$  for 27 cases out of 33. The depletion profiles of all 11 PCBs suggested a biphasic desorption behavior, under all three water flow rates (Figure 5.6). During the initial phase of desorption, which lasts approximately for 900 s, we observed a fast depletion of all 11 PCBs. After this early fast kinetic phase, we observed a slower depletion of the target analytes from the polymer. This prompted us to re-evaluate the main assumption in the one-compartment linear model, which is that PDMS can be considered as a single-compartment bulk phase.

We considered the possibility that diffusion within the polymer may be sufficiently slow that Eq. 5.3 is inadequate to correctly capture this mass transfer velocity. This hypothetical case would imply that published  $D_p$  values (Table 5.1) are erroneously high. To evaluate this possibility, we attempted to explain the laboratory desorption experiments using a one-dimensional finite difference model that allowed transient diffusion kinetics within the polymer phase as well as steady state diffusion through the WBL at the polymer-water interface [298]. To fit the model to the observed depletion curves of individual PCBs,  $D_p$  and  $\delta_w$  were treated as freely fitting parameters and  $D_w$  and  $\delta_p$  values were taken as known parameters. This approach failed to adequately explain the observed PCB depletion curves from the laboratory desorption experiment, regardless of the flow rate considered [298]. Based on these results, we concluded that the  $D_p$  values in Table 5.1 could not be rejected, and we discarded the hypothesis that transient diffusion behavior within the polymer was a mass transfer-limiting process during the laboratory desorption experiments.

Based on the numerical experiments described above, we arrived at the conclusion that the one-compartment linear model was inadequate to explain the observed PCB depletion kinetics in the laboratory desorption experiments. This was true regardless of whether we assumed either steady state or transient diffusion kinetics within the polymer phase. Taken together, these findings led us to reject the assumption that sorption to the polymer could be modeled as a single compartment.

### 5.4.2 Development and application of a two-compartment non-linear model of sorption kinetics

Several previous investigations have reported that the mass transfer between the PDMS and water is governed mainly by the sorption into the bulk polymer phase [158, 160, 163, 22, 299]. However, a few recent studies have suggested that adsorption of HOPs may occur on the PDMS surface [300, 301, 302].

Based on the findings discussed in the previous section, we developed a two-compartment non-linear model to explain the observed mass transfer kinetics of PCBs between water and PDMS. This model consisted of two polymer compartments, defined as "surface" and

"bulk", both of which contact a WBL (Figure 5.5). This model assumes that the two polymer compartments are additive, thus the total HOP mass in the polymer is the sum of HOP masses in the two compartments. The second main assumption of this model is that the two polymer compartments experience desorption independently, in parallel. This latter assumption is reasonable as long as the time scales of desorption kinetics of the two compartment are very different from each other.

By analogy to the one-compartment model, the mass flux of an HOP between each polymer compartment (surface or bulk) and bulk water can be formulated as:

$$F_{ps-w} = v_{tot-s}(C_w \cdot K_{psw} - C_s) \quad (5.11)$$

$$F_{pb-w} = v_{tot-b}(C_w \cdot K_{pbw} - C_{pb}), \quad (5.12)$$

where  $C_w$  is the concentration of the HOP in water;  $C_s$  is the concentration of the HOP in the surface polymer compartment, defined as the mass of HOPs in that compartment divided by the surface area of the polymer (mass length<sup>-2</sup>); and  $C_{pb}$  is the concentration of the HOP in the bulk polymer compartment, defined as the mass of HOP in that compartment divided by the total volume of the polymer (mass length<sup>-3</sup>). In Eqs. 5.11 and 5.12,  $v_{tot-s}$  is the velocity of chemical mass transfer between the surface polymer compartment and the bulk water phase (time<sup>-1</sup>),  $v_{tot-b}$  is the velocity of chemical mass transfer between the bulk polymer compartment and bulk water (length time<sup>-1</sup>),  $K_{psw}$  is the equilibrium partitioning coefficient of the chemical between the surface compartment and water (unit of length), and  $K_{pbw}$  is the unitless equilibrium partitioning coefficient of the chemical between the bulk polymer compartment and water. Based on the published  $D_p$  values reported in Table 5.1, we assume that diffusion in the PDMS phase is not the rate limiting step during mass transfer ( $\frac{\delta_p}{D_p} \ll \frac{\delta_w \cdot K_{pw}}{D_w}$ ). Thus we assume that mass transfer across the WBL is the rate limiting step [164, 21, 162, 161, 294]. Therefore,

$$v_{tot-s} = \frac{D_w}{K_{psw} \delta_w}, \quad (5.13)$$

$$v_{tot-b} = \frac{D_w}{K_{pbw} \delta_w}. \quad (5.14)$$

We defined an "apparent" surface concentration of HOPs, which has units of mass length<sup>-3</sup> as:

$$C_{ps} = \frac{C_s \cdot A_p}{V_p} \quad (5.15)$$

so that changes in the surface compartment concentration and changes in the bulk polymer compartment concentration can be considered in terms of common units. Based on the

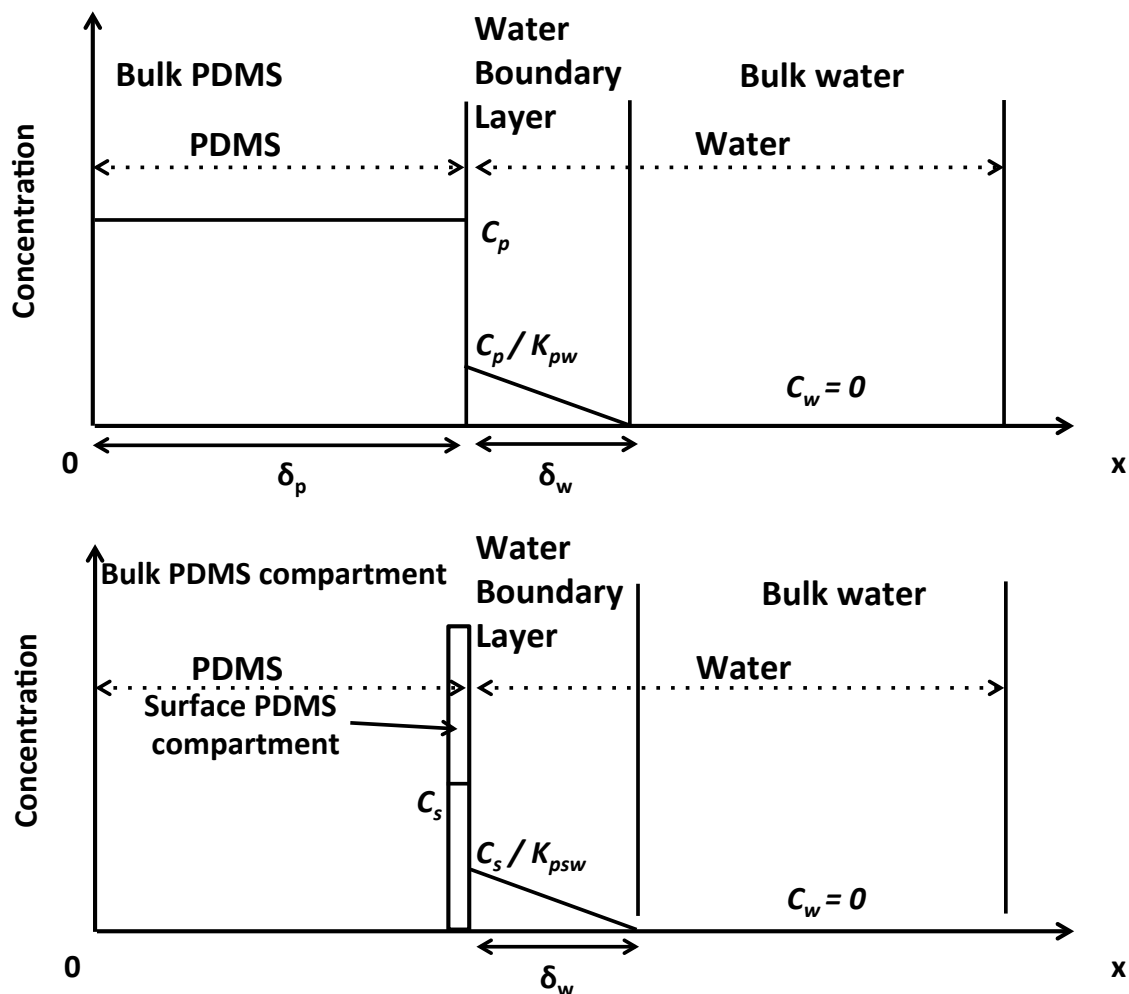


Figure 5.5 – Schematic of the two-compartment non-linear model in which concentration profiles are shown for PRCs during the laboratory desorption kinetic experiments. The top panel illustrates the model concentration profile of the PRC absorbed in bulk polymer and the PRC dissolved in water, and the bottom panel shows the the model concentration profiles of the PRCs adsorbed in the polymer between surface compartment and the PRC dissolved in water.  $C_{pb}$  is the concentration of the chemical in the bulk polymer compartment,  $C_s$  is the concentration of the chemical in the surface polymer compartment,  $K_{pbw}$  is the partitioning constant of the PRC between the bulk polymer and water, and  $K_{psw}$  is the surface sorption constant of the PRC.



assumptions of the two-compartment model, the time-dependent changes in concentration of the HOP in the two polymer compartments are characterized by the following differential equations:

$$\frac{dC_{ps}}{dt} = F_{ps-w} \cdot \frac{A_p}{V_p} \quad (5.16)$$

$$\frac{dC_{pb}}{dt} = F_{pb-w} \cdot \frac{A_p}{V_p} \quad (5.17)$$

If we substitute the flux equations (Eqs. 5.11 and 5.12) into Eqs. 5.16 and 5.17, we obtain:

$$\frac{dC_{ps}}{dt} = k_{ps} \left( \frac{C_w \cdot K_{psw}}{2\delta_p} - C_{ps} \right) \quad (5.18)$$

$$\frac{dC_{pb}}{dt} = k_{pb} (C_w \cdot K_{pbw} - C_{pb}) \quad (5.19)$$

where  $k_{ps}$  and  $k_{pb}$  are the rate constants of mass transfer of HOPs between the polymer compartments and water, with units of  $\text{time}^{-1}$ :

$$k_{ps} = \frac{D_w}{K_{psw}\delta_w} \quad (5.20)$$

$$k_{pb} = \frac{D_w}{2K_{pbw}\delta_w \cdot \delta_p} \quad (5.21)$$

### 5.4.3 Application of the two-compartment non-linear model to the laboratory desorption kinetics experiment

To apply Eqs. 5.18 and 5.19 to the laboratory desorption kinetics experiment, we assumed that:  $C_w=0$ ,  $C_{ps}(t=0)=C_{ps}^0$  and  $C_{pb}(t=0)=C_{pb}^0$ , consistent with the conditions of the experiment.  $C_{ps}^0$  is the initial apparent surface concentration of the PRC, and  $C_{pb}^0$  is the initial bulk concentration of that PRC. Thus, solving Eqs. 5.18 and 5.19 leads to:

$$C_{ps} = C_{ps}^0 \cdot \exp(-k_{ps} \cdot t) \quad (5.22)$$

$$C_{pb} = C_{pb}^0 \cdot \exp(-k_{pb} \cdot t). \quad (5.23)$$

The total concentration of PRC in the polymer (surface and bulk) changes with time according to:

$$C_p(t) = C_{ps}(t) + C_{pb}(t), \quad (5.24)$$

$$C_p(t) = C_{ps}^0 \cdot \exp(-k_{ps} \cdot t) + C_{pb}^0 \cdot \exp(-k_{pb} \cdot t). \quad (5.25)$$

Dividing both sides of Eq. 5.25 by the total initial concentration of PRCs in the polymer,  $C_p^0$ , we obtain:

$$\frac{C_p(t)}{C_p^0} = f_{ps} \cdot \exp(-k_{ps} \cdot t) + f_{pb} \cdot \exp(-k_{pb} \cdot t). \quad (5.26)$$

In Eq. 5.26,  $f_{ps}$  and  $f_{pb}$  represent the mass fraction of PRCs in each polymer compartment, such that  $f_{ps} + f_{pb} = 1$ , which is consistent with the assumption of additive compartments. Eq. 5.26 also assumes that the two compartments undergo mass transfer on different time frames, such that  $k_{ps} \gg k_{pb}$ , and therefore the compartments can be treated as approximately independent. Previous studies have shown that the mathematical expression given by Eq. 5.26 may be used to characterize the mass transfer of PRCs in a system of two sequential compartments, as long as the assumption of  $k_{ps} \gg k_{pb}$  is fulfilled [303, 304]. This model also has been used for describing multiphase mass transfer systems, such as the desorption of hydrophobic contaminants from sediment and soil [305, 306, 307, 308, 309, 310] and drug delivery in biological tissues [303].

We fitted Eq. 5.26 to the experimental depletion profiles of 11 PCBs, allowing the compound-specific parameters,  $k_{ps}$  and  $k_{pb}$ , to be freely fitted to each flow rate, by non-linear regression. The parameter  $f_{ps}$  was interpreted as independent of the water flow rate, and therefore we optimized this parameter by minimizing the root mean square error between the experimental data and the model estimate for each PCB at all three water flow rates. In other words, one value of  $f_{ps}$  was allowed for each PCB, such that the RMSE was minimized over all three water flow rates.

The two-compartment non-linear model successfully fitted the depletion profiles of all 11 PCBs at all three flow rates, employing Eq. 5.26. This model was able to describe the mass transfer from polymer to water of all PCBs for the water flow rates of 2 and 4 L min<sup>-1</sup> (Table 5.2 and Figure 5.6). The two compartment model exhibited some difficulties in fitting the depletion profiles of 5 out of 11 PCBs for the lowest water flow rate of 1 L min<sup>-1</sup>. This might be attributed to both experimental error and also the difficulties of the pumping system to maintain a constant water flow rate at 1 L min<sup>-1</sup>. Overall, the two compartment model appeared to be reasonably adequate for describing the depletion behavior of the 11 PCBs at all three water flow rates.

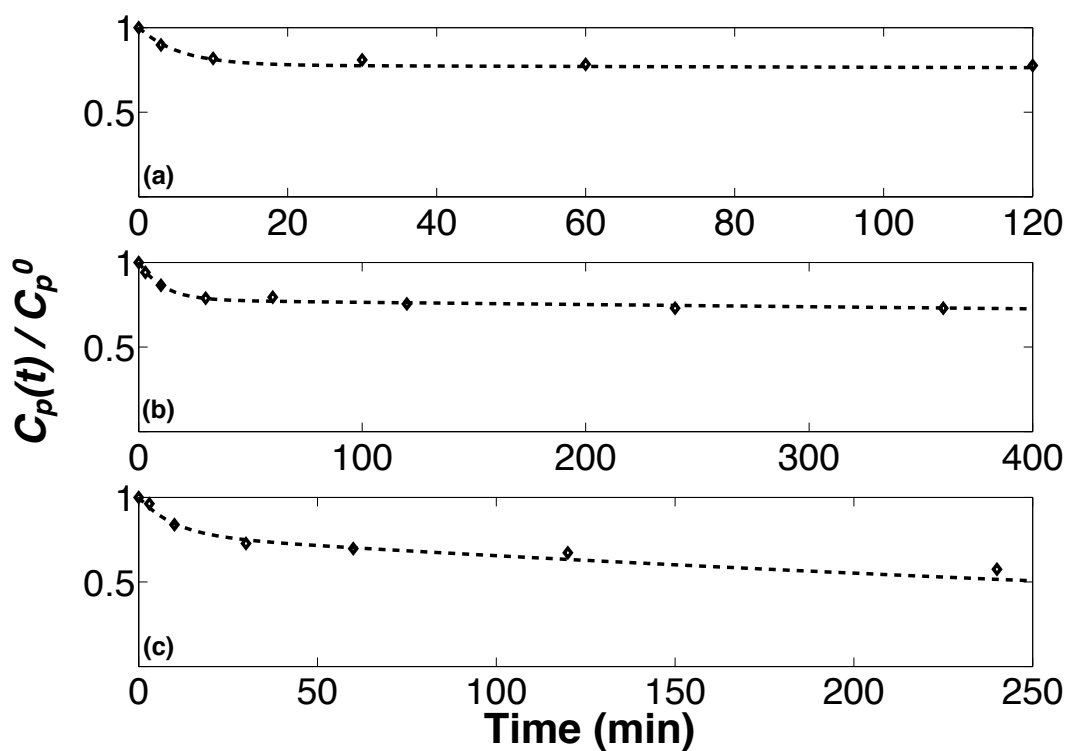


Figure 5.6 – The depletion profiles of PCB180 fitted with the two compartment model (Eq. 5.26) at: (a)  $1 \text{ L min}^{-1}$  water flow rate; (b)  $2 \text{ L min}^{-1}$  water flow rate; (c)  $4 \text{ L min}^{-1}$  water flow rate.

### The rate constants for surface and bulk mass transfer, $k_{ps}$ and $k_{pb}$

The fitting parameter  $k_{ps}$  was found to exceed  $k_{pb}$  by at least two orders of magnitude for all PCBs and all flow rates (Table 5.2). Therefore the assumption of polymer compartment independency was fulfilled. These two parameters represent the rate constants describing mass transfer between each polymer compartment (surface and bulk) and the water compartment. Based on their physical interpretation (Eq. 5.20 and 5.21),  $k_{ps}$  and  $k_{pb}$  are viewed to be dependent on both chemical properties and hydrological conditions.

The fitting parameter  $k_{ps}$  ranged between a low value of  $0.01670 \text{ min}^{-1}$ , observed for PCB27 with the water flow rate of  $1 \text{ L min}^{-1}$ , and a high value of  $1.1021 \text{ min}^{-1}$ , observed for PCB194 with  $1 \text{ L min}^{-1}$  water flow rate (Table 5.2). We did not observe any trends between fitted  $k_{ps}$  values and the physical and chemical properties of the 11 PCBs, such as  $K_{ow}$ ,  $D_w$ , or water solubility.  $k_{ps}$  also did not appear to be statistically associated with variations in the water flow rate. However, the 95% confidence interval (CI) of the fitting parameter,  $k_{ps}$ , revealed high uncertainty in this parameter. We analyzed this variability by dividing the upper bound of the CI to the lower bound of the CI, ( $\frac{CI_{upper}}{CI_{lower}}$ ). This ratio exhibited a value  $> 4$  for 23 out of 33 cases (Table 5.2), meaning that the fitted parameter has a high level of uncertainty. Thus the lack of trend between  $k_{ps}$  and the PCB properties may be attributed to the large uncertainty observed for  $k_{ps}$ .

The second fitting parameter  $k_{pb}$ , varied between a low value of  $0.09810 \times 10^{-3} \text{ min}^{-1}$  for PCB194 at the  $1 \text{ L min}^{-1}$  water flow rate, and a high value of  $1.954 \times 10^{-3} \text{ min}^{-1}$  for PCB27 at the  $4 \text{ L min}^{-1}$  water flow rate (Table 5.2). We also evaluated the statistical uncertainty of the fitting parameter  $k_{pb}$ . For  $k_{pb}$ , 20 out of 33 cases resulted in  $\frac{CI_{upper}}{CI_{lower}}$  values  $< 4$ , which indicated that this parameter was more successfully well-determined than  $k_{ps}$ . The  $\log 1/k_{pb}$  was found to be highly correlated with  $\log K_{pw}$ . Therefore  $\log 1/k_{pb}$  would also correlate with  $\log K_{ow}$  (Figure 5.7). The correlation coefficients between  $\log 1/k_{pb}$  and  $\log K_{ow}$  were exactly the same as the correlation coefficients between  $1/k_{pb}$  and  $\log K_{pw}$ . This similarity was due to the LFER slope of  $\sim 1$  [167], used for estimation of  $K_{pw}$  based on  $K_{ow}$ . The squared correlation coefficients between  $\log K_{ow}$  and  $\log k_{pb}$  were  $\geq 0.84$  for all three water flow rates (Figure 5.7). This is consistent with the assumption that the mass transfer of a HOP between bulk polymer compartment and water is controlled by the equilibrium partitioning coefficient of that HOP into the bulk PDMS, as illustrated by Eq. 5.21. However, linear regressions of both  $\log K_{ow}$  and  $\log K_{pw}$  versus  $\log 1/k_{pb}$  produces a slope  $< 1$  for all three flow rates. For the  $1 \text{ L min}^{-1}$  flow rate, the slope is 0.1874; for the  $2 \text{ L min}^{-1}$  flow rate, the slope is 0.1909; and for the  $4 \text{ L min}^{-1}$  flow rate, the slope is 0.0227. This indicates that  $1/k_{pb}$  has a much weaker dependence on  $K_{ow}$  (or  $K_{pw}$ ) than the linear model relationship given by Eq. 5.21. This suggests that the two-compartment model may be missing an important transport process or compartment. A sub-linear dependence of  $1/k_{pb}$  on  $K_{ow}$  also has been observed in previous studies that employed the one-compartment approach to model PDMS-water sorption kinetics of HOPs

[164, 162, 22, 311, 312, 294].

We briefly evaluated the possibility that diffusion within the bulk polymer phase may need to be considered. This was done by extending  $v_{tot-b}$  in Eq. 5.14 to include the term  $D_p/\delta_p$ , which describes diffusion within the bulk polymer phase, analogous to Eq. 5.5. At the fastest flow rate of 4 L min<sup>-1</sup>, the  $D_p/\delta_p$  term was found to account for less than 20% of the observed  $v_{tot-b}$  for all PCBs that were tested. At lower flow rates, the  $D_p/\delta_p$  term was a negligible contribution to  $v_{tot-b}$ . Inclusion of the  $D_p/\delta_p$  term into the rate constant,  $k_{pb}$ , did not lead to improved regressions between  $\log k_{pb}$  and  $\log K_{ow}$ . Based on these observations, diffusion within the polymer does not appear to be a dominant limitation to mass transfer for any of the conditions and compounds considered here. However, based on the uncertainties in the parameters  $D_p$  and  $v_{tot-b}$ , we cannot rule out the possibility that diffusion within the polymer may play an important role. At the present time, we have decided to neglect this process in the two-compartment model, since it adds needless complexity to model without aiding our interpretation of the datasets available here.

We also observed an increase in  $k_{pb}$  by increasing the water flow rate. This trend was attributed to the effect of the water flow rate on the thickness of the WBL,  $\delta_w$ . We estimated the thickness of WBL by solving Eq. 5.21 for  $\delta_w$ :

$$\delta_w = \frac{D_w A_p}{K_{pw} k_{pb} V_p}. \quad (5.27)$$

The data reported in Tables 5.1 and 5.2 were used for estimation of  $\delta_w$ . This estimated parameter,  $\delta_w$ , had an average value of 0.23  $\mu\text{m}$  for the 4 L min<sup>-1</sup> water flow rate. At this flow rate, the smallest  $\delta_w$  value was 0.0004  $\mu\text{m}$ , obtained for PCB194. The largest  $\delta_w$  value was 1.1  $\mu\text{m}$  obtained for PCB27. For the 2 L min<sup>-1</sup> water flow rate we found an average  $\delta_w$  of 1.03  $\mu\text{m}$ . The smallest  $\delta_w$  value for this water flow rate was 0.0069  $\mu\text{m}$  for PCB194 whereas the largest  $\delta_w$  was 4.7  $\mu\text{m}$ , obtained for PCB27. The average  $\delta_w$ , for 1 L min<sup>-1</sup> water flow rate, was 1.15  $\mu\text{m}$ , whereas the smallest and the largest  $\delta_w$  at this water flow rates were 0.0076  $\mu\text{m}$  and 5.2  $\mu\text{m}$ , respectively, obtained for PCB194 and PCB27.

Based on the estimates shown above, the lowest  $\delta_w$  values are physically unrealistic. These values are associated with the most hydrophobic PCBs (PCB194, PCB180, and PCB149). Additionally,  $\delta_w$  values exhibit a clear trend with respect to compound hydrophobicity;  $\delta_w$  is inversely correlated with  $\log K_{ow}$  according to a squared correlation coefficient of 0.92. However, according to the boundary layer model used here,  $\delta_w$  should be compound independent. The apparently unphysical behavior of the estimated  $\delta_w$  is consistent with the finding that  $\log 1/k_{pb}$  exhibits the wrong dependency on  $\log K_{ow}$ , as discussed in the previous paragraph. This suggests that an important transport process or compartment is not included in the present modeling approach. For practical purposes, the present estimates of  $\delta_w$  are viewed

as semi-quantitative, and these values allow comparisons with other studies that have used similar modeling approaches to estimate  $\delta_w$ .

We compared the magnitude of the average  $\delta_w$  of the present study to the same parameter reported for PCBs using the one compartment model and a batch system, where the water compartment was mixed using either a twister or by shaking the container [311, 312, 294, 167]. The averaged  $\delta_w$ , for the water flow rate of  $4 \text{ L min}^{-1}$ , was about five times smaller than the values reported by Jeannot and Cantwell, and tar Laak et al. [311, 312, 294], whereas for the smaller water flow rates (i.e.  $2 \text{ L min}^{-1}$  and  $1 \text{ L min}^{-1}$ ) the  $\delta_w$  was comparable to the literature reports [311, 312, 294].

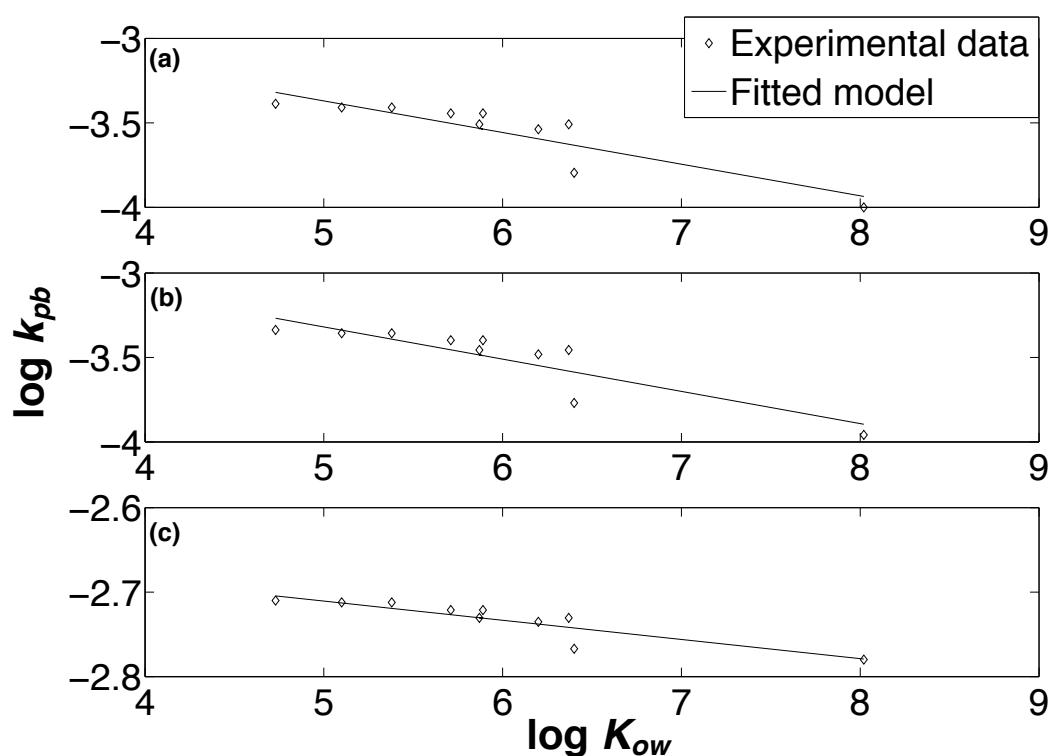


Figure 5.7 – The value of  $\log K_{ow}$  (Table 5.1) plotted vs the  $\log k_{pf}$  (Table 5.2) for: (a)  $1 \text{ L min}^{-1}$  water flow rate experiments ( $\log K_{pb} = -0.1874 \cdot \log K_{ow} - 2.4331$ ),  $R^2 = 0.86$ ; (b)  $2 \text{ L min}^{-1}$  water flow rate experiments ( $\log K_{pb} = -0.1909 \cdot \log K_{ow} - 2.3649$ ),  $R^2 = 0.84$ ; and (3)  $4 \text{ L min}^{-1}$  water flow rate experiments ( $\log K_{pb} = -0.0227 \cdot \log K_{ow} - 2.5969$ ),  $R^2 = 0.87$ .

### The surface and bulk polymer compartments, $f_{ps}$ and $f_{pb}$

To estimate  $f_{ps}$ , we treated this parameter as an optimization parameter (Table 5.2). We divided the interval between 0 and 1 (according to our model  $f_{ps}$  may vary between 0 and 1) into 500 points and fitted the other two fitting parameters,  $k_{ps}$  and  $k_{pb}$ , for each value of  $f_{ps}$ ,

Table 5.2 – The model parameters and the statistical parameters for 11 PCBs estimated with both three compartment and one compartment models.

| Compound | Two compartment model                 |   |   |          |                   | One compartment model |                |         |
|----------|---------------------------------------|---|---|----------|-------------------|-----------------------|----------------|---------|
|          | $f_{ps}^a$                            | $k_{ps}$ (95% confidence interval)<br>( $\text{min}^{-1}$ ) | $k_{pb}$ (95% confidence interval) $\times 1000$<br>( $\text{min}^{-1}$ ) | $R^{2b}$ | RMSE <sup>c</sup> | $k_e$                 | R <sup>2</sup> | RMSE    |
|          | Water flow rate 1 L $\text{min}^{-1}$ |   |   |          |                   |                       |                |         |
| PCB27    | 0.2310                                | 0.01670 (0.0014, 0.0415)                                    | 0.4113 (0.0033, 1.1796)   | 0.33     | 0.0529            | 0.002151              | 0.01           | 0.06434 |
| PCB31    | 0.2564                                | 0.0570 (0.0024, 0.0129)                                     | 0.4111 (0.1435, 1.8623)   | 0.59     | 0.0651            | 0.001380              | 0.15           | 0.06761 |
| PCB51    | 0.1795                                | 0.01240 (0.0051, 0.0220)                                    | 0.3922 (0.1189, 0.8297)   | 0.83     | 0.0241            | 0.001651              | 0.73           | 0.03050 |
| PCB52    | 0.2051                                | 0.01260 (0.0021, 0.0240)                                    | 0.3933 (0.0893, 0.5717)   | 0.61     | 0.0376            | 0.001804              | 0.46           | 0.04460 |
| PCB101   | 0.2051                                | 0.1845 (0.0570, 0.3241)                                     | 0.3573 (0.0287, 0.4321)   | 0.92     | 0.0251            | 0.002879              | 0.08           | 0.1029  |
| PCB105   | 0.2051                                | 0.3031 (0.0129, 0.7282)                                     | 0.3573 (0.0227, 1.1855)   | 0.92     | 0.0264            | 0.003530              | 0.06           | 0.09698 |
| PCB118   | 0.2308                                | 0.1634 (0.0389, 0.2831)                                     | 0.3114 (0.0360, 0.1974)   | 0.90     | 0.0295            | 0.003111              | 0.02           | 0.1177  |
| PCB138   | 0.2051                                | 0.2083 (0.0096, 0.4433)                                     | 0.2934 (0.0923, 0.4240)   | 0.75     | 0.0362            | 0.002523              | 0.07           | 0.09369 |
| PCB149   | 0.2051                                | 0.08350 (0.0374, 0.1359)                                    | 0.3114 (0.1454, 0.4813)   | 0.94     | 0.0222            | 0.002666              | 0.17           | 0.08014 |
| PCB180   | 0.2051                                | 0.2227 ( 0.0372, 0.1340)                                    | 0.1557 (0.0324, 0.1705)   | 0.99     | 0.00850           | 0.003069              | 0.08           | 0.1017  |
| PCB194   | 0.2308                                | 1.1021 (0.0203, 2.1172)                                     | 0.09810 (0.0397, 0.2537)  | 0.98     | 0.0138            | 0.003783              | 0.09           | 0.1585  |
|          | Water flow rate 2 L $\text{min}^{-1}$ |   |   |          |                   |                       |                |         |
| Compound | $f_{ps}^a$                            | $k_{ps}$ (95% confidence interval)<br>( $\text{min}^{-1}$ ) | $k_{pb}$ (95% confidence interval) $\times 1000$<br>( $\text{min}^{-1}$ ) | $R^{2b}$ | RMSE <sup>c</sup> | $k_e$                 | R <sup>2</sup> | RMSE    |
| PCB27    | 0.2308                                | 0.08500 (0.0696, 0.1283)                                    | 0.4572 (0.2314, 0.4693)   | 0.97     | 0.0198            | 0.001518              | 0.04           | 0.1086  |
| PCB31    | 0.2564                                | 0.2735 (0.0588, 0.4458)                                     | 0.4570 (0.1847, 0.8550)   | 0.90     | 0.0415            | 0.002003              | 0.04           | 0.1861  |
| PCB51    | 0.1795                                | 0.1650 ( 0.1127, 0.2480)                                    | 0.4367 (0.2849, 0.4681)   | 0.98     | 0.0149            | 0.001256              | 0.06           | 0.09815 |
| PCB52    | 0.2051                                | 0.0830 (0.0293, 0.1470)                                     | 0.4370 (0.2206, 0.6104)   | 0.94     | 0.0264            | 0.001452              | 0.10           | 0.1030  |
| PCB101   | 0.2051                                | 0.1555 (0.1029, 0.2168)                                     | 0.3970 (0.3319, 0.5159)   | 0.99     | 0.0128            | 0.001472              | 0.03           | 0.1150  |
| PCB105   | 0.2051                                | 0.0946 (0.0698, 0.1484)                                     | 0.3970 (0.2289, 0.3454)   | 0.98     | 0.0158            | 0.001314              | 0.15           | 0.1095  |
| PCB118   | 0.2308                                | 0.1312 (0.0908, 0.1682)                                     | 0.3460 (0.2066, 0.3540)   | 0.99     | 0.0127            | 0.001470              | 0.05           | 0.1296  |
| PCB138   | 0.2051                                | 0.1171 ( 0.0918, 0.1491)                                    | 0.3260 (0.2531, 0.3983)   | 0.99     | 0.0101            | 0.001351              | 0.03           | 0.1047  |
| PCB149   | 0.2051                                | 0.0745 ( 0.0591, 0.0951)                                    | 0.3460 (0.2380, 0.3681)   | 0.99     | 0.0109            | 0.001275              | 0.02           | 0.1007  |
| PCB180   | 0.2051                                | 0.1105 (0.0928, 0.1582)                                     | 0.1730 (0.1116, 0.2543)   | 0.97     | 0.0172            | 0.001310              | 0.20           | 0.1107  |
| PCB194   | 0.2308                                | 0.1020 ( 0.0613, 0.1393)                                    | 0.1090 (0.0407, 0.2698)   | 0.97     | 0.0172            | 0.001308              | 0.06           | 0.1116  |
|          | Water flow rate 4 L $\text{min}^{-1}$ |   |   |          |                   |                       |                |         |
| Compound | $f_{ps}^a$                            | $k_{ps}$ (95% confidence interval)<br>( $\text{min}^{-1}$ ) | $k_{pb}$ (95% confidence interval) $\times 1000$<br>( $\text{min}^{-1}$ ) | $R^{2b}$ | RMSE <sup>c</sup> | $k_e$                 | R <sup>2</sup> | RMSE    |
| PCB27    | 0.2308                                | 0.0982 (0.0164, 0.1372)                                     | 1.954 (1.1824, 2.6020)  | 0.95     | 0.0426            | 0.004175              | 0.50           | 0.1323  |
| PCB31    | 0.2564                                | 0.0278 (0.0055, 0.0517)                                     | 1.952 (0.4578, 1.4119)  | 0.79     | 0.0718            | 0.002870              | 0.65           | 0.09264 |
| PCB51    | 0.1795                                | 0.1267 (0.0398, 0.2339)                                     | 1.936 (1.4605, 2.0161)  | 0.98     | 0.0222            | 0.003299              | 0.61           | 0.09773 |
| PCB52    | 0.2051                                | 0.0804 (0.0014, 0.1633)                                     | 1.937 (1.1206, 2.0602)  | 0.95     | 0.0375            | 0.003407              | 0.57           | 0.1101  |
| PCB101   | 0.2051                                | 0.1526 (0.0282, 0.2855)                                     | 1.900 (1.2484, 1.9955)  | 0.96     | 0.0299            | 0.0034899             | 0.43           | 0.1206  |
| PCB105   | 0.2051                                | 0.09420 (0.0017, 0.2053)                                    | 1.903 (1.1651, 2.0607)  | 0.96     | 0.0343            | 0.003435              | 0.54           | 0.1117  |
| PCB118   | 0.2308                                | 0.1376 (0.0311, 0.2407)                                     | 1.856 (1.4376, 2.5452)  | 0.97     | 0.0334            | 0.004329              | 0.47           | 0.1311  |
| PCB138   | 0.2051                                | 0.08660 (0.0174, 0.2051)                                    | 1.856 (1.0514, 2.4133)  | 0.96     | 0.0344            | 0.003625              | 0.51           | 0.1222  |
| PCB149   | 0.2051                                | 0.1153 ( 0.0068, 0.1704)                                    | 1.713 (1.1817, 2.2104)  | 0.96     | 0.0298            | 0.003548              | 0.57           | 0.1123  |
| PCB180   | 0.2051                                | 0.1153 (0.0194, 0.1551)                                     | 1.710 (1.0876, 1.8191)  | 0.96     | 0.0298            | 0.003248              | 0.46           | 0.1150  |
| PCB194   | 0.2308                                | 0.1367 ( 0.0408, 0.2292)                                    | 1.663 (1.3614, 2.3009)  | 0.97     | 0.0302            | 0.004046              | 0.50           | 0.1224  |

<sup>a</sup> This parameter was optimized by dividing the 0 to 1 interval into 500 nodes and fitting the other two fitting parameters,  $k_{ps}$  and  $k_{pb}$  freely for each value of  $f_{ps}$ ; <sup>b</sup> The squared regression coefficient, representing the goodness of fit; <sup>c</sup> The root mean square error of the fit, which represents the distance between each experimental point and the model estimation.

employing Eq. 5.26. The  $f_{ps}$  value that produced the largest  $R^2$  and the smallest RMSE for all three water flow rates was considered the optimized  $f_{ps}$ .

The optimized value of  $f_{ps}$  varied between 0.1795, found for PCB51, to 0.2564 for PCB31. The magnitude of  $f_{ps}$  indicates that the surface sorption compartment contributed importantly to the observed PCB desorption kinetics.  $f_{ps}$  values exhibit little variability over the PCB set, and we did not observe any clear evidence of compound dependency in this property. Thus, according to the two-compartment model results, PCB desorption kinetics can be mostly explained by absorption into the bulk PDMS phase ( $f_{ps} \sim 80\%$ ), with a smaller fraction explained by surface adsorption to the PDMS surface ( $f_{ps} \sim 20\%$ ). This is in agreement with previous studies that have suggested that mass transfer between PDMS and water is governed mainly by sorption into the PDMS bulk phase [158, 160, 163, 22, 299].

### Sensitivity analysis of the model parameters

We evaluated the sensitivity of our model towards the optimization parameter  $f_{ps}$  and the fitting parameter  $k_{ps}$ . We also examined the effect of these parameters on the third fitting parameter  $k_{pb}$  under three different conditions: (1)  $k_{pb}$  was estimated while constraining  $k_{ps}$  at the average value of 0.1173 (calculated using the data in Table 5.2) and with  $f_{ps}$  as a simultaneous optimization parameter; (2)  $k_{pb}$  was estimated while constraining  $f_{ps}$  at the average value of 0.2145 (calculated using the data in Table 5.2) and leaving  $k_{ps}$  as a simultaneous optimization parameter; and (3)  $k_{pb}$  was estimated while setting both  $f_{ps}$  and  $k_{ps}$  at the average values of 0.2145 and 0.1173, respectively. As a point of reference, we used the  $k_{pb}$  values that had been estimated with all three parameters ( $k_{ps}$ ,  $k_{pb}$  and  $f_{ps}$ ) freely fitted, as given in Table 5.2.

Fitted values if  $k_{pb}$  appeared to be more sensitive to  $f_{ps}$  than to  $k_{ps}$  (Figure 5.8). With  $k_{ps}$  set to the average value of 0.1173, we observed a good agreement between the re-optimized  $k_{pb}$  values and the reference  $k_{pb}$  values for all three water flow rates. However, with  $f_{ps}$  constrained to an average value of 0.2145, re-optimized  $k_{pb}$  values exhibited less good agreement with the reference  $k_{pb}$  values. This effect was most severe for values obtained with the desorption experiment at 4 L min<sup>-1</sup> water flow rate. In the third case, where both  $f_{ps}$  and  $k_{ps}$  were set to the average values, the re-optimized  $k_{pb}$  values deviated far from the reference values shown in Table 5.2. These disagreements were most pronounced for the experiments with water flow rates of 1 and 4 L min<sup>-1</sup>. These outcomes suggest that the optimization parameters  $f_{ps}$  and the fitting parameter  $k_{ps}$  can not be constrained at the same time. However, the lack of sensitivity towards  $k_{ps}$  indicates that this parameter may be approximated by the average value of  $0.1173 \pm 0.073$  over all 11 PCBs and three water flow rates (excepting the aberrant  $k_{ps}$  value for PCB194 with 1 L min<sup>-1</sup> water flow rate). Considering the lack of trend between  $f_{ps}$  and the compounds properties, such as  $K_{ow}$ , water solubility and  $D_w$ , this parameter needs to be defined for each compound experimentally.



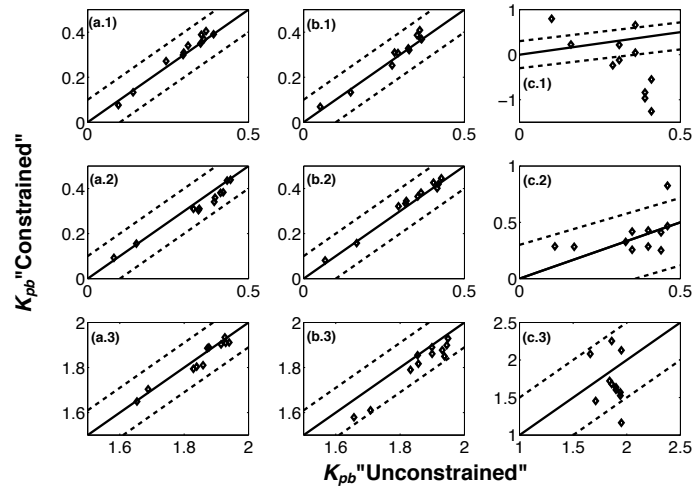


Figure 5.8 – The unconstrained  $k_{pb}$  vs the constrained  $k_{pb}$  estimated having: (a.1) 1 L min<sup>-1</sup> and  $k_{ps} = 0.1173$ ; (a.2) 2 L min<sup>-1</sup> and  $k_{ps} = 0.1173$ ; (a.3) 4 L min<sup>-1</sup> and  $k_{ps} = 0.1173$ ; (b.1) 1 L min<sup>-1</sup> and  $f_{ps} = 0.2051$ ; (b.2) 2 L min<sup>-1</sup> and  $f_{ps} = 0.2051$ ; (b.3) 4 L min<sup>-1</sup> and  $f_{ps} = 0.2051$ ; (c.1)  $f_{ps} = 0.2051$  and  $k_{ps} = 0.1173$ , and 1 L min<sup>-1</sup> water flow rate; (c.2)  $f_{ps} = 0.2051$  and  $k_{ps} = 0.1173$ , and 2 L min<sup>-1</sup> water flow rate; and (c.3)  $f_{ps} = 0.2051$  and  $k_{ps} = 0.1173$ , and 4 L min<sup>-1</sup> water flow rate.

### The surface adsorption coefficients of 11 PCBs

We estimated the surface adsorption coefficient ( $K_{psw}$ ) of 11 PCBs using Eq. 5.20. We solved Eq. 5.20 for  $K_{psw}$  and obtained:

$$K_{psw} = \frac{D_w}{k_{ps} \cdot \delta_w}. \quad (5.28)$$

We entered compound-specific  $D_w$ ,  $\delta_w$  and  $k_{ps}$  values for each water flow rate, in Eq. 5.28 for all 11 PCBs (Table 5.3). The  $K_{psw}$  values ranged from 0.28 (m) for PCB101 at the 1 L min<sup>-1</sup> water flow rate to 2.61 for PCB194 at the 4 L min<sup>-1</sup> water flow rate. We also considered a second approach for estimation of  $K_{psw}$ , which was independent of the desorption kinetics of the depletion experiment. We defined  $K_{psw}$  as follows:

$$K_{psw} = \frac{C_s}{C_w} \quad (5.29)$$

where  $C_s$  is the concentration of the HOP adsorbed on the surface of polymer. Assuming a partitioning equilibrium between two phases,  $C_w = (1 - f_{ps}) \cdot \frac{C_p}{K_{pw}}$ , and therefore Eq. 5.29 can be rewritten as follows:

$$K_{psw} = \left( \frac{f_{ps}}{1 - f_{ps}} \right) \cdot \left( \frac{V_p}{A_p} \right) \cdot K_{pw} \quad (5.30)$$

## Chapter 5. Accelerated sampler

Table 5.3 – The estimated polymer surface adsorption coefficient,  $K_{psw}$ , for 11 PCBs at three water flow rates.

| Compound | $K_{psw}^a$ (length)  |                       |                       | Flow rate independent (Eq. 5.30) |
|----------|-----------------------|-----------------------|-----------------------|----------------------------------|
|          | 1 L min <sup>-1</sup> | 2 L min <sup>-1</sup> | 4 L min <sup>-1</sup> |                                  |
| PCB27    | 0.36                  | 0.08                  | 0.29                  | 4.43                             |
| PCB31    | 1.07                  | 0.02                  | 1.04                  | 5.09                             |
| PCB51    | 1.09                  | 0.09                  | 0.53                  | 7.57                             |
| PCB52    | 2.04                  | 0.35                  | 1.59                  | 17.02                            |
| PCB101   | 0.28                  | 0.36                  | 1.76                  | 36.40                            |
| PCB105   | 0.25                  | 0.90                  | 4.31                  | 55.09                            |
| PCB118   | 0.39                  | 0.54                  | 2.67                  | 61.16                            |
| PCB138   | 0.61                  | 1.23                  | 8.60                  | 112.48                           |
| PCB149   | 2.39                  | 3.03                  | 13.85                 | 166.37                           |
| PCB180   | 0.50                  | 1.06                  | 10.24                 | 178.26                           |
| PCB194   | 2.61                  | 31.06                 | 349.68                | 8638.85                          |

<sup>a</sup> The value estimated using using Eq. 5.20, average  $\delta_w$  for each water flow rate, and the averaged  $k_{ps}$  of 0.1173.

Eq. 5.30 enabled us to estimated  $K_{psw}$  of 11 PCBs independently from the depletion experiment kinetics. The  $K_{psw}$  values estimated with Eqs. 5.30 vs 5.28 exhibited discrepancies of 1 to 3 orders of magnitude (Table 5.3). However, these different estimates were correlated with one another. The  $R^2$  for 4 L min<sup>-1</sup> water flow rate was 0.93. However, correlation between these two parameters, i.e.  $K_{psw}$  estimated using Eqs. 5.30 and 5.28, for 2 L min<sup>-1</sup> water flow rates appeared to be less good with a  $R^2$  of 0.67 (Figure 5.9). We did not observe any correlation between these two parameters for the case of the 1 L min<sup>-1</sup> water flow rate. Further investigations are needed in order to better understand the processes involved in the mass transfer of HOPs to the polymer surface.

### Application of the two compartment model to compound uptake

To apply the two-compartment model to compound uptake, we assume that the HOP concentration in both polymer compartments is zero at  $t = 0$ , and we assume that  $C_w$  is constant (and is not affected by the uptake). Based on these assumptions, the solution to equations 5.18 and 5.19 are:

$$C_{ps}(t) = \frac{C_w \cdot K_{psw}}{2\delta_p} (1 - \exp(-k_{ps} \cdot t)) \quad (5.31)$$

$$C_{pb}(t) = C_w \cdot K_{pbw} (1 - \exp(-k_{pb} \cdot t)). \quad (5.32)$$

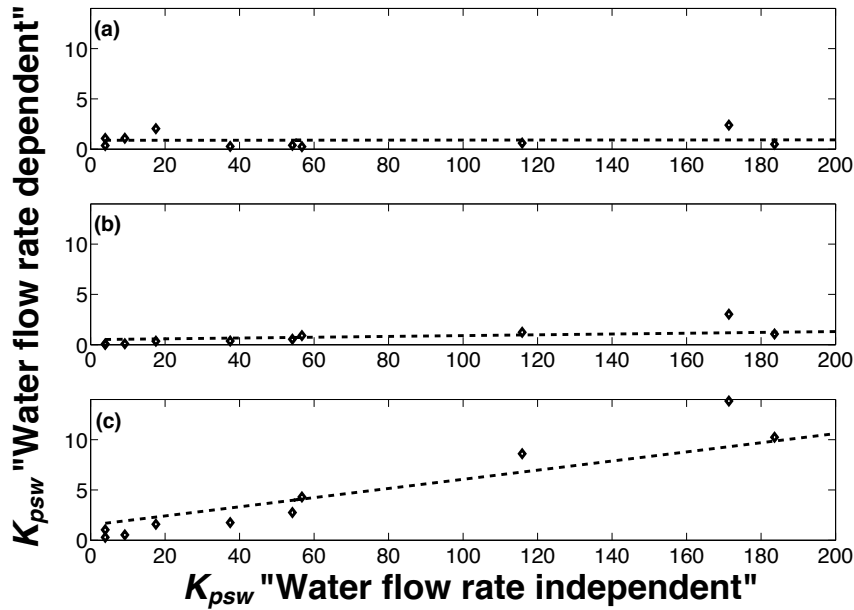


Figure 5.9 – The value of  $K_{psw}$  estimated using Eq. 5.28 vs the same parameter estimated using Eq. 5.30 for: (a)  $1 \text{ L min}^{-1}$  water flow rate; (b)  $2 \text{ L min}^{-1}$  water flow rate; and (c)  $4 \text{ L min}^{-1}$  water flow rate.

Under the assumption of two additive polymer compartments, the total polymer concentration variation of an HOP as a function of time can be formulated as:

$$C_p(t) = C_w \cdot \left( \frac{K_{psw}}{2\delta_p} (1 - \exp(-k_{ps} \cdot t)) + K_{pbw} (1 - \exp(-k_{pb} \cdot t)) \right). \quad (5.33)$$

The surface compartment may be neglected during the uptake of HOPs. We evaluated the relative contributions of the surface compartment and the bulk compartment during the uptake process. We used: the  $K_{psw}$  values of the desorption experiment at  $4 \text{ L min}^{-1}$  water flow rate (Table 5.3), the  $k_{ps}$  values listed in Table 5.2,  $k_{pb}$  values listed in Table 5.2, the exposure time of 200 min, and finally we assumed that  $K_{pbw} \approx K_{pw}$ . The contribution of the surface polymer compartment was  $< 5\%$  for all 11 PCBs at all three water flow rates. This implies that uptake kinetics may be approximately represented by neglecting the surface compartment, which gives:

$$C_p(t) = C_w K_{pw} (1 - \exp(-k_{pb} \cdot t)) \quad (5.34)$$

In this case  $k_{pb}$  may be estimated using the LFER established between  $\log k_{pb}$  and  $\log K_{ow}$  (Figure 5.7).

### Field evaluation of the novel sampler

We compared the accelerated sampler with conventional passive samplers for measurements of concentration of the truly dissolved fraction of 11 PCBs in the water column of Lake Geneva.

Amongst the 11 PCBs in this study, we were able to successfully detect 5 PCBs in the water column of the lake with both sampling methods, and four out of the five detected PCBs could be quantified by both sampling methodologies (Table 5.4). The two sampling methodologies produced concentration estimates that were in close agreement for all four quantified PCBs. Overall, the absolute concentration distribution (ACD) for all four compounds was  $\leq 50\%$ , which was within the acceptable experimental error interval [15], indicating the agreement between these two sampling methodologies. The largest discrepancies arose for the two PCBs that were very close to the method LOQ (PCB101 and PCB118). This agreement between the two methodologies demonstrates the adequacy of both the accelerated sampling approach and the two compartment model used for describing the accelerated sampler system.

This accelerated sampler is able to reach a method limit of quantification of  $0.001 \text{ pg L}^{-1}$  for these PCBs in the water column after only 2 h of sampling (Figure 5.10). Thus the accelerated sampler is able to capture the variations in the water column of an aquatic system with a time resolution of 2-5 h, whereas the passive sampling method has a time resolution of 4-8 weeks, depending on the hydrophobicity of the target analyte. Additionally, the accelerated sampler collects only the truly dissolved fraction of the target analyte in the water column, independently from the suspended solid and the dissolved organic matter of the aquatic system. This type of sampling is extremely difficult to perform using large volume sampling, whereas it has been made possible by the accelerated sampler. The accelerated sampler also overcame the issue of the sampling in the deep water column, which is a challenging task for both passive sampling and large volume sampling.

## 5.4. Results and discussion

Table 5.4 – The concentrations of four PCBs in the water column of Lake Geneva, measured using two different sampling methodologies.

| Compound | Passive samplers                 |                                  |   |                     | Accelerated sampler   |  |  |                     | ACD% <sup>d</sup> |
|----------|----------------------------------|----------------------------------|---|---------------------|---|--|--|---------------------|-------------------|
|          | $C_w$ June (pg L <sup>-1</sup> ) | $C_w$ July (pg L <sup>-1</sup> ) | Average<br>$C_w$ <sup>a</sup> (pg L <sup>-1</sup> ) | AE <sup>a</sup> (%) | June 12 <sup>th</sup><br>$C_w$ (pg L <sup>-1</sup> ) <sup>b</sup> | July 2 <sup>nd</sup><br>$C_w$ (pg L <sup>-1</sup> ) <sup>b</sup> | Average<br>$C_w$ (pg L <sup>-1</sup> ) | AE <sup>c</sup> (%) |                   |
| PCB52    | 0.043                            | 0.036                            | 0.040   | 25.0                | 0.033   | 0.043  | 0.038                                  | 20.7                | 5.6               |
| PCB101   | 0.0022                           | 0.0016                           | 0.0019  | 33.2                | 0.0019  | 0.0011   | 0.0015                                 | 37.7                | 38.5              |
| PCB118   | 0.0027                           | 0.0021                           | 0.0024  | 32.8                | 0.0011  | 0.0013   | 0.0012                                 | 3.5                 | 52.9              |
| PCB138   | 0.0052                           | 0.0056                           | 0.0053  | 17.5                | 0.0051  | 0.0058   | 0.0055                                 | 10.0                | 3.1               |
| PCB180   | nq <sup>e</sup>                  | nq <sup>e</sup>                  | nq <sup>e</sup>                                     | nq <sup>e</sup>     | nq <sup>e</sup>   | nq <sup>e</sup>  | -                                      | -                   | -                 |

<sup>a</sup> The value is determined based on 20 PDMS strips deployed at depths ranging from 70 m to 166.5 m; <sup>b</sup> Water column concentration has been estimated using Eq. 5.34, neglecting the polymer surface compartment; <sup>c</sup> The absolute error computed is based on 2 PDMS strips of the accelerated sampler field deployment; <sup>d</sup> The absolute concentration deviation (ACD) from the average value; <sup>e</sup> The concentration was smaller than the method limit of quantification (MLOQ) of 0.001 pg L<sup>-1</sup>, thus non-quantifiable "nq".

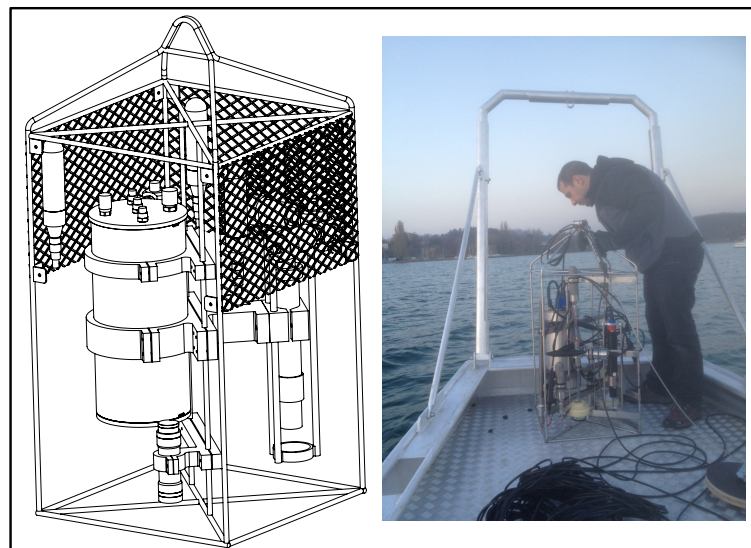


Figure 5.10 – Schematic of the accelerated sampler design and the finished prototype, built in collaboration with Angelos Mallios (WHOI). The field-test was carried out at a depth of 6 m in Lake Geneva.



## **6 Hydrophobic organic pollutant concentrations exhibit strong spatial gradients in the deep water column of Lake Geneva**

**Main author: Saer Samanipour**

**Contributions: This chapter was prepared by Saer Samanipour with editorial comments by J. Samuel Arey.**

**Angelos Mallios and Richard Camilli, from Woods Hole Oceanographic Institution (WHOI), contributed to the development and field test of the accelerated sampler.**

**Oscar Pizarro, from The University of Sydney, reconstructed MIR navigation data.**

### Abstract

It is frequently assumed that hydrophobic pollutants have uniform spatial distributions in surface water bodies such as lakes. We evaluated the spatial concentration distributions of 11 quantifiable hydrophobic organic pollutants (HOPs) in the water column of Lake Geneva, using both vertical and horizontal measurement transects. We successfully detected and quantified these 11 HOPs in 16 distinct water column sampling locations, using comprehensive two dimensional gas chromatography coupled to an electron capture detector (GC×GC- $\mu$ ECD). We further confirmed the identity of these target analytes in a selected subset of samples, employing GC×GC coupled to electron capture negative chemical ionization time-of-flight mass spectroscopy (ENCI-TOFMS). The observed concentration differences in a vertical profile from 70 to 166.5 m (bottom) depth ranged between a factor of 2 to 3. Based on sampling at 5 statistically grouped geographical locations in deep waters near the lake bottom, we observed horizontal concentration differences that varied between a factor of 2 to 60. We also analyzed 4 sediment samples collected from 4 different locations in the lake. We successfully detected and quantified 9 out of 29 target analytes in the sediment samples. Most of the quantified target analytes measured in both the water and sediment samples were found to be at/or near sediment-water partitioning equilibrium. Based on the spatial concentration distribution of our target analytes in both the water column and sediment of the lake, we were able to suggest potential source areas for several of the pollutants. To our knowledge, the present study is the most comprehensive report of concentration distributions of HOPs in the water column of a deep aquatic system.

### 6.1 Introduction

It is frequently assumed that HOPs exhibit uniform concentrations throughout the water column of an aquatic system [32, 41]. Accurate determination of trace concentrations of HOPs is logistically challenging and costly [17, 33, 63], and this has discouraged the acquisition of large measurement datasets needed to resolve spatial and temporal gradients of HOPs in aquatic systems. Consequently, assessments of aquatic HOPs and related environmental modeling efforts frequently rely on a few measurements taken at a single location in an aquatic system [42, 313, 314, 136, 47]. However, if it is the case that HOPs concentrations do exhibit substantial spatial variability in an aquatic system, then studies that conduct measurements at only a single location may commit significant errors in their estimates of inventories, sources, sinks, and exposures of these pollutants.

Little published data are available regarding the spatial distribution of HOPs in the water columns of aquatic systems. Most of these published data are focused on the shallow water column (depths < 10 m) and on the horizontal spatial distribution of HOPs [19, 34, 35, 36, 37, 21, 9, 38]. There are a few works that have evaluated the vertical gradient of HOPs in the deep water column of an aquatic system [51, 52, 53]. All of these studies indicated



the possibility of existence of significant vertical and/or horizontal gradients of HOPs in the water column. To our knowledge there is no published work that evaluates both vertical and horizontal concentration distributions of HOPs in the deep water column of an aquatic system.

HOPs can be introduced into the lake environment through different pathways, such as urban wastewater effluents and runoff, atmospheric deposition, tributaries, and air-water exchange [32, 39, 41, 34, 53, 35, 19]. Some HOPs, such as polychlorinated biphenyls (PCBs), organochlorinated pesticides, and polybrominated diphenylethers (PBDEs) have been the subject of production and use restrictions due to their environmental persistence and toxicity [249, 7].

Measuring these HOPs in complex environmental samples is an on-going challenge, due to their trace level concentrations [17], the presence of substantial matrix effects [52, 15, 53] and the logistical constraints involved [18, 24]. Our recent reports showed that the high separation power of comprehensive two dimensional gas chromatography (GC×GC) coupled to a highly sensitive detector, such as electron capture detector (ECD) and/or electron capture negative chemical ionization time-of-flight mass spectrometry (ENCI-TOFMS), enables the analyst to quantify trace level concentrations and also mitigate matrix effects [53, 15, 16]. In another recent study, we developed an accelerated sampler that can be deployed in the deep and shallow water column of an aquatic system and sample the truly dissolved fraction of HOPs in the water column within only a few hours [315]. This accelerated sampling system enabled us to overcome the logistical issues of the deep water sampling of HOPs. These advances made it possible to conduct measurements of HOPs at several locations in the deep water column of a large aquatic system, Lake Geneva.

In the present study, we analyzed for 29 HOPs along both vertical and horizontal transects in the deep water column of Lake Geneva. The sediments of the lake were also analyzed for these 29 target analytes at four different locations of the lake floor. We used the spatial distributions of these pollutant concentrations of the water column and sediment to evaluate the potential sources of the quantified pollutants and also to gain insight into the processes affecting their fate and transport in the lake. This is the first study that evaluates the concentration distribution of HOPs in the water column of a large aquatic system in both the vertical and horizontal directions.

## 6.2 Methods

### 6.2.1 Water sampling location

We sampled the water column of Lake Geneva, Switzerland, at 12 different geographic locations, using both conventional passive samplers and also a recently developed accelerated sampler. Lake Geneva is one of the largest fresh water resources in western Europe and it

## Chapter 6. Spatial distribution of Hydrophobic organic pollutants

provides drinking water to about 520,000 people [151]. The lake also receives treated effluents of several wastewater treatment plants (WWTP) bordering both the northern and the southern shores [153].

### Passive samplers deployment

We deployed passive samplers in the water column of the lake at depths ranging from 70 to 166.5 m (Figure 6.1). These passive samplers were deployed in duplicates at five different depths (70, 107, 147, 162 and 166.50 m) at a location having a total depth of 167 m. Thus the deepest sampler was situated 50 cm above the lake floor. We sampled the water column of the lake for three one-month long exposure periods during June, July and August of 2011. The passive sampling site was located at  $46^{\circ} 49' 82.88''$  N and  $6^{\circ} 58' 10.55''$  E, World Geodetic System, WGS84, 1,200 m distance from the northern shore of the lake and about 500 m distance from the outfall of the largest WWTP that emits effluent to the lake. We used solvent pre-washed stainless steel cages for deployment of the passive samplers. This deployment method enabled us to overcome both issues of biofilm formation. We used stainless steel chain and bottom release for the deployment of the cages.

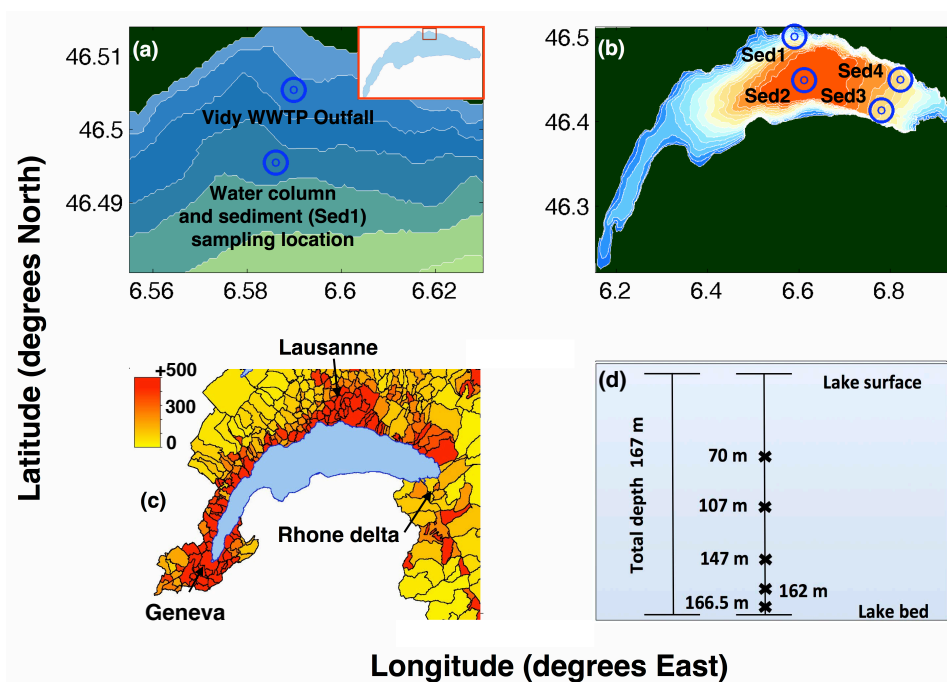


Figure 6.1 – Maps depicting (a) sampling location for the water column and sediment (Sed1) in Lake Geneva, with lake bathymetry contours of 45 m overlaid; (b) the four sediment sampling locations, with bathymetry contours of 20 m overlaid; and (c) population density of the Lake Geneva area, by municipality, 2007 (source: bfs.admin.ch). (d) Schematic showing depths at which the water column samplers were deployed.

### Accelerated sampler deployment

We employed a recently developed accelerated sampler [315] to measure the truly dissolved fraction of the target analytes in the deep water column of Lake Geneva. The accelerated sampler was deployed along 11 different trajectories using the human-occupied scientific MIR submersibles during the ELEMO field campaign in the summer of 2011 [151]. The trajectories ranged from 2-10 km in length and were conducted at an altitude of 2 to 5 m above the lake floor (Figure 6.2 and Table 6.1). The depths of the trajectories of the accelerated samplings varied between 100 and 310 m. The exposure times during the active sampling ranged from 70 to 180 min, using a sampler water flow rate of  $4 \text{ L min}^{-1}$  (Table 6.1).

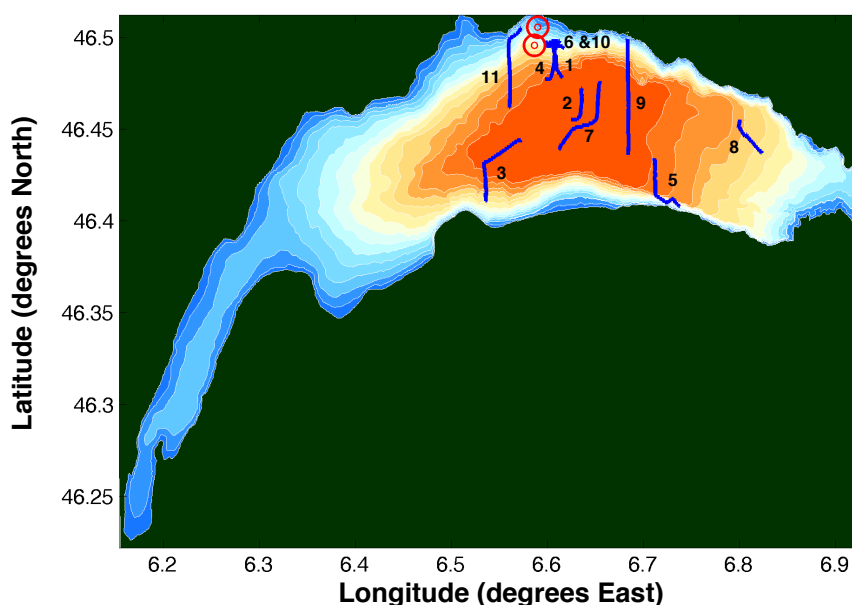


Figure 6.2 – MIR trajectories at different locations in Lake Geneva, depicted as blue lines, on a map of the lake in WGS84 coordinates. Bathymetry contours of 45 m are overlaid. Depicted numbers represent the trajectory number (Table 6.1). The red circles indicate the location of WWTP in Vidy Bay and the passive sampling location.

### Sediment samples

We collected sediment samples from four different locations in the lake (Figure 6.1). These sediment cores were collected either using a Benthos gravity corer from a boat (Sed1 and Sed4) or directly with the MIR submersibles (Sed2 and Sed3). The cores were collected at depths ranging from 80 (Sed4) to 310 m (Sed2).

## Chapter 6. Spatial distribution of Hydrophobic organic pollutants

Table 6.1 – Trajectories along which we deployed the accelerated sampler for measuring the truly dissolved fraction of our target analytes.

| Trajectories |            |                              |                 |                                    |
|--------------|------------|------------------------------|-----------------|------------------------------------|
| Number       | Date       | General Geographical area    | Depth range (m) | Accelerated sampler duration (min) |
| 1            | 04/07/2011 | Vidy Bay area                | 180-280         | 130                                |
| 2            | 05/07/2011 | Center of the lake           | 300-305         | 186                                |
| 3            | 07/07/2011 | Evian area                   | 200-300         | 120                                |
| 4            | 08/07/2011 | Vidy Bay area                | 190-280         | 116                                |
| 5            | 11/07/2011 | Rhône delta area             | 180-300         | 145                                |
| 6            | 12/07/2011 | Vidy Bay area                | 120-125         | 178                                |
| 7            | 12/07/2011 | Center of the lake           | 300-305         | 130                                |
| 8            | 14/07/2011 | Vevey area                   | 80-200          | 88                                 |
| 9            | 17/07/2011 | Center and Lutry area        | 80-286          | 52                                 |
| 10           | 02/08/2011 | Vidy Bay area                | 140-145         | 73                                 |
| 11           | 04/08/2011 | Center and the Vidy Bay area | 83-280          | 167                                |

All samples collected via conventional passive sampling and accelerated sampler, as well as experimental controls and sediment cores were immediately transported to the lab and stored at -20 °C.

### 6.2.2 Chemicals

We purchased analytical standard mixtures of 11 polychlorinated biphenyls (PCBs) and 18 organochlorinated pesticides from Sigma-Aldrich, Switzerland (Table 6.2). Analytical standards of PCB30, PCB50, PCB145 and PCB204 were also purchased from Sigma-Aldrich. We obtained ACS grade pentane, ACS grade methanol and pesticide grade hexane from VWR, Switzerland.

### 6.2.3 Sample preparation

#### Extraction of PDMS strips used for both passive samplers and the accelerated sampler

To measure the truly dissolved fraction of our target analytes in the water column of Lake Geneva (employing either the passive sampling methodology or the accelerated sampler), we used polydimethylsiloxane sheets (PDMS, AlteSil Laboratory Sheet, UK) having a thickness of 0.5 mm. These sheets were cut into PDMS strips of  $10 \times 1 \times 0.05 \text{ cm}^3$  with an average weight of  $1.98 \pm 0.2 \text{ g}$ . PDMS is an ideal sampling medium due to the linearity of the HOP mass transfer between water and PDMS for a wide range of  $K_{ow}$  values [164, 21]. The PDMS strips were cleaned using Soxhlet extraction with methanol for a period of 24 h. The clean strips were subsequently stored at -20 °C. 5 clean PDMS strips were utilized as PDMS blanks. Each clean PDMS strip was loaded with 20 ng of 4 (PCB30, PCB50, PCB145, and PCB204) performance reference compounds (PRCs). For the PRC loading of the strips we followed the protocol

Table 6.2 – The complete list of target analytes investigated in this study, their GC×GC-ENCI-TOFMS first dimension retention time  $t_{r1}$  (min), their GC×GC-ENCI-TOFMS second dimension retention time (s), and their positive identity confirmation in environmental samples using GC×GC-ENCI-TOFMS.

| Abbreviation  | Compound name  | $t_{r1}$ (min) | $t_{r2}$ (s) | Presence in the environmental samples confirmed by GC×GC-ENCI-TOFMS |                             |                  |
|---|--|----------------|--------------|---|-----------------------------|------------------|
|   |  |                |              | Water (passive sampling)  | Water (accelerated sampler) | Sediment samples |
| HOP1  | 2,4,5,6-tetrachloro- <i>m</i> -xylene                                | 25.10          | 2.60         | 3/3   | 2/2                         | 0/3              |
| HOP2  | $\alpha$ -hexachlorocyclohexane                                      | 26.8           | 2.95         | 0/3   | 0/2                         | 0/2              |
| HOP3  | $\gamma$ -hexachlorocyclohexane                                      | 27.07          | 3.54         | 3/3   | 2/2                         | 2/2              |
| HOP4  | $\beta$ -hexachlorocyclohexane                                       | 27.82          | 4.32         | 3/3   | 2/2                         | 1/2 <sup>a</sup> |
| HOP5  | $\delta$ -hexachlorocyclohexane                                      | 28.03          | 4.68         | 3/3   | 2/2                         | 1/2              |
| HOP6  | 2,2',5'-trichlorobiphenyl  | 28.50          | 3.21         | 0/3   | 0/2                         | 0/2              |
| HOP7  | 2,4,4'-trichlorobiphenyl   | 29.10          | 3.02         | 0/3   | 0/2                         | 0/2              |
| HOP8  | 1,4,5,6,7,8,8-heptachloro-3a,4,7,7a-tetrahydro-4,7-methano-1H-indene | 31.75          | 2.94         | 0/3   | 0/2                         | 0/2              |
| HOP9  | 2,2',3,5'-tetrachlorobiphenyl  | 31.60          | 3.28         | 0/3   | 0/2                         | 0/2              |
| HOP10   | aldrin   | 32.61          | 3.10         | 3/3   | 2/2                         | 1/2 <sup>a</sup> |
| HOP11   | 2,2',5,5'-tetrachlorobiphenyl  | 33.21          | 3.22         | 3/3   | 2/2                         | 1/2 <sup>a</sup> |
| HOP12   | heptachlor exo-epoxide   | 33.54          | 3.92         | 3/3   | 2/2                         | 1/2              |
| HOP13   | $\gamma$ -chlordane  | 34.14          | 2.80         | 0/3   | 0/2                         | 0/2              |
| HOP14   | 2,2',4,5,5'-pentachlorobiphenyl                                      | 35.53          | 3.62         | 3/3   | 2/2                         | 2/2              |
| HOP15   | $\beta$ -endosulfan  | 36.68          | 4.78         | 3/3   | 0/2 <sup>b</sup>            | 0/2              |
| HOP16   | $\alpha$ -chlordane  | 36.82          | 3.54         | 0/3   | 0/2                         | 0/2              |
| HOP17   | 1-chloro-4-[2,2-dichloro-1-(4-chlorophenyl)ethyl]benzene             | 37.39          | 3.40         | 0/3   | 0/2                         | 0/2              |
| HOP18   | 1,1-bis-(4-chlorophenyl)-2,2-dichloroethene                          | 38.62          | 4.20         | 3/3   | 2/2                         | 2/2              |
| HOP19   | endrin   | 38.20          | 4.50         | 3/3   | 2/2                         | 0/2              |
| HOP20   | 2,3',4,4',5'-pentachlorobiphenyl                                     | 39.22          | 4.24         | 3/3   | 1/2                         | 0/2              |
| HOP21   | endrin aldehyde  | 39.56          | 4.98         | 3/3   | 2/2                         | 2/2              |
| HOP22   | 2,2',3,3',4,4'-hexachlorobiphenyl                                    | 40.68          | 3.80         | 0/3   | 0/2                         | 0/2              |
| HOP23   | 2,2',3,5,5',6'-hexachlorobiphenyl                                    | 41.98          | 4.40         | 3/3   | 2/2                         | 0/2              |
| HOP24   | endosulfan sulfate   | 43.08          | 5.40         | 0/3   | 0/2                         | 0/2              |
| HOP25   | 1,1,1-trichloro-2,2-bis(4-chlorophenyl)ethane                        | 45.12          | 3.48         | 0/3   | 0/2                         | 0/2              |
| HOP26   | 2,2',3,4,4',5,5'-heptachlorobiphenyl                                 | 46.01          | 4.5          | 3/3   | 2/2                         | 0/2              |
| HOP27   | 1-chloro-4-[2,2-dichloro-1-(4-chlorophenyl)ethyl]benzene             | 48.52          | 4.53         | 0/3   | 0/2                         | 0/2              |
| HOP28   | methoxychlor   | 49.12          | 5.85         | 3/3   | 2/2                         | 0/2              |
| HOP29   | 2,2',3,3',4,4',5,5'-octachlorobiphenyl                               | 53.11          | 4.27         | 0/3   | 0/2                         | 0/2              |
| Performance reference compounds used for environmental sampling |  |                |              |   |                             |                  |
| PCB30   | 2,4,6-trichlorobiphenyl  | 28.95          | 4.32         | -   | -                           | -                |
| PCB50   | 2,2',4,6-tetrachlorobiphenyl   | 30.54          | 4.21         | -   | -                           | -                |
| PCB145  | 2,2',3,4,6,6'-hexachlorobiphenyl                                     | 42.30          | 3.87         | -   | -                           | -                |
| PCB204  | 2,2',3,4,4',5,6,6'-octachlorobiphenyl                                | 52.32          | 4.37         | -   | -                           | -                |

<sup>a</sup> This target analyte was only detected in sediment sample Sed1 but not in Sed2, analyzed by GC×GC-ENCI-TOFMS; <sup>b</sup> This target analyte was not detected by the accelerated sampler in any of the MIR trajectories, even though it was present in all 30 PDMS strips used for passive sampling.

## Chapter 6. Spatial distribution of Hydrophobic organic pollutants

---

Table 6.3 – List of target analytes successfully detected in the water column and sediments samples of the lake, employing GC×GC- $\mu$ ECD.

| Abbreviation | Successfully detected using GC×GC- $\mu$ ECD |                             |                  |
|--------------|--|-----------------------------|------------------|
|              | Water (passive sampling)                     | Water (accelerated sampler) | Sediment samples |
| HOP1         | 30/30  | 11/11                       | 0/4              |
| HOP2         | 0/30   | 0/11                        | 0/4              |
| HOP3         | 30/30  | 11/11                       | 4/4              |
| HOP4         | 30/30  | 11/11                       | 2/4              |
| HOP5         | 30/30  | 11/11                       | 2/4              |
| HOP6         | 0/30   | 0/11                        | 0/4              |
| HOP7         | 0/30   | 0/11                        | 0/4              |
| HOP8         | 0/30   | 0/11                        | 0/4              |
| HOP9         | 0/30   | 0/11                        | 0/4              |
| HOP10        | 30/30  | 11/11                       | 2/4              |
| HOP11        | 30/30  | 11/11                       | 2/4              |
| HOP12        | 30/30  | 11/11                       | 3/4              |
| HOP13        | 0/30   | 0/11                        | 0/4              |
| HOP14        | 30/30  | 11/11                       | 4/4              |
| HOP15        | 30/30  | 0/11                        | 0/4              |
| HOP16        | 0/30   | 0/11                        | 0/4              |
| HOP17        | 0/30   | 0/11                        | 0/4              |
| HOP18        | 30/30  | 11/11                       | 4/4              |
| HOP19        | 30/30  | 11/11                       | 0/4              |
| HOP20        | 30/30  | 11/11                       | 0/4              |
| HOP21        | 30/30  | 11/11                       | 3/4              |
| HOP22        | 0/30   | 0/11                        | 0/4              |
| HOP23        | 30/30  | 11/11                       | 0/4              |
| HOP24        | 0/30   | 0/11                        | 0/4              |
| HOP25        | 0/30   | 0/11                        | 0/4              |
| HOP26        | 30/30  | 11/11                       | 0/4              |
| HOP27        | 0/30   | 0/11                        | 0/4              |
| HOP28        | 30/30  | 11/11                       | 0/4              |
| HOP29        | 0/30   | 0/11                        | 0/4              |

developed by Booij et al [162]. We used 5 PRC-loaded strips in order to determine initial concentration of each PRC in the PDMS strips. The remaining PDMS strips were used for: conventional passive sampling; accelerated sampling; and controls. To determine the HOP mass on each strip, we extracted the strip using 20 mL pentane for 8 h, 3 consecutive times. The final extracts of 60 mL were reduced in volume and simultaneously solvent exchanged to 1 mL of hexane, employing a rotary evaporator. We did not perform any clean up on these final extracts. These water column extracts were stored at -20 °C until analysis.

As quality assurance measures, we analyzed 5 PDMS blanks, explained above; the solvent blanks, which were the solvents used during the extraction (hexane and pentane); an analytical blank, which was the extract of glassware and also the rotary evaporator; and 5 field blanks, which were PRC-loaded PDMS strips brought to the field but not deployed. The glassware used during the extractions was rinsed with solvent and baked in the oven overnight at 450 °C. For the external standard calibration curves, we performed the injections in increasing order of the concentration level. Thus the lower concentrations levels were injected before the higher levels. For both environmental samples and external standard analysis, we baked the GC systems at 300 °C before and after each injection.

### **Sediment sample extraction and clean up**

The center part of the top 1 cm of each sediment core was sampled. Therefore the sediment in contact with the plastic tube was discarded (Figure A.1). The sediment samples collected from the lake were air dried and homogenized according to EPA method EPA-823-B-01-002, revision of October 2001. We extracted approximately 0.5 g of each sediment sample using accelerated solvent extraction (ASE) with a modified version of EPA method 3545A, revision 1<sup>st</sup> February 2007 (Chapter 3, section B.2). This method was previously found to have high recoveries for a wide range of chemicals [53, 16] due to fact that this extraction method uses a minimal clean up process.

### **6.2.4 GC×GC-μECD and GC×GC-ENCI-TOFMS instrument conditions**

We analyzed both the water column extracts and sediment sample extracts by GC×GC-μECD. These analyses were performed on a Leco Corp GC×GC-μECD instrument, which is a modified Agilent 7890A GC system equipped with a split/splitless injector and a dual-stage quadrupole-jet modulator. The separation of the samples was carried out on a 30 m length, 0.25 mm inner diameter (i.d.), 0.25 μm film thickness RTX-1 column (Restek, USA) as the first dimension, and 2 m length, 0.1 mm i.d., 0.1 μm film thickness BPX-50 column as the second dimension (Restek, USA). The primary oven temperature was initially 45 °C, held for 1 min; then increased to 160 °C with a 2.5 °C min<sup>-1</sup> ramp. After holding at that temperature for 1 min, it was ramped to 300 °C at 1.8 °C min<sup>-1</sup>. The secondary oven temperature was started at 57 °C, held for 1 min and then increased to 172 °C with a ramp rate of 3.2 °C min<sup>-1</sup>. The secondary oven

## Chapter 6. Spatial distribution of Hydrophobic organic pollutants

---

temperature then was ramped to 312 °C min<sup>-1</sup> at a ramp rate of 2.8 °C min<sup>-1</sup>. We used helium as the carrier gas with a constant flow rate. Modulation periods of 15 s and 8 s were used for water column extracts and sediment extracts, respectively.

We used a GC×GC coupled to an electron capture negative chemical ionization time of flight mass spectrometer (ENCI-TOFMS) (Zoex Corp. USA) for the identity confirmation of our target analytes in selected water column extracts. We analyzed 3 water extracts from the passive sampling site and 2 water extracts from the accelerated sampler. For the instrument method and also for the identity confirmation of target analytes, we employed an already established method (Chapters 2, section 2.2.4) [15, 53].

### 6.2.5 Target analyte quantification in the environmental samples

#### Data processing prior to analyte quantification

To quantify target analytes by GC×GC-μECD, we employed external standard calibration with 5 concentration levels, using 3 replicates at each level. The chromatograms of standards and environmental samples were baseline corrected using the Eilers baseline [82], implemented via Matlab [93]. The three unitless baseline correction method parameters,  $\lambda$ ,  $p$  and  $d$ , were set to 10<sup>4</sup>, 0.02, and 2, respectively. We used the inverted watershed algorithm, implemented via GC Image (GC Image, LLC [81]) for the peak delineation. The peak delineation algorithm parameters were set to default. Our recent reports have shown the effectiveness of this combination of baseline correction and peak delineation methods for the quantification of target analytes and the elimination of matrix effects in complex environmental samples [15, 80]. We defined the method limit of qualification (LOQ) as the intercept of the external standard calibration curves and the method limit of detection as LOQ/3. Our LOQs were comparable to published LOQs for the same target analytes measured in the surface water of the Great Lakes, using conventional GC-MS [35, 19].

#### Determination of the water column concentrations of target analytes measured by passive samplers

Target analytes measured by passive sampling methodology were quantified as follows. Assuming that the mass transfer of HOPs across the water boundary layer is the rate limiting step, the depletion of the PRCs from the passive sampler material can be described as:

$$\frac{C_p(t)}{C_p^0} = \exp(-k_e \cdot t) \quad (6.1)$$

where  $C_p$  is the concentration of the PRC in the strip after environmental exposure,  $C_p^0$  is the initial concentration of the PRC in the strip,  $k_e$  is the rate constant of mass transfer, and



$t$  is the exposure time. The  $k_e$  values determined for the PRCs for the environmental field sampling period were used to establish a linear free energy relationship (LFER) with  $\log K_{ow}$  (octanol-water partitioning constant). The squared correlation coefficients,  $R^2$ , between  $\log K_{ow}$  and  $k_e$ , calculated based on 4 PRCs, were  $> 0.94$  for all the PDMS strips. These LFERs were then employed to estimate  $k_e$  for the target analytes. These  $k_e$  values were inserted into the uptake equation for estimation of the water column concentrations of the target analytes.

$$C_w = \frac{C_p(t)}{K_{pw} \cdot (1 - \exp(-k_e \cdot t))} \quad (6.2)$$

where  $C_w$  is the water column concentration of the target analyte and  $K_{pw}$  is the polymer-water partitioning equilibrium constant of that target analyte. We employed Eq. 6.2 to estimate the water column concentrations of target analytes measured with passive samplers.

Water column concentrations of target analytes were determined with the accelerated samplers method described in Chapter 5. For quantification of the water column concentrations measured using the accelerated sampler, we used the LFER established between  $\log K_{pw}$  and  $\log k_{pb}$  [315] to estimate the  $k_{pb}$  for our target analytes. The  $k_{pb}$  parameter was the rate of mass transfer of HOPs between the bulk polymer and water compartments. This LFER had a  $R^2$  of 0.87 for 11 PCBs. These estimated  $k_{pb}$  values then were utilized for estimation of the water column concentration of our target analytes according to Eq. 5.34 in Chapter 5.

## 6.3 Results and discussion

### 6.3.1 Successful detection and quantification of HOPs in the deep water column and sediments of Lake Geneva

We analyzed the 41 water column and 4 sediment samples for 29 target analytes, using GC×GC- $\mu$ ECD. We were able to successfully detect 15 out of 29 target analytes in all water column samples, including both the PDMS strips collected using passive sampling methodology and those of the accelerated sampler (Tables 6.2 and 6.3). With the exception of HOP15,  $\beta$ -endosulfan, we found 100% agreement in positive and negative detections between the two water column sampling methods. The accelerated sampler was not able to reach the concentration needed to detect  $\beta$ -endosulfan. This was attributed to the fact that PDMS is not an ideal material for sampling this compound. 11 target analytes out of 15 were successfully quantified in all 41 water column extracts.

We also analyzed four sediments samples of Lake Geneva, using GC×GC- $\mu$ ECD for detection and quantification of the target analytes. We detected 3 out of 29 target analytes in all four sediment samples (Table 6.2). The frequency of positive detection varied among the sediment samples collected from different locations in the lake. The highest number of positive detec-

## Chapter 6. Spatial distribution of Hydrophobic organic pollutants

---

tions was found for Sed1 (9 positive detections), collected in the Vidy Bay, whereas the lowest number of positive detections was observed in Sed2 in the center of the lake (4 successful detections). 7 out of 9 target analytes were successfully quantified in Sed1, 3 out of 9 were quantified in Sed2, 6 out of 9 were quantified in Sed3, and finally 7 out of 9 were quantified in Sed4.

We further confirmed the presence of the target analytes in selected water column and sediment samples employing GC×GC-ENCI-TOFMS (Table 6.2). We analyzed: three water extracts collected using the passive sampling method at the water column depth of 166.5 m; two water extracts collected employing the accelerated sampler for trajectories 7 (8M1) and 10 (15M1); and the two sediment extracts, Sed1 and Sed2 (Figure 6.1). For the water column samples, GC×GC-ENCI-TOFMS analysis confirmed the presence of all 15 target analytes that had also been successfully detected by GC×GC- $\mu$ ECD in these same samples. For the sediment samples, GC×GC-ENCI-TOFMS confirmed the presence of 9 target analytes that had been detected by GC×GC- $\mu$ ECD in these samples. For the analyzed sediment extracts, we found 100% agreement between the GC×GC-ENCI-TOFMS and GC×GC- $\mu$ -ECD positive detections and also negative detections. For the water column samples, with the exception of  $\beta$ -endosulfan, we found complete agreement between GC×GC-ENCI-TOFMS and GC×GC- $\mu$ -ECD for both the positive and negative detections.

### 6.3.2 Comparison of pollutant concentrations measured by passive sampler and by accelerated sampler

We compared the pollutant concentrations measured using conventional passive sampling with those measured by the accelerated sampler. Specifically, we compared the average water column concentrations of 14 successfully quantified target analytes during the months June, July and August as measured by passive samplers at 162 and 166.5 m depths with the average water column concentrations of these target analytes obtained by accelerated sampler during the trajectories 10 (August 2<sup>nd</sup>) and 6 (July 12<sup>th</sup>) (Table 6.4 and Figure 6.3). We chose these two MIR trajectories because they were both relatively short in length and were focused in an area roughly 500 m distance from the passive sampling location. The passive sampling site and the accelerated sampler trajectories were both located just outside of Vidy Bay.

The two sampling methodologies produced comparable water column concentrations for all 14 quantified pollutants (Table 6.4). The absolute concentration deviation (ACD, in %) ranged from 5.6% for HOP11 to 74.7% for HOP20. We observed the largest ACD values for compounds that had water column concentrations near the LOQ. For most of the target analytes the observed ACDs were within the acceptable range of experimental error. These results provide convincing validation of the use of the accelerated sampler for the determination of water column concentrations of HOPs in aquatic systems.

Table 6.4 – Water column concentrations of the 14 quantified target analytes, measured both by passive sampling and by the accelerated sampler, near the Vidy Bay.

| Target abbreviation | Water column concentration $\text{pg L}^{-1}$ |              |                |                 |                      |                      |                       |               |                      |                      |                  |
|---------------------|---|--------------|----------------|-----------------|----------------------|----------------------|-----------------------|---------------|----------------------|----------------------|------------------|
|                     | Passive sampling methodology                  |              |                |                 |                      | Accelerated sampler  |                       |               |                      |                      | Water            |
|                     | $C_w^a$ June                                  | $C_w^a$ July | $C_w^a$ August | Average $C_w^b$ | ASE <sup>c</sup> (%) | $C_w$ (trajectory 6) | $C_w$ (trajectory 10) | Average $C_w$ | ASE <sup>d</sup> (%) | ACD <sup>e</sup> (%) | LOQ <sup>f</sup> |
| HOP1                | 4.363   | 4.501        | 5.066          | 4.64            | 8.0                  | 3.512                | 4.250                 | 3.881         | 13.4                 | 13.3                 | 0.015            |
| HOP3                | 31.845  | 35.769       | 35.774         | 34.463          | 6.6                  | 42.530               | 45.990                | 44.260        | 5.5                  | 28.4                 | 0.008            |
| HOP4                | 9.286   | 5.265        | 7.368          | 7.306           | 27.5                 | 5.954                | 4.955                 | 5.455         | 12.9                 | 6.1                  | 0.012            |
| HOP5                | 0.703   | 0.633        | 0.663          | 0.67            | 5.8                  | 1.019                | 1.1463                | 1.0823        | 8.3                  | 62.4                 | 0.050            |
| HOP10               | 0.034   | 0.033        | 0.041          | 0.036           | 12.4                 | 0.054                | 0.039                 | 0.046         | 23.4                 | 29.3                 | 0.020            |
| HOP11               | 0.036   | 0.063        | 0.063          | 0.054           | 29.1                 | 0.032                | 0.043                 | 0.038         | 20.7                 | 5.6                  | 0.021            |
| HOP12               | 2.110   | 1.864        | 3.671          | 2.548           | 38.5                 | 1.959                | 1.682                 | 1.821         | 10.8                 | 28.5                 | 0.008            |
| HOP14               | 0.0011  | 0.0028       | 0.0022         | 0.002           | 44.5                 | 0.0019               | 0.0011                | 0.0015        | 37.7                 | 28.4                 | 0.0012           |
| HOP18               | 0.062   | 0.092        | 0.096          | 0.083           | 22.4                 | 0.076                | 0.040                 | 0.058         | 43.8                 | 30.3                 | 0.030            |
| HOP19               | 0.573   | 0.995        | 0.566          | 0.710           | 34.3                 | 0.401                | 0.661                 | 0.531         | 34.7                 | 25.2                 | 0.030            |
| HOP20               | 0.0032  | 0.0030       | 0.0068         | 0.0043          | 48.4                 | 0.0011               | 0.0011                | 0.0011        | 3.5                  | 74.7                 | 0.001            |
| HOP21               | 101.351                                       | 75.861       | 212.577        | 129.930         | 56.0                 | 52.76                | 47.18                 | 49.97         | 7.9                  | 61.5                 | 0.082            |
| HOP23               | 0.0013  | 0.0057       | 0.0059         | 0.0043          | 61.0                 | 0.0051               | 0.0059                | 0.0055        | 9.954                | 28.2                 | 0.002            |
| HOP28               | 0.760   | 0.791        | 0.786          | 0.779           | 2.2                  | 0.591                | 0.245                 | 0.418         | 58.5                 | 46.2                 | 0.025            |

<sup>a</sup> The average concentration is determined from 2 PDMS strips deployed as passive samplers at depths 166.5 and 162 m; <sup>b</sup> The average concentration is based on 6 PDMS strips deployed at depths 166.5 and 162 m during June, July and August of 2011; <sup>c</sup> The absolute standard error (ASE) is calculated over 6 PDMS strips as passive samplers; <sup>d</sup> The absolute standard error (ASE) is calculated over 2 PDMS strips deployed during the trajectories number 6 and 10; <sup>e</sup> ACD (%) is the absolute concentration deviation between the averaged water column concentration measured by passive samplers and the average water concentration measured by accelerated sampler; <sup>f</sup> Value is the method limit of quantification (LOQ) in  $\text{pg L}^{-1}$ .

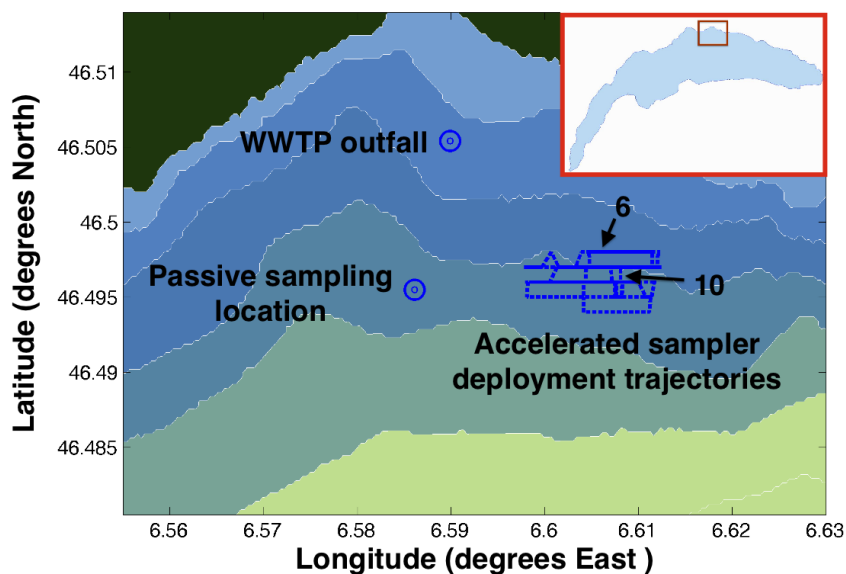


Figure 6.3 – Map of WWTP outfall, passive sampling locations and the two trajectories 6 and 10. Depicted numbers show the trajectory number (Table 6.1). Bathymetry contours of 20 m are overlaid.

### 6.3.3 Occurrence and general trends of the target analytes in the water column of Lake Geneva

We evaluated the water column concentration levels of 15 successfully detected target analytes in the lake. The truly dissolved concentration of these target analytes ranged between below LOQ ( $0.001 \text{ pg L}^{-1}$ ) for HOP26 to  $120 \text{ pg L}^{-1}$  for HOP21 during the trajectory 10M1 (Table 6.5). The levels of the target analytes were comparable to the levels of the same pollutants measured in the surface waters of the Great Lakes [35, 19]. These concentrations were several orders of magnitude smaller than that observed for the same compounds in the water samples from Strait of Johore, Singapore, East Lake, China, and Uluabat Lake, Turkey [36, 316, 317].

We observed significant spatial variability in the water column concentrations of some pollutants. For example, 2,4,5,6-tetrachloro-m-xylene (HOP1) exhibited an 80 fold variability in concentration in different sampling locations of the lake (Table 6.5). Endrin aldehyde (HOP21) exhibited 2.2 fold variability in concentration along the depth profile sampled near Vidy Bay (Figure 6.7). Some pollutants, such as  $\gamma$ -hexachlorocyclohexane (HOP3), exhibited comparatively homogeneous concentrations among the different sampling locations and depths.

In most cases, higher levels of pollutants were measured near to the shores of highly populated

Table 6.5 – Water column concentrations of the 15 detected pollutants measured at 12 different locations in the lake.

| Target analytes | Water column concentration (pg L <sup>-1</sup> ) |                 |                 |                 |                 |                 |                 |                 |                 |                 |                 | Literature reports from other surface water and marine systems |                              |
|-----------------|--|-----------------|-----------------|-----------------|-----------------|-----------------|-----------------|-----------------|-----------------|-----------------|-----------------|--|------------------------------|
|                 | Passive samplers                                 | Trajectories    |                 |                 |                 |                 |                 |                 |                 |                 |                 |  |                              |
|                 | <i>P<sub>Vidy</sub></i> <sup>a</sup>             | 1               | 2               | 3               | 4               | 5               | 6               | 7               | 8               | 9               | 10              | 11   |                              |
| HOP1            | 4.340  | 3.512           | 0.146           | 3.401           | 3.426           | 0.344           | 4.250           | 0.119           | 0.302           | 0.507           | 3.512           | 0.161  | - <sup>b</sup>               |
| HOP3            | 38.330   | 37.330          | 27.670          | 49.130          | 50.750          | 60.720          | 45.990          | 24.080          | 77.190          | 49.250          | 42.530          | 11.120   | 24.0-117 <sup>c</sup>        |
| HOP4            | 5.140  | 4.930           | 4.703           | 7.289           | 1.457           | 1.175           | 4.955           | 3.966           | 8.483           | 8.266           | 5.954           | 2.774  | 12300-60500 <sup>d</sup>     |
| HOP5            | 0.652  | 1.383           | 2.823           | 0.590           | 1.278           | 0.541           | 1.146           | 2.000           | 0.752           | 51.050          | 1.019           | 19.320   | 390-4620 <sup>d</sup>        |
| HOP10           | 0.031  | 0.032           | 0.075           | 0.166           | 0.099           | 0.053           | 0.039           | 0.053           | 0.045           | 0.076           | 0.054           | 0.024  | 49-446 <sup>d</sup>          |
| HOP11           | 0.041  | 0.047           | 0.013           | 0.019           | 0.051           | 0.016           | 0.043           | 0.013           | 0.027           | 0.045           | 0.032           | 0.014  | 130-470 <sup>f</sup>         |
| HOP12           | 1.93   | 1.547           | 0.386           | 3.095           | 2.872           | 0.992           | 1.682           | 0.402           | 0.798           | 1.340           | 1.959           | 0.428  | 0.1-2.0 <sup>e</sup>         |
| HOP14           | 0.0024   | 0.001           | nq <sup>g</sup> | nq <sup>g</sup> | 0.001           | nq <sup>g</sup> | 0.001           | nq <sup>g</sup> | nq <sup>g</sup> | nq <sup>g</sup> | 0.002           | nq <sup>g</sup>  | <0.005 <sup>f</sup>          |
| HOP18           | 0.074  | 0.056           | 0.031           | 0.293           | 0.025           | 0.059           | 0.040           | 0.022           | 0.038           | 0.225           | 0.076           | 0.029  | 11.4-36.6 <sup>c</sup>       |
| HOP19           | 0.990  | 0.541           | 0.161           | 0.235           | 0.254           | 0.205           | 0.661           | 0.168           | 0.334           | 0.560           | 0.401           | 0.179  | 7.47-72.2 <sup>c</sup>       |
| HOP20           | 0.0023   | 0.001           | nq <sup>g</sup> | nq <sup>g</sup> | 0.001           | nq <sup>g</sup> | 0.001           | nq <sup>g</sup> | nq <sup>g</sup> | nq <sup>g</sup> | 0.001           | nq <sup>g</sup>  | 0.35-1.09 <sup>f</sup>       |
| HOP21           | 58.30  | 108.300         | 23.930          | 40.580          | 42.300          | 34.750          | 47.180          | 26.040          | 49.730          | 120.100         | 52.760          | 47.430   | 10-486 <sup>d</sup>          |
| HOP23           | 0.0053   | 0.006           | nq <sup>g</sup> | nq <sup>g</sup> | 0.005           | nq <sup>g</sup> | 0.006           | nq <sup>g</sup> | nq <sup>g</sup> | nq <sup>g</sup> | 0.005           | nq <sup>g</sup>  | 330-6220 <sup>d</sup>        |
| HOP26           | nq <sup>g</sup>                                  | nq <sup>g</sup> | nq <sup>g</sup> | nq <sup>g</sup> | nq <sup>g</sup> | nq <sup>g</sup> | nq <sup>g</sup> | nq <sup>g</sup> | nq <sup>g</sup> | nq <sup>g</sup> | nq <sup>g</sup> | nq <sup>g</sup>  | <0.005-1630.000 <sup>f</sup> |
| HOP28           | 0.750  | 0.346           | 0.238           | 0.030           | 0.375           | 0.302           | 0.245           | 0.248           | 0.492           | 0.826           | 0.591           | 0.264  | 4000 <sup>d</sup>            |

<sup>a</sup> The average concentration is computed over 30 PDMS strips deployed during June, July and August 2011; <sup>b</sup> There are no published data available; <sup>c</sup> Concentrations in the surface water of the Great Lakes, taken from reference [19]; <sup>d</sup> Value is Beijing Guanting reservoir surface water column concentration, taken from reference [318]; <sup>e</sup> Concentrations in the surface water of the lower Great Lake (US), taken from reference [35]; <sup>f</sup> Concentration in the surface water in the East Lake, China, taken from reference [36]; <sup>g</sup> This compound was detected in the water column of Lake Geneva however its concentration was < LOQ.

areas such as Lausanne and Evian. For example, levels of HOP1, measured during the trajectory 6 in Vidy Bay, were about one order of magnitude higher than in the center of the lake and/or the Rhône River area. Additionally, the concentrations of pollutants measured in the Rhône River area (5) were typically similar to those measured in the center of the lake (7). Previous work in Lake Erie has revealed elevated concentrations up to 42 fold for pollutants measured near the Toledo, OH region compared to levels measured in the middle of that lake [35].

#### 6.3.4 Classification of the water column sampling locations and the variability within each class

We classified the 12 water column sampling locations into different categories based on variability in concentrations of the 15 target analytes at these different locations. For the classification, we used the Spearman rank-order correlation, which is a nonparametric statistical test used to define the correlation between two or more variables [319]. We also computed the *p* value, which indicates the significance level of the Spearman correlation coefficient,  $r_s$  (Table 6.6). To calculate  $r_s$ , we performed the Spearman test on the normalized concentration of each target analyte in each sampling location, using average concentration in all samples as the normalizing factor for each compound concentration. We considered a correlation between two trajectories statistically meaningful if the *p* value < 0.05 and an absolute  $r_s$  value > 0.6 for those trajectories.

## Chapter 6. Spatial distribution of Hydrophobic organic pollutants

---

The classification of the sampling locations resulted in 5 different categories (Figure 6.4). The first group contained trajectories 2 and 8, which represent the center of the lake (A). The second group contained the trajectories 9 and 11, representing the area in between Vidy Bay and the center of lake (B). The third group contained trajectories 1, 4, 6, 10, and the passive sampling site ( $P_{Vidy}$ ) viewed to represent Vidy Bay (C). The fourth group was trajectory 3 reflecting the Evian and Thonon area (D). Finally, the trajectories 5 and 8 formed the fifth group, interpreted as the Rhône River affected area (E). These categories were consistent with the geographical location of the trajectories and also with the current patterns of the lake [320, 321].

We evaluated the variability in concentration of each pollutant within each geographical category. For the center of the lake, the absolute concentration deviation from the average value (ACD) ranged between 3.0% for HOP12 to 25.0% for HOP10 and HOP18. We observed an ACD < 50% for all of quantified target analytes in Vidy Bay. For the Rhône delta area, we observed low ACD values for all quantified pollutants except for HOP4, which had an ACD of 70%. The highest level of variability was observed within the overlapping area between the center of the lake and Vidy Bay (trajectories 9 and 11), where the ACD varied between 73% for HOP18 to 109% for HOP19. Results of the Kruskal-Wallis test, with a  $p$  value < 0.01, indicated that the differences amongst the categories were larger than the variability within each geographical group.

### 6.3.5 Spatial distribution of HOPs in the deep water column

We analyzed the horizontal and vertical spatial distributions of the concentrations of 14 detected pollutants in the lake. For compounds that were detected at all 12 locations but not quantified at one or more locations, we used the LOQ at that location. The horizontal spatial distribution enabled us to evaluate large scale gradients between different locations, which may indicate regional pollutant sources and areal sinks. The vertical distributions at the passive sampling site were also used to make inferences about possible sources or sinks, on a more localized scale.

#### Horizontal concentration distributions of analyzed pollutants in the deep water column

We analyzed the horizontal concentration distributions of the 14 quantified pollutants in the deep water column of Lake Geneva. Overall pollutant concentrations were found to be the lowest in the center of the lake. Therefore, we considered the concentration of each pollutant in the center of the lake as the reference value. We normalized the average concentration of each pollutant in an individual geographical category by the concentration of that pollutant in the center of the lake (Figure 6.5).

Table 6.6 – The Spearman correlation coefficient,  $r_s$  [319], for the pollutants concentration data with respect to the different sampling locations and statistical significance test ( $p$  value) of the Spearman correlation coefficient.

| Trajectories | Spearman $r_s^a$ value |       |       |       |       |       |       |       |       |       |       | $P_{Vidy}^b$ |
|--------------|------------------------|-------|-------|-------|-------|-------|-------|-------|-------|-------|-------|--------------|
|              | 1                      | 2     | 3     | 4     | 5     | 6     | 7     | 8     | 9     | 10    | 11    |              |
| 1            | 1.00                   | -0.61 | -0.29 | 0.51  | -0.58 | 0.80  | -0.30 | -0.31 | -0.59 | 0.64  | -0.48 | 0.72         |
| 2            |                        | 1.00  | 0.29  | -0.46 | 0.73  | -0.63 | 0.97  | 0.83  | 0.54  | -0.58 | 0.65  | -0.69        |
| 3            |                        |       | 1.00  | -0.09 | 0.49  | -0.21 | 0.12  | 0.25  | 0.10  | -0.37 | -0.08 | -0.38        |
| 4            |                        |       |       | 1.00  | -0.14 | 0.64  | -0.26 | -0.38 | -0.83 | 0.61  | -0.69 | 0.47         |
| 5            |                        |       |       |       | 1.00  | -0.54 | 0.71  | 0.73  | 0.36  | -0.45 | 0.34  | -0.55        |
| 6            |                        |       |       |       |       | 1.00  | -0.44 | -0.35 | -0.85 | 0.71  | -0.75 | 0.78         |
| 7            |                        |       |       |       |       |       | 1.00  | 0.77  | 0.54  | -0.36 | 0.66  | -0.36        |
| 8            |                        |       |       |       |       |       |       | 1.00  | 0.42  | -0.31 | 0.52  | -0.38        |
| 9            |                        |       |       |       |       |       |       |       | 1.00  | -0.71 | 0.88  | -0.68        |
| 10           |                        |       |       |       |       |       |       |       |       | 1.00  | -0.59 | 0.79         |
| 11           |                        |       |       |       |       |       |       |       |       |       | 1.00  | -0.60        |
| $P_{Vidy}$   |                        |       |       |       |       |       |       |       |       |       |       | 1.00         |

| Trajectories | $p^c$ value |      |      |      |      |      |      |      |      |      |      | $P_{Vidy}^b$ |
|--------------|-------------|------|------|------|------|------|------|------|------|------|------|--------------|
|              | 1           | 2    | 3    | 4    | 5    | 6    | 7    | 8    | 9    | 10   | 11   |              |
| 1            | 1.00        | 0.02 | 0.30 | 0.05 | 0.03 | 0.00 | 0.28 | 0.26 | 0.02 | 0.01 | 0.07 | 0.00         |
| 2            |             | 1.00 | 0.30 | 0.08 | 0.00 | 0.01 | 0.01 | 0.00 | 0.04 | 0.03 | 0.01 | 0.01         |
| 3            |             |      | 1.00 | 0.74 | 0.07 | 0.45 | 0.67 | 0.37 | 0.71 | 0.17 | 0.77 | 0.16         |
| 4            |             |      |      | 1.00 | 0.61 | 0.01 | 0.34 | 0.16 | 0.00 | 0.02 | 0.01 | 0.08         |
| 5            |             |      |      |      | 1.00 | 0.04 | 0.00 | 0.00 | 0.19 | 0.09 | 0.22 | 0.04         |
| 6            |             |      |      |      |      | 1.00 | 0.10 | 0.20 | 0.00 | 0.00 | 0.00 | 0.00         |
| 7            |             |      |      |      |      |      | 1.00 | 0.00 | 0.04 | 0.19 | 0.01 | 0.18         |
| 8            |             |      |      |      |      |      |      | 1.00 | 0.12 | 0.26 | 0.05 | 0.16         |
| 9            |             |      |      |      |      |      |      |      | 1.00 | 0.00 | 0.00 | 0.01         |
| 10           |             |      |      |      |      |      |      |      |      | 1.00 | 0.02 | 0.00         |
| 11           |             |      |      |      |      |      |      |      |      |      | 1.00 | 0.02         |
| $P_{Vidy}$   |             |      |      |      |      |      |      |      |      |      |      | 1.00         |

<sup>a</sup> Spearman  $r_s$  value, which indicates the extent of correlation between two variables. An  $|r_s| > 0.6$  suggests a high level of correlation between the analyzed variables; <sup>b</sup> The average concentration is computed over 30 PDMS strips deployed during June, July and August 2011; <sup>c</sup>  $p$  value represents the meaningfulness of the  $r_s$  value. A  $p > 0.05$  indicates that the correlation between the two variable is not statistically meaningful.

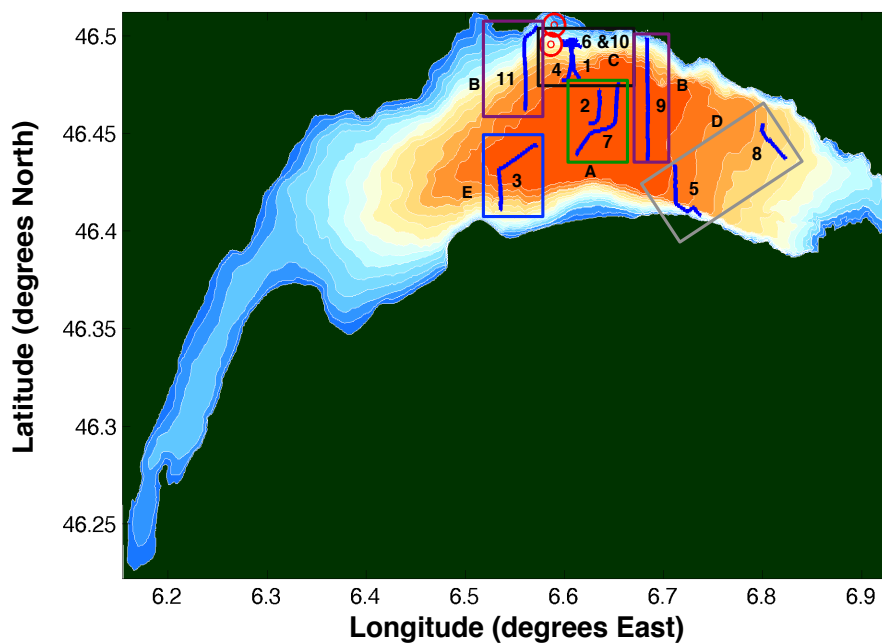


Figure 6.4 – Map showing MIR trajectories at different locations in Lake Geneva, in WGS84 coordinates. The rectangle in each color represents a different geographical category. Bathymetry contours of 45 m are overlaid. Depicted numbers represent the trajectory number (Table 6.1). The geographical categories are represented by capital letters.



In the water column samples taken at different locations in the lake, we observed three distinct spatial distribution patterns amongst the analyzed pollutants. For HOP3, HOP4, HOP10, HOP21, HOP26, and HOP28, we observed relatively homogenous concentrations in all sampled locations of the lake. The concentrations of these pollutants were within a factor of  $\leq 2$  compared to the center of the lake, at all sampled locations. These concentration variabilities amongst different geographical categories were not considered meaningful, indicating that the pollutants do not have a clear source or sink area. This was considered consistent with the European restrictions on the production and use of all of these pollutants. We observed a strong concentration decrease from one or more shorelines towards the center of the lake for the pollutants HOP1, HOP11, HOP12, HOP14, HOP19 and HOP20 (Figure 6.5). The magnitude of these concentration differences ranged between a factor of 6 and a factor of 80 in concentration. For pollutants such as HOP11, HOP12, HOP14, HOP19, and HOP20 the wastewater treatment plant in Vidy Bay is a historical point source [177, 262, 152]. Moreover, HOP11 and HOP19 were recently detected and quantified in the treated effluent of Vidy Bay's WWTP [16]. The pollutants HOP11, HOP14, HOP20 and HOP23 are polychlorinated biphenyls (PCBs), which historically were found to have elevated concentrations near the highly urbanized area of the northern shore of the lake [254]. The elevated concentrations observed in the Vidy Bay area for these compounds (relative to the center of the lake) indicates that the northern shores of the lake may be still today considered as a potential source of these compounds. For HOP1 and HOP12, the observed elevated concentrations in the nearshore areas of both Vidy Bay and Evian may indicate the involvement of these areas in the introduction of these pollutants into the lake. These two locations are both highly urbanized areas. Neither of these two target analytes were detected in Lausanne's Vidy WWTP effluent [16]. For HOP5 we observed a highly elevated concentration in the B geographical category, which is the intermediate area between the center of the lake and Vidy Bay. Between the two trajectories in this group, HOP5 had the highest concentration at trajectory 9. This may be attributed to the Venoge River tributary, which is known as a point source for agricultural and industrial pollutants [322]. For HOP18, we observed a higher concentration near the southern shores and also at the northern shore close to Lutry. This trend suggested that the southern shores of the lake near the highly populated areas of Evian and Thonon may be a source for this pollutant. For the high levels observed close to the shores of Lutry, in collaboration with colleagues in EPFL (Dr. Damien Bouffard) we are investigating the possibility of explaining these trends by the current patterns in the lake. However, further measurements of these compounds in the water column of the lake may be needed in order to gain a better understanding of the potential sources of these target analytes.

#### **Vertical concentration profiles of the analyzed pollutants in the water column**

We evaluated the vertical concentration distribution of our target analytes outside of Vidy Bay, between the water column depths of 70 and 167 m (Figure 6.1). We observed no statistically meaningful vertical gradients for HOP1, HOP3, HOP5, HOP10, HOP18, HOP19 and HOP26 (Figure 6.6). This homogenous vertical concentration distribution indicates that vertical mixing

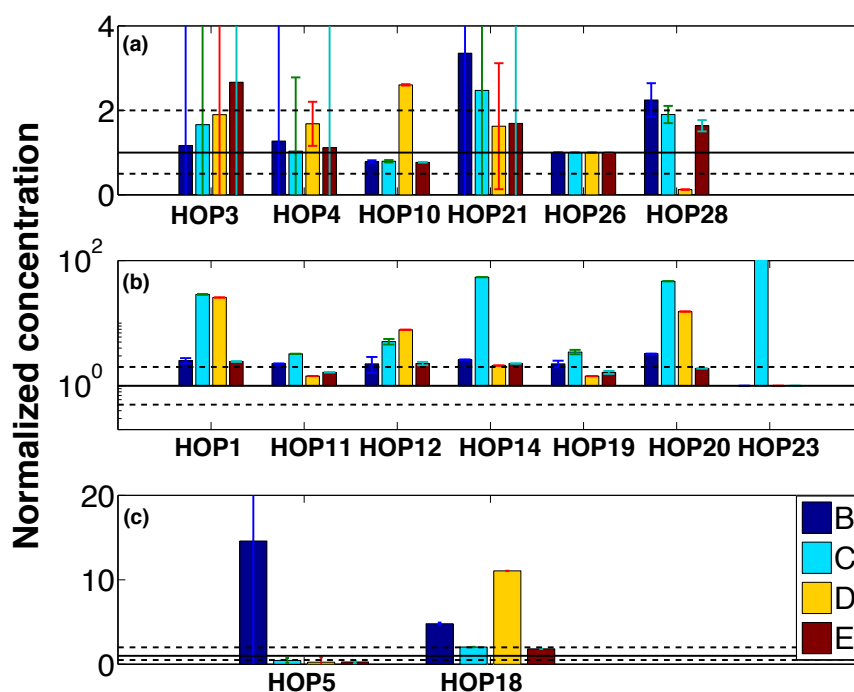


Figure 6.5 – The spatial distribution of: (a) the pollutants with no apparent gradient; (b) the pollutants with a statistically meaningful gradient from shoreline to the center of the lake; and (c) uncategorized target analytes, in Lake Geneva. The averaged concentration in each geographical category is normalized to the average concentration in the center of the lake. Each solid bar indicates an individual geographical category (see legend). The error bars indicate the variability within each geographical category ( $\pm$  standard deviations).

processes are more rapid than proximate source or removal processes for these compounds in this region of the lake. We observed similar trends for pentachloroorthiphenol, hexachlorobenzene, [52] and some brominated hydrocarbon compounds at this same sampling location [53]. For HOP11, HOP12, HOP20, HOP21, and HOP23, we observed lower concentrations at lesser depths and a gradual increase in their levels with increasing depth with the highest concentrations at the bottom of the lake (Figure 6.7). These pollutants were also found to be at/or near partitioning equilibrium between the sediment and water column of the lake at that location (discussed further in the next section). These observed elevated concentrations at the bottom of the water column might be attributed to the heavy past use of these pollutants [323, 324, 175] and present-day sediment resuspension at the bottom of the lake [140, 136], which may facilitate the introduction of these pollutants into the bottom waters of the lake. For HOP4, we observed a higher concentration both at lesser depths and at the bottom of the lake. This concentration trend may suggest the presence of a potential proximate source near the surface of the lake for this pollutant. Interestingly, HOP4 was successfully detected and quantified in the liquid phase of WWTP effluent of Vidy Bay [16], which is thus a potential source for this compound. However, further data are needed in order to better understand the potential sources and processes that affect these pollutants in the water column of the lake.

As mentioned in Chapter 3 of this thesis, the temperature profile of the water column of the lake at the passive sampling location proved insufficient for further inference about both vertical and horizontal concentration distribution of HOPs (Figure 3.4). More sophisticated modeling of the lake physics is needed in order to interpret the water mass mixing in this area.

#### 6.3.6 Occurrence of the target analytes in the sediments of the lake

The sediment concentrations of the quantified target analytes ranged between  $0.56 \text{ ng kg}^{-1}$  for HOP18 in Sed3 to  $147.13 \text{ ng kg}^{-1}$  for HOP3 in Sed2. Sed1 had the largest number of positive detections (9 out of 29) whereas Sed2 had the lowest number of positive detections and quantifications of (4 out of 29) analyzed pollutants (Table 6.7). The sediment concentrations of the quantified pollutants were about one order of magnitude smaller than the concentrations of the same pollutants reported at a different location in Lake Geneva (close to the outfall of Lausanne's WWTP in Vidy Bay) [177] whereas the sediment concentration of the same pollutants found to be two orders of magnitudes lower than their concentrations in Beijing Guanting reservoir sediments [318], and Gaobeidian Lake sediments, China [325]. For HOP10, HOP14, HOP18, and HOP21, the Sed1 sampling site had the highest concentration levels compared to the other three sediment samples. Compound HOP3 had the highest levels in Sed2, collected in the center of the lake, whereas HOP4 and HOP12 had the highest concentrations in Sed4. Sed3 had the highest concentrations for HOP5 and HOP11. The spatial distribution of these pollutants in the sediment samples may point to the presence of a source on the northern, north eastern, and/or eastern shores of the lake. This is consistent with the intensive industrial and agricultural development of these shore areas. The WWTP

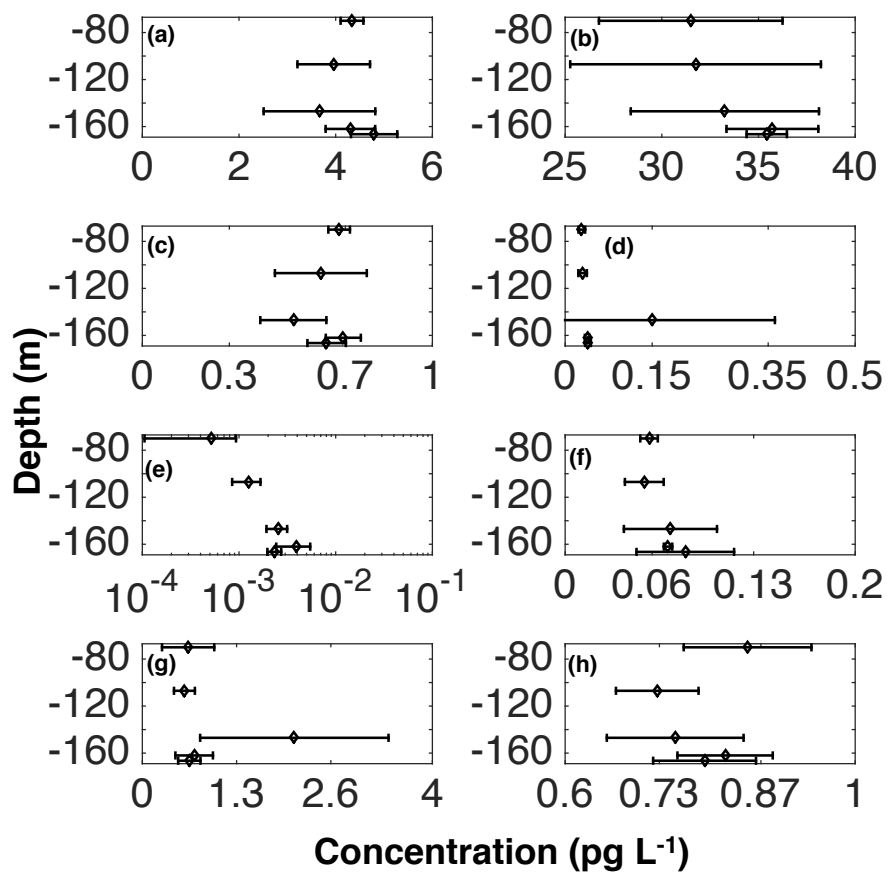


Figure 6.6 – The vertical concentration distribution of: (a) HOP1; (b) HOP3; (c) HOP5; (d) HOP10; (e) HOP14; (f) HOP18; (g) HOP19; and (h) HOP26. The error bars indicate the variability at each depth calculated over 6 PDMS strips ( $\pm 2$  standard deviations).

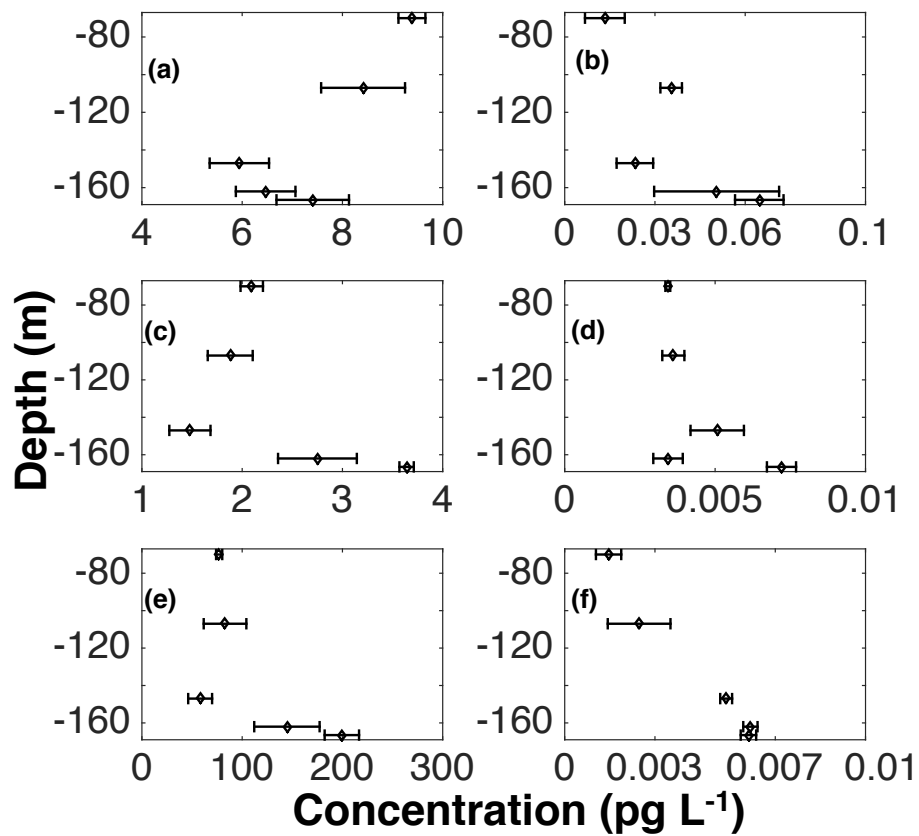


Figure 6.7 – The vertical concentration distribution of: (a) HOP4; (b) HOP11; (c) HOP12; (d) HOP20; (e) HOP21; and (f) HOP23. The error bars indicate the variability at each depth calculated over 6 PDMS strips ( $\pm 2$  standard deviations).

## Chapter 6. Spatial distribution of Hydrophobic organic pollutants

Table 6.7 – Sediment concentrations of the 15 pollutants at four sampling locations in Lake Geneva.

| Target analyte | Sediment concentration ng kg <sup>-1</sup> |                 |                 |                 | Literature reports<br>for sediments elsewhere |
|----------------|--|-----------------|-----------------|-----------------|---|
|                | Sed1                                       | Sed2            | Sed3            | Sed4            |   |
| HOP1           | nd <sup>a</sup>                            | nd <sup>a</sup> | nd <sup>a</sup> | nd <sup>a</sup> | _ <sup>b</sup>                                |
| HOP3           | 107.28                                     | 147.13          | 15.17           | 15.96           | 540.0 <sup>c</sup>                            |
| HOP4           | nq <sup>d</sup>                            | nd <sup>a</sup> | nd <sup>a</sup> | 52.00           | < 50 <sup>c</sup>                             |
| HOP5           | 1.02                                       | nd <sup>a</sup> | 5.00            | nd <sup>a</sup> | 52-467 <sup>e</sup>                           |
| HOP10          | 5.61                                       | nd <sup>a</sup> | nd <sup>a</sup> | 2.02            | 132-1300 <sup>e</sup>                         |
| HOP11          | nq <sup>d</sup>                            | nd <sup>a</sup> | 0.007           | nd <sup>a</sup> | 670.0 <sup>f</sup>                            |
| HOP12          | 6.13                                       | nd <sup>a</sup> | 3.30            | 10.04           | 370 <sup>c</sup>                              |
| HOP14          | 0.0076                                     | 0.0076          | 0.0013          | 0.0019          | 790.0 <sup>b</sup>                            |
| HOP18          | 25.04                                      | nq <sup>d</sup> | 0.56            | 4.13            | 150.0 <sup>c</sup>                            |
| HOP19          | nd <sup>a</sup>                            | nd <sup>a</sup> | nd <sup>a</sup> | nd <sup>a</sup> | 43.8-513 <sup>e</sup>                         |
| HOP20          | nd <sup>a</sup>                            | nd <sup>a</sup> | nd <sup>a</sup> | nd <sup>a</sup> | _ <sup>b</sup>                                |
| HOP21          | 20.18                                      | 3.18            | nd <sup>a</sup> | 0.93            | 36.6-147 <sup>d</sup>                         |
| HOP23          | nd <sup>a</sup>                            | nd <sup>a</sup> | nd <sup>a</sup> | nd <sup>a</sup> | 1200 <sup>c</sup>                             |
| HOP26          | nd <sup>a</sup>                            | nd <sup>a</sup> | nd <sup>a</sup> | nd <sup>a</sup> | 970 <sup>c</sup>                              |
| HOP28          | nd <sup>a</sup>                            | nd <sup>a</sup> | nd <sup>a</sup> | nd <sup>a</sup> | 35.4-352 <sup>d</sup>                         |

<sup>a</sup> Concentration of the target analyte was below limit of detection (< LOD); <sup>b</sup> No published data were available for the sediment concentration of this compound; <sup>c</sup> This is the measured concentration of the target analyte in Lake Geneva at a location near to the Vidy Bay WWTP outfall [177]; <sup>d</sup> This target analyte was detected in the sample using GC×GC-μECD and had its identity confirmed by GC×GC-ENCI-TOFMS, however, its concentration was < LOQ; <sup>e</sup> Sediment concentration measured at Beijing Guanting reservoir [318]; <sup>f</sup> Concentration measured in sediment samples in Gaobeidian Lake, China [325].

in Vidy Bay and the Rhône River both appeared to be involved in introduction of pollutants HOP18 and HOP4, respectively, into the lake. Previous works on the sediments of the lake also suggested the importance of these potential sources for the introduction of pollutants into the lake [254, 177, 16, 53]. However, further measurements would be needed to understand the magnitude of each of these potential sources.

### Evaluation of sediment water partitioning equilibrium of the analyzed pollutants

We evaluated the concentration distributions of the quantified pollutants between sediments and proximate water column samples. We only considered the target analytes quantified in both water and sediments. To evaluate whether these two compartments appeared to be at partitioning equilibrium, we compared the sediment-water concentration distribution ratio ( $C_s/C_w$ ) of each pollutant to the estimated  $K_d$  value. We estimated these  $K_d$  values assuming that the pollutants sorb only into the organic fraction of sediment, as indicated by the  $f_{oc}$ . Therefore the  $K_d$  was defined as [32]:

$$K_d = f_{oc} \cdot K_{oc} \quad (6.3)$$

To estimate the  $K_{oc}$  values of nonpolar pollutants having boiling point  $\leq 402$  °C, we employed a recently developed method based on GC×GC retention times [150]. For other pollutants, we used EPISuite to estimate the  $K_{oc}$  [168]. We assumed an  $f_{oc}$  of 0.056 for all locations, based on the measurement taken in the center of the lake [326]. A similar value  $f_{oc}$  of 0.059 was measured outside of Vidy Bay, about 200 m distance from the passive sampling location [177].

The sediment-water concentration distribution ratio ( $C_s/C_w$ ) of HOP3, HOP4, HOP10, HOP11, HOP14, and HOP18 at all locations (where  $C_s/C_w$  could be quantified) appeared to be approximately explained by partitioning equilibrium between water and sediment (Figure 6.8). The  $C_s/C_w$  values for these pollutants in Vidy Bay (at the location of Sed1) was calculated using Sed1 and the depth-averaged water column concentration of these compounds, based on passive sampling measurements during June-August 2011. HOP5 was observed to be near partitioning equilibrium at the location of Sed1. However, this pollutant had a  $\log C_s/C_w$  of 3.96 at the Rhône River area (Sed3 and trajectory 7M1), which was larger than the  $\log K_d$  value of 2.07. For HOP12, we observed comparable  $C_s/C_w$  values of 3.50 and 3.52 in Vidy Bay and also the Rhône River area to the  $K_d$  value of 2.49, whereas the same compound had a larger  $\log C_s/C_w$  of 4.10 at the Vevey area (Sed4 and 9M1 trajectory), compared to partitioning equilibrium constant of 2.49. The discrepancies observed between the  $C_s/C_w$  and the  $K_d$  values might be attributed to the non-equilibrium between the sediments and the water column. However, it may also be due to inherent error in the estimated  $K_d$  and also the assumption of sorption of these pollutants only into the organic carbon fraction of sediment, which does not take into account the presence of black carbon. Black carbon is an important material for the sorption of hydrophobic pollutants in some sediments [327, 328].

#### 6.3.7 Environmental implications

The water column of a lake is frequently considered as a well-mixed compartment for HOPs [32], which implies that the presence of vertical and horizontal gradients of these HOPs in the water column are negligible. However, some investigations have shown that this assumption may not be an accurate way to describe the spatial distribution of the hydrophobic compounds in the water column of an aquatic system [51, 53, 41, 47, 140, 35, 34]. In this study we reported the presence of statistically meaningful vertical gradients of hydrophobic pollutants in the water column of the lake. Concentrations varied by between a factor of two and three over 70 to 166.5 m depth at a single sampling site. These gradients were indicative of the processes affecting each pollutant in the water column at this area. We also report the presence of horizontal gradients of hydrophobic pollutants in the deep water column of the lake. For 6 target analytes out of 14, these concentration differences were larger than a factor of ten, which can not be considered as negligible. Additional data sets with higher temporal and spatial resolution would further aid in assessment of sources, sinks, and transport of HOPs in Lake Geneva. These results demonstrate that assessments of inventories, exposures, and inter-compartment transport may be significantly in error if they are based on water column

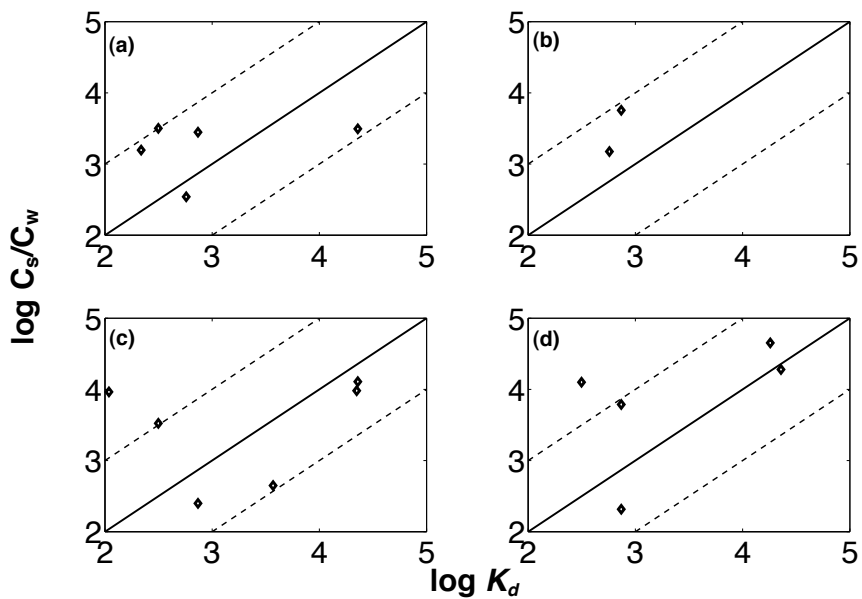


Figure 6.8 – The concentration distribution ratio,  $\log C_s/C_w$ , vs estimated  $\log K_d$  of the quantified pollutants in both sediment and water column samples of: (a) the location of Sed1, computed using the depth-averaged water column concentration measured by passive sampling; (b) the location Sed2, calculated using the average water column concentration over the trajectories 2 and 7; (c) the location Sed3, computed using water column concentrations from trajectory 5; and (d) the location Sed4, calculated using the water column concentrations from trajectory 8. The solid line represents the 1 to 1 line and the dash lines represent the plausible uncertainty in the estimated  $K_d$  value of one order of magnitude.



measurements at only a single location. Thus multimedia fate modeling of some pollutants would need to employ measurement datasets based on several sampling locations in order to represent the water column of this lake. These models also need to take advantage of the lake physics modeling and the water movement, which is non-trivial for complex aquatic systems [40, 140, 136], such as Lake Geneva.

Published data regarding the water column and sediment concentrations of hydrophobic organic pollutants are scarce due to difficulties in carrying out these types of measurements [19, 34, 35, 18, 17]. Even less common are measurements of both sediment and water at the same location and at the same time. The lack of data for both compartments has often led investigators to assess the potential pollutant sources by considering only one of the two compartments. However, the simultaneous consideration of both compartments presents considerable advantages. For example, our water column data reveal that the two highly urbanized areas of the northern shore and the southern shore may be potential sources of some of the analyzed pollutants, whereas the Rhône River did not appear to be a potential source for any of the pollutants. If we had considered the spatial concentration distribution of pollutants in only the analyzed sediments, we may have instead inferred the presence of a source in the northern and eastern shores of the lake, including the Rhône River. The highly urbanized area of Evian and Thonon would not have been considered as a potential source for these compounds. International Commission for the protection of waters of Lemman (CIPEL) carries out routine water sampling in the center of the lake [153]. Interestingly, by combining both the water column spatial distribution and the sediment spatial concentration distribution, we were able to better constrain the potential source areas of these pollutants into the lake. Our data clearly demonstrate the utility of investigating both compartments for an adequate assessment of the potential sources for hydrophobic organic pollutants in a deep and large lake such as Lake Geneva.



# 7 Conclusions

## 7.1 Main findings and implications

Chapter 2 of this thesis focused on the development of a highly sensitive analytical protocol for detection, quantification and identity confirmation of trace level PBPs in environmental samples. In particular, I investigated automated baseline correction and peak delineation algorithms for their ability to remove the matrix effect and quantify trace level PBPs in complex environmental samples analyzed by GC×GC- $\mu$ ECD and GC×GC-FID. By employing a suite of chemometric tests, I systematically assessed different baseline correction and peak delineation algorithms for their confidence and accuracy in target analyte quantification. The results of chemometric tests showed the crucial importance of the baseline correction algorithm for accurate peak integration. An aggressive baseline correction method systematically produced the best results for the chemometric tests, which indicated improved matrix effect removal. The results of the analytical protocol were also validated using a certified reference material. The validated analytical procedure led to the successful detection and quantification of 18 trace level target analytes, including 7 PAHs in a light diesel fuel and 11 chlorinated hydrocarbons in a lake water extract. In this chapter I also developed an accurate method for confident identity confirmation of PBPs in environmental samples. This method employs a "five point criterion", which consists of two GC×GC retention time matches and three m/z value matches between the standard peak and the suspect peak in environmental samples. This thesis is the first report of high mass accuracy GC×GC-ENCI-TOFMS data for novel and legacy PBPs. This chapter led to the development of a sensitive and accurate protocol for detection, identity confirmation, and quantification of trace level PBPs in environmental samples. Finally, this chapter also provides guidance for diagnosis of the matrix effect and biased calibration during the quantification of analytes using GC×GC with univariate detectors.

In Chapters 3 and 4, I evaluated the occurrence and wider fate and behavior of selected novel and legacy PBPs in the Lake Geneva environment. Target analytes were the novel PBPs, including 4BBP, TBB, HBB and PCTP, and several legacy PBPs, including pentaBDE technical mixture,

## Chapter 7. Conclusions

---

hexachlorobenzene (HCB) and PCNB. To confidently detect and quantify these analytes, the analytical procedure developed in Chapter 2 was employed. The water column concentrations of two novel brominated PBPs, 4BBP and TBB, were found to be 0.5-1.0 ng L<sup>-1</sup> at our sampling site, whereas the water column levels of PCTP laid between 3 ng L<sup>-1</sup> and 3000 ng L<sup>-1</sup>. 4BBP and PCTP were also detected and quantified in the sediments samples. Suspect screening of the GC×GC-ENCI-TOFMS data additionally revealed the presence of a potential precursor of PCTP, pentachloroethoxyanisole, in both the water and sediment samples. This is the first report of the levels of three of these novel PBPs (4BBP, TBB, and PCTP) in a lake environment. These chapters also investigate the potential pathways of introduction and elimination of these novel PBPs in the Lake Geneva environment. The occurrence of these novel PBPs and their relatively high water column concentrations warrants future investigations of these compounds in the environment, including the evaluation of their environmental risk.

In Chapter 3, the estimated partitioning properties of TBB and 4BBP were used for evaluation of the potential for bioaccumulation, long range transport, and Arctic contamination. We also estimated equilibrium partitioning distributions of these compounds between the water column and sediments of the lake. Based on both the estimated partitioning properties and the limited available occurrence data for these PBPs, we concluded that bioaccumulation, long range transport, and Arctic contamination likely play an important role in the global fate and behavior of these PBPs. Finally, we concluded that the highly urbanized area of the northern shore of the lake may be a source for these novel PBPs. Atmospheric deposition also may be a prominent source of these pollutants into the lake.

Chapter 5 of this thesis focuses on the development, modeling and field testing of an accelerated sampler of the TD fraction of PBPs in the deep and shallow water column of aquatic systems. Using this accelerated sampler, we were able to measure pg L<sup>-1</sup> levels of PBPs in water only after 2 h of sampling. We found an excellent agreement between the water column concentrations of PBPs measured employing the accelerated sampler when compared to the results of the established passive sampling methodology. The accelerated sampler enables high resolution (2-5 h) measurements of the TD fraction of trace level PBPs in both the deep and shallow water column of an aquatic system.

In Chapter 6, I employed the accelerated sampler developed in Chapter 5 for the measurement of the spatial distribution of PBPs in the water column of Lake Geneva. I detected and quantified 14 target PBPs in the water column, whereas 9 target PBPs were detected and quantified in sediments of the lake. The Lake Geneva concentrations of these PBPs were comparable to previously reported levels of the same compounds in the surface water of the Great Lakes. I established the presence of statistically meaningful gradients of several PBPs in both the vertical and the horizontal directions in the water column. Concentration differences varied between a factor of 2 to 3 in the vertical direction, whereas they varied between a factor of 6

to 80 in the horizontal direction. The vertical gradients appeared to be determined by both the potential sources of the PBPs and removal processes in the water column. The horizontal gradients appeared to be driven by the potential sources and also the pattern of currents in the lake. This dataset suggested that the highly urbanized areas of the northern and southern shores of the lake and also the Rhône River are likely to be sources of the analyzed PBPs. I also evaluated the partitioning equilibrium of the analyzed PBPs between the sediment and the water column of the lake in different locations. The analyzed pollutants were found to be near partitioning equilibrium between the two compartments.

## 7.2 Remaining challenges

As I discussed in Chapter 3, the estimated water column concentration of PCTP is highly related to  $pK_a$ , the apparent  $K_{sw}$  of PCTP, and the environmental pH. The two parameters,  $pK_a$  and the apparent  $K_{sw}$  of PCTP, should be measured experimentally or better constrained in order to produce a more accurate estimate of the water column concentration of PCTP.

In the two-compartment mass transfer model (Chapter 5), the nature of the mass transfer occurring between the polymer surface compartment and the bulk water is not yet clear. Further modeling and analysis are needed to better explain the mass transfer between these compartments.

The spatial concentration distribution of the quantified pollutants in the water column of the lake may be further interpreted with the aid of physical modeling of the lake water mass and further measurements of potential source inputs including tributaries, WWTP effluents, and atmosphere.

## 7.3 Future work

The detection and quantification of the novel PBPs TBB, 4BB, and PCTP in the Lake Geneva environment may increase interest in further investigating of these pollutants across the globe. Further ecotoxicological studies are needed in order to assess the risk posed by the presence of these novel PBPs in the Lake Geneva environment.

In this thesis, I produced also demonstrated the utility of exploring the spatial distributions of the novel and legacy PBPs in the water column and sediments of the lake. This dataset can be used for fate modeling purposes to further investigate the different processes affecting these pollutants in the water column and sediments of the lake.



# **A Supporting information to Chapter 3: Overlooked Persistent and Bioaccumulative Brominated Pollutants in the Deep Water Column of Lake Geneva: 1,3,5-tribromobenzene and 4-bromobiphenyl**

A modified version of this chapter was submitted as Supporting Information to *Environ. Sci. Technol.*, (es-2015-01534y).

## **A.1 Passive sampling methodology**

We employed a passive sampling technique [21] for measurement of the target analytes in the water column of Lake Geneva. Assuming that the mass transfer across the water boundary layer is the rate limiting step in the mass transfer between water and the PDMS strip, the PRC depletion from the PDMS strip can be explained with the following equation [329, 164, 162, 22, 30].

$$\frac{C_t}{C_0} = \exp(-k_e \cdot t) \quad (\text{A.1})$$

where  $t$  is the exposure time,  $C_t$  is the concentration of each PRC in the strip after exposure, the  $C_0$  is the initial concentration of each PRC in the strip, and the  $k_e$  is the rate of exchange

## Appendix A. SI to Chapter 3: Overlooked brominated pollutants in Lake Geneva

Table A.1 – The ASE recovery (%), and the squared correlation coefficient ( $R^2$ ) of external standard calibration curves of each target analyte.

| Compound                               | Acronym | Extraction recovery (%) | $R^2$ |
|--|---------|-------------------------|-------|
| 4-bromobiphenyl                        | 4BBP    | 92.8                    | 0.998 |
| 1,3,5-tribromobenzene                  | TBB     | 96.1                    | 0.989 |
| hexabromobenzene                       | HBB     | 95.5                    | 0.993 |
| 2,3,4,5,6-pentabromoethylbenzene       | PBEB    | 102.0                   | 0.999 |
| 2,2',4,4'-tetrabromodiphenyl ether     | BDE47   | 92.0                    | 0.999 |
| 2,2',4,4',5-pentabromodiphenyl ether   | BDE99   | 85.4                    | 0.985 |
| 2,2',4,4',6-pentabromodiphenyl ether   | BDE100  | 87.2                    | 0.996 |
| 2,2',4,4',5,5'-hexabromodiphenyl ether | BDE153  | 81.3                    | 0.991 |
| 2,2',4,4',5,5'-hexabromobiphenyl       | HBBP    | 83.0                    | 0.954 |

between water and strips for each PRC. The  $k_e$  of each target analyte was estimated using a linear free energy relationship (LFER) established between the log  $K_{ow}$  and the observed  $k_e$  values of PRCs. The LFERs for all the PDMS strips had a squared correlation coefficient ( $R^2$ )  $\sim$  0.94 ( $N = 4$ ). By inserting the estimated  $k_e$  of each target analyte into the uptake equation, we were able to estimate the water concentration of the target analyte [329, 164, 162, 22, 30]:

$$C_w = \frac{C_t}{K_{sw} \cdot (1 - \exp(-k_e \cdot t))} \quad (\text{A.2})$$

where  $C_w$  is the truly dissolved concentration of the target analyte and  $K_{sw}$  is the partition coefficient of the target analyte between sampler and water [329].

### A.2 Sediment samples extraction and clean up

For the sediment extraction we employed the ASE technique based on EPA Method 3545A, which enabled us to perform the extraction and the clean up steps together [330, 16]. The extraction cell consisted of the following layers (from inlet to outlet): a layer of activated Florisil, a layer of diatomaceous earth, 0.5 g of dried sample, a layer of diatomaceous earth, and a layer of the sodium sulfate. The extraction was carried out at 100 °C and 1500 psi for 5 min, using a 50/50 solution of acetone and hexane. The extraction was repeated 3 times. A flush at 60% of the extraction cell volume was set and the nitrogen purge time lasted 60 s. The volume of final extract was reduced to 1 mL and simultaneously switched to hexane, using rotary evaporation. Extraction recoveries for individual target analytes were defined by spiking a sample-less cell with 40 ng of each target analyte and performing the extraction. The extraction recoveries varied between 81% and 102% (Table B.1). We defined the method blank as extraction and analysis of a sample-less cell. We also analyzed the individual solvents used for the sediment sample extraction in order to define the ASE solvent blanks.



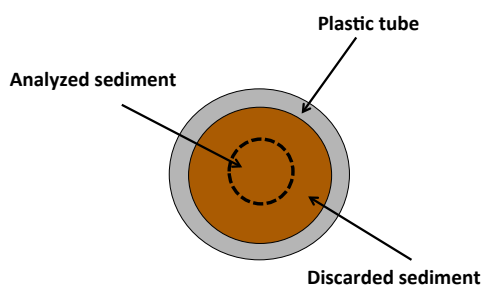


Figure A.1 – A simplified diagram of the analyzed part of the sediment samples.

### A.3 GC×GC- $\mu$ ECD and GC×GC-ENCI-TOFMS analysis conditions

GC×GC- $\mu$ ECD and GC×GC-ENCI-TOFMS instrument conditions were optimized in previous studies, with the goal of obtaining excellent separation of our target analytes in complex environmental samples [15, 16].

For GC×GC- $\mu$ ECD analysis we used helium as the carrier gas, and separations were carried out with a constant flow rate of  $1.5 \text{ mL min}^{-1}$ . The main oven temperature program was:  $45 \text{ }^\circ\text{C}$  initially held for 1 min; then increased to  $160 \text{ }^\circ\text{C}$  at  $2.5 \text{ }^\circ\text{C min}^{-1}$  and held for another minute; and then increased to  $300 \text{ }^\circ\text{C}$  at  $1.8 \text{ }^\circ\text{C min}^{-1}$  and held for 10 min. The second column oven was programmed as:  $57 \text{ }^\circ\text{C}$  held for 1 min; then increased with a ramp rate of  $3.2 \text{ }^\circ\text{C min}^{-1}$  to  $172 \text{ }^\circ\text{C}$  and held for 1 min; and finally increased to  $312 \text{ }^\circ\text{C}$  at  $2.8 \text{ }^\circ\text{C min}^{-1}$  and held at that temperature for 33.4 min. We employed the same instrument oven program for analysis of all samples and all standards mixtures. All injections were carried out in splitless mode. After each injection (i.e., either sample or standard mixture) the instrument ovens were baked out at  $300 \text{ }^\circ\text{C}$  for 30 min. The injector port liner was replaced between the standards injections and samples injections in order to avoid carryover. Modulation periods of 15 s and 8 s were used during the analysis of the water column samples and the sediment extracts, respectively. All chromatograms were acquired using ChromaTOF software (Leco, Corp. USA) with a frequency of 50 Hz.

The GC×GC-ENCI-TOFMS separation was carried out on a 30 m length, 0.25 mm inner diameter (i.d.),  $0.25 \text{ }\mu\text{m}$  film thickness RXI-1MS column (Restek, USA) as the first dimension, and a 1 m length, 0.1 mm i.d.,  $0.1 \text{ }\mu\text{m}$  film thickness BPX-50 column (Restek, USA) as the second dimension. We used helium as the carrier gas and methane as the ionization agent. The separations were carried out using the following oven temperature program: the first column oven temperature was initially  $32 \text{ }^\circ\text{C}$  and held at that temperature for 1 min; then increased to  $300 \text{ }^\circ\text{C}$  at  $4.5 \text{ }^\circ\text{C min}^{-1}$  and then held for another minute. The second column oven was programmed as:  $67 \text{ }^\circ\text{C}$  held for 1 min; then increased to  $300 \text{ }^\circ\text{C}$  at  $4.2 \text{ }^\circ\text{C min}^{-1}$  and held for 1 min. We used  $250 \text{ }^\circ\text{C}$  as the transfer line temperature and  $220 \text{ }^\circ\text{C}$  as the ionization

## Appendix A. SI to Chapter 3: Overlooked brominated pollutants in Lake Geneva

temperature. All injections were carried out in splitless mode with an injection volume of 1  $\mu\text{L}$ . An 8 s modulation period was used during the analysis. The TOFMS acquired 50 spectra per second with a mass resolution of 4000 (full width at half maximum) and a mass accuracy of  $\pm 5$  milli-mass-units (mmu) over the calibrated mass range of 50 to 600  $m/z$ . The detector was operated at 2234 V and the ionization source emission current was 0.1 mA.

### A.4 Target quantification

Table A.2 – The parameter settings for inverted watershed delineation algorithms implemented in the GC Image software. Each parameter in the table is explained in the user manual of GC Image software.

| Blob detection and peak delineation<br>with inverted watershed algorithm |                         |       |                    |
|--|-------------------------|-------|--------------------|
| Signal smoothing   |                         |       |                    |
| Parameter  | before peak delineation | Value | Units              |
| First column   |                         | 0.1   | pixel              |
| Second column  |                         | 1     | pixel              |
| Parameter  | Blob filter             | Value | Units              |
| Minimum area   |                         | 15    | pixel              |
| Minimum volume   |                         | 0.0   | detector intensity |
| Minimum peak   |                         | 10    | unitless           |

To quantify target analytes in lake water extracts and sediment samples, we used a five level external standard method (0.005, 0.01, 0.05, 0.1 and 0.5  $\mu\text{g L}^{-1}$ ) with three replicates at each level of concentration for each target analyte. The integrated signal-to-noise ratios (S/N) of all detected target analytes were  $> 100$  for the lowest concentration levels of the calibration method, lake water extracts, and the sediment samples. A  $S/N > 100$  guarantees that the integrated signal is larger than instrument limit of quantification (LOQ) [76]. We defined the instrument LOQ as  $10 \times S/N$ . The method LOQ was defined as the absolute value of the offset of the external standard calibration regression [15] (Table 3.1 in the main text) and the method LOD was defined as  $LOQ/3$ . Throughout the text of the thesis, the term "LOQ" refers to the method LOQ.

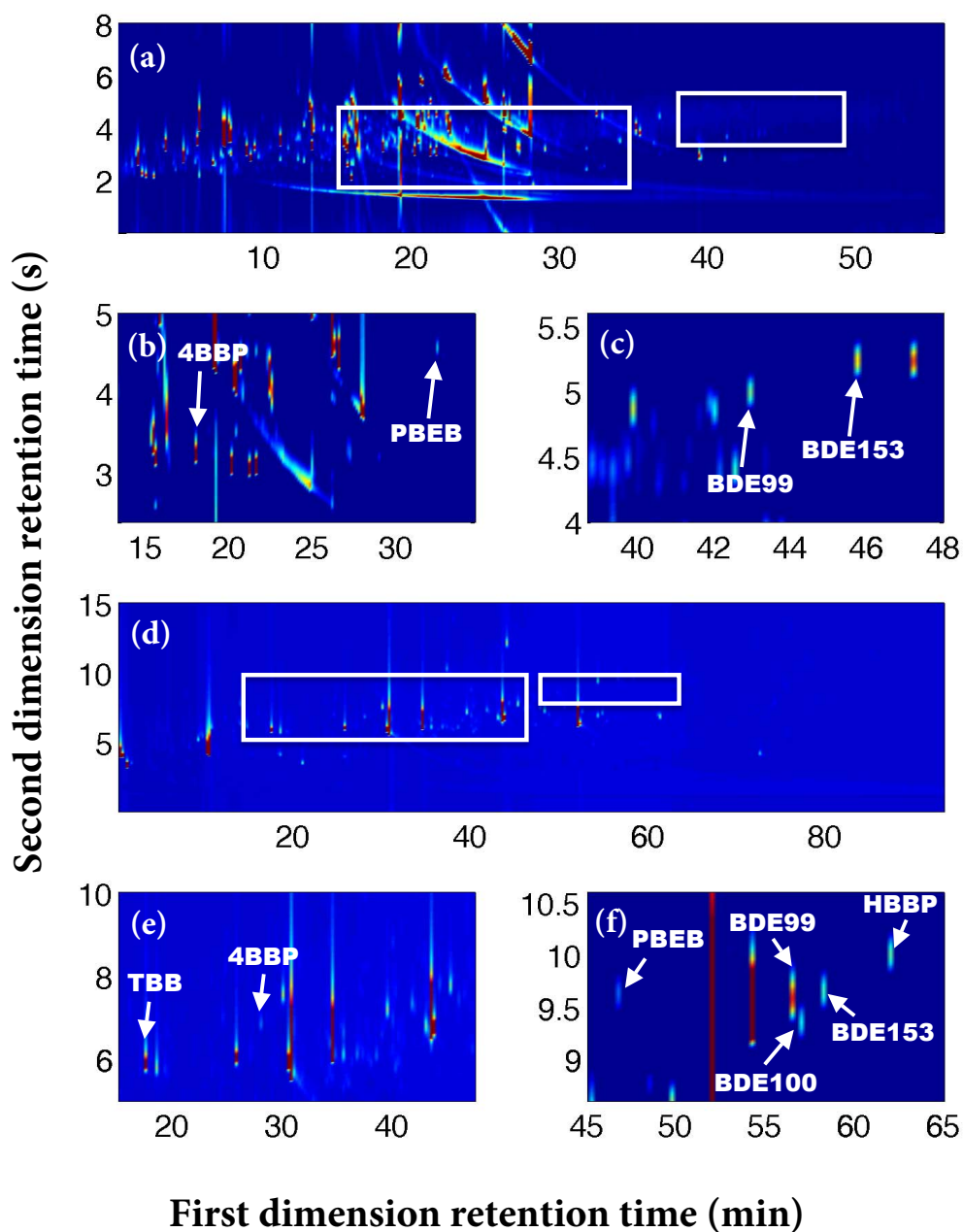


Figure A.2 – (a) GC $\times$ GC- $\mu$ ECD chromatogram of sediment extract, (b) the left-hand-side zoomed-in subregion of the sediment extract chromatogram, (c) the right-hand-side zoomed-in subregion of the sediment extract chromatogram, (d) GC $\times$ GC- $\mu$ ECD chromatogram of water column extract, (e) the left-hand-side zoomed-in subregion of the water extract chromatogram, and (f) the right-hand-side zoomed-in subregion of the water extract chromatogram.

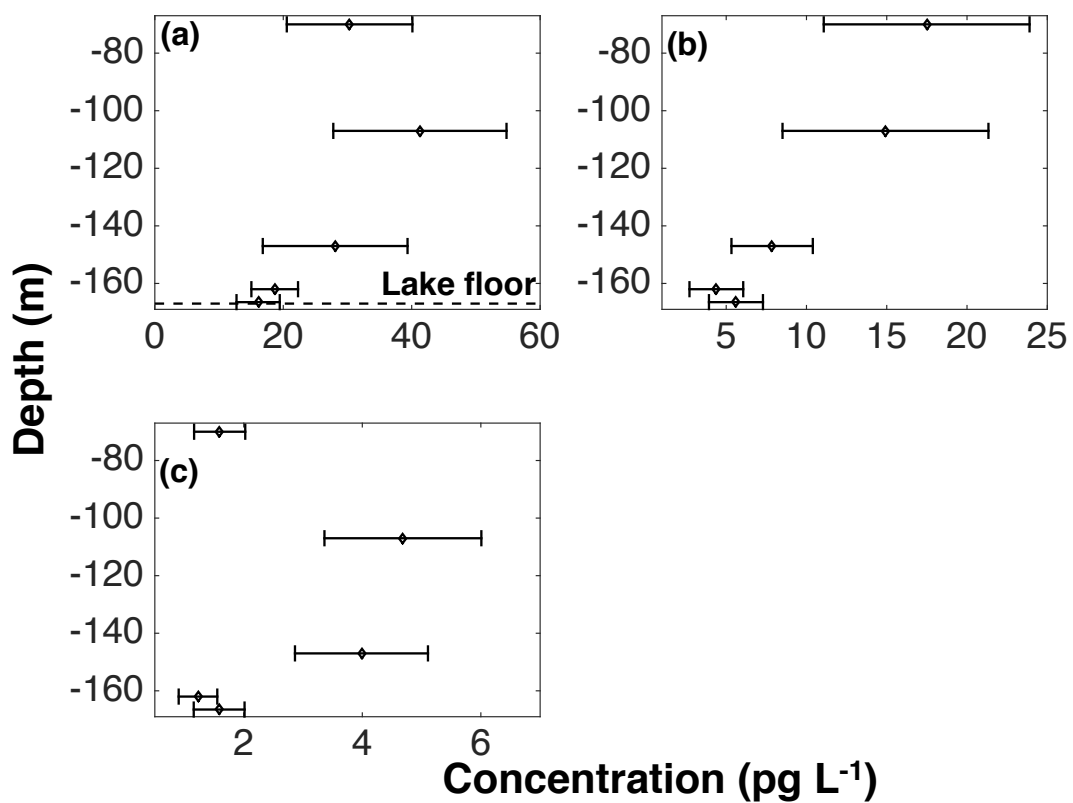


Figure A.3 – Dissolved water column concentrations with respect to depth for (a) BDE99; (b) BDE100; and (c) HBBP. The error bars represent the concentration variability at each depth, based on 6 individual measurements taken at each depth over separate sampling periods (June, July, August, 2011).

#### A.4. Target quantification

Table A.3 – The truly dissolved concentrations of the target analytes in the water column of Lake Geneva and their relative standard error, RSE (%)<sup>a</sup>, based on two replicates measured at each depth.

| 4BBP concentration (pg/L) in the water column of Lake Geneva   |                   |         |                   |         |                     |         |  |
|--|-------------------|---------|-------------------|---------|---------------------|---------|--|
| Depth (m)  | June <sup>b</sup> | RSE (%) | July <sup>b</sup> | RSE (%) | August <sup>b</sup> | RSE (%) | Kruskal-Wallis <i>p</i> value <sup>c</sup> [109] |
| 70   | 718               | 24      | 505               | 1       | 562                 | 12      | < 0.01   |
| 107  | 667               | 2       | 389               | 25      | 688                 | 12      |  |
| 147  | 748               | 33      | 554               | 98      | 567                 | 3       |  |
| 162  | 758               | 10      | 634               | 3       | 656                 | 8       |  |
| 166.5  | 650               | 11      | 609               | 6       | 668                 | 19      |  |
| TBB concentration (pg/L) in the water column of Lake Geneva    |                   |         |                   |         |                     |         |  |
| Depth (m)  | June <sup>b</sup> | RSE (%) | July <sup>b</sup> | RSE (%) | August <sup>b</sup> | RSE (%) | Kruskal-Wallis <i>p</i> value <sup>c</sup> [109] |
| 70   | 1210              | 28      | 703               | 25      | 892                 | 14      | 0.11   |
| 107  | 861               | 4       | 490               | 22      | 673                 | 23      |  |
| 147  | 800               | 2       | 596               | 38      | 450                 | 11      |  |
| 162  | 720               | 30      | 490               | 5       | 467                 | 27      |  |
| 166.5  | 549               | 35      | 587               | 4       | 528                 | 8       |  |
| PBEB concentration (pg/L) in the water column of Lake Geneva   |                   |         |                   |         |                     |         |  |
| Depth (m)  | June <sup>b</sup> | RSE (%) | July <sup>b</sup> | RSE (%) | August <sup>b</sup> | RSE (%) | Kruskal-Wallis <i>p</i> value <sup>c</sup> [109] |
| 70   | 8                 | 43      | 7                 | 4       | 6                   | 22      | 0.01, 0.8 <sup>e</sup>                           |
| 107  | 9                 | 339     | 7                 | 22      | 4 <sup>d</sup>      | 79      |  |
| 147  | 6                 | 18      | 14 <sup>d</sup>   | 155     | 7                   | 4       |  |
| 162  | 7                 | 6       | 8                 | 7       | 7                   | 2       |  |
| 166.5  | 7                 | 2       | 8                 | 16      | 8                   | 92      |  |
| BDE99 concentration (pg/L) in the water column of Lake Geneva  |                   |         |                   |         |                     |         |  |
| Depth (m)  | June <sup>b</sup> | RSE (%) | July <sup>b</sup> | RSE (%) | August <sup>b</sup> | RSE (%) | Kruskal-Wallis <i>p</i> value <sup>c</sup> [109] |
| 70   | 52                | 88      | 14                | 6       | 25                  | 42      | 0.6  |
| 107  | 58                | 83      | 10                | 30      | 56                  | 32      |  |
| 147  | 54                | 94      | 15                | 92      | 15                  | 18      |  |
| 162  | 12                | 13      | 17                | 9       | 27                  | 63      |  |
| 166.5  | 23                | 41      | 16                | 3       | 9                   | 46      |  |
| BDE100 concentration (pg/L) in the water column of Lake Geneva |                   |         |                   |         |                     |         |  |
| Depth (m)  | June <sup>b</sup> | RSE (%) | July <sup>b</sup> | RSE (%) | August <sup>b</sup> | RSE (%) | Kruskal-Wallis <i>p</i> value <sup>c</sup> [109] |
| 70   | 27                | 89      | 3                 | 8       | 22                  | 73      | 0.4  |
| 107  | 28                | 107     | 3                 | 53      | 13                  | 50      |  |
| 147  | 4                 | 22      | 6                 | 94      | 14                  | 11      |  |
| 162  | 4                 | 6       | 1                 | 34      | 8                   | 47      |  |
| 166.5  | 5                 | 20      | 3                 | 52      | 10                  | 9       |  |
| BDE153 concentration (pg/L) in the water column of Lake Geneva |                   |         |                   |         |                     |         |  |
| Depth (m)  | June <sup>b</sup> | RSE (%) | July <sup>b</sup> | RSE (%) | August <sup>b</sup> | RSE (%) | Kruskal-Wallis <i>p</i> value <sup>c</sup> [109] |
| 70   | nd <sup>f</sup>   | -       | nd <sup>f</sup>   | -       | 2                   | 2       | <0.01  |
| 107  | nd <sup>f</sup>   | -       | nd <sup>f</sup>   | -       | 6                   | 28      |  |
| 147  | nd <sup>f</sup>   | -       | nd <sup>f</sup>   | -       | 5                   | 6       |  |
| 162  | nd <sup>f</sup>   | -       | nd <sup>f</sup>   | -       | 2                   | 7       |  |
| 166.5  | nd <sup>f</sup>   | -       | nd <sup>f</sup>   | -       | 2                   | 10      |  |
| HBBP concentration (pg/L) in the water column of Lake Geneva   |                   |         |                   |         |                     |         |  |
| Depth (m)  | June <sup>b</sup> | RSE (%) | July <sup>b</sup> | RSE (%) | August <sup>b</sup> | RSE (%) | Kruskal-Wallis <i>p</i> value <sup>c</sup> [109] |
| 70   | nd <sup>f</sup>   | -       | nd <sup>f</sup>   | -       | 2                   | 2       | <0.01  |
| 107  | nd <sup>f</sup>   | -       | nd <sup>f</sup>   | -       | 5                   | 28      |  |
| 147  | nd <sup>f</sup>   | -       | nd <sup>f</sup>   | -       | 4                   | 6       |  |
| 162  | nd <sup>f</sup>   | -       | nd <sup>f</sup>   | -       | 2                   | 7       |  |
| 166.5  | nd <sup>f</sup>   | -       | nd <sup>f</sup>   | -       | 2                   | 10      |  |

<sup>a</sup> The RSE (%) is the relative standard error of each measurement computed using the standard deviation between two replicates at each depth; <sup>b</sup> The reported concentration is an average between two replicates in each depth; <sup>c</sup> The Kruskal-Wallis test was used to evaluate the concentration variability over different time periods. A Kruskal-Wallis *p* value of  $\leq 0.01$  indicates that the three sampling periods gave statistically different concentration, whereas a *p* value of  $> 0.1$  indicates that the concentrations of the three periods were statistically identical; <sup>d</sup> This value was found to be an outlier based on Dixon-Q<sub>95%</sub>-test [331]; <sup>e</sup> This Kruskal-Wallis *p* value was calculated after excluding the two outliers; <sup>f</sup> The target analyte was not detected in the water column of the lake.

Table A 4 – Estimated chemical and physical properties of the constituents of the pentabDE technical mixture.

| Chem. Phys. proper.                       | Compound name                            |  |  |  |                        |
|---|--|--|--|--|------------------------|
|   | BDE47                                    | BDE99                                    | BDE100                                 | BDE153                                 | HBBP                   |
| Melting point (°C)                        | 161.73 <sup>a</sup>                      | 182.80 <sup>a</sup>                      | 182.80 <sup>a</sup>                    | 197.14 <sup>a</sup>                    | 198.09 <sup>a</sup>    |
| Boiling point (°C)                        | 405.51 <sup>a</sup>                      | 436.21 <sup>a</sup>                      | 436.21 <sup>a</sup>                    | 466.91 <sup>a</sup>                    | 468.94 <sup>a</sup>    |
| P <sub>s</sub> (mm Hg)                    | ×10 <sup>-8a</sup>                       | 3.1×10 <sup>-8a</sup>                    | 3.25×10 <sup>-6a</sup>                 | 3.38×10 <sup>-7a</sup>                 | 3.32×10 <sup>-7a</sup> |
| Water solubility (mg/L)                   | 0.054 <sup>c</sup> , 0.0109 <sup>d</sup> | 0.011 <sup>c</sup> , 0.0024 <sup>d</sup> | 0.011 <sup>c</sup>                     | 0.002 <sup>c</sup>                     | 0.001 <sup>c</sup>     |
| K <sub>h</sub> (atm·m <sup>3</sup> /mole) | 1.18×10 <sup>-6a</sup>                   | 1.18×10 <sup>-6a</sup>                   | 4.71×10 <sup>-7a</sup>                 | 1.65×10 <sup>-6a</sup>                 | 0.001 <sup>c</sup>     |
| log K <sub>aw</sub>                       | -3.92 <sup>a</sup>                       | -4.32 <sup>a</sup>                       | -4.32 <sup>a</sup>                     | -4.72 <sup>a</sup>                     | -4.17 <sup>a</sup>     |
| log K <sub>ow</sub>                       | 6.77 <sup>a</sup> , 6.81 <sup>d</sup>    | 6.84 <sup>a</sup> , 7.32 <sup>d</sup>    | 7.66 <sup>a</sup> , 7.24 <sup>d</sup>  | 8.55 <sup>a</sup> , 7.90 <sup>d</sup>  | 9.10 <sup>a</sup>      |
| log K <sub>oa</sub>                       | 10.53 <sup>a</sup>                       | 11.31 <sup>a</sup>                       | 11.98 <sup>a</sup>                     | 12.15 <sup>a</sup>                     | 13.27 <sup>a</sup>     |
| log K <sub>oc-w</sub> (L/kg)              | 4.73 <sup>a</sup> , 4.41 <sup>e</sup>    | 4.76 <sup>a</sup> , 4.22 <sup>e</sup>    | 5.218 <sup>a</sup> , 4.07 <sup>e</sup> | 5.710 <sup>a</sup> , 3.99 <sup>e</sup> | 7.897 <sup>a</sup>     |
| log K <sub>D<sub>OC</sub>-w</sub> (L/kg)  | 6.321 <sup>f</sup>                       | 6.384 <sup>f</sup>                       | 7.130 <sup>f</sup>                     | 7.941 <sup>f</sup>                     | 8.441 <sup>f</sup>     |
| log K <sub>p<sub>DMS</sub>-w</sub>        | 6.13 <sup>g</sup> , 6.61 <sup>h</sup>    | 6.25 <sup>g</sup> , 7.16 <sup>h</sup>    | 6.77 <sup>g</sup> , 7.01 <sup>h</sup>  | 6.70 <sup>h</sup>                      | 6.95 <sup>g</sup>      |
| log BCF                                   | 4.13 <sup>a</sup>                        | 4.18 <sup>a</sup>                        | 3.80 <sup>a</sup>                      | 3.37 <sup>a</sup>                      | 3.68 <sup>a</sup>      |
| Direct photolysis half life, τ (h)        | 9 <sup>i</sup>                           | 4 <sup>i</sup>                           | 54 <sup>i</sup>                        | 2 <sup>i</sup>                         | 9 <sup>i</sup>         |

<sup>a</sup> Estimated using EPISuite [168]; <sup>b</sup> Hardy et al [154]; <sup>c</sup> Yalkowsky et al [216]; <sup>d</sup> Braekvelt et al [218]; <sup>e</sup> Estimated using the method developed by Kwan et al [141]; <sup>f</sup> Estimated using the method developed by Schwarzenbach et al [32]; <sup>g</sup> Perron et al [220]; <sup>h</sup> Estimated using the method developed by Booi et al [219]; <sup>i</sup> The photoreaction was carried out in cyclohexane solvent and in the presence of helium atmosphere [174]; <sup>j</sup> The photoreaction was carried out using a UV-vis light source in cyclohexane solvent and in the presence of helium atmosphere [175].

# B Supporting information to Chapter 4: Pentachlorothiophenol, a newly identified aquatic pollutant

## B.1 Water concentration estimation of the target analytes

Assuming that the mass transfer through the aqueous boundary layer is the rate limiting step [21, 164], the mass transfer of individual PRC between water and PDMS material is defined as:

$$\frac{C_t}{C_0} = \exp(-k_e \cdot t) \quad (\text{B.1})$$

where  $C_t$  is an individual PRC concentration in the sampler at time  $t$ ,  $C_0$  is the initial concentration of the same PRC in the sampler, and the  $k_e$  is the rate of mass transfer between the sampler and water for that specific PRC. We found a good agreement between the measured mass transfer rates of our PRCs and reported values in literature [265]. The  $k_e$  values estimated based on the depletion levels of PRCs were used to create a linear free energy relationship (LFER) with  $\log K_{ow}$  for each PDMS strip. The squared correlation coefficients ( $R^2$ ) of these LFERs were  $\sim 0.94$  for all analyzed PDMS strips. We employed these LFERs to estimate the  $k_e$  value for the target analytes. For estimation of water concentration of our target analytes, we used the estimated  $k_e$  inserted into the uptake equation (Eq. B.2).

$$C_w = \frac{C_t}{K_{sw} \cdot (1 - \exp(-k_e \cdot t))} \quad (\text{B.2})$$

## Appendix B. Pentachlorothiophenol, a newly identified aquatic pollutant

---

where  $C_w$  is the concentration of the truly dissolved fraction of the target analyte and  $K_{sw}$  is the partitioning coefficient of the target analyte between water and the sampler [297].

### B.1.1 Preprocessing and extraction of the PDMS strips

The PDMS strips ( $10 \times 1 \times 0.05 \text{ cm}^3$ ) were extracted using Soxhlet extraction with methanol for 24 hours [22, 165, 166, 167] and were stored in a freezer ( $-20 \text{ }^\circ\text{C}$ ). Five of the clean strips were used as the PDMS blank. The strips were loaded with four PRCs (PCB 30, PCB 50, PCB 145, PCB 204), having a concentration of  $20 \text{ ng g}^{-1}$  each. The details of the PRC loading process are explained elsewhere [162]. Five loaded strips were used for determination of the initial concentration of each PRC in the strips. After the environmental deployment, we extracted the strips by soaking them in 20 mL of pentane for eight hours [295], three successive times. The final extract had a volume of 60 mL and was reduced in volume and simultaneously switched to 1 mL of hexane using a rotary evaporator, then stored at  $-20 \text{ }^\circ\text{C}$  until analysis. No further clean up step was included in our sample preparation.

For quality assurance, we analyzed four different types of blanks. These were: the 5 PDMS blanks (explained above); the solvent blanks, which were the solvents employed for extraction (pentane and hexane); 3 field blanks, which were extracts of loaded strips brought to the field but not deployed; and the method blank, which was a solvent extract of the rotary evaporation glassware and the other glassware used for the extraction.

## B.2 Sediment samples extraction and clean up

The surface sediments of the lake were analyzed, employing ASE technique based on EPA method 3545A (Figure A.1). This method enabled us to perform the extraction and the clean up steps together [16, 53]. The extraction cell from inlet to outlet consisted of the following layers: a layer of activated Florisil, a layer of diatomaceous earth, 0.5 g of dried sample, a layer of diatomaceous earth, and a layer of the sodium sulfate. The sediment samples were extracted for 5 min with a solution of acetone and hexane at 50% (volume), at  $100 \text{ }^\circ\text{C}$  and at 1500 psi, 3 consecutive times. The solvent flush was set to 60% of the volume of the extraction cell and the purge time was 60 s. The volume of final extract was reduced and switched to 1 mL of hexane using rotary evaporator. The extraction recoveries were calculated for individual target analytes by spiking a sample-less cell with 40 ng of each target analyte and carrying out the extraction (Table B.1). The method blank was defined by extraction and analysis of a sample-less cell and the solvent blank was defined via analysis of all the solvents involved in the extraction.



### B.3. GC×GC- $\mu$ ECD and GC×GC-ENCI-TOFMS instrument conditions

Table B.1 – The ASE extraction recovery (%) and the  $R^2$  of external standard calibration curves of each target analyte.

| Compound                | Acronym | Recovery (%) | $R^2$ |
|-------------------------|---------|--------------|-------|
| pentachlorothiophenol   | PCTP    | 80.1         | 0.989 |
| hexachlorobenzene       | HCB     | 119.3        | 0.993 |
| pentachloronitrobenzene | PCNB    | 85.1         | 0.991 |

### B.3 GC×GC- $\mu$ ECD and GC×GC-ENCI-TOFMS instrument conditions

We obtained an excellent separation of our target analytes by optimizing the GC×GC- $\mu$ ECD and GC×GC-ENCI-TOFMS instrument conditions in our previous studies [16, 53, 15].

The GC×GC- $\mu$ ECD instrument was set to the constant flow of helium, having a flow rate of 1.5 mL min<sup>-1</sup>. The main oven temperature program was the following: 45 °C held for 1 minute; increased to 160 °C at 2.5 °C min<sup>-1</sup> held for another minute; then from 160 °C to 300 °C at 1.8 °C min<sup>-1</sup> and held for 10 minutes. The secondary oven was programmed at 57 °C held for one min then ramped to 172 °C at 3.2 °C min<sup>-1</sup> and held for one minute at 172 °C; then ramped from 172 °C to 312 °C at 2.8 °C min<sup>-1</sup> and it kept at that temperature for 33.4 minutes. Modulation periods of 15 s and 8 s were used for analysis of water column samples and sediment samples, respectively. All of the injections were performed in splitless mode. We used this oven temperature program for all of our samples. All chromatograms were acquired using ChromaTOF (Leco, Corp. USA) with a  $\mu$ ECD sampling rate of 50 Hz.

The GC×GC-ENCI-TOFMS separations were carried out using a 30 m length, 0.25 mm (i.d.), 0.25  $\mu$ m film thickness RXI-1MS column (Restek, USA) as the first dimension, and a 1 m length BPX-50 column (Restek, USA) with 0.1 mm i.d. and 0.1  $\mu$ m film thickness as the second dimension. Helium and methane were used as the carrier gas and as the ionization agent, respectively. We programmed the oven temperature program as follows: the first column oven temperature was started at 32 °C and was held at that temperature for 1 min; then increased to 300 °C at 4.5 °C min<sup>-1</sup> and then held one minute. The second column oven was programmed as: 67 °C held for 1 minute; then increased to 300 °C at 4.2 °C min<sup>-1</sup> and held for 1 minute. The transfer line temperature was set at 250 °C and the ionization temperature was 220 °C. We injected 1  $\mu$ L of each sample in splitless mode, and during the runs we used a modulation period of 8 s. The mass range of the TOFMS was set between 50 to 600 m/z and it acquired 50 spectra per second via GCsquare (Zoex), with a mass resolution of 4000 (full width at half maximum) and a mass accuracy of  $\pm 5$  milli-mass-units (mmu) over the calibrated mass range (i.e., 50 to 600 m/z). The ionization source emission current was 0.1 mA and the detector was operated at 2234 V.

## B.4 Computational estimates of aqueous $pK_a$ values

We estimated the aqueous acid dissociation constant ( $pK_a$ ) of PCTP with quantum chemical computations.  $pK_a$  values were assessed by taking advantage of the linear free energy relationship (LFER) that is observed between experimental and computed  $pK_a$  data within a functional group family [332, 333]. To establish the LFER, we evaluated computational  $pK_a$  values for seven compounds having known experimental  $pK_a$  values with sulfur as the dissociation functional group, including thiophenol, 4-chlorothiophenol, cysteine, 3-mercaptopropionic acid, mercaptan, hydrogen sulfide, and hydrogen disulfide. Raw, "uncorrected" theoretical  $pK_a$  values were calculated as follows:

$$\log k_a^{uncorrected} = \frac{\Delta G_{aq,rxn}^{dep}}{2.303RT} \quad (\text{B.3})$$

where  $\Delta G_{aq,rxn}^{dep}$  is the Gibbs free energy of the dissociation reaction in aqueous phase. Gas phase geometry optimizations and Gibbs free energy calculations of the neutral species and the deprotonated compounds were performed with the CBS-QB3 composite method [274, 275], which is known to give good results for the gas phase proton attachment energy used in  $pK_a$  calculations [334, 335, 336, 337, 338]. Solvation free energies were simulated with the SMD continuum solvation model with the B2PLYPD/aug-cc-pVTZ model chemistry.

### B.4.1 Free energy of the proton in aqueous phase

A value of  $-6.28 \text{ kcal mol}^{-1}$  was assigned to the free energy of the proton in gas phase,  $G_{gas}^{H^+}$  [334]. This was converted from 1 atm to 1 M standard state at 298 K by adding a factor of  $1.89 \text{ kcal mol}^{-1}$ . To this term we added the free energy of solvation of the proton,  $\Delta G_{solv}^{H^+} = -263.12 \text{ kcal mol}^{-1}$  [335]. The resulting value of  $-267.51 \text{ kcal mol}^{-1}$  was employed for  $G_{aq}^{H^+}$  in the 1 M aqueous standard state and was used for computations of free energy of aqueous dissociation reaction in Eq B.3. The value for  $G_{gas}^{H^+}$  becomes cancelled out in the LFER that we applied to estimate a  $pK_a$  value of 4.3 for PCTP.

### B.4.2 Quantum chemical computation of the $K_{sw}^{app}$

To estimate the  $K_{sw}^{app}$  of PCTP according to Eq. 4.1 and Figure B.1, we needed to estimate the PDMS-water partition coefficient for the protonated species,  $K_{HA-sw}$ , the PDMS-water partition coefficient of the deprotonated species,  $K_{A-sw}$ , and aqueous acidic dissociation coefficient,  $pK_a$ . The partition coefficient of both the protonated species and deprotonated species of PCTP between PDMS and water phase can be computed by taking advantage of computed solvation free energies and the thermodynamic cycle [341, 342, 343] shown in

Table B.2 – Experimental  $pK_a$  data, uncorrected quantum chemical  $pK_a$ , LFER corrected  $pK_a$  and the absolute deviation (AD) between the LFER estimated  $pK_a$  and the experimental value for 7 sulfur-containing compounds.

| Compounds                | Experimental $pK_a$ | Uncorrected Quantum Chemical $pK_a$ | Quantum Chemical LFER $pK_a$ | AD   |
|--------------------------|---------------------|-------------------------------------|------------------------------|------|
|                          | hydrogen disulfide  | 5.00 <sup>a</sup>                   | 6.41                         |      |
| 4-chloro-thiophenol      | 7.50 <sup>b</sup>   | 9.75                                | 6.74                         | 0.76 |
| thiophenol               | 7.81 <sup>b</sup>   | 11.59                               | 7.60                         | 0.21 |
| hydrogen sulfide         | 6.83 <sup>c</sup>   | 12.36                               | 7.96                         | 1.13 |
| cysteine                 | 8.50 <sup>a</sup>   | 14.69                               | 9.05                         | 0.56 |
| 3-mercaptopropionic acid | 10.40 <sup>d</sup>  | 15.48                               | 9.42                         | 0.98 |
| mercaptan                | 10.30 <sup>a</sup>  | 17.60                               | 10.42                        | 0.12 |
| pentachlorothiophenol    |                     | 4.48                                | 4.26                         |      |

<sup>a</sup> Value is taken from reference [283]; <sup>b</sup> Value is taken from reference [282]; <sup>c</sup> Value is taken from reference [339]; <sup>d</sup> Value is taken from reference [340].

Figure B.1:

$$\log K_{AB} = \frac{\Delta G_B - \Delta G_A}{2.303RT} \quad (\text{B.4})$$

where  $K_{sw}$  is the partition coefficient of each species (i.e. neutral and ionized) between the PDMS phases and water phase,  $\Delta G_B$  is the solvation free energy of the PCTP species in PDMS at 1M standard state,  $\Delta G_A$  is the solvation free energy of the PCTP species in water at 1M standard state,  $R$  is the molar gas constant and  $T$  is the temperature. The SMD solvent model is not parametrized to simulate PDMS condensed phase. Therefore we used *n*-hexadecane solvent as a model proxy of PDMS. We validated this approach by performing further calculations for  $K_{AB}^{app}$  of four additional ionizable compounds: 2,4-dichlorophenol, 2,4,6-trichlorophenol, 2,3,4,6-tetrachlorophenol and pentachlorophenol. The two partitioning phases chosen for these additional calculations were water and polyacrylate fiber, based on the availability of experimental data [344]. In order to mimic the polyacrylate fibre (PA) we assigned the solvent as propylacetate (pa) in the model. This method enabled us to successfully estimate  $K_{PA-w}^{app}$  with an absolute deviation from experimental data of  $\leq 1.1$  log units for all four chlorophenols (Table B.3).

## B.5 Quality assurance

For the quality control purposes sodium sulfate and Florisil<sup>®</sup> were heated to 600 °C for 24 hours. All glassware were washed with MilliQ water and rinsed with hexane ACS grade and baked overnight at 450 °C. Additionally, we baked the GC×GC ovens at 300 °C for 30 min after each injection. Injection port liners were changed between standard injections and sample injections.

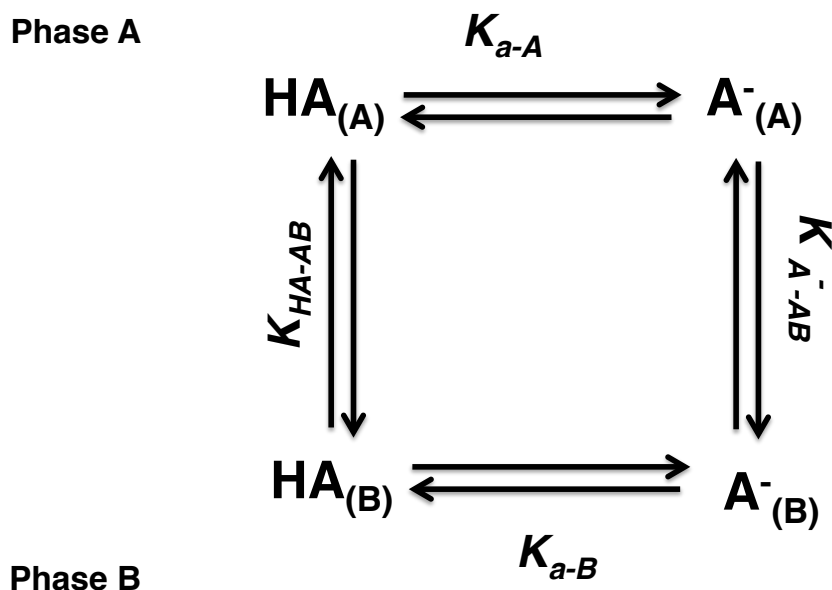


Figure B.1 – Thermodynamic cycle of the partitioning of an acidic compound, HA, between two phases A and B.  $K_{a-A}$  is the acid dissociation coefficient in phase A,  $K_{a-B}$  is the acid dissociation coefficient in phase B,  $K_{HA-AB}$  is the partition coefficient of the associated acid between the two phases, and  $K_{A^{-}-AB}$  is the partition coefficient of the dissociated acid between the two phases.

Table B.3 – Estimated partitioning coefficient of selected chlorinated phenols between water and propylacetate, their  $K_{pa-w}^{app}$  (estimated using Eq. 4.1 assuming a pH of 2), their  $pK_a$ , and the experimental  $K_{PA-w}^{app}$  reported by Escher et al carried out at pH=2 [344].

| Compounds                 | $pK_a$            | $\log K_{pa-w}^{HA}$ | $\log K_{pa-w}^{A^{-}}$ | $\log K_{pa-w}^{app}$ | $\log K_{PA-w}^{app}$ | AD <sup>a</sup> |
|---------------------------|-------------------|----------------------|-------------------------|-----------------------|-----------------------|-----------------|
| 2,6-dichlorophenol        | 6.97 <sup>b</sup> | 2.87                 | -6.29                   | 2.87                  | 2.60                  | 0.3             |
| 2,4,6-trichlorophenol     | 6.15 <sup>b</sup> | 3.32                 | -5.06                   | 3.32                  | 2.89                  | 0.4             |
| 2,3,4,6-tetrachlorophenol | 5.40 <sup>c</sup> | 3.63                 | -4.02                   | 3.63                  | 2.91                  | 0.72            |
| pentachlorophenol         | 4.75 <sup>c</sup> | 4.05                 | -3.04                   | 4.05                  | 2.93                  | 1.12            |

<sup>a</sup> The absolute deviation (AD), in log units, between the estimated apparent and experimental values; <sup>b</sup> The value is taken from the reference [345]; <sup>c</sup> The value is taken from reference [346].

Table B.4 – Truly dissolved concentrations of PCTP and HCB at our sampling site in the water column of Lake Geneva.

| Concentration (ng L <sup>-1</sup> ) of PCTP in the water column of Lake Geneva |                   |                      |                   |                      |                     |                      |                                     |
|--|-------------------|----------------------|-------------------|----------------------|---------------------|----------------------|-------------------------------------|
| Depth (m)  | June <sup>a</sup> | RSE (%) <sup>b</sup> | July <sup>a</sup> | RSE (%) <sup>b</sup> | August <sup>a</sup> | RSE (%) <sup>b</sup> | Kruskal-Wallis <i>p</i> value [109] |
| 70   | 197.26            | 52.5                 | 136.97            | 32.0                 | 116.60              | 65.6                 | 0.6                                 |
| 107  | 297.29            | 48.0                 | 97.68             | 25.7                 | 135.10              | 6.7                  |                                     |
| 147  | 89.01             | 43.6                 | 458.87            | 124.4                | 272.59              | 5.0                  |                                     |
| 162  | 130.53            | 22.9                 | 159.76            | 15.6                 | 197.34              | 11.2                 |                                     |
| 166.5  | 254.37            | 37.2                 | 193.16            | 26.2                 | 404.05              | 94.7                 |                                     |
| Average concentration (ng L <sup>-1</sup> ) <sup>d</sup>                       | 193.69            | 40.9 <sup>e</sup>    | 209.29            | 44.8 <sup>e</sup>    | 225.15              | 36.6 <sup>e</sup>    |                                     |

| Concentration (ng L <sup>-1</sup> ) of HCB in the water column of Lake Geneva |                   |                      |                   |                      |                     |                      |  |
|---|-------------------|----------------------|-------------------|----------------------|---------------------|----------------------|--|
| Depth (m)   | June <sup>a</sup> | RSE (%) <sup>b</sup> | July <sup>a</sup> | RSE (%) <sup>b</sup> | August <sup>a</sup> | RSE (%) <sup>b</sup> | Kruskal-Wallis <i>p</i> <sup>c</sup> value [109] |
| 70  | 0.035             | 52.5                 | 0.155             | 102.6                | 0.050               | 52.2                 | 0.8  |
| 107   | 0.053             | 48.0                 | 0.120             | 73.4                 | 0.057               | 15.2                 |  |
| 147   | 0.016             | 43.6                 | 0.058             | 29.6                 | 0.061               | 20.0                 |  |
| 162   | 0.023             | 22.7                 | 0.062             | 32.8                 | 0.054               | 14.8                 |  |
| 166.5   | 0.045             | 37.1                 | 0.057             | 24.2                 | 0.071               | 46.1                 |  |
| Average concentration (ng L <sup>-1</sup> ) <sup>d</sup>                      | 0.034             | 40.72 <sup>e</sup>   | 0.090             | 52.5 <sup>e</sup>    | 0.059               | 29.7 <sup>e</sup>    |  |

<sup>a</sup> The reported concentration is an average of two replicates in each depth; <sup>b</sup> The RSE (%) is the relative standard error of each measurement computed using the standard deviation between two replicates at each depth; <sup>c</sup> The *p* value evaluated the differences in the concentration of the target analytes from month to month. A *p* value > 0.05 indicated that the differences in the concentration observed during different months were not statistically meaningful; <sup>d</sup> The concentration averaged over five depths for each month; <sup>e</sup> The RSE (%) is the relative standard error of the concentration over five depths for each month.

To ensure the absence of biased calibration, we computed the test for proportionality of the integrated signal (ARF) on our external standard calibration method (ESM) data set, Eq. 2.8. The deviation of ARF from a value of 1 was smaller than 20% for all of our target analytes, which indicated the absence of incorrigible error introduced during the data processing. We also compiled the offset error values for our target analytes, in order to make sure that the ESM is adequate for quantification of our target analytes in the environmental sample. The instrument limit of quantification LOQ was defined as the 10 times S/N. The method LOQ was defined as the offset of the external standard calibration method. Throughout this manuscript, the term "LOQ" refers to the method LOQ. All detected target analytes in the analyzed samples had a S/N > 100, which indicated that the integrated signals for the target analytes were larger than the instrument LOQ [76]. These tests and their implications have been explained in detail elsewhere [15].

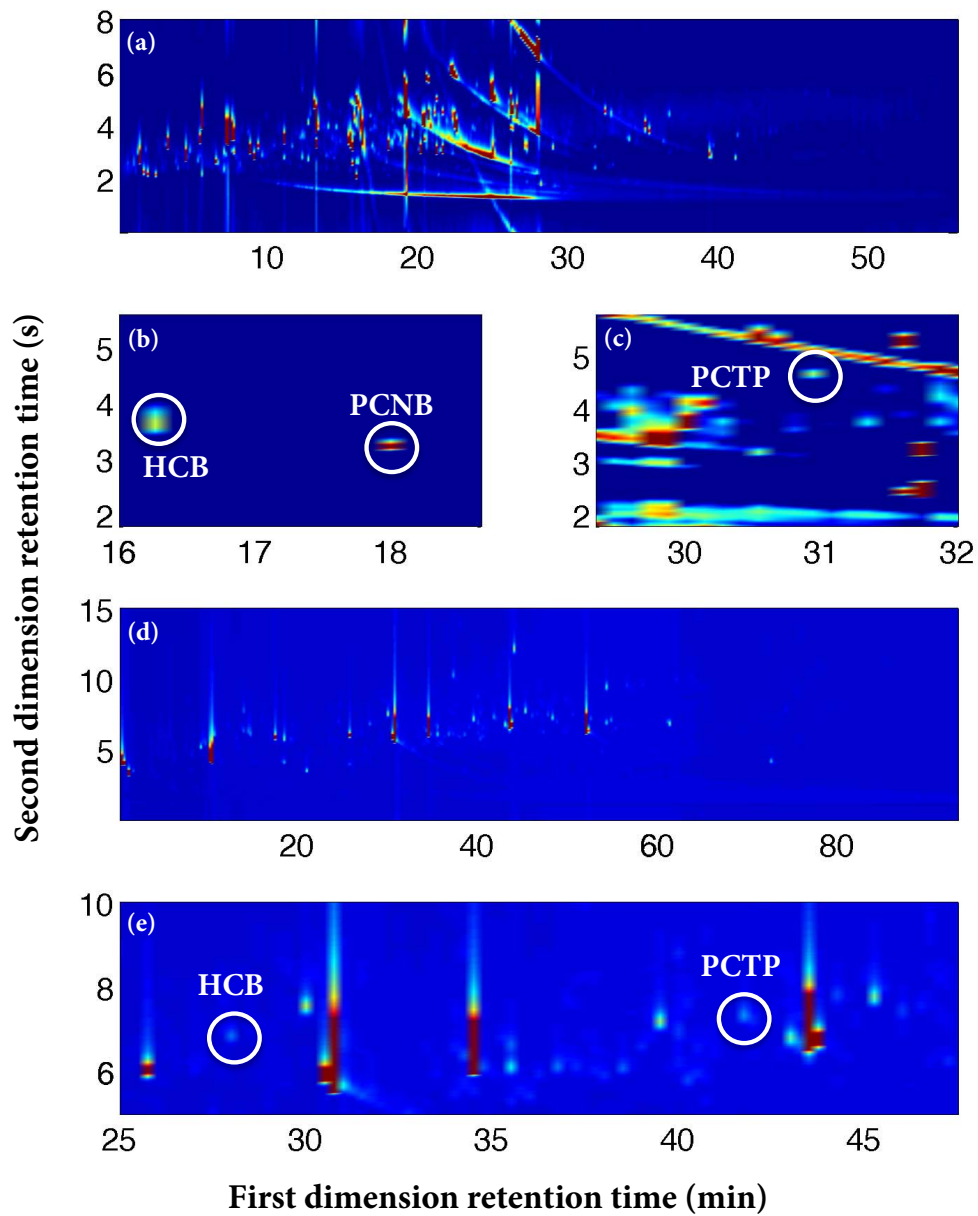


Figure B.2 – GC×GC-μECD data showing: (a) the sediment extract chromatogram; (b) and (c) zoomed in subregions of the sediment extract chromatogram; (d) the water column extract chromatogram; and (e) zoomed in subregion in the water column extract chromatogram.

## Bibliography

- [1] P. H. Howard and D. C. Muir, "Identifying New Persistent and Bioaccumulative Organics Among Chemicals in Commerce. III: By products, Impurities, and Degradation Products," *Environ. Sci. Technol.*, 2013.
- [2] D. C. Muir and P. H. Howard, "Are there other persistent organic pollutants? a challenge for environmental chemists," *Environ. Sci. Technol.*, vol. 40, no. 23, pp. 7157–7166, 2006.
- [3] P. H. Howard and D. C. Muir, "Identifying new persistent and bioaccumulative organics among chemicals in commerce," *Environ. Sci. Technol.*, vol. 44, no. 7, pp. 2277–2285, 2010.
- [4] D. C. Muir and P. H. Howard, "Are there other persistent organic pollutants? A challenge for environmental chemists," *Environ. Sci. Technol.*, vol. 40, no. 23, pp. 7157–7166, 2006.
- [5] C. Rovida and T. Hartung, "Re-evaluation of animal numbers and costs for in vivo tests to accomplish REACH legislation requirements for chemicals—a report by the transatlantic think tank for toxicology," *Altex*, vol. 26, no. 3, pp. 187–208, 2009.
- [6] R. E. Clement, E. J. Reiner, and S. P. Bhavsar, "Organohalogen contaminants of emerging concern in Great Lakes fish: a review," *Anal. Bioanal. Chem.*, vol. 404, pp. 2639–2658, Aug. 2012.
- [7] G. Klečka, C. Persoon, and R. Currie, "Chemicals of emerging concern in the great lakes basin: an analysis of environmental exposures," *Rev. Environ. Contam. Toxicol.*, vol. 207, pp. 1–93, 2010.
- [8] D. Ueno, C. Darling, M. Alae, L. Campbell, G. Pacepavicius, C. Teixeira, and D. Muir, "Detection of hydroxylated polychlorinated biphenyls (OH-PCBs) in the abiotic environment: surface water and precipitation from Ontario, Canada," *Environ. Sci. Technol.*, vol. 41, no. 6, pp. 1841–1848, 2007.
- [9] D. Ueno, C. Darling, M. Alae, G. Pacepavicius, C. Teixeira, L. Campbell, R. J. Letcher, Å. Bergman, G. Marsh, and D. Muir, "Hydroxylated polybrominated diphenyl ethers (OH-PBDEs) in the abiotic environment: surface water and precipitation from Ontario, Canada," *Environ. Sci. Technol.*, vol. 42, no. 5, pp. 1657–1664, 2008.

## Bibliography

---

- [10] T. Meyer, D. C. Muir, C. Teixeira, X. Wang, T. Young, and F. Wania, "Deposition of brominated flame retardants to the Devon Ice Cap, Nunavut, Canada," *Environ. Sci. Technol.*, vol. 46, no. 2, pp. 826–833, 2011.
- [11] E. Skoczyńska, P. Korytár, and J. d. Boer, "Maximizing Chromatographic Information from Environmental Extracts by GC×GC-ToF-MS," *Environ. Sci. Technol.*, vol. 42, pp. 6611–6618, Sept. 2008.
- [12] K. Arinaitwe, D. C. Muir, B. T. Kiremire, P. Fellin, H. Li, and C. Teixeira, "Polybrominated diphenyl ethers and alternative flame retardants in air and precipitation samples from the northern Lake Victoria region, east Africa," *Environ. Sci. Technol.*, vol. 48, no. 3, pp. 1458–1466, 2014.
- [13] K. J. Jobst, L. Shen, E. J. Reiner, V. Y. Taguchi, P. A. Helm, R. McCrindle, and S. Backus, "The use of mass defect plots for the identification of (novel) halogenated contaminants in the environment," *Anal. Bioanal. Chem.*, vol. 405, pp. 3289–3297, Jan. 2013.
- [14] M. Pena-Abaurrea, K. J. Jobst, R. Ruffolo, L. Shen, R. McCrindle, P. A. Helm, and E. J. Reiner, "Identification of potential novel bioaccumulative and persistent chemicals in sediments from Ontario (Canada) using scripting approaches with GC×GC-TOFMS analysis," *Environ. Sci. Technol.*, vol. 48, no. 16, pp. 9591–9599, 2014.
- [15] S. Samanipour, P. Dimitriou-Christidis, J. Gros, A. Grange, and J. S. Arey, "Analyte quantification with comprehensive two-dimensional gas chromatography: Assessment of methods for baseline correction, peak delineation, and matrix effect elimination for real samples," *J. Chromatogr. A*, vol. 1375, pp. 123–139, 2015.
- [16] P. Dimitriou-Christidis, A. Bonvin, S. Samanipour, J. Hollender, R. Rutler, J. Westphale, J. Gros, and J. S. Arey, "GC×GC quantification of priority and emerging nonpolar organic micropollutants in all types of wastewater streams: Analysis methodology, chemical occurrence, and partitioning," *Environ. Sci. Technol.*, vol. In press, 2015.
- [17] D. Muir and E. Sverko, "Analytical methods for PCBs and organochlorine pesticides in environmental monitoring and surveillance: a critical appraisal," *Anal. Bioanal. Chem.*, vol. 386, no. 4, pp. 769–789, 2006.
- [18] D. Muir and R. Lohmann, "Water as a new matrix for global assessment of hydrophilic POPs," *TRAC-Trends Anal. Chem.*, vol. 46, pp. 162–172, 2013.
- [19] M. Venier, R. A. Hites, A. Dove, S. M. Backus, and K. Romanak, "Flame retardants and legacy chemicals in Great Lake's water," *Environ. Sci. Technol.*, vol. 48, no. 16, pp. 9563–9572, 2014.
- [20] S. L. Kaserzon, D. W. Hawker, K. Booij, D. S. O'Brien, K. Kennedy, E. L. Vermeirssen, and J. F. Mueller, "Passive sampling of perfluorinated chemicals in water: In-situ calibration," *Environ. Pollut.*, vol. 186, pp. 98–103, 2014.



- [21] K. Booij, B. N. Zegers, and J. P. Boon, "Levels of some polybrominated diphenyl ether (PBDE) flame retardants along the Dutch coast as derived from their accumulation in SPMDs and blue mussels (*Mytilus edulis*)," *Chemosphere*, vol. 46, no. 5, pp. 683–688, 2002.
- [22] I. J. Allan, K. Booij, A. Paschke, B. Vrana, G. A. Mills, and R. Greenwood, "Field performance of seven passive sampling devices for monitoring of hydrophobic substances," *Environ. Sci. Technol.*, vol. 43, no. 14, pp. 5383–5390, 2009.
- [23] R. Greenwood, G. Mills, and B. Vrana, *Passive sampling techniques in environmental monitoring*, vol. 48. Elsevier, 2007.
- [24] R. Lohmann, K. Booij, F. Smedes, and B. Vrana, "Use of passive sampling devices for monitoring and compliance checking of POP concentrations in water," *Environ. Sci. Pollut. R.*, vol. 19, no. 6, pp. 1885–1895, 2012.
- [25] A. R. Schneider, A. Paolicchi, and J. E. Baker, "The use of solid-phase microextraction to rapidly measure dissolved PCBs in natural waters," *Int. J. Environ. An. Ch.*, vol. 86, no. 11, pp. 789–803, 2006.
- [26] N. Estoppey, A. Schopfer, J. Omlin, P. Esseiva, E. L. Vermeirssen, O. Delémont, and L. F. De Alencastro, "Effect of water velocity on the uptake of polychlorinated biphenyls (PCBs) by silicone rubber (SR) and low-density polyethylene (LDPE) passive samplers: An assessment of the efficiency of performance reference compounds (PRCs) in river-like flow conditions," *Sci. Total Environ.*, vol. 499, pp. 319–326, 2014.
- [27] R. Lohmann and D. Muir, "Global aquatic passive sampling (AQUA-GAPS): Using passive samplers to monitor POPs in the waters of the world," *Environ. Sci. Technol.*, vol. 44, no. 3, pp. 860–864, 2010.
- [28] J. Llorca, C. Gutiérrez, E. Capilla, R. Tortajada, L. Sanjuán, A. Fuentes, and I. Valor, "Constantly stirred sorbent and continuous flow integrative sampler: New integrative samplers for the time weighted average water monitoring," *J. Chromatogr. A*, vol. 1216, no. 31, pp. 5783–5792, 2009.
- [29] A. Kot-Wasik, B. Zabiegała, M. Urbanowicz, E. Dominiak, A. Wasik, and J. Namieśnik, "Advances in passive sampling in environmental studies," *Anal. Chim. Acta*, vol. 602, no. 2, pp. 141–163, 2007.
- [30] K. Booij, B. Vrana, and J. N. Huckins, *Theory, modelling and calibration of passive samplers used in water monitoring*, vol. 48. Elsevier Amsterdam, 2007.
- [31] G. Petrick, D. E. Schulz-Bull, V. Martens, K. Scholz, and J. C. Duinker, "An in-situ filtration/extraction system for the recovery of trace organics in solution and on particles tested in deep ocean water," *Mar. Chem.*, vol. 54, no. 1, pp. 97–105, 1996.

## Bibliography

---

- [32] R. P. Schwarzenbach, P. M. Gschwend, and D. M. Imboden, *Environmental Organic Chemistry*. John Wiley & Sons, 2003.
- [33] W. Xu, X. Wang, and Z. Cai, "Analytical chemistry of the persistent organic pollutants identified in the Stockholm Convention: A review," *Anal. Chim. Acta*, vol. 790, pp. 1–13, 2013.
- [34] C. A. McDonough, M. A. Khairy, D. C. Muir, and R. Lohmann, "Significance of population centers as sources of gaseous and dissolved PAHs in the Lower Great Lakes," *Environ. Sci. Technol.*, vol. 48, no. 14, pp. 7789–7797, 2014.
- [35] M. Khairy, D. Muir, C. Teixeira, and R. Lohmann, "Spatial trends, sources, and air–water exchange of organochlorine pesticides in the Great Lakes basin using low density polyethylene passive samplers," *Environ. Sci. Technol.*, vol. 48, no. 16, pp. 9315–9324, 2014.
- [36] J. Ge, M. Liu, X. Yun, Y. Yang, M. Zhang, Q. X. Li, and J. Wang, "Occurrence, distribution and seasonal variations of polychlorinated biphenyls and polybrominated diphenyl ethers in surface waters of the East Lake, China," *Chemosphere*, vol. 103, pp. 256–262, 2014.
- [37] A. Möller, Z. Xie, R. Sturm, and R. Ebinghaus, "Polybrominated diphenyl ethers (PBDEs) and alternative brominated flame retardants in air and seawater of the European Arctic," *Environ. Pollut.*, vol. 159, no. 6, pp. 1577–1583, 2011.
- [38] S. S. Streets, S. A. Henderson, A. D. Stoner, D. L. Carlson, M. F. Simcik, and D. L. Swackhamer, "Partitioning and bioaccumulation of PBDEs and PCBs in Lake Michigan," *Environ. Sci. Technol.*, vol. 40, no. 23, pp. 7263–7269, 2006.
- [39] P. M. Gschwend and R. A. Hites, "Fluxes of polycyclic aromatic hydrocarbons to marine and lacustrine sediments in the northeastern United States," *Geochim. Cosmochim. Ac.*, vol. 45, no. 12, pp. 2359–2367, 1981.
- [40] R. Carafa, D. Marinov, S. Dueri, J. Wollgast, J. Ligthart, E. Canuti, P. Viaroli, and J. Zaldívar, "A 3D hydrodynamic fate and transport model for herbicides in Sacca di Goro coastal lagoon (Northern Adriatic)," *Mar. Pollut. Bull.*, vol. 52, no. 10, pp. 1231–1248, 2006.
- [41] R. Lohmann, K. Breivik, J. Dachs, and D. Muir, "Global fate of POPs: current and future research directions," *Environ. Pollut.*, vol. 150, no. 1, pp. 150–165, 2007.
- [42] C. Bogdal, M. Scheringer, P. P. Schmid, M. Bläuenstein, M. Kohler, and K. Hungerbühler, "Levels, fluxes and time trends of persistent organic pollutants in Lake Thun, Switzerland: Combining trace analysis and multimedia modeling," *Sci. Total Environ.*, vol. 408, pp. 3654–3663, Aug. 2010.
- [43] A. Mudroch, K. Kaiser, M. Comba, and M. Neilson, "Particle-associated PCBs in Lake Ontario," *Sci. Total Environ.*, vol. 158, pp. 113–125, 1994.

- [44] M. F. Simcik, S. J. Eisenreich, and P. J. Lioy, "Source apportionment and source/sink relationships of PAHs in the coastal atmosphere of Chicago and Lake Michigan," *Atmos. Environ.*, vol. 33, no. 30, pp. 5071–5079, 1999.
- [45] L. Melymuk, M. Robson, S. A. Csiszar, P. A. Helm, G. Kaltenecker, S. Backus, L. Bradley, B. Gilbert, P. Blanchard, L. Jantunen, *et al.*, "From the city to the lake: Loadings of PCBs, PBDEs, PAHs and PCMs from Toronto to Lake Ontario," *Environ. Sci. Technol.*, vol. 48, no. 7, pp. 3732–3741, 2014.
- [46] W. D. Hafner and R. A. Hites, "Potential sources of pesticides, PCBs, and PAHs to the atmosphere of the Great Lakes," *Environ. Sci. Technol.*, vol. 37, no. 17, pp. 3764–3773, 2003.
- [47] S. N. Meijer, J. Dachs, P. Fernandez, L. Camarero, J. Catalan, S. Del Vento, B. Van Drooge, E. Jurado, and J. O. Grimalt, "Modelling the dynamic air–water–sediment coupled fluxes and occurrence of polychlorinated biphenyls in a high altitude lake," *Environ. Pollut.*, vol. 140, no. 3, pp. 546–560, 2006.
- [48] P. Sun, P. Blanchard, K. A. Brice, and R. A. Hites, "Trends in polycyclic aromatic hydrocarbon concentrations in the Great Lakes atmosphere," *Environ. Sci. Technol.*, vol. 40, no. 20, pp. 6221–6227, 2006.
- [49] D. R. Oros, D. Hoover, F. Rodigari, D. Crane, and J. Sericano, "Levels and distribution of polybrominated diphenyl ethers in water, surface sediments, and bivalves from the San Francisco Estuary," *Environ. Sci. Technol.*, vol. 39, no. 1, pp. 33–41, 2005.
- [50] K. Cailleaud, J. Forget-Leray, S. Souissi, D. Hilde, K. LeMenach, and H. Budzinski, "Seasonal variations of hydrophobic organic contaminant concentrations in the water-column of the Seine Estuary and their transfer to a planktonic species *Eurytemora affinis* (Calanoïda, copepoda). Part 1: PCBs and PAHs," *Chemosphere*, vol. 70, pp. 270–280, Dec. 2007.
- [51] J. Dachs, J. M. Bayona, C. Raoux, and J. Albaigés, "Spatial, vertical distribution and budget of polycyclic aromatic hydrocarbons in the western Mediterranean seawater," *Environ. Sci. Technol.*, vol. 31, no. 3, pp. 682–688, 1997.
- [52] S. Samanipour, *Overlooked persistent and bioaccumulative pollutants in Lake Geneva: their measurement, occurrence, and concentration distribution in the water column and sediments (Chapter III)*. PhD thesis, EPFL, 2015.
- [53] S. Samanipour, D. Nabi, and J. S. Arey, "Overlooked persistent and bioaccumulative brominated pollutants in the deep water column of Lake Geneva: 1,3,5-tribromobenzene and 4-bromobiphenyl," *Environ. Sci. Technol.*, submitted 2015.

## Bibliography

---

- [54] W. Bertsch, "Two-dimensional gas chromatography. concepts, instrumentation, and applications—part 2: Comprehensive two-dimensional gas chromatography," *J. High Res. Chromatog.*, vol. 23, no. 3, pp. 167–181, 2000.
- [55] G. S. Frysinger, R. B. Gaines, and E. B. Ledford, "Quantitative determination of BTEX and total aromatic compounds in gasoline by comprehensive two-dimensional gas chromatography (GC×GC)," *J. High Res. Chromatog.*, vol. 22, no. 4, pp. 195–200, 1999.
- [56] S. Peters, G. Vivó-Truyols, P. J. Marriott, and P. J. Schoenmakers, "Development of an algorithm for peak detection in comprehensive two-dimensional chromatography," *J. Chromatogr. A*, vol. 1156, no. 1, pp. 14–24, 2007.
- [57] J. M. Amigo, T. Skov, and R. Bro, "ChromATHography: solving chromatographic issues with mathematical models and intuitive graphics," *Chem. Rev.*, vol. 110, no. 8, pp. 4582–4605, 2010.
- [58] J. A. Murray, "Qualitative and quantitative approaches in comprehensive two-dimensional gas chromatography," *J. Chromatogr. A*, vol. 1261, pp. 58–68, 2012.
- [59] J. Beens, H. Boelens, R. Tijssen, and J. Blomberg, "Quantitative aspects of comprehensive two-dimensional gas chromatography (GC×GC)," *J. High Res. Chromatog.*, vol. 21, no. 1, pp. 47–54, 1998.
- [60] R. B. Gaines, E. B. Ledford, and J. D. Stuart, "Analysis of water samples for trace levels of oxygenate and aromatic compounds using headspace solid-phase microextraction and comprehensive two-dimensional gas chromatography," *J. Microcolumn Sep.*, vol. 10, no. 7, pp. 597–604, 1998.
- [61] C. Cordero, C. Bicchi, D. Joulain, and P. Rubiolo, "Identification, quantitation and method validation for the analysis of suspected allergens in fragrances by comprehensive two-dimensional gas chromatography coupled with quadrupole mass spectrometry and with flame ionization detection," *J. Chromatogr. A*, vol. 1150, no. 1, pp. 37–49, 2007.
- [62] M. Kallio and T. Hyötyläinen, "Simple calibration procedure for comprehensive two-dimensional gas chromatography," *J. Chromatogr. A*, vol. 1200, no. 2, pp. 264–267, 2008.
- [63] A. M. Muscalu, E. J. Reiner, S. N. Liss, T. Chen, G. Ladwig, and D. Morse, "A routine accredited method for the analysis of polychlorinated biphenyls, organochlorine pesticides, chlorobenzenes and screening of other halogenated organics in soil, sediment and sludge by GC×GC- $\mu$ ECD," *Anal. Bioanal. Chem.*, vol. 401, no. 8, pp. 2403–2413, 2011.
- [64] M. Adahchour, J. Beens, R. Vreuls, and U. Brinkman, "Recent developments in comprehensive two-dimensional gas chromatography (GC×GC): II. modulation and detection," *TrAC-Trends Anal. Chem.*, vol. 25, no. 6, pp. 540–553, 2006.

- [65] J. T. Matos, R. M. Duarte, and A. C. Duarte, "Trends in data processing of comprehensive two-dimensional chromatography: state of the art," *J. Chromatogr. B*, vol. 910, pp. 31–45, 2012.
- [66] K. M. Pierce, J. C. Hoggard, R. E. Mohler, and R. E. Synovec, "Recent advancements in comprehensive two-dimensional separations with chemometrics," *J. Chromatogr. A*, vol. 1184, no. 1, pp. 341–352, 2008.
- [67] G. Vivó-Truyols, J. Torres-Lapasió, A. Van Nederkassel, Y. Vander Heyden, and D. Massart, "Automatic program for peak detection and deconvolution of multi-overlapped chromatographic signals: Part II: Peak model and deconvolution algorithms," *J. Chromatogr. A*, vol. 1096, no. 1, pp. 146–155, 2005.
- [68] P. G. Stevenson, M. Mnatsakanyan, G. Guiochon, and R. A. Shalliker, "Peak picking and the assessment of separation performance in two-dimensional high performance liquid chromatography," *Analyst*, vol. 135, no. 7, pp. 1541–1550, 2010.
- [69] S. E. Reichenbach, M. Ni, V. Kottapalli, and A. Visvanathan, "Information technologies for comprehensive two-dimensional gas chromatography," *Chemometr. Intell. Lab.*, vol. 71, no. 2, pp. 107–120, 2004.
- [70] K. M. Pierce, B. Kehimkar, L. C. Marney, J. C. Hoggard, and R. E. Synovec, "Review of chemometric analysis techniques for comprehensive two dimensional separations data," *J. Chromatogr. A*, vol. 1255, pp. 3–11, 2012.
- [71] H. M. McNair and J. M. Miller, *Basic gas chromatography*. John Wiley & Sons, 2011.
- [72] W. Youden, "Technique for testing accuracy of analytical data," *Anal. Chem.*, vol. 19, no. 12, pp. 946–950, 1947.
- [73] M. J. Cardone, P. J. Palermo, and L. B. Sybrandt, "Potential error in single-point-ratio calculations based on linear calibration curves with a significant intercept," *Anal. Chem.*, vol. 52, no. 8, pp. 1187–1191, 1980.
- [74] M. Cardone, "Detection and determination of error in analytical methodology. II: Correction for corrigible systematic error in the course of real sample analysis," *J. Assoc. Off. Anal. Chem.*, vol. 66, no. 5, pp. 1283–1294, 1983.
- [75] M. J. Cardone, "New technique in chemical assay calculations. 2. Correct solution of the model problem and related concepts," *Anal. Chem.*, vol. 58, no. 2, pp. 438–445, 1986.
- [76] K. Danzer and L. A. Currie, "Guidelines for calibration in analytical chemistry. part I. Fundamentals and single component calibration (IUPAC Recommendations 1998)," *Pure Appl. Chem.*, vol. 70, no. 4, pp. 993–1014, 1998.
- [77] K. S. Booksh and B. R. Kowalski, "Theory of analytical chemistry," *Anal. Chem.*, vol. 66, no. 15, pp. 782A–791A, 1994.

## Bibliography

---

- [78] P. Gemperline, *Practical guide to chemometrics*. CRC press, 2012.
- [79] J. S. Arey, R. K. Nelson, and C. M. Reddy, "Disentangling oil weathering using GC×GC. 1. Chromatogram analysis," *Environ. Sci. Technol.*, vol. 41, no. 16, pp. 5738–5746, 2007.
- [80] J. Gros, C. M. Reddy, C. Aeppli, R. K. Nelson, C. A. Carmichael, and J. S. Arey, "Resolving biodegradation patterns of persistent saturated hydrocarbons in weathered oil samples from the Deepwater Horizon disaster," *Environ. Sci. Technol.*, vol. 48, pp. 1628–1637, 2014.
- [81] S. E. Reichenbach, M. Ni, D. Zhang, and E. B. Ledford Jr, "Image background removal in comprehensive two-dimensional gas chromatography," *J. Chromatogr. A*, vol. 985, no. 1, pp. 47–56, 2003.
- [82] P. H. Eilers, "Parametric time warping," *Anal. Chem.*, vol. 76, no. 2, pp. 404–411, 2004.
- [83] J. Harynuk, A. Kwong, and P. Marriott, "Modulation-induced error in comprehensive two-dimensional gas chromatographic separations," *J. Chromatogr. A*, vol. 1200, no. 1, pp. 17–27, 2008.
- [84] I. Latha, S. E. Reichenbach, and Q. Tao, "Comparative analysis of peak-detection techniques for comprehensive two-dimensional chromatography," *J. Chromatogr. A*, vol. 1218, no. 38, pp. 6792–6798, 2011.
- [85] A. Paulina de la Mata, K. D. Nizio, and J. J. Harynuk, "Integration parameters and their effects on quantitative results with two-step peak summation quantitation in comprehensive two-dimensional gas chromatography," *J. Chromatogr. A*, vol. 1255, pp. 190–195, 2012.
- [86] R. C. Allen, M. G. John, S. C. Rutan, M. R. Filgueira, and P. W. Carr, "Effect of background correction on peak detection and quantification in online comprehensive two-dimensional liquid chromatography using diode array detection," *J. Chromatogr. A*, vol. 1254, pp. 51–61, 2012.
- [87] EU-Commission, "Commission decision ec 2002/657 of 12 August 2002 implementing council directive 96/23/ec concerning the performance of analytical methods and the interpretation of results," *Off. J. Eur. Communities L*, vol. 221, 2002.
- [88] R. A. Hites, E. Stemmler, B. Arbogast, W. Budde, M. Deinzer, R. Dougherty, J. Eichelberger, R. Foltz, and C. Grimm, "Interlaboratory comparison of methane electron capture negative ion mass spectra," *Anal. Chem.*, vol. 60, no. 8, pp. 781–787, 1988.
- [89] D. Barcelo, "Applications of gas chromatography—mass spectrometry in monitoring environmentally important compounds," *TrAC-Trends Anal. Chem.*, vol. 10, no. 10, pp. 323–329, 1991.

- [90] L. J. Schmidt and R. J. Hesselberg, "A mass spectroscopic method for analysis of AHH-inducing and other polychlorinated biphenyl congeners and selected pesticides in fish," *Arch. Environ. Contam. Toxicol.*, vol. 23, no. 1, pp. 37–44, 1992.
- [91] M. J. La Guardia, R. C. Hale, E. Harvey, and D. Chen, "Flame-retardants and other organohalogens detected in sewage sludge by electron capture negative ion mass spectrometry," *Environ. Sci. Technol.*, vol. 44, no. 12, pp. 4658–4664, 2010.
- [92] G. T. Tomy, G. A. Stern, D. C. Muir, A. T. Fisk, C. D. Cymbalisty, and J. B. Westmore, "Quantifying C<sub>10</sub>-C<sub>13</sub> polychloroalkanes in environmental samples by high-resolution gas chromatography/electron capture negative ion high-resolution mass spectrometry," *Anal. Chem.*, vol. 69, no. 14, pp. 2762–2771, 1997.
- [93] The mathworks, "Guide, matlab user's," 1998.
- [94] H. Parastar, J. R. Radović, M. Jalali-Heravi, S. Diez, J. M. Bayona, and R. Tauler, "Resolution and quantification of complex mixtures of polycyclic aromatic hydrocarbons in heavy fuel oil sample by means of GC×GC-TOFMS combined to multivariate curve resolution," *Anal. Chem.*, vol. 83, no. 24, pp. 9289–9297, 2011.
- [95] S. E. Reichenbach, P. W. Carr, D. R. Stoll, and Q. Tao, "Smart templates for peak pattern matching with comprehensive two-dimensional liquid chromatography," *J. Chromatogr. A*, vol. 1216, no. 16, pp. 3458–3466, 2009.
- [96] L. Cuadros-Rodriguez, L. Gámiz-Gracia, E. M. Almansa-López, and J. M. Bosque-Sendra, "Calibration in chemical measurement processes. II. A methodological approach," *TrAC-Trends Anal. Chem.*, vol. 20, no. 11, pp. 620–636, 2001.
- [97] K. S. Booksh and B. R. Kowalski, "Calibration method choice by comparison of model basis functions to the theoretical instrumental response function," *Anal. Chem. Acta*, vol. 348, no. 1, pp. 1–9, 1997.
- [98] A. C. Olivieri, N. M. Faber, J. Ferré, R. Boqué, J. H. Kalivas, and H. Mark, "Uncertainty estimation and figures of merit for multivariate calibration (IUPAC Technical Report)," *Pure Appl. Chem.*, vol. 78, no. 3, pp. 633–661, 2006.
- [99] K. Booksh, J. M. Henshaw, L. W. Burgess, and B. R. Kowalski, "A second-order standard addition method with application to calibration of a kinetics-spectroscopic sensor for quantitation of trichloroethylene," *J. Chemometr.*, vol. 9, no. 4, pp. 263–282, 1995.
- [100] J. C. Miller and J. N. Miller, "Basic statistical methods for analytical chemistry. part I. Statistics of repeated measurements. A review," *Analyst*, vol. 113, no. 9, pp. 1351–1356, 1988.
- [101] M. J. Cardone, "New technique in chemical assay calculations. 1. A survey of calculational practices on a model problem," *Anal. Chem.*, vol. 58, no. 2, pp. 433–438, 1986.

## Bibliography

---

- [102] M. J. Cardone, S. A. Willavize, and M. E. Lacy, "Method validation revisited: a chemometric approach," *Pharm. Res.*, vol. 7, no. 2, pp. 154–160, 1990.
- [103] R. C. Castells and M. A. Castillo, "Systematic errors: detection and correction by means of standard calibration, Youden calibration and standard additions method in conjunction with a method response model," *Anal. Chem. Acta*, vol. 423, no. 2, pp. 179–185, 2000.
- [104] A. D. Jorgensen, K. C. Picel, and V. C. Stamoudis, "Prediction of gas chromatography flame ionization detector response factors from molecular structures," *Anal. Chem.*, vol. 62, no. 7, pp. 683–689, 1990.
- [105] T. Holm, "Aspects of the mechanism of the flame ionization detector," *J. Chromatogr. A*, vol. 842, no. 1, pp. 221–227, 1999.
- [106] J. Lovelock, "The electron capture detector: Theory and practice," *J. Chromatogr. A*, vol. 99, pp. 3–12, 1974.
- [107] F. Allegrini and A. C. Olivieri, "Analytical figures of merit for partial least-squares coupled to residual multilinearization," *Anal. Chem.*, vol. 84, no. 24, pp. 10823–10830, 2012.
- [108] D. L. Massart, A. Dijkstra, and L. Kaufman, "Evaluation and optimization of laboratory methods and analytical procedures," *Elsevier*, 1978.
- [109] W. H. Kruskal and W. A. Wallis, "Use of ranks in one-criterion variance analysis," *J. Amer. Statist. Assoc.*, vol. 47, no. 260, pp. 583–621, 1952.
- [110] R. C. Dougherty, "Negative chemical ionization mass spectrometry," *Anal. Chem.*, vol. 53, no. 4, pp. 625A–636A, 1981.
- [111] P. Korytár, J. Parera, P. Leonards, J. De Boer, and U. Brinkman, "Quadrupole mass spectrometer operating in the electron-capture negative ion mode as detector for comprehensive two-dimensional gas chromatography," *J. Chromatogr. A*, vol. 1067, no. 1, pp. 255–264, 2005.
- [112] A. C. Olivieri, "Analytical advantages of multivariate data processing. One, two, three, infinity?," *Anal. Chem.*, vol. 80, no. 15, pp. 5713–5720, 2008.
- [113] E. Cequier, A. C. Ionas, A. Covaci, R. M. Marcé, G. Becher, and C. Thomsen, "Occurrence of a broad range of legacy and emerging flame retardants in indoor environments in Norway," *Environ. Sci. Technol.*, vol. 48, no. 12, pp. 6827–6835, 2014.
- [114] L. J. Carter, "Michigan's PBB incident: Chemical mix-up leads to disaster," *Science*, vol. 192, no. 4236, pp. 240–243, 1976.
- [115] K. Betts, "New flame retardants detected in indoor and outdoor environments," *Environ. Sci. Technol.*, vol. 42, no. 18, pp. 6778–6778, 2008.



- [116] E. Webster, D. Mackay, and F. Wania, "Evaluating environmental persistence," *Environ. Toxicol. Chem.*, vol. 17, no. 11, pp. 2148–2158, 1998.
- [117] A. Covaci, S. Harrad, M. A.-E. Abdallah, N. Ali, R. J. Law, D. Herzke, and C. A. de Wit, "Novel brominated flame retardants: a review of their analysis, environmental fate and behaviour," *Environ. Int.*, vol. 37, no. 2, pp. 532–556, 2011.
- [118] R. C. Hale, M. Alaei, J. B. Manchester-Neesvig, H. M. Stapleton, and M. G. Ikonou, "Polybrominated diphenyl ether flame retardants in the North American environment," *Environ. Int.*, vol. 29, no. 6, pp. 771–779, 2003.
- [119] A. Salamova and R. A. Hites, "Discontinued and alternative brominated flame retardants in the atmosphere and precipitation from the Great Lakes basin," *Environ. Sci. Technol.*, vol. 45, no. 20, pp. 8698–8706, 2011.
- [120] J. Gieroń, A. Grochowalski, and R. Chrzęszcz, "PBB levels in fish from the Baltic and North seas and in selected food products from Poland," *Chemosphere*, vol. 78, no. 10, pp. 1272–1278, 2010.
- [121] C. A. de Wit, M. Alaei, and D. C. Muir, "Levels and trends of brominated flame retardants in the Arctic," *Chemosphere*, vol. 64, no. 2, pp. 209–233, 2006.
- [122] R. J. Law, C. R. Allchin, J. De Boer, A. Covaci, D. Herzke, P. Lepom, S. Morris, J. Tronczynski, and C. A. De Wit, "Levels and trends of brominated flame retardants in the European environment," *Chemosphere*, vol. 64, no. 2, pp. 187–208, 2006.
- [123] M. Kohler, M. Zennegg, C. Bogdal, A. C. Gerecke, P. Schmid, N. V. Heeb, M. Sturm, H. Vonmont, H.-P. E. Kohler, and W. Giger, "Temporal trends, congener patterns, and sources of octa-, nona-, and decabromodiphenyl ethers (PBDE) and hexabromocyclododecanes (HBCD) in Swiss lake sediments," *Environ. Sci. Technol.*, vol. 42, no. 17, pp. 6378–6384, 2008.
- [124] A. C. Gerecke, P. Schmid, C. Bogdal, M. Kohler, M. Zennegg, and N. V. Heeb, "Brominated flame retardants–endocrine-disrupting chemicals in the Swiss environment," *CHIMIA*, vol. 62, no. 5, pp. 352–357, 2008.
- [125] C. Bogdal, P. Schmid, M. Kohler, C. E. Müller, S. Iozza, T. D. Bucheli, M. Scheringer, and K. Hungerbühler, "Sediment record and atmospheric deposition of brominated flame retardants and organochlorine compounds in Lake Thun, Switzerland: lessons from the past and evaluation of the present," *Environ. Sci. Technol.*, vol. 42, no. 18, pp. 6817–6822, 2008.
- [126] M. Alaei, P. Arias, A. Sjödin, and Å. Bergman, "An overview of commercially used brominated flame retardants, their applications, their use patterns in different countries/regions and possible modes of release," *Environ. Int.*, vol. 29, no. 6, pp. 683–689, 2003.

## Bibliography

---

- [127] Å. Bergman, A. Rydén, R. J. Law, J. de Boer, A. Covaci, M. Alaee, L. Birnbaum, M. Petreas, M. Rose, and S. Sakai, "A novel abbreviation standard for organobromine, organochlorine and organophosphorus flame retardants and some characteristics of the chemicals," *Environ. Int.*, vol. 49, pp. 57–82, 2012.
- [128] G. Zhao, H. Zhou, X. Liu, K. Li, P. Zhang, W. Wen, and Y. Yu, "PHAHs in 14 principal river sediments from Hai River basin, China," *Sci. Total Environ.*, vol. 427, pp. 139–145, 2012.
- [129] P. Morris, J. Quensen, J. Tiedje, and S. Boyd, "Reductive debromination of the commercial polybrominated biphenyl mixture Firemaster BP6 by anaerobic microorganisms from sediments.," *Appl. Environ. Microb.*, vol. 58, no. 10, pp. 3249–3256, 1992.
- [130] D. L. Bedard and H. M. Van Dort, "Complete reductive dehalogenation of brominated biphenyls by anaerobic microorganisms in sediment," *Appl. Environ. Microb.*, vol. 64, no. 3, pp. 940–947, 1998.
- [131] D. L. Bedard, H. Van Dort, and K. A. Deweerdt, "Brominated biphenyls prime extensive microbial reductive dehalogenation of Aroclor 1260 in Housatonic river sediment," *Appl. Environ. Microb.*, vol. 64, no. 5, pp. 1786–1795, 1998.
- [132] Y. Yamaguchi, "Basic researches on environmental behavior of organobrominated flame retardants," Master's thesis, 1984.
- [133] Y. Yamaguchi, M. Kawano, R. Tatsukawa, and S. Moriwaki, "Hexabromobenzene and its debrominated compounds in human adipose tissues of Japan," *Chemosphere*, vol. 17, no. 4, pp. 703–707, 1988.
- [134] Y. Yamaguchi, M. Kawano, and R. Tatsukawa, "Tissue distribution and excretion of hexabromobenzene and its debrominated metabolites in the rat," *Arch. Environ. Contam. Toxicol.*, vol. 17, no. 6, pp. 807–812, 1988.
- [135] I. Watanabe, T. Kashimoto, and R. Tatsukawa, "Hexabromobenzene and its debrominated compounds in river and estuary sediments in Japan," *Bull. Environ. Contam. Tox.*, vol. 36, no. 1, pp. 778–784, 1986.
- [136] S. Dueri, J. Castro-Jiménez, and J.-M. Zaldívar, "Modelling the influence of thermal stratification and complete mixing on the distribution and fluxes of polychlorinated biphenyls in the water column of Ispra Bay (Lake Maggiore)," *Chemosphere*, vol. 75, no. 9, pp. 1266–1272, 2009.
- [137] M. Gorga, E. Martínez, A. Ginebreda, E. Eljarrat, and D. Barceló, "Determination of PBDEs, HBB, PBEB, DBDPE, HBCD, TBBPA and related compounds in sewage sludge from Catalonia (Spain)," *Sci. Total Environ.*, vol. 444, pp. 51–59, 2013.
- [138] P. Guerra, M. Alaee, B. Jiménez, G. Pacepavicius, C. Marvin, G. MacInnis, E. Eljarrat, D. Barceló, L. Champoux, and K. Fernie, "Emerging and historical brominated flame retardants in peregrine falcon (*Falco peregrinus*) eggs from Canada and Spain," *Environ. Int.*, vol. 40, pp. 179–186, 2012.

- [139] S. Newton, U. Sellström, and C. A. de Wit, "Emerging flame retardants, PBDEs, and HBCDDs in indoor and outdoor media in Stockholm, Sweden," *Environ. Sci. Technol.*, vol. 49, no. 5, pp. 2912–2920, 2015.
- [140] E. Jurado, J.-M. Zaldívar, D. Marinov, and J. Dachs, "Fate of persistent organic pollutants in the water column: Does turbulent mixing matter?," *Mar. Pollut. Bull.*, vol. 54, no. 4, pp. 441–451, 2007.
- [141] C. S. Kwan, H. Takada, K. Mizukawa, M. Torii, T. Koike, R. Yamashita, M. Saha, and E. C. Santiago, "PBDEs in leachates from municipal solid waste dumping sites in tropical Asian countries: phase distribution and debromination," *Environ. Sci. Pollut. Res.*, vol. 20, no. 6, pp. 4188–4204, 2013.
- [142] V. Lenters, C. Thomsen, L. A. Smit, B. A. Jönsson, H. S. Pedersen, J. K. Ludwicki, V. Zvezdai, A. H. Piersma, G. Toft, and J. P. Bonde, "Serum concentrations of polybrominated diphenyl ethers (PBDEs) and a polybrominated biphenyl (PBB) in men from Greenland, Poland and Ukraine," *Environ. Int.*, vol. 61, pp. 8–16, 2013.
- [143] M. Tian, S.-J. Chen, J. Wang, X.-B. Zheng, X.-J. Luo, and B.-X. Mai, "Brominated flame retardants in the atmosphere of e-waste and rural sites in southern China: Seasonal variation, temperature dependence, and gas-particle partitioning," *Environ. Sci. Technol.*, vol. 45, no. 20, pp. 8819–8825, 2011.
- [144] E. Barón, E. Eljarrat, and D. Barceló, "Gas chromatography/tandem mass spectrometry method for the simultaneous analysis of 19 brominated compounds in environmental and biological samples," *Anal. Bioanal. Chem.*, vol. 406, no. 29, pp. 7667–7676, 2014.
- [145] A. Papachlimitzou, J. L. Barber, S. Losada, P. Bersuder, and R. J. Law, "A review of the analysis of novel brominated flame retardants," *J. Chromatogr. A*, vol. 1219, pp. 15–28, 2012.
- [146] P. Haglund, K. Löfstrand, A. Malmvärn, A. Bignert, and L. Asplund, "Temporal variations of polybrominated dibenzo-p-dioxin and methoxylated diphenyl ether concentrations in fish revealing large differences in exposure and metabolic stability," *Environ. Sci. Technol.*, vol. 44, no. 7, pp. 2466–2473, 2010.
- [147] K. Kalachova, J. Pulkrabova, T. Cajka, L. Drabova, and J. Hajslova, "Implementation of comprehensive two-dimensional gas chromatography–time-of-flight mass spectrometry for the simultaneous determination of halogenated contaminants and polycyclic aromatic hydrocarbons in fish," *Anal. Bioanal. Chem.*, vol. 403, no. 10, pp. 2813–2824, 2012.
- [148] K. R. Robrock, P. Korytár, and L. Alvarez-Cohen, "Pathways for the anaerobic microbial debromination of polybrominated diphenyl ethers," *Environ. Sci. Technol.*, vol. 42, no. 8, pp. 2845–2852, 2008.

## Bibliography

---

- [149] P. Korytár, P. Leonards, J. De Boer, and U. Brinkman, "Group separation of organohalogenated compounds by means of comprehensive two-dimensional gas chromatography," *J. Chromatogr. A*, vol. 1086, no. 1, pp. 29–44, 2005.
- [150] D. Nabi, J. Gros, P. Dimitriou-Christidis, and J. S. Arey, "Mapping Environmental Partitioning Properties of Nonpolar Complex Mixtures by Use of GC×GC," *Environ. Sci. Technol.*, vol. 48, no. 12, pp. 6814–6826, 2014.
- [151] A. Wüest, F. S. Anselmetti, J. S. Arey, B. W. Ibelings, J.-L. Loizeau, T. Vennemann, and U. Lemmin, "Into the abyss of Lake Geneva: the elemo interdisciplinary field investigation using the MIR submersibles," *Aquat. Sci.*, vol. 76, no. 1, pp. 1–6, 2014.
- [152] F. Bonvin, R. Rutler, N. Chèvre, J. Halder, and T. Kohn, "Spatial and temporal presence of a wastewater-derived micropollutant plume in Lake Geneva," *Environ. Sci. Technol.*, vol. 45, no. 11, pp. 4702–4709, 2011.
- [153] CIPEL, "*Commission internationale pour la protection des eaux du Léman.*" <http://www.cipel.org>.
- [154] M. Hardy, "The toxicology of the three commercial polybrominated diphenyl oxide (ether) flame retardants," *Chemosphere*, vol. 46, no. 5, pp. 757–777, 2002.
- [155] M. Zennegg, M. Kohler, A. C. Gerecke, and P. Schmid, "Polybrominated diphenyl ethers in whitefish from Swiss lakes and farmed rainbow trout," *Chemosphere*, vol. 51, no. 7, pp. 545–553, 2003.
- [156] B. V. Pepich, B. Prakash, M. M. Domino, T. A. Dattilio, D. J. Munch, and E. K. Price, "Development of US EPA method 527 for the analysis of selected pesticides and flame retardants in the UCMR survey," *Environ. Sci. Technol.*, vol. 39, no. 13, pp. 4996–5004, 2005.
- [157] F. Stuer-Lauridsen, "Review of passive accumulation devices for monitoring organic micropollutants in the aquatic environment," *Environ. Pollut.*, vol. 136, no. 3, pp. 503–524, 2005.
- [158] T. Górecki and J. Namieśnik, "Passive sampling," *TrAC-Trends Anal. Chem.*, vol. 21, no. 4, pp. 276–291, 2002.
- [159] P. Beneš and E. Steinnes, "*In situ* dialysis for the determination of the state of trace elements in natural waters," *Water Res.*, vol. 8, no. 11, pp. 947–953, 1974.
- [160] J. Namieśnik, B. Zabiegała, A. Kot-Wasik, M. Partyka, and A. Wasik, "Passive sampling and/or extraction techniques in environmental analysis: a review," *Anal. Bioanal. Chem.*, vol. 381, no. 2, pp. 279–301, 2005.
- [161] J. N. Huckins, J. D. Petty, J. A. Lebo, F. V. Almeida, K. Booij, D. A. Alvarez, W. L. Cranor, R. C. Clark, and B. B. Mogensen, "Development of the permeability/performance reference

- compound approach for in situ calibration of semipermeable membrane devices," *Environ. Sci. Technol.*, vol. 36, no. 1, pp. 85–91, 2002.
- [162] K. Booij, F. Smedes, and E. M. van Weerlee, "Spiking of performance reference compounds in low density polyethylene and silicone passive water samplers," *Chemosphere*, vol. 46, no. 8, pp. 1157–1161, 2002.
- [163] B. Vrana, G. Mills, R. Greenwood, J. Knutsson, K. Svensson, and G. Morrison, "Performance optimisation of a passive sampler for monitoring hydrophobic organic pollutants in water," *J. Environ. Monitor.*, vol. 7, no. 6, pp. 612–620, 2005.
- [164] T. P. Rusina, F. Smedes, J. Klanova, K. Booij, and I. Holoubek, "Polymer selection for passive sampling: A comparison of critical properties," *Chemosphere*, vol. 68, no. 7, pp. 1344–1351, 2007.
- [165] P. Mayer, J. Tolls, J. L. Hermens, and D. Mackay, "Peer reviewed: equilibrium sampling devices," *Environ. Sci. Technol.*, vol. 37, no. 9, pp. 184A–191A, 2003.
- [166] P. Mayer, U. Karlson, P. S. Christensen, A. R. Johnsen, and S. Trapp, "Quantifying the effect of medium composition on the diffusive mass transfer of hydrophobic organic chemicals through unstirred boundary layers," *Environ. Sci. Technol.*, vol. 39, no. 16, pp. 6123–6129, 2005.
- [167] J.-H. Kwon, T. Wuethrich, P. Mayer, and B. I. Escher, "Dynamic permeation method to determine partition coefficients of highly hydrophobic chemicals between poly (dimethylsiloxane) and water," *Anal. Chem.*, vol. 79, no. 17, pp. 6816–6822, 2007.
- [168] U.S. Environmental Protection Agency, Office of Pollution Prevention and Toxics: Washington, DC, "Exposure assessment tools and models, estimation program interface (EPI) Suite, Version 3.12;," <http://www.epa.gov/oppt/exposure/pubs/episuitedl.htm>, 2005.
- [169] W. Meylan, R. Boethling, D. Aronson, P. Howard, and J. Tunkel, "Chemical structure-based predictive model for methanogenic anaerobic biodegradation potential," *Environ. Toxicol. Chem.*, vol. 26, no. 9, pp. 1785–1792, 2007.
- [170] T. M. Kolic, L. Shen, K. MacPherson, L. Fayez, T. Gobran, P. A. Helm, C. H. Marvin, G. Arsenault, and E. J. Reiner, "The analysis of halogenated flame retardants by GC-HRMS in environmental samples," *J. Chromatogr. Sci.*, vol. 47, no. 1, pp. 83–91, 2009.
- [171] E. Hoffmann, *Mass spectrometry*. Wiley Online Library, 1996.
- [172] D. Bouffard and U. Lemmin, "Kelvin waves in Lake Geneva," *J. Great Lakes Res.*, vol. 39, no. 4, pp. 637–645, 2013.
- [173] J. Yen, W. Liao, W. Chen, and Y. Wang, "Interaction of polybrominated diphenyl ethers (PBDEs) with anaerobic mixed bacterial cultures isolated from river sediment," *J. Haz. Mat.*, vol. 165, no. 1, pp. 518–524, 2009.

## Bibliography

---

- [174] J. D. Raff and R. A. Hites, "Deposition versus photochemical removal of PBDEs from Lake Superior air," *Environ. Sci. Technol.*, vol. 41, no. 19, pp. 6725–6731, 2007.
- [175] US National Library of Medicine, "*Toxicology Data Network.*" Hazardous Substances Data Bank, Website: <http://toxnet.nlm.nih.gov>.
- [176] A. M. Razmi, D. A. Barry, U. Lemmin, F. Bonvin, T. Kohn, and R. Bakhtyar, "Direct effects of dominant winds on residence and travel times in the wide and open lacustrine embayment: Vidy Bay (Lake Geneva, Switzerland)," *Aquat. Sci.*, vol. 76, no. 1, pp. 59–71, 2014.
- [177] J. Poté, L. Haller, J.-L. Loizeau, A. G. Bravo, V. Sastre, and W. Wildi, "Effects of a sewage treatment plant outlet pipe extension on the distribution of contaminants in the sediments of the Bay of Vidy, Lake Geneva, Switzerland," *Bioresour. Technol.*, vol. 99, no. 15, pp. 7122–7131, 2008.
- [178] H. P. H. Arp, T. Møskeland, P. L. Andersson, and J. R. Nyholm, "Presence and partitioning properties of the flame retardants pentabromotoluene, pentabromoethylbenzene and hexabromobenzene near suspected source zones in Norway," *J. Environ. Monitor.*, vol. 13, no. 3, pp. 505–513, 2011.
- [179] P. Guerra, E. Eljarrat, and D. Barceló, "Analysis and occurrence of emerging brominated flame retardants in the Llobregat River basin," *J. Hydrol.*, vol. 383, no. 1, pp. 39–43, 2010.
- [180] S. L. Klosterhaus, H. M. Stapleton, M. J. La Guardia, and D. J. Greig, "Brominated and chlorinated flame retardants in San Francisco Bay sediments and wildlife," *Environ. Int.*, vol. 47, pp. 56–65, 2012.
- [181] F. Thevenon, N. D. Graham, A. Herbez, W. Wildi, and J. Poté, "Spatio-temporal distribution of organic and inorganic pollutants from Lake Geneva (Switzerland) reveals strong interacting effects of sewage treatment plant and eutrophication on microbial abundance," *Chemosphere*, vol. 84, no. 5, pp. 609–617, 2011.
- [182] S. D. Shaw and K. Kannan, "Polybrominated diphenyl ethers in marine ecosystems of the American continents: foresight from current knowledge," *Rev. Environ. Health*, vol. 24, no. 3, pp. 157–230, 2009.
- [183] "Preparation method of 4-bromo-4-iodobiphenyl," July 17 2013. CN Patent App. CN 201,310,139,730.
- [184] A. Nonn, "Process for bromination of biphenyl with BrCl," Apr. 21 1992. US Patent 5,107,044.
- [185] H. Swaine, "Agents rodenticides," Sept. 9 1992. EP Patent 0,147,052.
- [186] R. Radhakrishnan, M. Cyr, and S. Pyles, "Method for synthesizing pifrenidone," Aug. 27 2013. US Patent 8,519,140.

- [187] "Method for preparing 1,3,5-trimethoxybenzene," May 30 2012. CN Patent App. CN 201,010,555,746.
- [188] "Organic conjugated polymer film, its synthetic method and its application," May 15 2013. CN Patent 102,492,117.
- [189] R. Perry, "Preparation of poly(benz(ox, imid, thi)azole) polymers," Jan. 13 1993. EP Patent App. EP19,920,111,331.
- [190] F. Wania, "Assessing the potential of persistent organic chemicals for long-range transport and accumulation in polar regions," *Environ. Sci. Technol.*, vol. 37, no. 7, pp. 1344–1351, 2003.
- [191] C. A. de Wit, "An overview of brominated flame retardants in the environment," *Chemosphere*, vol. 46, no. 5, pp. 583–624, 2002.
- [192] A. Bignert, M. Olsson, W. Persson, S. Jensen, S. Zakrisson, K. Litzén, U. Eriksson, L. Häggberg, and T. Alsberg, "Temporal trends of organochlorines in Northern Europe, 1967–1995. Relation to global fractionation, leakage from sediments and international measures," *Environ. Pollut.*, vol. 99, no. 2, pp. 177–198, 1998.
- [193] C. A. de Wit, D. Herzke, and K. Vorkamp, "Brominated flame retardants in the Arctic environment—trends and new candidates," *Sci. Total Environ.*, vol. 408, no. 15, pp. 2885–2918, 2010.
- [194] F. A. Gobas, W. de Wolf, L. P. Burkhard, E. Verbruggen, and K. Plotzke, "Revisiting bioaccumulation criteria for POPs and PBT assessments," *Integr. Environ. Assess. Manage.*, vol. 5, no. 4, pp. 624–637, 2009.
- [195] G. Zhao, Z. Wang, H. Zhou, and Q. Zhao, "Burdens of PBBs, PBDEs, and PCBs in tissues of the cancer patients in the e-waste disassembly sites in Zhejiang, China," *Sci. Total Environ.*, vol. 407, no. 17, pp. 4831–4837, 2009.
- [196] K. Krysiak-Baltyn, J. Toppari, N. Skakkebaek, T. S. Jensen, H. Virtanen, K.-W. Schramm, H. Shen, T. Vartiainen, H. Kiviranta, and O. Taboureau, "Country-specific chemical signatures of persistent environmental compounds in breast milk," *Int. J. Androl.*, vol. 33, no. 2, pp. 270–278, 2010.
- [197] J. A. Arnot and F. A. Gobas, "A review of bioconcentration factor (BCF) and bioaccumulation factor (BAF) assessments for organic chemicals in aquatic organisms," *Environ. Rev.*, vol. 14, no. 4, pp. 257–297, 2006.
- [198] J.-P. Wu, Y.-T. Guan, Y. Zhang, X.-J. Luo, H. Zhi, S.-J. Chen, and B.-X. Mai, "Several current-use, non-pbde brominated flame retardants are highly bioaccumulative: evidence from field determined bioaccumulation factors," *Environ. Int.*, vol. 37, no. 1, pp. 210–215, 2011.

## Bibliography

---

- [199] J.-P. Wu, Y.-T. Guan, Y. Zhang, X.-J. Luo, H. Zhi, S.-J. Chen, and B.-X. Mai, "Trophodynamics of hexabromocyclododecanes and several other non-PBDE brominated flame retardants in a freshwater food web," *Environ. Sci. Technol.*, vol. 44, no. 14, pp. 5490–5495, 2010.
- [200] J. Verreault, W. A. Gebbink, L. T. Gauthier, G. W. Gabrielsen, and R. J. Letcher, "Brominated flame retardants in glaucous gulls from the Norwegian Arctic: more than just an issue of polybrominated diphenyl ethers," *Environ. Sci. Technol.*, vol. 41, no. 14, pp. 4925–4931, 2007.
- [201] L. T. Gauthier, C. E. Hebert, D. C. Weseloh, and R. J. Letcher, "Current-use flame retardants in the eggs of herring gulls (*Larus argentatus*) from the Laurentian Great Lakes," *Environ. Sci. Technol.*, vol. 41, no. 13, pp. 4561–4567, 2007.
- [202] J.-P. W. Desforges, N. J. Dangerfield, P. Shaw, and P. S. Ross, "Heightened biological uptake of PBDEs relative to PCBs near source revealed by sediment and plankton profiles along a coastal transect in British Columbia," *Environ. Sci. Technol.*, vol. 48, no. 12, pp. 6981–6988, 2014.
- [203] M. Pena-Abaurrea, A. Covaci, and L. Ramos, "Comprehensive two-dimensional gas chromatography–time-of-flight mass spectrometry for the identification of organobrominated compounds in bluefin tuna," *J. Chromatogr. A*, vol. 1218, no. 39, pp. 6995–7002, 2011.
- [204] L. Jacobs, S. Chou, and J. Tiedje, "Field concentrations and persistence of polybrominated biphenyls in soils and solubility of PBB in natural waters," *Environ. Health Persp.*, vol. 23, p. 1, 1978.
- [205] J. L. Hesse and R. A. Powers, "Polybrominated biphenyl (PBB) contamination of the Pine River, Gratiot, and Midland Counties, Michigan," *Environ. Health Persp.*, vol. 23, p. 19, 1978.
- [206] D.-H. Lim and C. M. Lastoskie, "A dynamic multimedia environmental and bioaccumulation model for brominated flame retardants in Lake Huron and Lake Erie, USA," *Environ. Toxicol. Chem.*, vol. 30, no. 5, pp. 1018–1025, 2011.
- [207] J. B. Manchester-Neesvig, K. Valters, and W. C. Sonzogni, "Comparison of polybrominated diphenyl ethers (PBDEs) and polychlorinated biphenyls (PCBs) in Lake Michigan salmonids," *Environ. Sci. Technol.*, vol. 35, no. 6, pp. 1072–1077, 2001.
- [208] A. Sjödin, L.-Y. Wong, R. S. Jones, A. Park, Y. Zhang, C. Hodge, E. DiPietro, C. McClure, W. Turner, and L. L. Needham, "Serum concentrations of polybrominated diphenyl ethers (PBDEs) and polybrominated biphenyl (PBB) in the United States population: 2003–2004," *Environ. Sci. Technol.*, vol. 42, no. 4, pp. 1377–1384, 2008.



- [209] R. J. Law, M. Alaei, C. R. Allchin, J. P. Boon, M. Lebeuf, P. Lepom, and G. A. Stern, "Levels and trends of polybrominated diphenylethers and other brominated flame retardants in wildlife," *Environ. Int.*, vol. 29, no. 6, pp. 757–770, 2003.
- [210] J. A. Szymańska, "Hepatotoxicity of brominated benzenes: relationship between chemical structure and hepatotoxic effects in acute intoxication of mice," *Arch. Toxicol.*, vol. 72, no. 2, pp. 97–103, 1997.
- [211] J. Szymańska, E. Bruchajzer, S. Sporny, and J. Piotrowski, "Changes in selected indicators of liver impairment after repeated administration of mono- and polybromobenzenes in mice," *B. Environ. Contam. Tox.*, vol. 61, no. 1, pp. 22–30, 1998.
- [212] T. Damstra, W. Jurgelski Jr, H. S. Posner, V. B. Vouk, N. J. Bernheim, J. Guthrie, M. Luster, and H. L. Falk, "Toxicity of polybrominated biphenyls (PBBs) in Domestic and laboratory animals," *Environ. Health Persp.*, vol. 44, p. 175, 1982.
- [213] S. Safe and O. Hutzinger, "Polychlorinated biphenyls (PCBs) and polybrominated biphenyls (PBBs): biochemistry, toxicology, and mechanism of action," *Crit. Rev. Toxicol.*, vol. 13, no. 4, pp. 319–395, 1984.
- [214] C. Zhu, L. Kong, H. Hong, Q. Huang, and L. Wang, "Acute toxicity of substituted biphenyls to daphnia magna and quantitative structure-activity relationship study," *Toxicol. Environ. Chem.*, vol. 68, no. 3-4, pp. 267–273, 1999.
- [215] J. Cristale, A. Katsoyiannis, A. J. Sweetman, K. C. Jones, and S. Lacorte, "Occurrence and risk assessment of organophosphorus and brominated flame retardants in the River Aire (UK)," *Environ. Pollut.*, vol. 179, pp. 194–200, 2013.
- [216] S. Yalkowsky and R. Dannenfelser, "AqueSol database of aqueous solubility." College of Pharmacy, University of Arizona, Tucson, AZ, 1992.
- [217] W. Doucette and A. Andren, "Estimation of octanol/water partition coefficients: Evaluation of six methods for highly hydrophobic aromatic hydrocarbons," *Chemosphere*, vol. 17, no. 2, pp. 345–359, 1988.
- [218] E. Braekevelt, S. A. Tittlemier, and G. T. Tomy, "Direct measurement of octanol–water partition coefficients of some environmentally relevant brominated diphenyl ether congeners," *Chemosphere*, vol. 51, no. 7, pp. 563–567, 2003.
- [219] K. Booij, H. E. Hofmans, C. V. Fischer, and E. M. Van Weerlee, "Temperature-dependent uptake rates of nonpolar organic compounds by semipermeable membrane devices and low-density polyethylene membranes," *Environ. Sci. Technol.*, vol. 37, no. 2, pp. 361–366, 2003.
- [220] M. M. Perron, R. M. Burgess, E. M. Suuberg, M. G. Cantwell, and K. G. Pennell, "Performance of passive samplers for monitoring estuarine water column concentrations: 2. Emerging contaminants," *Environ. Toxicol. Chem.*, vol. 32, no. 10, pp. 2190–2196, 2013.

## Bibliography

---

- [221] T. Vermeire, D. Jager, B. Bussian, J. Devillers, K. Den Haan, B. Hansen, I. Lundberg, H. Niessen, S. Robertson, H. Tyle, *et al.*, "European union system for the evaluation of substances (euses). principles and structure," *Chemosphere*, vol. 34, no. 8, pp. 1823–1836, 1997.
- [222] "REACH - Registration, Evaluation, Authorisation and Restriction of Chemicals, <http://ec.europa.eu/enterprise/sectors/chemicals/reach>."
- [223] Toxicology data network, "Pentachlorothiophenol," March 2012.
- [224] H. W. Engels, *Ullmann's Encyclopedia of Industrial Chemistry*, vol. 4 of *Rubber, Chemicals and Additives*. John Wiley & Sons, 7th ed ed., 2008.
- [225] R. F. Dietrich and W. A. Gay, "Process for producing pentachloronitrobenzene," June 12 1984. US Patent 4,454,362.
- [226] L. P. Cornils B, *Ullmann's Encyclopedia of Industrial Chemistry*, vol. 5 of *Dicarboxylic Acids, Aliphatic*. John Wiley & Sons, 7th ed ed., 2008.
- [227] P. Mosier-Boss and S. Lieberman, "Surface-enhanced raman spectroscopy substrate composed of chemically modified gold colloid particles immobilized on magnetic microparticles," *Anal. Chem.*, vol. 77, no. 4, pp. 1031–1037, 2005.
- [228] T. Benz, H. Hagenmaier, C. Lindig, and J. She, "Occurrence of the sulphur analogue of octachlorodibenzo-p-dioxin in the environment and investigations on its potential source," *Anal. Bioanal. Chem.*, vol. 344, no. 6, pp. 286–291, 1992.
- [229] R. Mora Torres, C. Grosset, R. Steiman, J. Alary, and J. Fourier, "Liquid chromatography study of degradation and metabolism of pentachloronitrobenzene by four soil micromycetes," *Chemosphere*, vol. 33, no. 4, pp. 683–692, 1996.
- [230] L. Mayring, G. Renner, and H. Prigge, "Sulphur-containing metabolites of the fungicides pentachloronitrobenzene (PCNB) and hexachlorobenzene (HCB) II. Mass spectra," *Chemosphere*, vol. 13, no. 7, pp. 731–737, 1984.
- [231] G. Renner and C. Hopfer, "Metabolic studies on pentachloronitrobenzene (PCNB) in cress," *Chemosphere*, vol. 12, no. 7, pp. 967–970, 1983.
- [232] G. Renner and G. Ruckdeschel, "Effects of pentachloronitrobenzene and some of its known and possible metabolites on fungi," *Appl. Environ. Microb.*, vol. 46, no. 3, pp. 765–768, 1983.
- [233] D. G. Rusness and G. L. Lamoureux, "Pentachloronitrobenzene metabolism in peanut. 2. Characterization of chloroform-soluble metabolites produced in vivo," *J. Agr. Food Chem.*, vol. 28, no. 6, pp. 1070–1077, 1980.
- [234] N. B. Murthy and D. D. Kaufman, "Degradation of pentachloronitrobenzene (PCNB) in anaerobic soils," *J. Agr. Food Chem.*, vol. 26, no. 5, pp. 1151–1156, 1978.

- [235] J. Betts, S. P. James, and W. Thorpe, "The metabolism of pentachloronitrobenzene and 2,3,4,6-tetrachloronitrobenzene and the formation of mercapturic acids in the rabbit," *Biochem. J.*, vol. 61, no. 4, p. 611, 1955.
- [236] C. den Besten, M. M. Bennik, M. van Iersel, M. A. Peters, C. Teunis, and P. J. van Bladeren, "Comparison of the urinary metabolite profiles of hexachlorobenzene and pentachlorobenzene in the rat," *Chem-Biol. Interact.*, vol. 90, no. 2, pp. 121–137, 1994.
- [237] W. Müller, I. Scheunert, K. Rozman, W. Kögel, D. Freitag, E. Richter, F. Coulston, and F. Korte, "Comparative metabolism of hexachlorobenzene and pentachloronitrobenzene in plants, rats, and rhesus monkeys," *Ecotox. Environ. Safe.*, vol. 2, no. 3, pp. 437–445, 1978.
- [238] M. Rizzardini and A. G. Smith, "Sex differences in the metabolism of hexachlorobenzene by rats and the development of porphyria in females," *Biochem. Pharmacol.*, vol. 31, no. 22, pp. 3543–3548, 1982.
- [239] I. Bauer, S. Weigelt, and W. Ernst, "Biotransformation of hexachlorobenzene in the blue mussel (*Mytilus edulis*)," *Chemosphere*, vol. 19, no. 10, pp. 1701–1707, 1989.
- [240] D. Okutman Tas and S. G. Pavlostathis, "Microbial reductive transformation of pentachloronitrobenzene under methanogenic conditions," *Environ. Sci. Technol.*, vol. 39, no. 21, pp. 8264–8272, 2005.
- [241] D. O. Tas and S. G. Pavlostathis, "Occurrence, toxicity, and biotransformation of pentachloronitrobenzene and chloroanilines," *Crit. Rev. Env. Sci. Tec.*, vol. 44, no. 5, pp. 473–518, 2014.
- [242] J. To-Figueras, C. Barrot, M. Sala, R. Otero, M. Silva, M. D. Ozalla, C. Herrero, J. Corbella, J. Grimalt, and J. Sunyer, "Excretion of hexachlorobenzene and metabolites in feces in a highly exposed human population.," *Environ. Health Persp.*, vol. 108, no. 7, p. 595, 2000.
- [243] P. H. Howard, *Handbook of Environmental Fate and Exposure Data: For Organic Chemicals, Volume III Pesticides*, vol. 3. CRC press, 1991.
- [244] Y. Fushiwaki, N. Tase, A. Saeki, and K. Urano, "Pollution by the fungicide pentachloronitrobenzene in an intensive farming area in Japan," *Sci. Total Environ.*, vol. 92, pp. 55–67, 1990.
- [245] O. Wurl and J. P. Obbard, "Chlorinated pesticides and pcbs in the sea-surface microlayer and seawater samples of singapore," *Mar. Pollut. Bull.*, vol. 50, no. 11, pp. 1233–1243, 2005.
- [246] J. To-Figueras, M. Sala, R. Otero, C. Barrot, M. Santiago-Silva, M. Rodamilans, C. Herrero, J. Grimalt, and J. Sunyer, "Metabolism of hexachlorobenzene in humans: association between serum levels and urinary metabolites in a highly exposed population.," *Environ. Health Persp.*, vol. 105, no. 1, p. 78, 1997.

## Bibliography

---

- [247] F. Khan, D. Prakash, and R. Jain, "Development of an HPLC method for determination of pentachloronitrobenzene, hexachlorobenzene and their possible metabolites," *BMC Chem. Biol.*, vol. 11, no. 1, p. 2, 2011.
- [248] D. Carrizo, J. O. Grimalt, N. Ribas-Fito, M. Torrent, and J. Sunyer, "Pentachlorobenzene, hexachlorobenzene, and pentachlorophenol in children's serum from industrial and rural populations after restricted use," *Ecotox. Environ. Safe.*, vol. 71, no. 1, pp. 260–266, 2008.
- [249] P. E. Hagen and M. P. Walls, "The stockholm convention on persistent organic pollutants," *Natural Resources & Environment*, vol. 19, no. 4, pp. 49–52, 2005.
- [250] S. Iozza, J. Hüttig, M. Reth, Z. Zencak, and M. Oehme, "Analysis of chlorinated paraffins in different biological and non-biological matrices—an overview," *Organohalog. Compd.*, vol. 68, pp. 2404–2407, 2006.
- [251] P. Korytár, J. Parera, P. Leonards, J. De Boer, and U. Brinkman, "Quadrupole mass spectrometer operating in the electron-capture negative ion mode as detector for comprehensive two-dimensional gas chromatography," *J. Chromatogr. A*, vol. 1067, no. 1, pp. 255–264, 2005.
- [252] W. Yang, Z.-Q. Yu, L. Xiang-Fan, F. Jia-Liang, Z. Dong-Ping, R. Guo-Fa, S. Guo-Ying, and F. Jia-Mo, "Qualitative analysis of some emerging halogenous pollutions in fish sample by comprehensive two-dimensional gas chromatography/time-of-flight mass spectrometry," *Chinese J. Anal. Chem.*, vol. 40, no. 8, pp. 1187–1193, 2012.
- [253] M.-c. He, Y. Sun, X.-r. Li, and Z.-f. Yang, "Distribution patterns of nitrobenzenes and polychlorinated biphenyls in water, suspended particulate matter and sediment from mid-and down-stream of the Yellow River (China)," *Chemosphere*, vol. 65, no. 3, pp. 365–374, 2006.
- [254] R. Thomas, J. Vernet, and R. Frank, "ΣDDT, PCBs, and HCB in the sediments of Lake Geneva and the Upper Rhône River," *Environ. Geol.*, vol. 5, no. 3, pp. 103–113, 1983.
- [255] "Lake Geneva-Lure fishing Website;" <http://leurres.ch/leman-en.html>.
- [256] K. Aswald, G. Burgermeister, L. Machado, and J. Mowrer, "Etude préliminaire de la pollution du Léman par les PCB," *Institut du Génie de l'Environnement, Suisse*, 1979.
- [257] J. Mowrer, K. Åswald, G. Burgermeister, L. Machado, and J. Tarradellas, "PCB in a Lake Geneva ecosystem," *Ambio*, pp. 355–358, 1982.
- [258] G. Monod and G. Keck, "PCBs in lake Geneva (lake Lemman) fish," *B. Environ. Contam. Tox.*, vol. 29, no. 5, pp. 570–576, 1982.
- [259] G. Monod, "Egg mortality of Lake Geneva charr (*Salvelinus alpinus* L.) contaminated by PCB and DDT derivatives," *B. Environ. Contam. Tox.*, vol. 35, no. 1, pp. 531–536, 1985.

- [260] D. Ortelli, P. Edder, and S. Ramseier, "Métaux et micropolluants organiques dans les eaux du léman (metals and organic micropollutants in Geneva Lake waters)," tech. rep., CIPEL, 2010.
- [261] J. Poté, N. Goldscheider, L. Haller, J. Zopfi, F. Khajehnouri, and W. Wildi, "Origin and spatial-temporal distribution of faecal bacteria in a bay of Lake Geneva, Switzerland," *Environ. Monit. Assess.*, vol. 154, no. 1-4, pp. 337–348, 2009.
- [262] B. Morasch, F. Bonvin, H. Reiser, D. Grandjean, L. F. De Alencastro, C. Perazzolo, N. Chèvre, and T. Kohn, "Occurrence and fate of micropollutants in the Vidy Bay of Lake Geneva, Switzerland. Part II: Micropollutant removal between wastewater and raw drinking water," *Environ. Toxicol. Chem.*, vol. 29, no. 8, pp. 1658–1668, 2010.
- [263] A. Kot, B. Zabiegała, and J. Namieśnik, "Passive sampling for long-term monitoring of organic pollutants in water," *TRAC-Trends Anal. Chem.*, vol. 19, no. 7, pp. 446–459, 2000.
- [264] K. Booiij, B. Vrana, and J. N. Huckins, "Theory, modelling and calibration of passive samplers used in water monitoring," *Passive sampling techniques in environmental monitoring*, vol. 48, p. 141, 2007.
- [265] T. P. Rusina, F. Smedes, M. Koblizkova, and J. Klanova, "Calibration of silicone rubber passive samplers: experimental and modeled relations between sampling rate and compound properties," *Environ. Sci. Technol.*, vol. 44, no. 1, pp. 362–367, 2009.
- [266] M. J. Frisch, G. W. Trucks, H. B. Schlegel, G. E. Scuseria, M. A. Robb, J. R. Cheeseman, G. Scalmani, V. Barone, B. Mennucci, G. A. Petersson, H. Nakatsuji, M. Caricato, X. Li, H. P. Hratchian, A. F. Izmaylov, J. Bloino, G. Zheng, J. L. Sonnenberg, M. Hada, M. Ehara, K. Toyota, R. Fukuda, J. Hasegawa, M. Ishida, T. Nakajima, Y. Honda, O. Kitao, H. Nakai, T. Vreven, J. A. Montgomery, Jr., J. E. Peralta, F. Ogliaro, M. Bearpark, J. J. Heyd, E. Brothers, K. N. Kudin, V. N. Staroverov, R. Kobayashi, J. Normand, K. Raghavachari, A. Rendell, J. C. Burant, S. S. Iyengar, J. Tomasi, M. Cossi, N. Rega, J. M. Millam, M. Klene, J. E. Knox, J. B. Cross, V. Bakken, C. Adamo, J. Jaramillo, R. Gomperts, R. E. Stratmann, O. Yazyev, A. J. Austin, R. Cammi, C. Pomelli, J. W. Ochterski, R. L. Martin, K. Morokuma, V. G. Zakrzewski, G. A. Voth, P. Salvador, J. J. Dannenberg, S. Dapprich, A. D. Daniels, Ö. Farkas, J. B. Foresman, J. V. Ortiz, J. Cioslowski, and D. J. Fox, "Gaussian-09 Revision D.01." Gaussian Inc. Wallingford CT 2009.
- [267] S. Grimme, "Semiempirical hybrid density functional with perturbative second-order correlation," *J. Chem. Phys.*, vol. 124, no. 3, p. 034108, 2006.
- [268] T. Schwabe and S. Grimme, "Double-hybrid density functionals with long-range dispersion corrections: higher accuracy and extended applicability," *Phys. Chem. Chem. Phys.*, vol. 9, no. 26, pp. 3397–3406, 2007.
- [269] E. R. Davidson, "Comment on "Comment on Dunning's correlation-consistent basis sets"," *Chem. Phys. Lett.*, vol. 260, no. 3, pp. 514–518, 1996.

## Bibliography

---

- [270] T. H. Dunning Jr, "Gaussian basis sets for use in correlated molecular calculations. I. The atoms boron through neon and hydrogen," *J. Chem. Phys.*, vol. 90, no. 2, pp. 1007–1023, 1989.
- [271] T. H. Dunning Jr, K. A. Peterson, and A. K. Wilson, "Gaussian basis sets for use in correlated molecular calculations. X. The atoms aluminum through argon revisited," *J. Chem. Phys.*, vol. 114, no. 21, pp. 9244–9253, 2001.
- [272] R. A. Kendall, T. H. Dunning Jr, and H. R. J., "Electron affinities of the first-row atoms revisited. Systematic basis sets and wave functions," *J. Chem. Phys.*, vol. 96, pp. 6796–6806, 1992.
- [273] A. V. Marenich, C. J. Cramer, and D. G. Truhlar, "Universal solvation model based on solute electron density and on a continuum model of the solvent defined by the bulk dielectric constant and atomic surface tensions," *J. Phys. Chem. B*, vol. 113, no. 18, pp. 6378–6396, 2009.
- [274] J. A. Montgomery Jr, M. J. Frisch, J. W. Ochterski, and G. A. Petersson, "A complete basis set model chemistry. VI. Use of density functional geometries and frequencies," *J. Chem. Phys.*, vol. 110, no. 6, pp. 2822–2827, 1999.
- [275] J. A. Montgomery Jr, M. J. Frisch, J. W. Ochterski, and G. A. Petersson, "A complete basis set model chemistry. VII. Use of the minimum population localization method," *J. Chem. Phys.*, vol. 112, no. 15, pp. 6532–6542, 2000.
- [276] C. Lee, W. Yang, and R. G. Parr, "Development of the Colle-Salvetti correlation-energy formula into a functional of the electron density," *Phys. Rev. B*, vol. 37, no. 2, p. 785, 1988.
- [277] A. D. Becke, "Density-functional exchange-energy approximation with correct asymptotic behavior," *Phys. Rev. A*, vol. 38, no. 6, p. 3098, 1988.
- [278] A. McLean and G. Chandler, "Contracted Gaussian basis sets for molecular calculations. I. Second row atoms,  $Z=11-18$ ," *J. Chem. Phys.*, vol. 72, no. 10, pp. 5639–5648, 1980.
- [279] H. C. Tülp, K. Fenner, R. P. Schwarzenbach, and K.-U. Goss, "pH-Dependent sorption of acidic organic chemicals to soil organic matter," *Environ. Sci. Technol.*, vol. 43, no. 24, pp. 9189–9195, 2009.
- [280] C. T. Jafvert, J. C. Westall, E. Grieder, and R. P. Schwarzenbach, "Distribution of hydrophobic ionogenic organic compounds between octanol and water: organic acids," *Environ. Sci. Technol.*, vol. 24, no. 12, pp. 1795–1803, 1990.
- [281] G. O. Spessard, "ACD Labs/LogP dB 3.5 and ChemSketch 3.5," *J. Chem. Inf. Comp. Sci.*, vol. 38, no. 6, pp. 1250–1253, 1998.

- [282] M. Altarawneh, T. Dar, and B. Z. Dlugogorski, "Thermochemical parameters and  $pK_a$  values for chlorinated congeners of thiophenol," *J. Chem. Eng. Data*, vol. 57, no. 6, pp. 1834–1842, 2012.
- [283] J. J. Warren, T. A. Tronic, and J. M. Mayer, "Thermochemistry of proton-coupled electron transfer reagents and its implications," *Chem. Rev.*, vol. 110, no. 12, pp. 6961–7001, 2010.
- [284] J. R. Kucklick, T. F. Bidleman, L. L. McConnell, M. D. Walla, and G. P. Ivanov, "Organochlorines in the water and biota of Lake Baikal, Siberia," *Environ. Sci. Technol.*, vol. 28, no. 1, pp. 31–37, 1994.
- [285] R. Vilanova, P. Fernández, C. Martínez, and J. O. Grimalt, "Organochlorine pollutants in remote mountain lake waters," *J. Environ. Qual.*, vol. 30, no. 4, pp. 1286–1295, 2001.
- [286] J. O. Grimalt, B. L. Van Drooge, A. Ribes, R. M. Vilanova, P. Fernandez, and P. Appleby, "Persistent organochlorine compounds in soils and sediments of European high altitude mountain lakes," *Chemosphere*, vol. 54, no. 10, pp. 1549–1561, 2004.
- [287] M. Winkler, J. Headley, and K. Peru, "Optimization of solid-phase microextraction for the gas chromatographic–mass spectrometric determination of synthetic musk fragrances in water samples," *J. Chromatogr. A*, vol. 903, no. 1, pp. 203–210, 2000.
- [288] F. Hernández, J. Sancho, M. Ibáñez, E. Abad, T. Portolés, and L. Mattioli, "Current use of high-resolution mass spectrometry in the environmental sciences," *Anal. Bioanal. Chem.*, vol. 403, no. 5, pp. 1251–1264, 2012.
- [289] I. Hilber, P. Mäder, R. Schulin, and G. S. Wyss, "Survey of organochlorine pesticides in horticultural soils and there grown cucurbitaceae," *Chemosphere*, vol. 73, no. 6, pp. 954–961, 2008.
- [290] P. Schmid, C. Bogdal, Z. Wang, V. Azara, R. Haag, and U. von Arx, "Releases of chlorobenzenes, chlorophenols and dioxins during fireworks," *Chemosphere*, vol. 114, pp. 158–164, 2014.
- [291] S. Canonica, B. Hellrung, and J. Wirz, "Oxidation of phenols by triplet aromatic ketones in aqueous solution," *The Journal of Physical Chemistry A*, vol. 104, no. 6, pp. 1226–1232, 2000.
- [292] D. O'Brien, T. Komarova, and J. F. Mueller, "Determination of deployment specific chemical uptake rates for SPMD and PDMS using a passive flow monitor," *Mar. Pollut. Bull.*, vol. 64, no. 5, pp. 1005–1011, 2012.
- [293] T. P. Rusina, F. Smedes, and J. Klanova, "Diffusion coefficients of polychlorinated biphenyls and polycyclic aromatic hydrocarbons in polydimethylsiloxane and low-density polyethylene polymers," *J. Appl. Polym. Sci.*, vol. 116, no. 3, pp. 1803–1810, 2010.

## Bibliography

---

- [294] T. L. ter Laak, F. J. Busser, and J. L. Hermens, "Poly (dimethylsiloxane) as passive sampler material for hydrophobic chemicals: effect of chemical properties and sampler characteristics on partitioning and equilibration times," *Anal. Chem.*, vol. 80, no. 10, pp. 3859–3866, 2008.
- [295] P. Mayer, W. H. Vaes, and J. L. Hermens, "Absorption of hydrophobic compounds into the poly (dimethylsiloxane) coating of solid-phase microextraction fibers: High partition coefficients and fluorescence microscopy images," *Anal. Chem.*, vol. 72, no. 3, pp. 459–464, 2000.
- [296] F. Smedes, R. W. Geertsma, T. v. d. Zande, and K. Booij, "Polymer- water partition coefficients of hydrophobic compounds for passive sampling: Application of cosolvent models for validation," *Environ. Sci. Technol.*, vol. 43, no. 18, pp. 7047–7054, 2009.
- [297] B. Vrana, G. A. Mills, M. Kotterman, P. Leonards, K. Booij, and R. Greenwood, "Modelling and field application of the chemcatcher passive sampler calibration data for the monitoring of hydrophobic organic pollutants in water," *Environ. Pollut.*, vol. 145, no. 3, pp. 895–904, 2007.
- [298] J. Politano, S. Samanipour, and J. S. Arey, "Numerical modeling of diffusion and boundary layer-controlled mass transfer during accelerated sampling of bioaccumulative micro-pollutants with poly(dimethylsiloxane) materials (PDMS) deployed in natural waters," LMCE Semester project report, available on request., EPFL, 2014.
- [299] E. Baltussen, P. Sandra, F. David, H.-G. Janssen, and C. Cramers, "Study into the equilibrium mechanism between water and poly (dimethylsiloxane) for very apolar solutes: Adsorption or sorption?," *Anal. Chem.*, vol. 71, no. 22, pp. 5213–5216, 1999.
- [300] A. Gaspar and F. A. Gomez, "Application of surface plasmon resonance spectroscopy for adsorption studies of different types of components on poly (dimethylsiloxane)," *Anal. Chim. Acta*, vol. 777, pp. 72–77, 2013.
- [301] M. W. Toepke and D. J. Beebe, "PDMS absorption of small molecules and consequences in microfluidic applications," *Lab Chip*, vol. 6, no. 12, pp. 1484–1486, 2006.
- [302] H. Makamba, J. H. Kim, K. Lim, N. Park, and J. H. Hahn, "Surface modification of poly (dimethylsiloxane) microchannels," *Electrophoresis*, vol. 24, no. 21, pp. 3607–3619, 2003.
- [303] M. Holz and A. Fahr, "Compartment modeling," *Adv. Drug Deliver. Rev.*, vol. 48, no. 2, pp. 249–264, 2001.
- [304] J. Birdwell, R. L. Cook, and L. J. Thibodeaux, "Desorption kinetics of hydrophobic organic chemicals from sediment to water: A review of data and models," *Environ. Toxicol. Chem.*, vol. 26, no. 3, pp. 424–434, 2007.
- [305] G. Cornelissen, P. C. van Noort, and H. A. Govers, "Mechanism of slow desorption of organic compounds from sediments: a study using model sorbents," *Environ. Sci. Technol.*, vol. 32, no. 20, pp. 3124–3131, 1998.



- [306] G. Cornelissen, H. Rigterink, M. M. Ferdinandy, and P. C. van Noort, "Rapidly desorbing fractions of PAHs in contaminated sediments as a predictor of the extent of bioremediation," *Environ. Sci. Technol.*, vol. 32, no. 7, pp. 966–970, 1998.
- [307] G. Cornelissen, P. van Noort, and H. A. Govers, "Desorption kinetics of chlorobenzenes, polycyclic aromatic hydrocarbons, and polychlorinated biphenyls: sediment extraction with Tenax<sup>®</sup> and effects of contact time and solute hydrophobicity," *Environ. Toxicol. Chem.*, vol. 16, no. 7, pp. 1351–1357, 1997.
- [308] G. Cornelissen, P. C. van Noort, J. R. Parsons, and H. A. Govers, "Temperature dependence of slow adsorption and desorption kinetics of organic compounds in sediments," *Environ. Sci. Technol.*, vol. 31, no. 2, pp. 454–460, 1997.
- [309] P. van Noort, G. Cornelissen, T. E. ten Hulscher, B. A. Vrind, H. Rigterink, and A. Belfroid, "Slow and very slow desorption of organic compounds from sediment: influence of sorbate planarity," *Water Res.*, vol. 37, no. 10, pp. 2317–2322, 2003.
- [310] S. C. Wu and P. M. Gschwend, "Sorption kinetics of hydrophobic organic compounds to natural sediments and soils," *Environ. Sci. Technol.*, vol. 20, no. 7, pp. 717–725, 1986.
- [311] M. A. Jeannot and F. F. Cantwell, "Mass transfer characteristics of solvent extraction into a single drop at the tip of a syringe needle," *Anal. Chem.*, vol. 69, no. 2, pp. 235–239, 1997.
- [312] M. A. Jeannot and F. F. Cantwell, "Solvent microextraction into a single drop," *Anal. Chem.*, vol. 68, no. 13, pp. 2236–2240, 1996.
- [313] V. Vasquez, J. Curren, S.-L. Lau, M. Stenstrom, and I. Suffet, "A field studies and modeling approach to develop organochlorine pesticide and PCB total maximum daily load calculations: Case study for Echo Park Lake, Los Angeles, CA," *Sci. Total Environ.*, vol. 409, no. 19, pp. 4010–4015, 2011.
- [314] X. Xia, P. K. Hopke, T. M. Holsen, and B. S. Crimmins, "Modeling toxaphene behavior in the Great Lakes," *Sci. Total Environ.*, vol. 409, no. 4, pp. 792–799, 2011.
- [315] S. Samanipour, J. Politano, S. Dasari, and J. S. Arey, *Overlooked persistent and bioaccumulative pollutants in Lake Geneva: their measurement, occurrence, and concentration distribution in the water column and sediments (Chapter V)*. Phd thesis, EPFL, 2015.
- [316] C. Basheer, H. K. Lee, and J. P. Obbard, "Determination of organochlorine pesticides in seawater using liquid-phase hollow fibre membrane microextraction and gas chromatography–mass spectrometry," *J. Chromatogr. A*, vol. 968, no. 1, pp. 191–199, 2002.
- [317] N. Barlas, İ. Çok, and N. Akbulut, "The contamination levels of organochlorine pesticides in water and sediment samples in Uluabat Lake, Turkey," *Environ. Monit. Assess.*, vol. 118, no. 1-3, pp. 383–391, 2006.

## Bibliography

---

- [318] N. Xue, X. Xu, and Z. Jin, "Screening 31 endocrine-disrupting pesticides in water and surface sediment samples from Beijing Guanting reservoir," *Chemosphere*, vol. 61, no. 11, pp. 1594–1606, 2005.
- [319] G. U. Yule, *An Introduction to the Theory of Statistics*. C. Griffin Ltd., 1919.
- [320] A. M. Razmi, D. A. Barry, D. Bouffard, and U. Lemmin, "Typical near surface layer current patterns in Lake Geneva's main basin (Grand Lac)," in *American Geophysical Union's 47th annual Fall Meeting*, no. EPFL-POSTER-204663, 2014.
- [321] A. Razmi, D. Barry, D. Bouffard, N. Le Dantec, U. Lemmin, and A. Wuest, "Gyre formation within embayments of a large lake (Lake Geneva, Switzerland)," in *AGU Fall Meeting Abstracts*, vol. 1, p. 1657, 2013.
- [322] N. Estoppey, J. Omlin, A. Schopfer, P. Esseiva, E. L. Vermeirssen, O. Delémont, and L. F. De Alencastro, "Low density polyethylene (LDPE) passive samplers for the investigation of polychlorinated biphenyl (PCB) point sources in rivers," *Chemosphere*, vol. 118, pp. 268–276, 2015.
- [323] J. Vijgen, P. Abhilash, Y. F. Li, R. Lal, M. Forter, J. Torres, N. Singh, M. Yunus, C. Tian, A. Schäffer, and R. Weber, "Hexachlorocyclohexane (HCH) as new Stockholm Convention POPs—a global perspective on the management of Lindane and its waste isomers," *Environ. Sci. Pollut. Res.*, vol. 18, no. 2, pp. 152–162, 2011.
- [324] K. Breivik, J. M. Pacyna, and J. Münch, "Use of  $\alpha$ -,  $\beta$ - and  $\gamma$ -hexachlorocyclohexane in Europe, 1970–1996," *Sci. Total Environ.*, vol. 239, no. 1, pp. 151–163, 1999.
- [325] X. Li, Q. Zhang, J. Dai, Y. Gan, J. Zhou, X. Yang, H. Cao, G. Jiang, and M. Xu, "Pesticide contamination profiles of water, sediment and aquatic organisms in the effluent of Gaobeidian wastewater treatment plant," *Chemosphere*, vol. 72, no. 8, pp. 1145–1151, 2008.
- [326] F. Thevenon, L. F. d. Alencastro, J.-L. Loizeau, T. Adatte, D. Grandjean, W. Wildi, and J. Poté, "A high-resolution historical sediment record of nutrients, trace elements and organochlorines (DDT and PCB) deposition in a drinking water reservoir (Lake Brêt, Switzerland) points at local and regional pollutant sources," *Chemosphere*, vol. 90, no. 9, pp. 2444–2452, 2013.
- [327] A. Accardi-Dey and P. M. Gschwend, "Assessing the combined roles of natural organic matter and black carbon as sorbents in sediments," *Environ. Sci. Technol.*, vol. 36, no. 1, pp. 21–29, 2002.
- [328] G. Cornelissen, Ö. Gustafsson, T. D. Bucheli, M. T. Jonker, A. A. Koelmans, and P. C. van Noort, "Extensive sorption of organic compounds to black carbon, coal, and kerogen in sediments and soils: mechanisms and consequences for distribution, bioaccumulation, and biodegradation," *Environ. Sci. Technol.*, vol. 39, no. 18, pp. 6881–6895, 2005.

- [329] T. P. Rusina, F. Smedes, M. Koblizkova, and J. Klanova, "Calibration of silicone rubber passive samplers: experimental and modeled relations between sampling rate and compound properties," *Environ. Sci. Technol.*, vol. 44, no. 1, pp. 362–367, 2010.
- [330] A. Hussen, R. Westbom, N. Megersa, L. Mathiasson, and E. Björklund, "Development of a pressurized liquid extraction and clean-up procedure for the determination of  $\alpha$ -endosulfan,  $\beta$ -endosulfan and endosulfan sulfate in aged contaminated Ethiopian soils," *J. Chromatogr. A*, vol. 1103, no. 2, pp. 202–210, 2006.
- [331] R. Dean and W. Dixon, "Simplified statistics for small numbers of observations," *Anal. Chem.*, vol. 23, no. 4, pp. 636–638, 1951.
- [332] J. Ho and M. L. Coote, "A universal approach for continuum solvent  $pK_a$  calculations: are we there yet?," *Theor. Chem. Acc.*, vol. 125, no. 1-2, pp. 3–21, 2010.
- [333] S. Zhang, "A reliable and efficient first principles-based method for predicting  $pK_a$  values. 4. Organic bases," *J. Comput. Chem.*, vol. 33, no. 31, pp. 2469–2482, 2012.
- [334] M. D. Liptak and G. C. Shields, "Accurate  $pK_a$  calculations for carboxylic acids using complete basis set and Gaussian-n models combined with CPCM continuum solvation methods," *J. Am. Chem. Soc.*, vol. 123, no. 30, pp. 7314–7319, 2001.
- [335] M. D. Liptak and G. C. Shields, "Experimentation with different thermodynamic cycles used for  $pK_a$  calculations on carboxylic acids using complete basis set and Gaussian-n models combined with CPCM continuum solvation methods," *Int. J. Quantum Chem.*, vol. 85, no. 6, pp. 727–741, 2001.
- [336] M. D. Liptak, K. C. Gross, P. G. Seybold, S. Feldgus, and G. C. Shields, "Absolute  $pK_a$  determinations for substituted phenols," *J. Am. Chem. Soc.*, vol. 124, no. 22, pp. 6421–6427, 2002.
- [337] R. Casasnovas, J. Frau, J. Ortega-Castro, A. Salvà, J. Donoso, and F. Muñoz, "Absolute and relative  $pK_a$  calculations of mono and diprotic pyridines by quantum methods," *J. Mol. Struct. THEOCHEM*, vol. 912, no. 1, pp. 5–12, 2009.
- [338] A. A. Isse and A. Gennaro, "Absolute potential of the standard hydrogen electrode and the problem of interconversion of potentials in different solvents," *J. Phys. Chem. B*, vol. 114, no. 23, pp. 7894–7899, 2010.
- [339] A. Fischer, *Acidität der Sulfane und Zusammensetzung der wässrigen Alkalipolysulfidlösungen*. PhD thesis, Diss. Techn. Wiss. ETH Zürich, Nr. 3018,0000. Ref.: Schwarzenbach, G.; Korref.: Günthard, HH, 1960.
- [340] Q. Fernando and H. Freiser, "Chelating properties of  $\beta$ -mercaptopropionic acid," *J. Am. Chem. Soc.*, vol. 80, no. 18, pp. 4928–4931, 1958.
- [341] D. J. Giesen, M. Z. Gu, C. J. Cramer, and D. G. Truhlar, "A universal organic solvation model," *J. Org. Chem.*, vol. 61, no. 25, pp. 8720–8721, 1996.

## Bibliography

---

- [342] W. H. Vaes, E. Urrestarazu Ramos, H. J. Verhaar, C. J. Cramer, and J. L. Hermens, "Understanding and estimating membrane/water partition coefficients: Approaches to derive quantitative structure property relationships," *Chem. Res. Toxicol.*, vol. 11, no. 8, pp. 847–854, 1998.
- [343] C. J. Cramer, *Essentials of Computational Chemistry: Theories and Models*. John Wiley & Sons, 2013.
- [344] B. I. Escher, M. Berg, J. Mühlemann, M. A. Schwarz, J. L. Hermens, W. H. Vaes, and R. P. Schwarzenbach, "Determination of liposome/water partition coefficients of organic acids and bases by solid-phase microextraction," *Analyst*, vol. 127, no. 1, pp. 42–48, 2002.
- [345] B. I. Escher, R. P. Schwarzenbach, and J. C. Westall, "Evaluation of liposome-water partitioning of organic acids and bases. 1. Development of a sorption model," *Environ. Sci. Technol.*, vol. 34, no. 18, pp. 3954–3961, 2000.
- [346] D. D. Perrin, *Dissociation constants of organic bases in aqueous solution*. Butterworths, 1972.

# Saer SAMANIPOUR

## PERSONAL DATA

---

DATE OF BIRTH: 14 January 1984  
ADDRESS: Ch. de Rionza 11, 1020 Renens, Switzerland  
PHONE: +41 (0)79 435 3457  
EMAIL: [saersamani@gmail.com](mailto:saersamani@gmail.com)  
[saer.samanipour@epfl.ch](mailto:saer.samanipour@epfl.ch)

## EDUCATION

---

|                        |   |
|------------------------|---|
| From:<br>DECEMBER 2010 | PhD in CHEMISTRY, <b>Ecole Polytechnique Fédérale de Lausanne (EPFL)</b> , Switzerland.   |
| To:<br>JUNE 2015       | Thesis: "Overlooked persistent and bioaccumulative pollutants (PBPs) in Lake Geneva: their measurement, occurrence, and concentration distribution in the water and sediments."<br><br>  Advisor: Prof. J. Samuel AREY<br><br>Focus: This thesis investigated the occurrence of legacy and novel PBPs in a deep aquatic system and specifically in Lake Geneva by taking advantage of the resolution power of comprehensive two-dimensional gas chromatography (GC×GC). |
| JUNE 2010              | Master of Science (MSc) in CHEMISTRY, <b>University of Camerino</b> , Italy. <b>110/110 summa cum laude</b>   Major: Analytical chemistry<br>Thesis: "Kinetic model, HPLC-DAD method development and optimization of Lycopen extraction from tomatoes."<br><br>  Advisor: Dr. Paolo PASSAMONTI  |
| DECEMBER 2008          | Bachelor of Science (BSc) in CHEMISTRY, <b>University of Camerino</b> , Italy. <b>110/110 summa cum laude</b>   Major: Physical chemistry<br>Thesis: "Thermal engines and their efficiency and irreversibility."<br><br>  Advisor: Prof. Bernard Howard LAVENDA   |

## AWARDS AND HONORS

---

|           |   |
|-----------|---|
| Current   | Reviewer for <i>J. Chrom. A.</i> and <i>Chem. Eng. Commun.</i>                              |
| 2015      | Swiss Chemical Society (SCS), Analytical chemistry division, travelling award.              |
| 2014      | Swiss Chemical Society (SCS) traveling award.   |
| 2009-2010 | Research scholarship based on academic merit, funded by the <b>University of Camerino</b> . |

## RESEARCH EXPERIENCE

---

|                      |  |
|----------------------|--|
| From:<br>JULY 2009   | Research assistant, <b>University of Camerino</b> .  |
| To:<br>NOVEMBER 2010 | Focus: the aim of this project was extraction, purification and isolation of natural dyes from plants, for the industrial production of these dyes. During this project, I developed an optimized extraction method for isolation of Indigo from Woad, using the Design of Experiment methodology (DoE). |

## TEACHING EXPERIENCE

---

2014 | Teaching assistant for "Fate and behavior of organic pollutants", **EPFL**.

2012-2013 | Teaching assistant for "Quantitative methods II", **EPFL**.

2012 | Teaching assistant for "Numerical analysis II", **EPFL**.

2011 | Teaching assistant for "Water and wastewater treatment", **EPFL**.

## SCHOLARLY MEMBERSHIP

---

Swiss Chemical Society (SCS) membership.

## RELEVANT INFORMATION

---

June 2013 | "Summer school in environmental systems analysis", **EAWAG**, Switzerland.

February 2013 | "Matlab programming", Basic level, **EPFL**, Switzerland.

October 2012 | "Training for GC×GC", **ZOEX**, Amsterdam, Netherlands.

January 2012 | "Scientific writing", **EPFL**, Switzerland.

November 2009 | "Design of Experiment", Basic level, **S-in**, Vicenza, Italy.

## LANGUAGES

---

PERSIAN: Mother tongue  
ENGLISH: Fluent  
ITALIAN: Fluent

## JOURNAL PUBLICATIONS

---

### Published work

1. Dimitriou-Christidis, P.; Bonvin, A.; **Samanipour, S.**; Hollender, J.; Rutler, R.; Westphale, J.; Gros, J. and Arey, J. S., GC×GC quantification of priority and emerging nonpolar organic micropollutants in all types of wastewater streams: analysis methodology, chemical occurrence, and partitioning. *Environ. Sci. Technol.* **2015**, (*In press*).
2. **Samanipour, S.**; Dimitriou-Christidis, P.; Grange, A.; Gros, J.; Arey, J. S., Analyte quantification with comprehensive two-dimensional gas chromatography: Assessment of

methods for baseline correction, peak delineation and matrix effect elimination. *J. Chromatogr. A* **2015**, 1375, 123-139.

3. Alibabaei, L.; Giovannetti, R.; **Samanipour, S.**, Structure investigations of binary azeotrope of diethyl amine-acetone by FT-IR and H-NMR spectroscopy. *Spectrochim. Acta A* **2009**, 72, 390-393.

## Unpublished work

1. **Samanipour, S.**; Nabi, D.; Arey, J. S., Overlooked persistent and bioaccumulative brominated pollutants in deep water column and sediments of Lake Geneva (Switzerland): detection, quantification, their fate, and behavior. *Environ. Sci. Technol.* **2015**, (Submitted).
2. **Samanipour, S.**; Trogolo, D.; Zushi, Y.; Arey, J. S., Pentachlorothiophenol, a newly identified aquatic pollutant in the water column and sediments of Lake Geneva, Switzerland. *Environ. Sci. Technol.* **2015**, (To be submitted).
3. **Samanipour, S.**; Mallios, A.; Politano, J.; Dasari, S.; Camilli, R.; Gerecke, A. and Arey, J. S., Development, modeling and field test of a novel sampler of the truly dissolved fraction of organic pollutants in deep and shallow water. *J. Chromatogr. A*, (In preparation).
4. **Samanipour, S.**; Riano, S.; Buoffard, D.; Wüest, J. and Arey, J. S., Spatial and temporal distribution of hydrophobic persistent and bioaccumulative pollutants in the water column of Lake Geneva, Switzerland. *Environ. Sci. Technol.*, (In preparation).

## CONFERENCES

---

### Oral contributions

1. **Samanipour, S.** and Arey, J. S., Pollutant distributions between sediments and the benthic water column in a deep lake: Application of passive sampling and GC×GC to less-studied and legacy halogenated contaminants in Lake Geneva. **ContaSed March 2015**, Ascona, Switzerland.
2. **Samanipour, S.**; Nabi, D.; Arey, J. S., Concentration and trends of novel brominated hydrocarbons in the water column and sediments of Lake Geneva (Switzerland): detection and quantification using GC×GC- $\mu$ ECD and GC×GC-ENCI-TOFMS. Presented at **EuChEMS September 2014**, Istanbul, Turkey.

### Poster contributions

1. **Samanipour, S.**; Cecchi, T. and Passamonti, P., Lycopene extraction kinetic model. **CF2010: Il XXXIX congresso nazionale di chimica fisica, September 2010**, Stresa, Italy.
2. **Samanipour, S.**; Cecchi, T. and Passamonti, P., Optimization of Lycopene extraction by design of experiment. **XXII convegno nazionale della divisione di chimica analitica della società chimica Italiana, September 2010**, Como, Italy.

### Other contributions

1. Arey, J. S.; **Samanipour, S.**; Nabi, D.; Dimitriou-Christidis, P. and Gros, J., Advances in trace detection, quantification, and partitioning property estimation of bioaccumula-

- tive pollutants with GC×GC. Presented at SETAC Europe 25th Annual Meeting, **May 2015**, Barcelona, Spain.
2. Mallios, A.; Pizarro, O.; Arey, J. S.; **Samanipour, S.** et al., Synoptic identification of greenhouse gas sources and sinks in Lake Léman. Aquatic Sciences Meeting, **February 2015**, Granada, Spain.
  3. Arey, J. S.; **Samanipour, S.**; Nabi, D.; Dimitriou-Christidis, P. and Gros, J., Detection, quantification, and partitioning property estimation of less-studied bioaccumulative pollutants in aquatic environments using GC×GC- $\mu$ ECD and GC×GC-ENCI-TOFMS. Presented at The 6th Multidimensional Chromatography Workshop, **January 2015**, Toronto, Canada.

## REFERENCES

---

- Prof. J. Samuel Arey  
  
EPFL ENAC IIE LMCE  
GR C2 544 (Bâtiment GR)  
Station 2  
1015 Lausanne  
Switzerland  
Phone: +41 (0)21 693 8031  
Email: samuel.arey@epfl.ch
  
- Dr. Richard Camilli  
  
Mailstop 07  
Woods Hole Oceanographic Institution  
Woods Hole, MA 02543  
USA  
Phone: +1 508 289 3796  
Email: rcamilli@whoi.edu
  
- Dr. Petros Dimitriou-Christidis  
  
Firmenich SA  
Route Des Jeunes 1, Les Acacias  
1211 Geneva  
Switzerland  
Phone: +41 (0)22 780 3768  
Email: petros.dimitriou.christidis@firmenich.com